

**Investigation of Vitrimer Epoxy Resins for Carbon Fiber Reinforced
Polymers and Fiber Metal Laminates**

Dissertation

zur Erlangung des akademischen Grades

Dr.-Ing.

eingereicht an der

Mathematisch-Naturwissenschaftlich-Technischen Fakultät

der Universität Augsburg

von

Natascha Sarah Dosoudil



Erstgutachter: Prof. Dr. Markus Sause

Zweitgutachter: Prof. Dr.-Ing. Dietmar Koch

Mündliche Prüfung: Augsburg, 15.03.2022

Abstract

In this thesis, various vitrimer epoxy polymers were investigated for use in carbon fiber reinforced and hybrid metal composite materials. First, the reactivity and processing of the neat resin material was determined. Mechanical performance and thermal properties of the resins, carbon fiber reinforced polymers (CFRP) and fiber metal laminates (FML) were comprehensively characterized. Thus, influencing variables and correlations were determined and, on this basis, design criteria and target parameters for vitrimer matrix materials were set to create vitrimer polymer materials efficient for use in high-performance composites. To analyze and highlight the added value of vitrimer epoxies, especially the dynamic properties of the polymers were tested. The ability for relaxation and the potential for recycling and repair of different resins was compared. Finally, three resin formulations were selected which are suitable for use in structural components due to their static properties and which offer added value concerning sustainability due to their dynamic properties.

Kurzzusammenfassung

In dieser Arbeit wurde eine Vielzahl an vitrimeren Epoxidharzen für den Gebrauch in Carbonfaser-verstärkten sowie Metall-Hybrid-Verbundwerkstoffen untersucht. Zunächst wurden die Reaktivität und die Verarbeitung der reinen Harze bestimmt. Die thermischen und mechanischen Eigenschaften der reinen Harze sowie von Kohlenstofffaserverstärkten Kunststoff (CFK) - und Fasermetall-Hybridlaminat (FML) - Materialien wurden umfassend charakterisiert. Dabei wurden Einflussgrößen und Zusammenhänge ermittelt und basierend darauf Designkriterien und Zielparameter für vitrimere Matrixmaterialien festgelegt, um diese effizient in Hochleistungs-Verbundmaterial einsetzen zu können. Um den Mehrwert des Materials zu analysieren und herauszustellen wurden insbesondere die dynamischen Eigenschaften der Kunststoffe getestet. Die Relaxationsfähigkeit des Materials, das Recycling- sowie Reparaturpotential verschiedener Harzmischungen wurde verglichen. Schließlich wurden drei Harzmischungen ausgewählt, welche sich sowohl hinsichtlich ihrer statischen Eigenschaften für den Einsatz in Strukturbauteilen eignen als auch hinsichtlich ihrer dynamischen Eigenschaften einen Mehrwert auf Grund ihrer Nachhaltigkeit bieten.

Contents

Abstract	I
Kurzzusammenfassung	II
Contents	III
List of Abbreviations	VII
1 Introduction	1
1.1 Motivation	1
1.2 Objectives	1
2 Fundamentals	3
2.1 Polymers.....	3
2.1.1 Thermoplastics.....	3
2.1.2 Thermosets.....	4
2.1.2.1 Phase Transitions of Thermosetting Polymers.....	4
2.1.2.2 Structure of Epoxy Resins	6
2.1.2.3 Curing Mechanism of Epoxy and Amine	7
2.1.2.4 Curing Mechanism of Epoxy and Carboxylic Acid.....	9
2.1.2.5 Curing Mechanism of Epoxy and Thiol	10
2.1.3 Vitrimers.....	11
2.1.3.1 General Definition and Properties.....	11
2.1.3.2 Variety of Dynamic Polymer Chemistry	14
2.1.3.3 Disulfide Exchange Mechanism.....	16
2.1.3.4 Thiol-Disulfide Reaction.....	24
2.2 Carbon Fiber Reinforced Polymers (CFRP).....	27
2.2.1 General Information	27
2.2.2 Mechanical Parameters and Transversal Isotropy.....	28
2.3 Fiber Metal Laminates (FMLs)	29

Contents

2.4	Potential of Vitrimers for CFRP and FML	35
3	Methods.....	37
3.1	Thermal Analysis	37
3.1.1	Differential Scanning Calorimetry (DSC)	37
3.1.2	Thermogravimetric Analysis (TGA)	37
3.1.3	Dynamic Mechanical Analysis (DMA).....	38
3.1.3.1	Rheometry.....	38
3.1.3.2	Single Cantilever DMA	39
3.2	Gel Permeation Chromatography (GPC).....	40
3.3	Quasi-Static Mechanical Tests.....	41
3.3.1	Tensile Test	41
3.3.2	Compression Test.....	42
3.3.3	Bending Test.....	43
3.3.4	Butt-Joint Test.....	45
3.3.5	Shear Tests	45
3.3.5.1	Apparent Interlaminar Shear Strength (ILSS) Test	45
3.3.5.2	Tensile Test of $\pm 45^\circ$ Laminates	46
3.3.5.3	V-Notched Rail Shear Test.....	47
3.4	Fracture Mechanics - Double Cantilever Beam (DCB) Test	49
3.5	High Strain-Rate Test – Charpy Impact.....	52
4	Materials and Sample Preparation.....	54
4.1	Base Materials	54
4.1.1	Resin Components	54
4.1.2	Type of Carbon Fiber Material.....	58
4.2	Overview of Resin Formulations	58
4.3	Prepreg Materials	63
4.4	General Sample Preparation.....	64

4.4.1	Neat Resin Specimens.....	64
4.4.2	CFRP Specimens	65
4.4.3	FML Specimens.....	67
5	Results and Discussion	69
5.1	Curing Behavior	69
5.1.1	Gel Time Measurements (<i>t_{gel}</i>)	69
5.1.2	Cure Time	74
5.1.3	Discussion	75
5.2	Glass Transition Temperature (<i>T_g</i>)	76
5.2.1	DSC	76
5.2.2	Rheological Measurements.....	77
5.2.3	Discussion	78
5.3	Degradation Temperature (<i>T_d</i>)	79
5.4	Mechanical Performance at Room Temperature.....	84
5.4.1	Neat Resin	85
5.4.2	CFRP	88
5.4.3	FML	94
5.4.4	Benchmarking	100
5.4.5	Discussion	103
5.5	Mechanical Performance at Elevated Temperatures.....	105
5.5.1	Mechanical Stability of the CFRP (DMA Measurements)	106
5.5.2	Mechanical Stability of the FML (DMA Measurements)	108
5.5.3	Discussion	108
5.6	Water Absorption and Media Resistivity of the CFRP and FML	108
5.6.1	Accelerated Conditioning (<i>H₂O</i>)	109
5.6.2	Salt Spray Test (<i>NaCl</i>).....	115
5.6.3	Media Resistivity (<i>HCl, NaOH, Ca(OH)₂, CaCl₂</i>)	121

Contents

5.6.4	Discussion	123
5.7	Dynamic Properties.....	125
5.7.1	Network Structure	125
5.7.2	Relaxation Behavior.....	126
5.7.3	Flow Tests on Vitrimer Neat Resin to Assess Reparability	131
5.7.4	Recycling of Vitrimer Neat Resin.....	135
5.7.5	Interim Conclusion	142
5.7.6	Repair Potential of Vitrimer Composites.....	143
5.7.7	Recyclability of Vitrimer Composites	147
5.7.8	Discussion	149
5.8	Summary	152
6	Conclusions and Outlook	161
	Definitions and Parameter Conventions	164
	References	165
	List of Figures	171
	List of Tables.....	175
	Acknowledgements	177
	Appendix	178

List of Abbreviations

Abbreviation	Meaning
ARALL	Aramid Aluminum Laminate
APhD	4-Aminophenyl disulfide
BDE	Bond dissociation energy
BFDGE	Diglycidylether of Bisphenol F
BGPDS	Bis(4-glycidioxyphenyl)disulfide
CARALL	Carbon Reinforced Aluminum Laminate
CFRP	Carbon Fiber Reinforced Polymer
CTE	Coefficient of Thermal Expansion
DBU	Diazabicycloundecene
DCB	Double Cantilever Beam
DDS	Diaminodiphenyl sulfone, Dapsone, Aradur (9964-1)
DGEBA, DGE	Diglycidylether of Bisphenol A, Diglycidylether
DMA	Dynamic Mechanical Analysis
DPDS	Diphenyl disulfide
DSC	Differential Scanning Calorimetry
DTPA	Dithiopropionic acid
DTT	Dithiothreitol
EPS	Epoxy-functional polysulfide
FML	Fiber Metal Laminate
FTIR	Fourier Transform Infrared Spectroscopy
FVF	Fiber Volume Fraction
GFRP	Glas Fiber Reinforced Polymer
GLARE	Glas Laminate Aluminum Reinforced Epoxy
GPC	Gas Permeation Chromatography
HMDA	Hexamethylene diamine
ILSS	Interlaminar Shear Strength
MDA	4,4'-Methylene dianiline
2-ME	2-Mercaptoethanol
PACM	4,4'-Methylenebis(cyclohexylamine)
TBP	Tributylphosphine

List of Abbreviations

TGA

Thermogravimetric Analysis

1 Introduction

Today there is a demand for high-performance materials which are also sustainable. Composite materials offer high potential for lightweight construction and design capabilities for a great variety of applications. Carbon Fiber Reinforced Polymers and Fiber Metal Laminates require a polymer as adhesive for fibers and metal layers.

1.1 Motivation

Sustainability and resource efficiency are important issues in industry. So, reuse, recycling, repair and remanufacturing of materials is desired and at best closed loop supply chains are aspired. Also, an extension of the life cycle of component parts is targeted. Much research is done in the field of new and innovative materials.

Lightweight construction is of great importance for many industrial sectors such as automotive and aerospace industry, shipbuilding, and many others. In this way, weight and thus materials and energy and consequently costs can be saved. For example, composite materials such as carbon fiber reinforced polymers are much lighter and exhibit higher specific strength and stiffness compared to steel. Hybrid composites like fiber metal laminates, in turn, combine the advantages of fiber reinforced polymers and metals.

Usually, thermoplastic or thermosetting matrix materials are used for composite materials. The matrix component of composites offers a great possibility to improve sustainability of fiber composites. In the last decades, intensive research was done in the field of innovative polymers with thermo-activated formability, repair potential and on-demand recyclability. Vitrimers are a specific class of polymers which combine the advantages of thermoplastic polymers (reversible formability, recyclability, room-temperature storability) and thermosetting polymers (mechanical performance, media resistivity, good adhesion to metal).

1.2 Objectives

The aim of this thesis is to formulate and investigate different thermosetting epoxy-based vitrimer resins regarding their network structure as well as to test and compare their standard irreversible or static properties (reactivity, thermal properties, mechanical performance) and reversible or dynamic network properties (relaxation behavior, reparability, recycling potential). A comprehensive characterization is performed to evaluate whether the formulated vitrimer matrix

Introduction

materials exhibit and combine the advantages of thermoplastic and thermosetting materials and to what extent. Besides pure resin tests, the vitrimer resins are used as matrix material in fiber reinforced composites and their influence on material properties and their suitability for use in composite materials is discussed. It is aspired to create resins with mechanical performance competitive to standard materials and sustainability as well. Four key requirements are set for the resin of choice. The material shall maintain its mechanical stability up to 100 °C to ensure suitability for a wide range of structural applications. The relaxation time should be relatively fast to enable forming process in a reasonable timescale. The target value corresponds to the relaxation ability of a vitrimer epoxy resin reported in literature which was already used in CFRP and has a glass transition temperature (T_g) far above 100 °C, but very high cost. [1] The cost of neat resin should not exceed EUR 20 per kg to be useful for several branches. And, last but not least, the resin shall be recyclable with chemicals not hazardous for the environment or human health and offer reparability. Figure 1.1 represents the target criteria used for resin development.

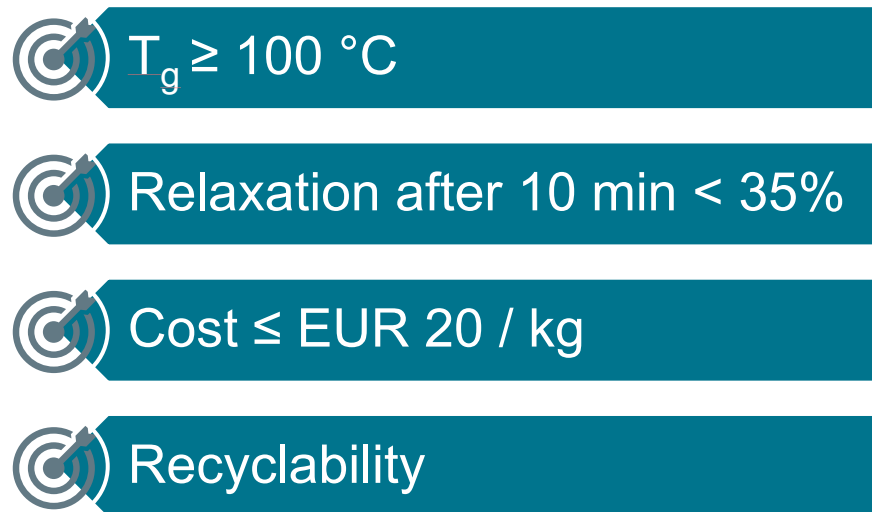


Figure 1.1: Target criteria for resin development

2 Fundamentals

2.1 Polymers

Polymers are chemical substances composed of macromolecules. Macromolecules have a high relative molecular mass and are created by polymerization reaction of monomers. The schematic structure of polymers is shown in Figure 2.1.

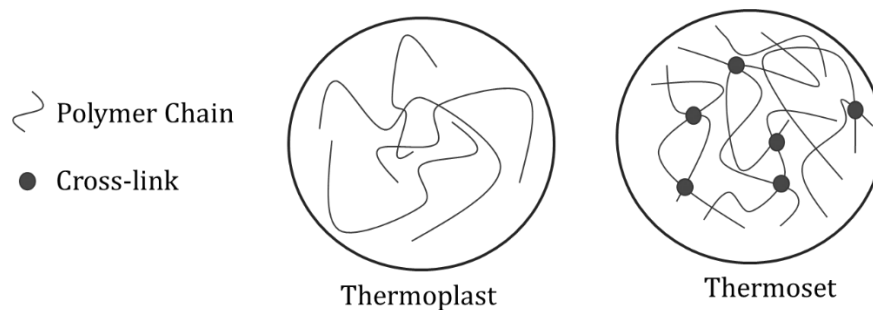


Figure 2.1: Schematic structure of polymers (following [2])

There is a great variety of polymer materials, but a distinction can be made between two main classes of polymers: thermosets and thermoplastics. These two groups exhibit significant differences in their molecular structure. There are also elastomers, but these are not discussed in detail here. [2]

2.1.1 Thermoplastics

Thermoplastics consist of linear or branched polymer chains which are held together by weak physical interactions like Van der Waals forces. Amorphous thermoplastics (e.g., PS, PES) have randomly oriented macromolecules and thus they soften over a broad range of temperatures around their T_g . Semi-crystalline thermoplastics (e.g., PP, PE, P6, PA66, PPS, PEEK) exhibit crystalline regions where the molecular chains are ordered and tightly packed, so they have a sharp melting point T_m . The structural difference is shown in Figure 2.2. Thermoplastics are rather ductile materials and can be reversibly molten and solidified by heating and cooling. [2] As matrix material in fiber metal laminates, their weak adhesion to metal is disadvantageous.

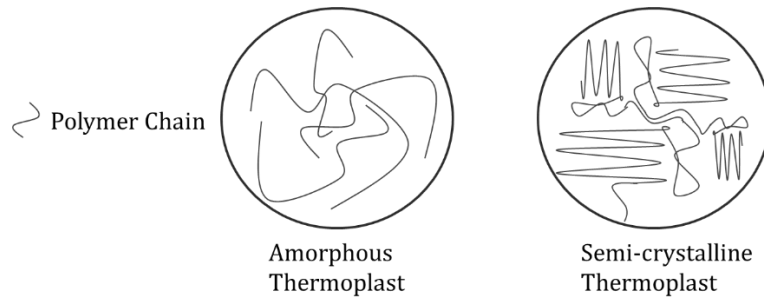


Figure 2.2: Microstructure of amorphous and semi-crystalline thermoplastic polymers (following [2])

2.1.2 Thermosets

Thermosets are strongly crosslinked networks connected via covalent chemical bonds. Thermosets irreversibly solidify by a curing reaction either temperature dependent (hot-melt systems) or temperature independent (by mixing of a two-component system). They are rather brittle and form covalent bonds to inorganic substrates like metals, which is the reason why they are well suitable for fiber metal laminates.

The main difference is that due to their molecular structure thermoplastics can be reshaped, repaired and recycled, whereas thermosets have high mechanical properties, good chemical resistance and high thermal stability.

2.1.2.1 Phase Transitions of Thermosetting Polymers

During cure, thermosetting resins undergo three states: liquid, gel and solid. The curing reaction is associated with a significant viscosity increase of the resin material. This transition behavior is a function of time and temperature which is illustrated in the so called time-temperature transformation (TTT) diagrams as shown schematically for thermosetting resins in Figure 2.3.

DYNAMIC MECHANICAL ANALYSIS (DMA)

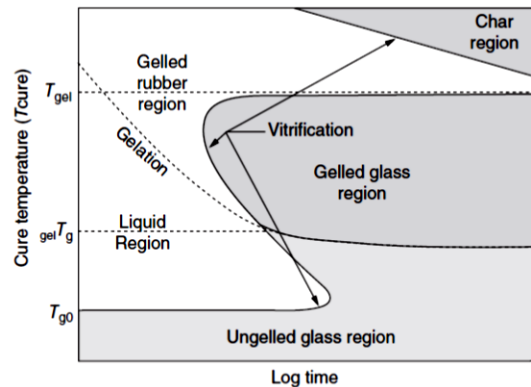


Figure 2.3: Schematic TTT-diagram for thermosetting resins [3]

The gelation curve relates the time for reaching the gel point to the isothermal temperature of cure. With proceeding curing reaction there is a significant T_g evolution as a function of the degree of conversion α . This relation represents the diffusion control of the reaction and is described by the DiBenedetto equation. [4]

The glass transition of thermosetting resins is defined as the reversible transition from the rubbery to the glassy state. There are three important glass transition temperatures in the TTT-diagram: The $T_{g,0}$ of the uncured sample, the $T_{g,gel}$ where gelation and vitrification occur simultaneously, respectively where the vitrification and gelation curves intersect, and the $T_{g,max}$ of the fully cured sample. [3]

The gel-point marks the end of flowability and the onset of insolubility. Then, a molecular network exists which reaches throughout the whole sample. (See chapter 3.1.3.1 for evaluation of gel-point using rheometry method.) Vitrification means the shift of the reaction from chemically to diffusion-controlled and occurs when T_g exceeds T_{cure} . [3]

There is no single method to measure the exact cure time. There are several methods to measure the change of properties related to curing of the material. A curing degree of 100% is never reached in practice because there are still reactants in the volume which could not meet each other. [2] The viscosity change during cure can be measured or monitored by rheometry. When the complex viscosity does not significantly change anymore, then the completion of the reaction can be assumed. This method lacks accuracy, as the viscosity no longer changes measurably

while the material reaches the last missing percent of maximum degree of conversion. The conversion can be verified with FTIR as well, which measures the presence before and the absence of oxirane groups after curing. However, the sensitivity of the FTIR must be taken into account. Another pragmatic way to determine a reasonable cure time is isothermal DSC measurements. Therefore, a constant temperature is held for a certain time which is followed by a second measurement step with heating ramp. When residual enthalpy is observable in the second step, the material needs to be cured longer. To achieve a precise value, this procedure becomes laborious since several measurements must be performed. Fast heating and cooling are required to obtain precise results. With modern DSC equipment, preferably flash DSC, isothermal measurements can be utilized as well to define the cure time. When two or more methods are combined, the higher value must be considered, and the measurement results are closer to reality. [3] A theoretical or mathematical approach (e.g., based on DSC measurements) to investigate and predict cure times is thermokinetic modelling.

Logically, cure temperature must be set over the temperature $T_{g,1}$, where vitrification occurs. The cure temperature depends on the degree of cure desired, which significantly influences the plastic properties. For example, lowering the maximum degree of cure by a few percent can noticeably increase the toughness properties of some resins. When full cure is targeted, the cure temperature can be set to $T_{cure} > T_{g,max} + 20\text{ }^{\circ}\text{C}$, for example and must be substantially lower than the decomposition temperature of the material. Unreacted resin material has potentially lower thermal resistance than the cured material, what should be looked out for in processing and may require two or multi-stage curing cycles. Furthermore, post-curing (at e.g., $T_{cure} + 50\text{ }^{\circ}\text{C}$) can be performed to relax residual stresses in the material. [4]

2.1.2.2 Structure of Epoxy Resins

The term epoxy resin is applied to both the prepolymer and the cured resin. Cured epoxy thermosets usually exhibit thermal stability, excellent adhesion, mechanical strength and chemical stability to many solvents. [5] Epoxy resin prepolymers contain the characteristic oxirane group, which is illustrated in Figure 2.4. Due to the ring strain, epoxides are highly reactive.

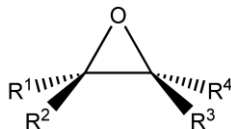
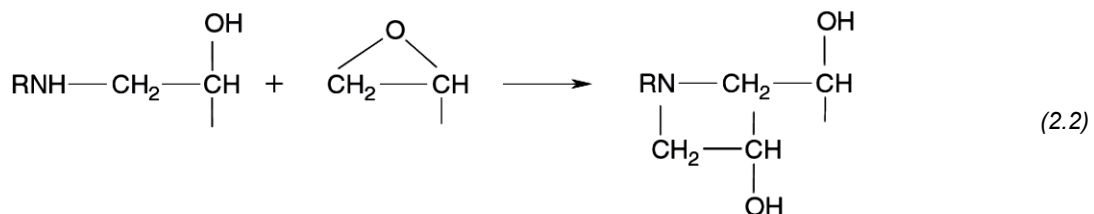
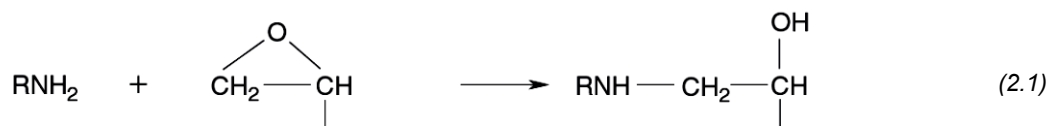


Figure 2.4: Structural chemical formula of the oxirane ring (epoxy group) (following [6])

Epoxy resins are polyadducts (i.e. products of chain growth polymerization). The most prominent prepolymer is the aromatic diglycidylether of bisphenol A (DGEBA) molecule which is synthesized from bisphenol A and epichlorohydrin. This diepoxide monomer has a molecular weight M_w of 340 g/mol. Aliphatic diglycidylethers (DGE) are used as reactive diluents or flexibilizers. [6]

2.1.2.3 Curing Mechanism of Epoxy and Amine

The reaction mechanism of epoxide resins with amine hardeners is a step-growth polymerization and has complex kinetics due to the number of different intermediate and reaction products involved, the autocatalysis of the ring-opening step and the changing concentration of the different molecules during the proceeding reaction. A lot of research has already been done on this curing mechanism, which is not yet fully understood. Ehlers et al., for example, conducted a study on the epoxy-amine reaction in 2007 to elucidate the participating polymerization reaction types and transition states. It is an S_N^2 addition mechanism and shows second-order kinetics. [7] The following two equations (2.1- 2.2) show a simplified scheme of the epoxy amine curing mechanism [8]:



Referring to equation (2.1), the reaction starts with a nucleophilic attack by the primary amine nitrogen (with high electron density due to the free electron pair) on the electrophilic carbon (with low electron density) of the epoxy group. Breaking the $C - O$ bond opens the ring and relieves the ring strain as this is the energetically more favorable state. This results in a negative charge on the oxygen and a positive charge on the nitrogen. The oxygen anion attracts a hydrogen from the ammonium nitrogen, forming a hydroxyl group and reforming an amine group which can react with another epoxy ring. The product is a secondary alcohol. The hydroxyl groups catalyze the reaction, which is an autocatalytic mechanism. Theoretically, there is a competing reaction: Etherification occurs when the hydroxyl groups generated during cure react with the epoxy ring forming ether bonds. [9]

Referring to equation (2.2), the least hindered end of the epoxide is attacked by another nucleophilic nitrogen and another secondary alcohol is built as well as a tertiary amine which is no longer reactive without an active hydrogen. Subsequently, other epoxy groups attach to the other amine group of the diamine, connecting two epoxy chains and forming crosslinks. Diamines can form four bonds and quickly increase the molecular weight along the curing reaction. [9] The result of the epoxy-amine reaction is a three-dimensionally crosslinked network as shown in Figure 2.5.

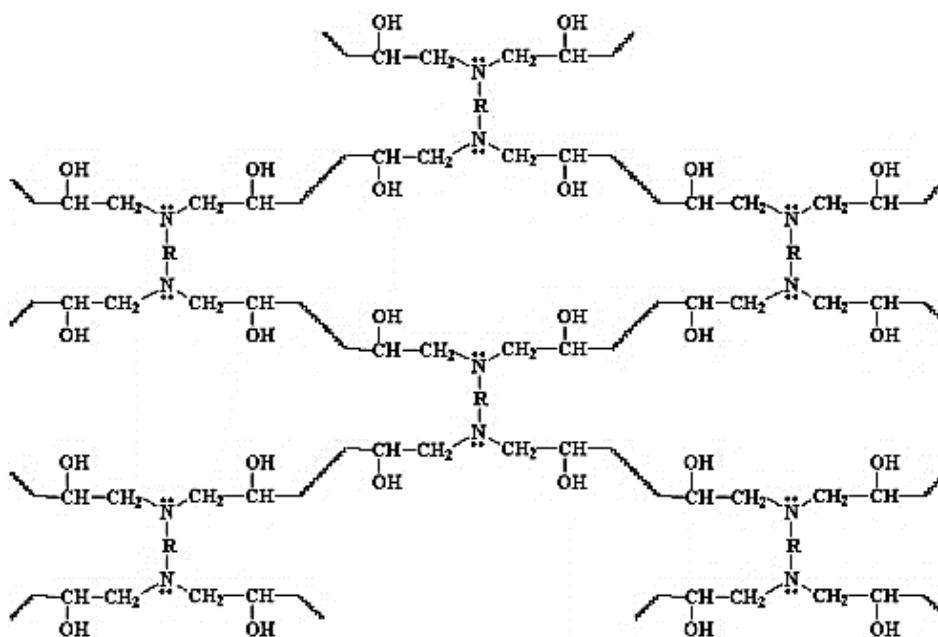


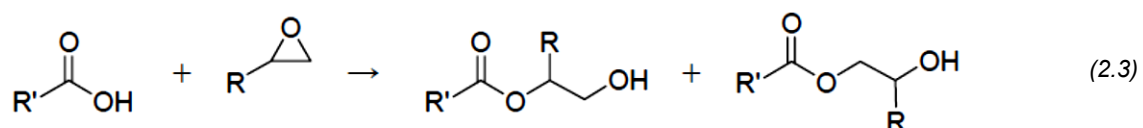
Figure 2.5: Schematic epoxy-amine network structure [10]

Besides amine curing agents there are other chemicals used which enable rapid cure times in the range of a few minutes. Furthermore, accelerators can be used to further decrease the cure time. [6, 11] These reactions exhibit very complex reaction mechanisms due to the variety of different possible reaction paths and intermediate species involved, which are furthermore dependent on the temperature profile applied. [12]

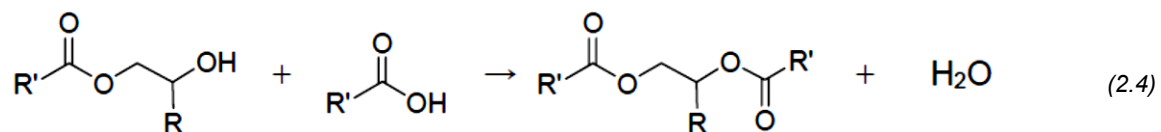
The reaction of aromatic amines can be catalyzed with BF_3 for example, but the epoxy product formed exhibits higher brittleness and slightly different material properties than without catalyst.

2.1.2.4 Curing Mechanism of Epoxy and Carboxylic Acid

The reaction of an epoxy group with a carboxyl group can occur without a catalyst. The uncatalyzed reaction usually leads to four reaction products. In the ring opening reaction (2.3) two reaction products are formed: the ester of the primary hydroxyl group and the ester of the secondary hydroxyl group.

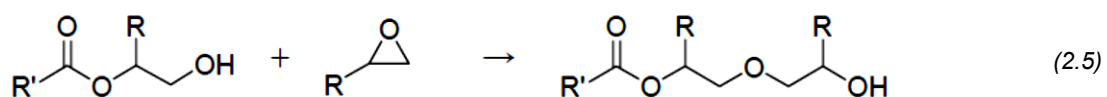


When temperatures are high enough, esterification (2.4) of the reaction product also takes place.

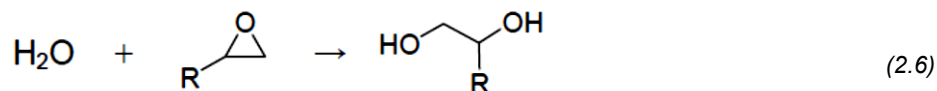


Fundamentals

An additional reaction which takes place is the reaction of the hydroxyl groups obtained from the ring opening reaction with epoxy groups leading to ether formation (2.5). The formation of the ether groups will occur only when an excess of epoxy groups is present.



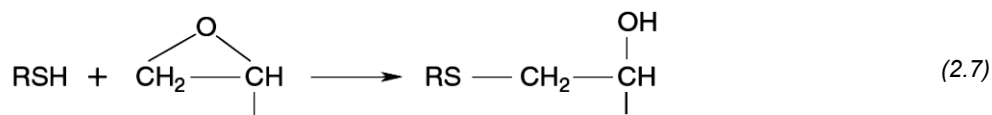
The water formed can lead to hydrolysis (2.6) of the epoxy group.



[13]

2.1.2.5 Curing Mechanism of Epoxy and Thiol

In the case of thiol reacting with epoxy, the $-SH$ group opens the ring in an addition reaction (2.7).



When the reactivity is too low, catalysis with primary and secondary amines is possible. [8]

2.1.3 Vitrimers

2.1.3.1 General Definition and Properties

A relatively new class of polymers was found by Ludwig Leibler and his co-workers, who introduced the term “vitriimer” for materials which combine the advantages of thermosets and thermoplastics. [14] Vitrimers are organic polymers with a cross-linked network structure very similar to thermosets and are classified as covalent adaptive networks (CANs) of associative nature (see Figure 2.6), which means that they do not depolymerize upon heating. Thus, vitrimers have a constant cross-link density and exhibit no loss of network integrity. [15] A specific chemical reaction or bond (incorporated) in the network is responsible for the dynamic behavior. Classical production and processing methods of thermoplastic and thermosetting materials are applicable.

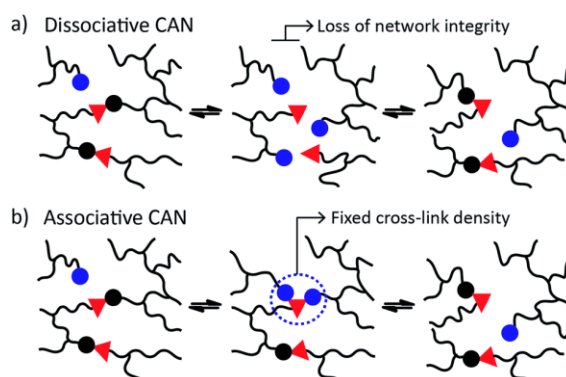


Figure 2.6: Schematic representation of associative and dissociative CANs [15]

As described in the previous chapters 2.1.1 and 2.1.2, thermoplastic polymers consist of molecular chains held together by weak physical interactions and therefore can be molten. Thermoplastics are of dissociative nature and their viscosity drop is described by the Williams-Landel-Ferry model. [16] Raising the temperature leads to a significant decrease of viscosity. Thermosetting polymers exhibit a covalent network structure. They are not fusible but degrade at high temperatures.

Vitrimers exhibit special viscoelastic properties. By increasing the temperature, the dynamic exchange reactions are accelerated to the extent that the material can macroscopically flow like viscoelastic fluids. The dynamic bonds incorporated in the network structure of vitrimers lead to

Fundamentals

formability. At low temperatures, the exchange reactions are immeasurably slow (frozen) and the material behaves like standard thermosets.

All organic compounds including polymers are fragile glass-formers. Inorganic materials like silica are usually strong glass formers and organic as well as polymer liquids are fragile glass formers. In contrast, vitrimers are strong organic glass formers and show Arrhenius-like gradual viscosity change. [14] In general, the broadness of the glass transition gives a measure for the rate of viscosity change. [15]

The viscoelastic behavior of vitrimers is described by two transition temperatures. T_g is the classical glass transition temperature between the glassy and rubbery state of the polymer where long-range coordinated molecular motion begins. At temperatures above T_g , the irreversible/static network of the polymer has enough energy to overcome the rotation barriers of the covalent bonds to allow the reversible parts of the network to exchange and segmental molecular motion is possible. T_g depends on the cross-link density and on the intrinsic rigidity of the monomers. [15]

T_v is the topology freezing temperature and derives from reversible exchange reactions. At T_v , the transition of the material behavior occurs when the timescale of dynamic exchange reaction in the network is faster than the deformation of the material. Then, the material is able to rearrange its topology, which results in softening or macroscopic flow. [17] T_v depends on the exchange reaction kinetics and the density of exchangeable bonds.

Figure 2.7 shows the temperature-dependent viscosity change of elastomer and thermoset vitrimers.

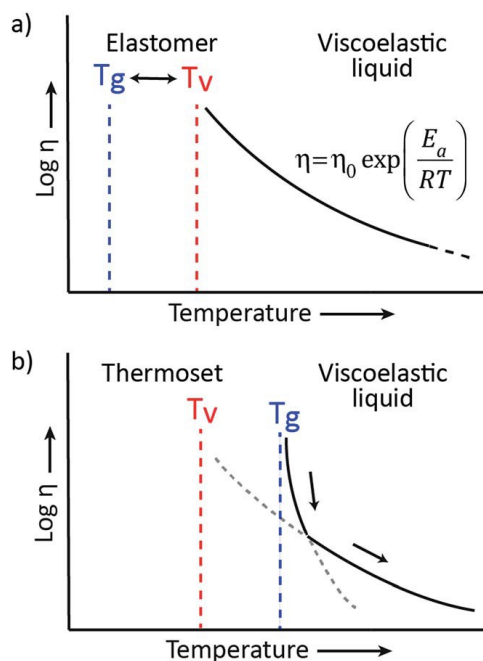


Figure 2.7: Representation of viscosity change of a) elastomer and b) thermoset vitrimers [15]

Below T_g , network-rearrangement kinetics are diffusion-controlled, and network topology rearrangements are dominated by segmental motion. The material shows Williams-Landel-Ferry behavior. Above T_g , exchange kinetics change from diffusion controlled to exchange reaction controlled following the Arrhenius law. [15]

Vitrimers are mainly investigated for their “self-healing”, “malleability” and “recycling” potential. In this context, fusibility is meant less in the actual physical sense than the softening of the material. Under the influence of temperature, vitrimers soften and can be reshaped. There are vitrimers that are capable of self-healing and those that can be repaired, which normally requires an external force and heat.

Three strategies exist for self-healing materials. Encapsulation of a healing agent (e.g., microcapsules) is called extrinsic self-healing. The disadvantage is that healing is only possible one time. Another strategy to obtain a self-healing polymeric material is blending of immiscible thermoplastic and thermosetting polymers. When the polymer is damaged, upon heating, the thermoplastic component flows into the damaged areas of the thermoset component and restores mechanical properties. [18] In contrast, intrinsic self-healing means that specific reversible chemical bonds reform to heal the material. Its advantage is the possibility of multiple healing

Fundamentals

steps. Reversible behavior of polymers can either result from covalent (chemical bonds, e.g., disulfides) or non-covalent (supramolecular/physical interactions, e.g., hydrogen bonds) exchange mechanisms. For the latter one, mechanical performance and media resistivity is worse. Reverlink™ from Arkema, for example, is a combination of chemical and physical cross-links. Its reversibility is of supramolecular nature and results from *H*-bond exchange. [19]

Recycling potential means if and how much of the input material can be recovered and in what quality; whether it is possible to recover the monomers or resin and harder and, in the case of FRP, whether the fibers remain in good quality when resin and fibers are separated by a recycling process. The severity of the recycling conditions and the temperature and time necessary also play a role in the assessment of the recycling potential.

2.1.3.2 Variety of Dynamic Polymer Chemistry

Regarding the chemistry of vitrimers, a huge variety of different polymer materials (epoxy-amine, epoxy-anhydride, polyurethane, polyimine, etc.) and of different functional groups and chemical reactions responsible for the dynamic exchange reactions (disulfide exchange, transesterification, Diels-Alder reaction, etc.) exists. In the following, an overview of recent research is given, subdivided according to the nature of the dynamic exchange reaction. Vitrimer functionalities were recently reviewed by Zou and by Denissen. [15, 20]

Transesterification

Leibler and co-workers showed the vitrimer behavior by the example of epoxy-anhydride thermosets which show reversible transesterification reaction [14]. Transesterification vitrimers can be tuned by catalysts and are frequently reported in literature with different polymer materials. [21–26] Transesterification is applied not only to neat resin materials but already to fiber composite materials. [27]

Diels-Alder Reaction

Another type of vitrimer material is based on the Diels-alder reaction. [28–31] In contrast to transesterification, Diels-alder functionality is dissociative in nature. The reaction takes place between a dien and dienophile. Due to the decrease of cross-link density by heat treatment, the viscosity drop is more abrupt. This concept is also proven in fiber reinforced composites [32] and commercially available as prepreg material from Evonik Industries.

Transimination

Transimination offers another route to obtain vitrimer behavior with thermosets. Polyimine (imine bond: $C = N$) networks can undergo covalent imine exchange reactions in the absence of any catalyst. As a result, polyimines are malleable, repairable and recyclable. Taynton et al. prepared and tested such networks with T_g values ranging from 18 to 146 °C [33] and demonstrated the advantageous use of polyimine as matrix material in fiber reinforced composites as well [34]. Polyimine vitrimers are commercially available from Mallinda [35].

Transamination

Vinylogous urethanes are also able to undergo stress relaxation and network rearrangement. Via transamination, they present another example of dynamic covalent polymers. Reversible urea bonds are responsible for catalyst-free transamination reactivity. [36–38]

Disulfide Exchange

The concept of dynamic disulfide exchange is intensively studied and reported in literature. [39] Disulfide exchange is an associative vitrimer mechanism. Disulfide containing polymers were investigated as neat resin material as well as matrix for fiber reinforced composites [1, 40]. Thus, disulfide groups were incorporated in for example epoxies [41] or polyurethanes [42–44]. With disulfide vitrimers, very high T_g values of 187 °C are achievable [45].

The resin materials investigated in the framework of this study are epoxy polymers and contain dynamic disulfide bonds which enable the material to perform dynamic exchange reactions. Besides temperature as a stimulus, UV radiation can be used to cleave the disulfide bonds, and the presence of a catalyst can enhance this process.

Dynamic covalent disulfide bonds combine robustness and reversibility of the material. Structural rigidity (mechanical performance and chemical stability), formability, good processability and facile degradability are the main advantages of vitrimers. Thus, they have the potential for new applications, closed loop life cycles and therefore more sustainability.

The variety of vitrimer materials is nearly unlimited. Furthermore, vitrimer properties are also feasible with selenium chemistry [46], metal ligand-interactions [39], and several other functionalities as well. There is always a tradeoff between a high T_g , mechanical performance and media resistivity as well as low healing temperature. If a high elastic modulus is desired, it is

usually accompanied by a high T_g and thus by a high healing temperature. The healing temperature and elastic modulus of different self-healing materials is plotted in Figure 2.8. [40]

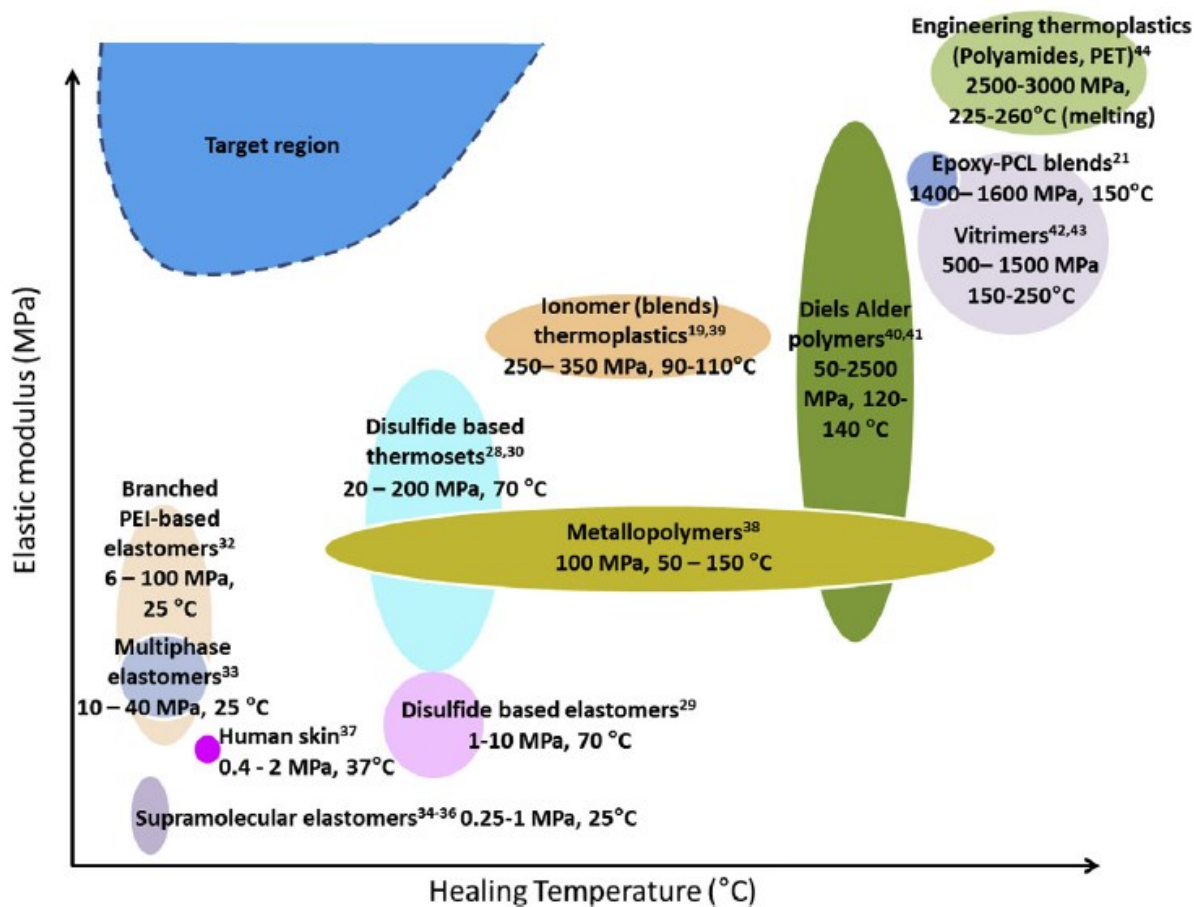


Figure 2.8: Overview of elastic modulus versus healing temperature of a wide range of intrinsic self-healing polymer matrices developed in the past decade [40]

Other new types of associative exchangeable chemistries are listed by Zhou [47].

2.1.3.3 Disulfide Exchange Mechanism

Sulfur chemistry is very versatile. [48] Disulfides are promising candidates for self-healing materials. [49] Many authors proposed a [2+2] metathesis reaction mechanism for disulfide exchange. [50–53] In this case, break and formation of two $S-S$ bonds would occur simultaneously. In 2016, Matxain et al. theoretically studied the reaction mechanism of disulfide

exchange. The $S - S$ bond strength strongly depends on the molecular structure. Another crucial factor for the exchange reaction to take place is hydrogen bonding between molecular chains to favor the contact among disulfides. The bonding energies of the disulfides and the hydrogen bonding are in the same order of magnitude. [49] Further studies about this reaction mechanism can be found in literature. [43, 53, 54]

Matxain analyzed the reaction barriers, $S - S$ bond lengths and angles as well as the transition states of disulfide exchange. He found no computational evidence for the existence of the [2+2] metathesis. Instead, it can be assumed that a [2+1] radical reaction mechanism takes place, which is schematically shown in Figure 2.9. [49]

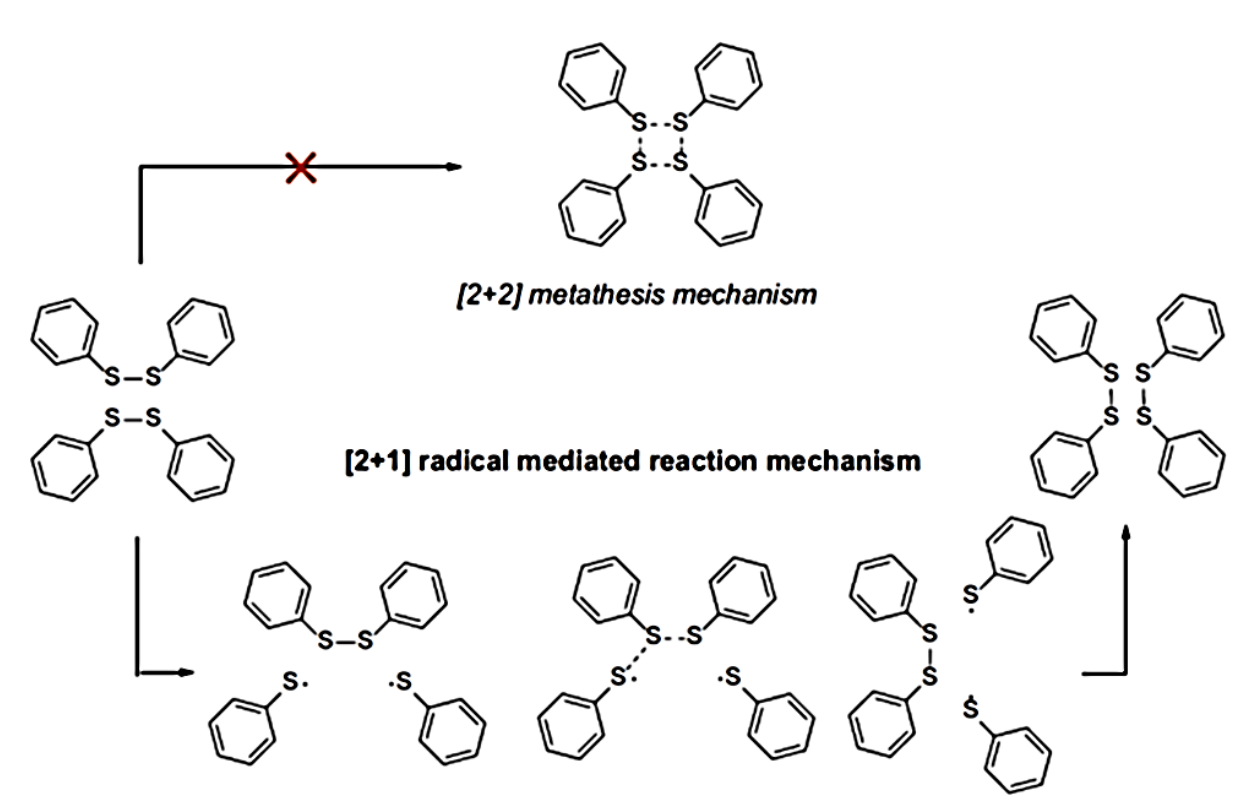


Figure 2.9: [2+1] Radical mediated disulfide exchange mechanism [55]

Fundamentals

In this case, homolytical cleavage of a disulfide bond leads to the formation of two sulfur-centered radicals that attack another $S - S$ bond through a three-membered transition state, producing new radicals, in a single displacement reaction, and finally another $S - S$ bond. [49]

Influence of Molecular Structure

Whereas the bond dissociation energy (BDE) strongly depends on the molecular structure of the disulfide compound, the reaction barrier (activation energy) for disulfide exchange is around 10 kcal mol^{-1} regardless of the substituent used. Drawing from all the results of Matxain, it was concluded that radical formation and H -bonding prevail over kinetics.

The electronic conditions as well as the substituents improve or worsen the efficiency of disulfide exchange. Depending on whether the substituents have an electron donating or electron withdrawing effect on the disulfides, the exchange reaction is either activated or deactivated. Furthermore, the electron density in the phenyl ring (Ph) is important. Atoms with a positive inductive effect (+I) are favorable as well. For weakening the $S - S$ bond (low BDE), key factors are delocalization and conjugation. The presence of double bonds, lone electron pairs and phenyl rings favors an extended delocalization. A low BDE correlates with high distance between the sulfur atoms ($S - S$ bond length), low bond order (BO) and low spin density (ρ) on the sulfur atom, which all favors the disulfide exchange reaction. [49]

In general, aryl substituted (aromatic) disulfides have a lower BDE to generate free radicals than their alkyl (aliphatic) counterparts and their sulfenyl radicals are more stable. [56] A very promising candidate for effective disulfide exchange is the aryl substituted disulfide with $-NH_2$ substituents in para position. Furthermore, there are two alkyl substituted molecules, thiuram and dendralene, which are suitable as well. Dendralene even has a lower BDE than 4-Aminophenyl disulfide (APhD). Thiuram has a BDE similar to unsubstituted Diphenyl disulfide (DPDS). Table 2.1 shows characterizing values for the disulfide bond of the four compounds mentioned above. [49] Further values and information can be found in the specified source.

Table 2.1: Calculated values of various disulfide bonds [49]

	Bond dissociation energy	Spin density	Bond order	Excitation energy	Average S-S bond length
symbol	BDE	ρ	BO(σ_{SS})	λ	r_{S-S}^{ave}
unit	Kcal mol ⁻¹	1	1	nm	Å
PhS-SPh	48.00	0.809	0.979	319.9	2.09
NH₂PhS-SPhNH₂	41.28	0.726	0.946	320.5	2.13
Dendralene	38.74	0.642	0.965	295.6	2.12
Thiuram	48.94	0.52	0.968	474.5	2.12

Stimuli

Depending on the properties or quality of the disulfide bond and the material itself, different stimuli (temperature, UV radiation) can be used to trigger the exchange reaction. Furthermore, the presence of a catalyst (e.g., tertiary amines, phosphines) can be used as well to promote the reaction. [50, 57]

Other

Disulfide exchange is an isodesmic reaction, which by definition has no reaction enthalpy and thus is not measurable by DSC. [21] The presence of sulfenyl radicals is also responsible for a mechanochromic effect in epoxy materials containing aromatic disulfides. This phenomenon enables visual detection of material damages. [55]

Disulfide Exchange Mechanism in Literature

There are several studies reported in literature where disulfide containing materials show reparability. To demonstrate this capability of the material, de Luzuriaga et al. successfully stacked several thin cured vitrimer CFRP sheets onto each other and hot-pressed them again to obtain one multilayered CFRP sheet. In their study, APhD was used as hardener material for epoxy monomers. Furthermore, already tested and thus delaminated ILSS samples of vitrimer CFRP were fully repaired by hot-pressing them at 200 °C and 100 bar for 5 minutes. Comparing the strength values of pristine and repaired specimens, the successful recovery of the material was proven. In another experiment, they ground fully cured specimens and hot-pressed them to sheets again. [1]

Lei et al. demonstrated the self-healing ability of cross-linked (aliphatic) disulfide polymers (prepared with EPS25) at room temperature under alkaline conditions (Diazabicycloundecene (DBU)) and the presence of Tributylphosphine (TBP) as catalyst. Firstly, a polymer sample was fractured into two pieces. The tensile strength restored after 24 h of healing at room temperature with a healing efficiency of 91%. Without TBP, only 13% healing efficiency was observed, which resulted from dangling chains and hydrogen bonding. Control samples without disulfide bonds did not show any healing effect.

Raising the temperature to 60 °C significantly accelerated the disulfide exchange, which resulted in healing times of only 2 h. To demonstrate multiple self-healing ability of the material, several healing cycles were performed. Insensitivity of the reaction to air was proven by separating the two pieces for a time before recombination. Furthermore, a cylindrical polymer specimen was compressed and successfully remolded at room temperature for 48 h to flat geometry. Chopped polymer was also compressed and successfully reshaped to flat geometry. When disulfide exchange and self-healing already occur at room temperature, the material shows significant creep as well. [57]

Lafont et al. investigated the restoration of cohesive and adhesive properties of disulfide containing rubbers. Self-healing ability is highly dependent on the density and mobility of the disulfide bonds present in the material. EPS25 (aliphatic) and EPS70 (partially aromatic) was used as disulfide containing epoxy prepolymers. The T_g values of the material ranged between -46 and -3.6 °C. The higher the difference between the healing temperature and the T_g value of the material, the shorter the recovery time. Cohesion was exponentially recovered as function of time.

EPS25 led to shorter healing times than EPS70, thus aromatic segments increase rigidity of the material, whereas enhanced molecular mobility favors healing. The higher the healing temperature, the shorter the healing time. Another factor which contributes to a good and fast healing is when the polymer chains with disulfide bonds are close enough to increase the probability of dynamic bond exchange. EPS70 led to higher adhesive strength than EPS25. [58]

Canadell et al. tested the influence of different disulfide concentrations on the self-healing properties of epoxy resin-based rubber where EPS25 was used as disulfide-containing prepolymer. The T_g of the material was about $-35\text{ }^\circ\text{C}$. The material was heated to $60\text{ }^\circ\text{C}$ for healing. Correlation between an increasing disulfide content and more efficient healing was found. The longer the healing times, the better the healing efficiency. As in all the afore mentioned papers, reproducibility of healing via disulfide exchange was proven by repetitive healing experiments. The material showed solubility in solvents which selectively break the disulfide bonds. At temperatures above $100\text{ }^\circ\text{C}$ a significant macroscopic flow of the material was observed. It is assumed that healing is better applicable for low T_g materials since the mobility of polymer chains for higher T_g materials is limited and impedes the interchange of disulfides. [59] Due to a large variety of disulfide containing monomers, many different cross-linked materials can be designed.

Takahashi et al. synthesized a new disulfide component in which the disulfide groups are incorporated in a diepoxide monomer. This component is bis(4-glycidyoxyphenyl)disulfide (BGPDS). In contrast to other studies, they recently tested the degradation behavior of disulfide containing epoxy thermosets via disulfide-exchange mechanism instead of thiol-disulfide exchange reaction. Therefore, diphenyl disulfide (DPDS) molecule was used as exchange partner.

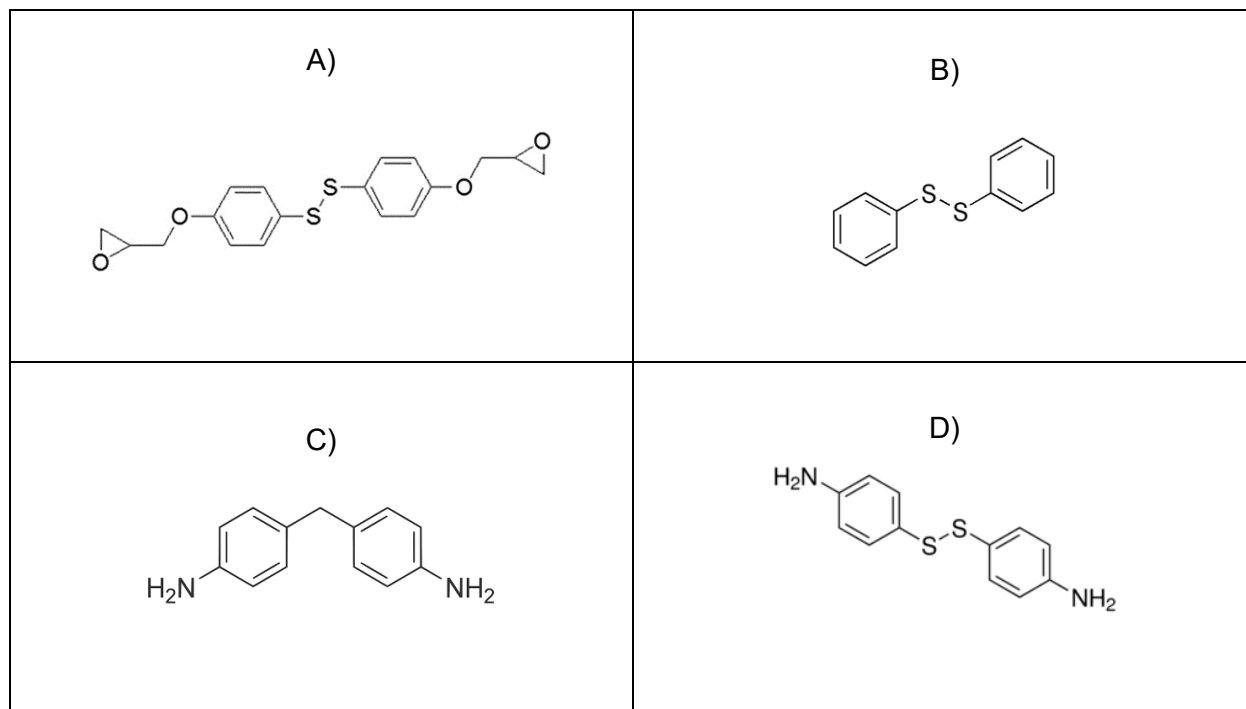


Figure 2.10: A) Disulfide-containing diepoxide BGPDS [60], B) Diphenyl disulfide (DPDS) [60], C) Methylene dianiline (MDA) [61], D) 4-Aminophenyl disulfide (APhD) [61]

Except for the disulfide bridge, BGPDS is similar to the standard DGEBA. Different combinations of static and dynamic diepoxides and diamines were tested (aromatic: DGEBA, BGPDS, APhD, MDA; aliphatic: Hexamethylenediamine HMDA). The structural formulas of BGPDS, DPDS, MDA and APhD are shown in Figure 2.10.

The aim was to improve degradability and achieve complete solubility of the resin by using BGPDS, to achieve a proper distribution and a higher number of disulfide bonds, and to fragment the polymer network into smaller pieces. The T_g values of the resins tested ranged from 120 to 180 °C. Table 2.2 shows the influence of the disulfide bond on the T_g and T_d .

Table 2.2: Comparison of similar diepoxides and diamines with and without a disulfide bond [60]

Diepoxide	Diamine	T _g (DSC) [°C]	T _d (TGA) [°C]
DGEBA	MDA	180	374
DGEBA	APhD	166	292
BGPDS	MDA	151	290
BGPDS	APhD	121	287

Incorporation of disulfide bonds does not significantly lower the tensile strength. Therefore, these disulfides containing thermosetting resins combine structural rigidity and facile degradability. By using BGPDS in combination with DTDA the disulfide bonds are present in the resin component as well as in the hardener component.

Two recycling procedures were tested at room temperature and at 100 °C:

- 1) Photo-induced degradation under N_2 and with DPDS
- 2) Degradation in the presence of DBU (base), DPDS and dioxane

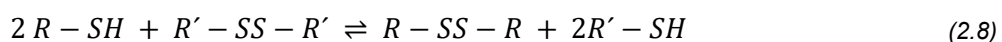
The degradation at room temperature was not sufficient. At elevated temperature, all resins containing BGPDS fully degraded within 60 minutes or less. Using only APhD as dynamic component the degradation efficiency was only 20%, the resin remained undissolved and only swelled. When APhD was used instead of MDA in combination with BGPDS, the degradation time was only slightly faster. With APhD and DGEBA larger fragments were obtained than with BGPDS and MDA. The smallest fragments were obtained when BGPDS and APhD were used.

A control sample without disulfide bonds was tested to confirm that the degradation behavior derives solely from the disulfide exchange reaction. Thus, diepoxides have two reactive sites and diamines have four reactive sites – each molecule, APhD and BGPDS, which each has one disulfide bond– the disulfide containing diepoxide led to 33% dynamic bonds and the disulfide containing diamine only led to 20% dynamic bonds in total. The main reason for insufficient degradation was the large fragment size and poor detachability from the network rather than the lack of swelling ability. [60]

2.1.3.4 Thiol-Disulfide Reaction

Reaction mechanism

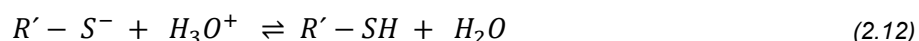
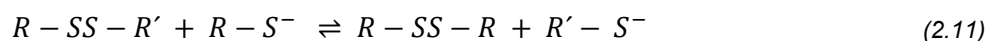
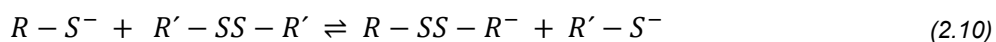
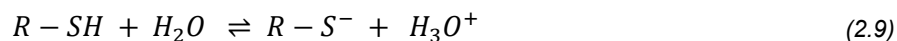
The thiol-disulfide reaction is utilized for the recycling of disulfide containing polymers. Disulfide bonds are cleaved by reducing agents with thiol-functionality. This exchange reaction occurs via a reversible S_N2 mechanism which is a nucleophilic substitution with second-order kinetics. The overall reaction (2.8) is [62]:



Fernandes and Ramos theoretically studied the reaction mechanism and determined the corresponding free energies, transition structures, charge densities and solvent effects. [63]

The key component is the deprotonated form of the thiol compound ($-SH$), the thiolate anion ($-S^-$), which is a stronger nucleophile than the thiol. Thus, the concentration of the thiolate anion is pH-dependent, raising the pH to alkaline conditions promotes the reaction kinetics [55].

The detailed mechanism (2.9-2.12) is:



The thiolate anion reacts with the disulfide bond via a nucleophilic attack and the disulfide bond is displaced by the thiolate anion. [62]

Reaction Conditions, Reagents and Solvents

There are several influencing factors for the thiol-disulfide exchange reaction described in literature. Between the pH of the solution and the thiol chemical a Brønsted correlation exists, which means that the acidity of the reducing agent influences the rate constant of the reaction. Furthermore, the solvent influences the reaction kinetics. In polar aprotic solvents (e.g., DMSO, DMF) the rate of thiol-disulfide exchange is 10^3 times faster than in polar protic solvents (e.g., water, methanol). [64] As already mentioned, it is also possible to use catalysts or radiation to promote the exchange reaction.

When the pH equals the pK_a of the thiol, the reaction rate is maximum. Commonly 2-Mercaptoethanol (2-ME) ($pK_a = 9,2$) or Dithiothreitol (DTT) ($pK_a = 9,6$) is used as a reducing agent for disulfide bonds. However, 2-ME is considered toxic and DTT is very costly. To achieve fast and complete reduction, a thiol compound with high reduction potential and high nucleophilicity is required. [65]

A further decisive factor for the recycling efficiency is the material itself and its interaction with the chemicals. [62, 65] The cross-linking density of the polymer influences the penetration of the chemicals into the network. [55, 60] Steric hindrance is a further reason why not all reducing agents work equally well with each material, causing the disulfides to remain inaccessible for the thiol groups. [64] A main parameter which thermodynamically influences the reaction is temperature. The possibility of oxidation of free thiol anions in air is a drawback of this reaction type.

Literature Review and Examples

The reaction of disulfides is experimentally investigated in proteins, hydrogels as well as elastomeric and thermosetting polymers. Recycling of disulfide containing polymers comprises solubilization and fragmentation of the polymer.

In 1990, Tesoro and Sastri performed an early study on the cleavage and reformation of disulfide bonds in epoxy polymers. Different curing agents containing disulfide bonds, inter alia APhD, were used. After grinding the polymer to powder to increase the surface area, the reduction reaction was carried out in a solution of diglyme, *HCl*, water and TBP (reducing agent) under N_2 at 60 and 100 °C. For complete solubilization the cross-linking density, which can be adjusted by the choice of resin and hardener component and by their stoichiometric ratio, is crucial. The

Fundamentals

reformation of disulfide bonds was carried out using an iodine solution (re-oxidation agent) in diglyme. [61] The T_g value measured by DMA with 5 K/min was 176 °C, but the evaluation criterion was not mentioned.

In 2015, Johnson et al. studied the effect of disulfide content, temperature and stoichiometric ratio on the degradation of disulfide-based epoxy thermosets in 100% 2-ME at room temperature and at 80 °C. Bisphenol-F diglycidyl ether (BFDGE) was combined with 4,4'-Methylenebis(cyclohexylamine) (PACM) and APhD. The curing agents PACM and APhD were mixed on-stoichiometrically (1:1, amine hydrogens to epoxy groups) and off-stoichiometrically (1.5:1, amine hydrogens to epoxy groups) in different ratios to each other (100:0, 75:25, 50:50, 25:75, 0:100). All on-stoichiometric polymer samples had T_g values above 130 °C and T_d values above 300 °C. The off-stoichiometric resins had T_g values above 100 °C. All T_g values were evaluated by the maximum of the tan delta peak of DMA measurement with 2 K/min heating rate.

There was no significant influence of incorporated disulfide bonds on the mechanical properties of the original polymer. After immersion in 2-ME the disulfide content correlated with the mechanical properties. 75% APhD was the threshold value for an adequate penetration of the thiol compound into the polymer. The specific thiol-based cleavage was proven by comparing the behavior of disulfide polymers in 2-ME to a reference solution without thiols. At room temperature, the tightly crosslinked polymer samples remain unaffected. Raising the temperature to 80 °C led to good degradation, whereas a reference polymer without disulfide bonds only swelled under same conditions.

Since the on-stoichiometric samples only ruptured into solid fragments and did not completely liquify, off-stoichiometric samples were prepared to lower the cross-linking density and ease the penetration of reducing agent into the network structure. The weight gain due to swelling was higher and the degradation was faster compared to on-stoichiometric samples. However, by loosening the network due to a greater distance between crosslinks, the T_g value decreased and the mechanical as well as chemical properties can be assumed to have deteriorated. In general, these disulfide-containing epoxies proved to be robust materials in extreme environments and at the same time capable of controlled degradation. [5]

De Luzuriaga et al. immersed a disulfide epoxy CFRP in different chemical agents at room temperature, but the material only dissolved in the thiol-containing 2-ME/DMF solution. [1]

Only a few studies were performed on the re-oxidation of reduced disulfide-containing polymers to regain the resin material. Sastri and Tesoro recovered the dissolved polymer by oxidation with iodine in diglyme. [66]

2.2 Carbon Fiber Reinforced Polymers (CFRP)

2.2.1 General Information

Carbon Fibers

Carbon fibers offer outstanding mechanical properties among fiber materials and simultaneously a low density. They exhibit extremely high strength and stiffness and a low elongation at break. Their diameter is between 5-10 μm . The organic carbon fiber exhibits anisotropic material behavior. The atomic structure consists of hexagonal graphene layers with only weak physical bonding via Van der Waals forces between the planes, which are responsible for the fiber's low transverse strength. Within the graphene layers strong covalent bonds result in high tensile strength and modulus of this fiber type. The production process includes the precursor production (mostly PAN), spinning to precursor fibers, the stabilization, carbonization and optionally graphitization process as well. The fibers produced in this way are then surface treated, sized and wound on spools. [67]

Fiber Reinforced Polymers

Fiber reinforced polymers (FRP) are a subcategory of composite materials. They consist of a fiber reinforcement – in this case continuous carbon fibers – and an embedding polymer matrix. The matrix transfers the loads to the fibers via the interphase (adhesion) between them. Furthermore, the tasks of the matrix component are to fix the fibers in the desired geometry, to support the fibers under compression loading to avoid kinking and to protect them against environmental influences.

There are four paradoxes which explain the superior mechanical properties of fiber reinforced composites. The first paradox states that the experimental strength of a solid material is lower than its theoretical strength. For plastic materials this applies also to their modulus. The second paradox states that a material in fiber form has a significant higher tensile strength than the same material in bulk form. Furthermore, the thinner the fiber, the higher the strength. The third paradox states that the lower the clamping length, the higher the measured strength of a single fiber

filament, because the probability of defects and their effects is lower. Due to uniform embedding of fibers in matrix, the effective clamping length is approximately zero. The fourth paradox of composite materials states that the composite can absorb stresses which would break the weaker individual component. The stronger component can use a higher share of its theoretical strength when loaded in the composite as if it was loaded alone. [68]

The mechanical performance of FRP depends on the fiber type and length, the matrix material (thermoplastic, thermosetting or elastomer polymers) used, the orientation of fibers, the production process and the fiber volume content. With FRP composites, a wide range of material properties and versatile design possibilities are feasible. The requirements of the resin material strongly depend on the desired application. The distinct advantages of continuous FRP, especially CFRP, are their high specific strength and modulus, their lightweight potential, good corrosion resistance and low thermal expansion. Due to their anisotropy along the preferential direction, they enable load adapted design and weight savings. The disadvantages in general are high costs, long cycle times, low automatization of manufacturing processes and low recyclability.

Within the framework of this study only thermosetting pre-impregnated fabrics (prepregs) are used for manufacturing FRP and FML samples. The production route of prepreg material is as follows: The resin components are mixed and heated to achieve a reasonable viscosity for fiber impregnation. The resin is rolled as a film onto a release paper. The fibers are unwound from spools, spread to the desired prepreg width and rolled onto the resin film. Both materials together are wound up on a roll, which then must be stored refrigerated to avoid unwanted chemical reaction between resin and hardener.

2.2.2 Mechanical Parameters and Transversal Isotropy

A key parameter of CFRP is the fiber volume fraction which significantly influences the material properties. Due to the nature of CFRP, its properties are highly directional. The Poisson ratio describes the expansion or contraction of a material perpendicular to the direction of loading. One parameter can be calculated for isotropic material (e.g., neat resin) and two for transversely isotropic material (e.g., unidirectional FRP). The Poisson ratio ν_{ij} (2.13) is related to the contraction in j -direction when an extension in i -direction is applied.

$$\nu_{ij} = -\frac{\varepsilon_j}{\varepsilon_i} \quad (2.13)$$

For transversely isotropic material, the plane of symmetry reduces the number of constants (2.14):

$$E_{\perp} = E_2 = E_3, \quad G_{\parallel\perp} = G_{13} = G_{12}, \quad \nu_{\parallel\perp} = \nu_{13} = \nu_{12} \quad (2.14)$$

The following equations (2.15-2.17) are valid for transversely isotropic material:

$$\nu_{\parallel\perp} = -\frac{\varepsilon_{\perp}}{\varepsilon_{\parallel}} \quad (2.15)$$

$$\frac{E_{\parallel}}{\nu_{\parallel\perp}} = \frac{E_{\perp}}{\nu_{\perp\parallel}}, \quad \nu_{\parallel\perp} = \nu_{\perp\parallel} \quad (2.16)$$

$$G_{\perp\perp} = \frac{E_{\perp}}{2(1 + \nu_{\perp\perp})} \quad (2.17)$$

This means that five independent constants exist for transversely isotropic materials: E_{\parallel} , E_{\perp} , $G_{\parallel\perp}$, $\nu_{\parallel\perp}$ and $\nu_{\perp\perp}$.

2.3 Fiber Metal Laminates (FMLs)

Fiber metal laminates (FMLs) are hybrid composites consisting of alternating metal and FRP layers as shown in Figure 2.11 and combine the advantages of both.

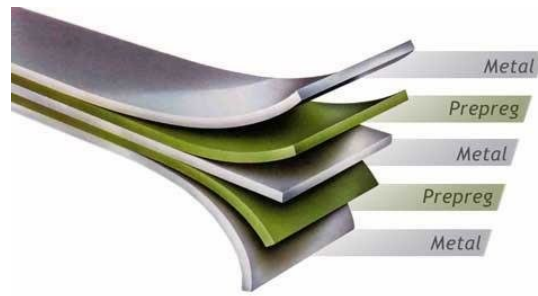


Figure 2.11: Layer structure of FML [69]

FMLs offer a great possibility of variation and thus can be tailor-made for several requirements and applications. There are three basic ways to influence the material properties: by selecting the component materials (fiber type, kind of metal, matrix polymer), by choosing a layer structure (order, thickness and number of layers [70, 71], fiber orientation, interlayers) and by modifying the interface (adhesion promoter, surface treatment). Metal volume fraction and fiber volume fraction further characterize the laminate. [72] As interlayer for example elastomer layers [73] are used to balance differences in thermal expansion. Glas Fiber Reinforced Polymer (GFRP) layers for example are used to prevent corrosion in Carbon Reinforced Aluminum Laminates (CARALL).

A coding system is used to describe FML materials. For example: GLARE 4B-4/3-0.4 is a Glas Reinforced Epoxy (GLARE) laminate, constructed according to definition of Grade 4B. Four layers of metal and three layers of fiber are used. The thickness of each metal layer is 0.4 mm. [72]

FMLs have improved fatigue and impact properties as well as higher fracture toughness and corrosion resistance compared to monolithic aluminum material. Furthermore, FMLs exhibit lower weight than pure metal. [74] The metal layer acts as a diffusion barrier and reduces moisture absorbance. Figure 2.12 compares the fatigue life of monolithic aluminum and GLARE FMLs.

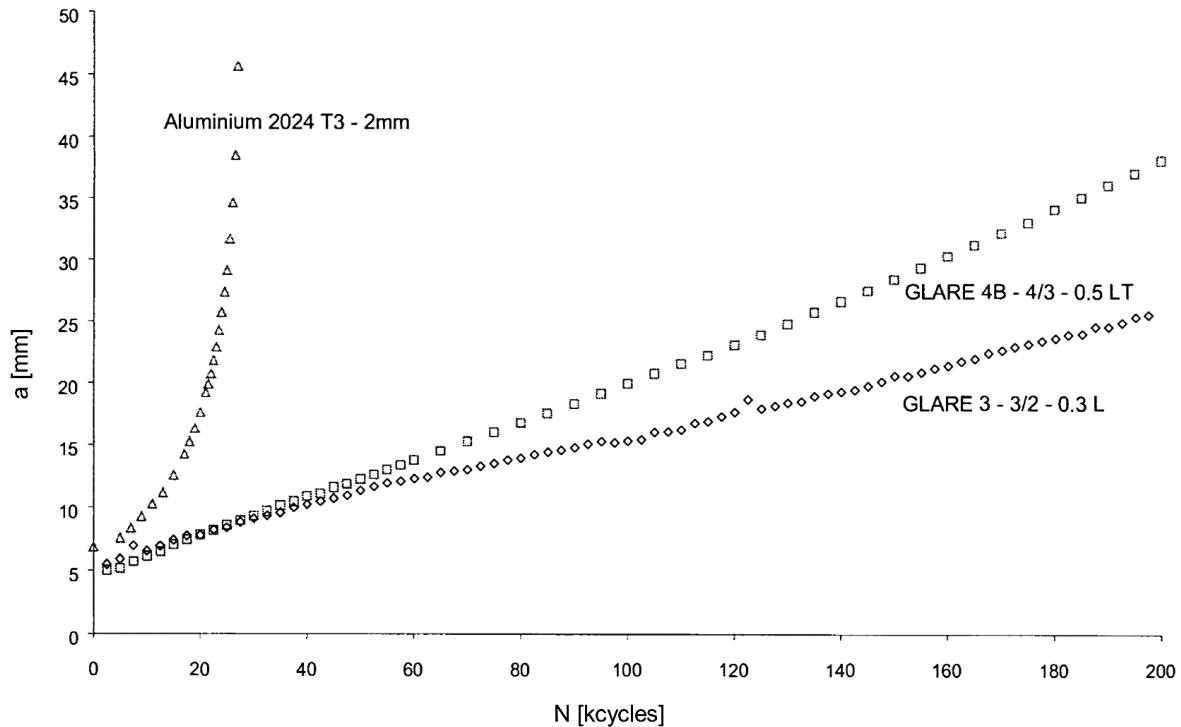


Figure 2.12: Crack growth curve of aluminum 2024-T3 and Glare FMLs for constant amplitude fatigue loading [72]

In contrast to pure CFRP, due to the metal fraction the failure behavior of FML is more ductile and FMLs exhibit less or no splintering compared to FRPs. Furthermore, the incorporation of metal leads to more isotropic properties of FML compared to FRP. The increased isotropy and ductility are responsible for improved blunt notch strength. Bearing strength and impact strength are increased as well.

The layered structure is responsible for the unique properties of FMLs. Due to the fiber bridging mechanism illustrated in Figure 2.13, crack propagation is significantly reduced. When a crack is initiated in the aluminum layer, load is transferred to the interface and to the fibers, which results in a balanced occurrence of delamination and fiber loading.

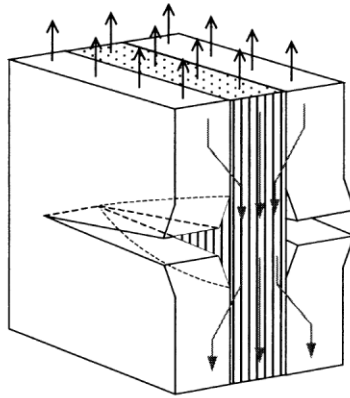


Figure 2.13: Delamination and fiber bridging in FMLs [72]

Therefore, crack propagation is stable, stress intensities at the crack tips are lowered and the crack propagation has a much higher share of the fatigue life of the material than the crack initiation period compared to monolithic aluminum. The failure of the material is more predictable. The stiffer the fiber, the more efficient the crack bridging mechanism, wherefore, because of their stiffness, carbon fibers are preferable. Improved resistance against crack growth leads to slower crack growth rates and thus longer maintenance intervals of aircraft structures, which reduces cost. [75]

As shown in Figure 2.14, the stress-strain curve of FMLs lies between pure metal and pure FRP material.

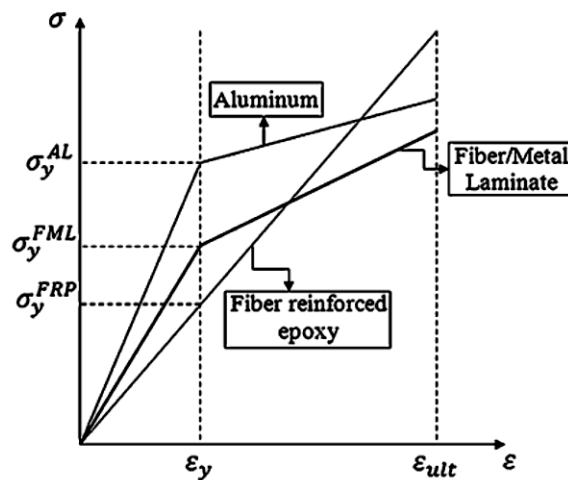


Figure 2.14: Schematic illustration of stress-strain curves of aluminum, FRP and FML [76]

Different components and interfaces are present in the FML material and therefore, failure behavior is complex. Several types of defects and damage can be distinguished. Figure 2.15 shows the order and interaction of damage occurrence in FML.

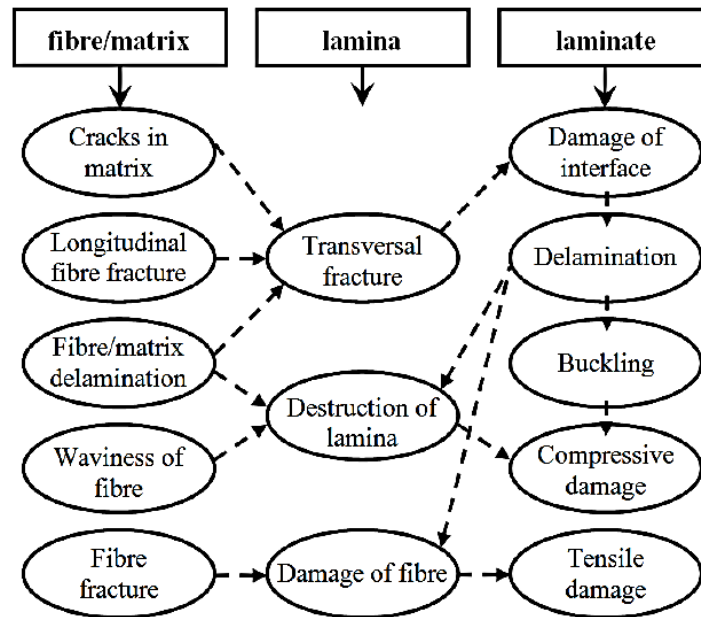


Figure 2.15: Types and levels of damage in FML [77]

As mentioned above, substitution of the fiber type is one approach to vary FML material properties. The first FML material was ARALL (aramid fiber reinforced aluminum). Aramid fibers were embedded in an epoxy matrix and combined with aluminum layers. [78]

Thus, ARALL has poor fatigue performance when cyclic compressive load is applied, and thus, glass fibers exhibit higher compressive stability, aramid fibers were replaced by glass fibers and GLARE was born. [79] Glass fibers also improve the impact and burn-through resistance of FML. Tensile strength of GLARE is higher than of ARALL. [75]

By again changing the fiber type of FML to carbon, a further improvement of material performance is possible. Carbon fibers have higher specific strength and stiffness than aramid and glass fibers.

Fundamentals

Elongation of break is limited. [80] With CARALL (carbon fiber reinforced aluminum) excellent crack growth characteristics are realized and especially stiffness is significantly increased. On the other hand, by using carbon fibers other issues than thermal stresses after curing resulting from different thermal expansion coefficients of carbon fibers and aluminum, as well as the risk of galvanic corrosion arises from the potential difference of carbon fibers and aluminum. [69, 81]

While ARALL and GLARE are standardized in different grades and are commercially available, there is a huge gap between the multitude of different FML materials presented and investigated in literature and the few actual applications. [75] For FML, the variety of design is almost without limit.

Another approach was to change the sort of metal constituent used for FML. For example, FML with stainless steel [82], titanium [83] and magnesium [84] are reported as alternatives to aluminum. Aluminum has the best specific mechanical properties and is beneficial in terms of cost. Magnesium has a low density but also a low hardness. Therefore, relatively thick layers need to be used which tend to less buckling or kinking. Titanium is highly stable against temperature, has low thermal expansion, is light but expensive and its surface treatment is difficult. Stainless steel significantly reduces corrosion issues, but adhesion to the FRP is worse than for aluminum and only thin layers can be used due to its high density. [75]

Challenges of FML material exist in physical nature (adhesion of layers, galvanic corrosion, thermal stresses due to mismatch of thermal expansion coefficients), relating to manufacturing process (cycle time, effort, flexibility) and life cycle (repair, processing, recycling). [72, 75]

Choosing either thermoplastic (e.g., PA6 [85], PEEK [86]) or thermosetting (e.g., epoxy) matrices further influence FML properties and manufacturing as well. In general, adhesion to metal is worse for thermoplastic matrices. Higher process temperatures are required which results in higher thermal stresses. Thermoplastic FMLs are formable and recyclable. Thermoplastics exhibit higher toughness, lower manufacturing cost and are repairable. [85, 87]

In general, thermosetting matrices exhibit higher stiffness and strength as well as a better temperature performance. They require lower process temperatures. The adhesion of thermoset matrix to metal is generally sufficient without extra surface treatment of the metal component. Cycle times vary depending on the resin system used. However, their brittleness is disadvantageous. Once cured, thermosetting FML is not formable, which is why it must be manufactured in the final geometry desired. [70]

2.4 Potential of Vitrimers for CFRP and FML

Using vitrimers for FRP and FML has several advantages. As previously mentioned in chapter 2.1.3, vitrimers are formable, processable and recyclable. Depending on the chemical composition used, below T_g vitrimers may exhibit the same advantages – mechanical performance, media resistivity and temperature stability – as thermosets. When vitrimers are used as matrix material in FRP, a classic prepreg process can be used. The advantages of prepregging over other FRP manufacturing processes such as RTM processes are a guaranteed and high achievable fiber volume fraction, consistent material properties, reliability (low void content) and easy lay-up process. [88] Furthermore, this means that already existing processes, molds and plants can be used, so no extra investment is required. And in addition, vitrimer resins eliminate drawbacks of standard thermosetting prepregs.

Thermosetting prepregs are partially cured (B-staged) and then refrigerated to prevent further curing or ageing of the material and to ensure processability of the material into cured parts. Vitrimer prepregs can be fully cured and thus, can be stored at room temperature. Therefore, with precured vitrimer prepregs, roll-to-roll processes are possible. Vitrimers also enable the reprocessing or recycling of scrap material and cured parts. As the recycling process is a simple dissolution process without damaging the fiber material, virgin-like fiber properties are maintained and no significant loss of mechanical performance was observed. [1] While thermosetting materials must be cured in the final geometry, thermoplastic materials can be produced as plate material and can be reversibly formed into the desired shape. For FML, vitrimers are favorable for the same reasons as for FRP material and because of their good adhesion to metal. Also, recycling of FML is greatly simplified since metal and vitrimer FRP layers can easily be separated by solely heating of the laminate sheets.

Recycling routes for thermoplastic polymers are relatively easy and well established. The material is melted and subsequently formed again. Likewise, it is the case for thermoplastic FRP. Carbon fiber recycling is of high importance because of the high cost and its consumption in great amounts. For thermosetting FRP, different recycling routes exist (mechanical, thermal, chemical recycling). With those state-of-the-art recycling methods several disadvantages arise. Mechanical fragmentation or milling usually has a high demand of energy and high cost. Furthermore, it results in significant downcycling of the material. This means that the fiber cannot be reincorporated in the same high-tech applications and the commercial value of the material is significantly decreased. Thermal recycling or pyrolysis lowers the mechanical properties compared to virgin

Fundamentals

carbon fibers. Chemical recycling requires harsh conditions which lead to harmful environmental impacts and damages the fibers. [89]

It is impossible to regain the matrix material of classical thermosetting FRP. For chemical recycling of thermosets and especially for the use of milder conditions, special thermosetting resins with low T_g and low media stability are required. Vitrimers offer the possibility to regain the matrix as well and might be a promising alternative to standard thermosets concerning recyclability. [90]

There are three state-of-the-art repair methods for FRP. The first method is patching of new material on the damaged area, where the damaged FRP is removed and replaced by metal plates or repairplies which are patched onto this area. Therefore, holes need to be drilled in the material which results in further mechanical damage and adds weight to the component. Another method is using adhesives and repair plies to repair damaged FRP structures. No drill holes are required. The damaged area is also removed, adhesion is improved by previous surface treatment and repair plies are applied onto the area. A disadvantage is that under field conditions clean surfaces are not easy to realize and intact fibers are also damaged and removed. A relatively novel approach is to encapsulate healing agents into the material, but which act as defects and thus, lower the mechanical properties. [89] So dynamic covalent bonds such as disulfides (vitrimers), may be a favorable alternative to previous repair strategies. [90]

In summary, there seems to be a trade-off between the T_g , the mechanical properties and media resistivity and therefore a limited applicability concerning load-bearing capacity and operating temperature on the one hand and the recyclability and reparability of the polymers as well as the recovery of undamaged carbon fiber on the other hand. The remarkable advantages of vitrimers are their preservation of material value (less downcycling), resource efficiency, sustainability and their potential for closed loop supply chains.

3 Methods

In the following chapter all methods of thermal analysis as well as mechanical testing that were performed to determine the material behavior and properties are described.

3.1 Thermal Analysis

For processing the samples with the vitrimer resin mixtures formulated, it is essential to have detailed knowledge about the reactivity of the raw materials and the thermal stability of the cured/manufactured material. Therefore, different methods of thermal analysis were used for characterization.

3.1.1 Differential Scanning Calorimetry (DSC)

For DSC measurements two pans with a sample and a reference are put in an oven and both subjected to a defined temperature program which can be either isothermal (constant T) or dynamic (constant heating rate). The temperature of the two pans is controlled by thermocouples. The measuring cell is usually flushed with nitrogen. While the temperature of both pans is kept the same, thermal effects from physical and chemical processes (phase transitions, chemical reactions) of the sample result in differences of the heat flow proportional to the temperature difference, which are measured and recorded as DSC signal. There are endothermic and exothermic effects to be distinguished which either release or consume heat. The change in enthalpy ΔH is obtained by integration of the heat flow peak/DSC signal. [91]

The most important effects within the scope of this study were the curing reaction of the resin, which can be observed as a significant exothermic peak in the DSC thermogram, as well as the endothermic glass transition step of the thermosetting polymers.

The instrument used was a DSC Q100 from TA Instruments. The measurements were evaluated according to ISO 11357-2 and ISO 11357-3 standards.

3.1.2 Thermogravimetric Analysis (TGA)

TGA is a method of thermal analysis where the mass change of a sample due to physical and chemical processes is measured by a thermobalance as function of time and temperature. The resulting thermogram gives information about the thermal stability and the maximum usage

Methods

temperatures of the sample. The typical heating rate the sample is subjected to is 10 K/min and the furnace is commonly flushed with N_2 or air/ O_2 . At the inflection points of the TGA signal its first derivative shows significant peaks which resemble characteristic temperatures for the sample tested where the mass loss rate is maximum. [92]

The instrument used was a Q500 from TA Instruments. The measurements were performed according to DIN EN ISO 11358-1.

3.1.3 Dynamic Mechanical Analysis (DMA)

3.1.3.1 Rheometry

DMA measurements of liquids are referred to as rheological measurements. Rheology describes the deformation behavior of solids and the flow behavior of liquids under shear. Rheometry refers to measurement methods to determine rheological properties of material as a function of time, temperature and frequency. The material is sinusoidally stressed in shear (excitation) and with a phase shift a shear deformation/strain (response) results. The measured quantities are the storage modulus (G') and the loss modulus (G'') which give information about the elastic and viscous properties of a material. G' represents the energy which is stored in the material and G'' is the amount of kinetic energy that is converted into heat dissipation or acoustic emission. The relation of those two quantities is defined as $\tan \delta$ (3.1). [3]

$$\tan \delta = \frac{G''}{G'} \quad (3.1)$$

The behavior of viscoelastic materials like polymers is intermediate between that of a Hooke's ideal elastic solid and an ideal viscous Newtonian fluid. For this study either isothermal temperature programs were used to evaluate the gel time of the fresh neat resin material (investigation of reactivity) or temperature ramps to measure the glass transition temperature T_g of the already cured resin material.

The G'/G'' modulus crossover method is commonly used to determine the gel-point where the molecular weight is maximum and only the density increases by further crosslinking. [93, 94] The glass transition temperature increases with increasing degree of cure until $T_{g,max}$ is reached or T_g exceeds the process temperature, then vitrification occurs (see also chapter 2.1.2.1).

The favored criterion to select T_g from rheometric measurements as an onset of the glass transition region is the peak in G'' which indicates the initial drop of G' where the material changes from the glassy state into the transition to a rubber-like state [95]. With this criterion used the upper use temperature to maintain the mechanical performance of the material is defined. It is also possible to determine T_g using the $\tan \delta$ peak, but it rather indicates the transition midpoint or inflection point of the decreasing $\log G'$ curve where the softening point has already been exceeded. [3]

The measurements were conducted using an oscillating plate-plate rheometer setup as shown in Figure 3.1 of the type AR 2000ex from TA Instruments. The frequency during the measurements was 1 Hz, the gap was 1000 μm and the plates size was 25 mm in diameter. The applicable standard was DIN EN 3291.

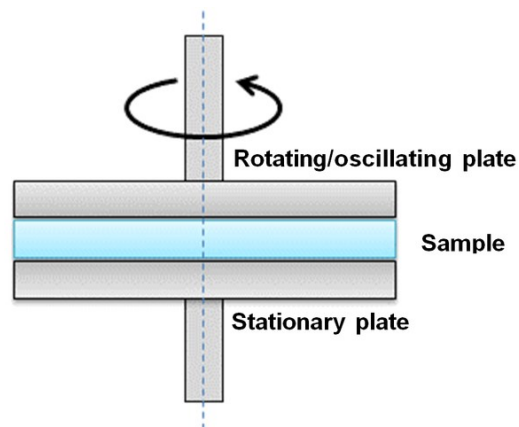


Figure 3.1: Oscillating plate-plate rheometer [96]

3.1.3.2 Single Cantilever DMA

DMA is a method of mechanical spectroscopy, which means the experimental determination of time, temperature and frequency dependent mechanical properties. DMA measurements are performed on plastics, CFRP and FML materials as well. Therefore, the single-cantilever mode was used to apply a sinusoidal stress to the sample. The instrument used was a Q800 DMA from TA Instruments and the applicable standard was DIN EN ISO 6721-1. The same principles as

mentioned above in section 3.1.3.1 are valid. The G' , G'' and $\tan \delta$ values were obtained as a function of time and temperature. [3]

3.2 Gel Permeation Chromatography (GPC)

GPC is a method to separate molecules (analytes) by their size, more precisely by their hydrodynamic volume. A microporous column is used as stationary phase. A solvent is used as mobile phase (eluent). Smaller molecules enter the pores and are retained wherefore their retention time is extended. As a result, larger molecules flow faster through the column.

Polymer standards (e.g., polystyrene) with a known and narrow distribution of molecular mass are used for calibration. The relative molecular mass measured is related to the calibration polymer. At this point it must be noted that the molecules of the calibration polymer are linear in contrast to other possible molecules under consideration which can be branched molecules as well.

After elution, the different weights of the molecules are monitored by detectors. RI and UV detectors indirectly measure the concentration by weight of the analytes. As a result of GPC, the distribution of the molecular mass is obtained as a chromatogram and the number average molecular weight M_n and the weight average molecular weight M_w can be calculated by the following formulas (3.2-3.4):

$$M_n = \frac{\sum w_i}{\sum w_i/M_i} \quad (3.2)$$

$$M_w = \frac{\sum w_i \times M_i}{\sum w_i} \quad (3.3)$$

$$D = \frac{M_w}{M_n} \quad (3.4)$$

For evaluation, the elugram is divided into i equidistant stripes and it is assumed that each stripe contains only macromolecules of a certain hydrodynamic volume or molar mass. M_i is the molecular weight and w_i is the mass fraction of the macromolecules in one stripe.

The polydispersity D describes the width of distribution. With GPC a polymer is characterized by means of the broadness and shape of its molecular mass distribution. [97] GPC was performed according to DIN EN 55672-1.

3.3 Quasi-Static Mechanical Tests

For quasi-static testing the specimen loading is relatively slow, shock-free and constantly rising until failure. [98]

3.3.1 Tensile Test

This test gives information about the brittleness or ductility respectively the fracture behavior of a material. It determines the mechanical properties tensile strength σ_t and Young's modulus E_t of the material. The sample is elongated at a constant rate of extension. The developing force F is monitored until a significant force drop is observed. The basic equations of mechanical testing in tension are the following (3.5-3.7):

$$\sigma_t = \frac{F}{A} \quad (3.5)$$

$$\varepsilon = \frac{\Delta l}{l_0} \quad (3.6)$$

$$E_t = \frac{\Delta\sigma_t}{\Delta\varepsilon} = \frac{\Delta\sigma_t}{0.0025 - 0.0005} \quad (3.7)$$

The elongation ε is the relation of the change in length Δl during testing and the initial length l_0 of the specimen. The tensile strength σ_t is defined as the force F related to the cross-sectional area A of the specimen. The tensile modulus E_t is the relation of the resulting stress to strain and is

Methods

the slope of the linear-elastic region of the stress-strain diagram. The strain range to determine the tensile modulus of elasticity is $0.05\% \leq \varepsilon \leq 0.25\%$. [98, 99] Tensile testing was performed according to DIN EN ISO 527 standard and a Zwick/Roell Z250 testing machine was used.

3.3.2 Compression Test

During compression testing the specimen is loaded in the opposite direction to tension testing and the compressive strength σ_{cM} and modulus E_c are obtained [99]. On an atomic level the molecules are forced together during compression testing in contrast to being forced apart during tensile testing. A Zwick universal testing machine was used. The applicable standard was DIN EN ISO 14126. The compression test procedure with shear loading as illustrated in Figure 3.2 was used.

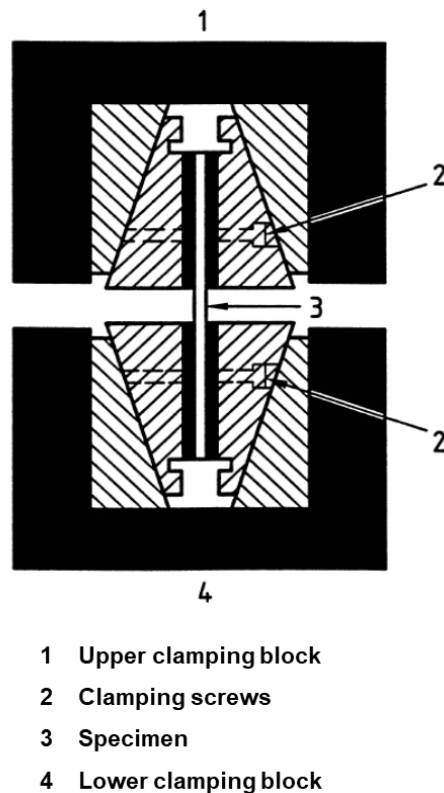


Figure 3.2: Compression test with shear loading [100]

The strain range for modulus evaluation is analogous to the tensile and bending test. The material properties were calculated by the following equations (3.8, 3.9):

$$\sigma_{cM} = \frac{F_{max}}{bh} \quad (3.8)$$

$$E_c = \frac{\sigma_c'' - \sigma_c'}{\varepsilon_{f2}'' - \varepsilon_{f2}'} = \frac{\Delta\sigma_c}{0.0025 - 0.005} \quad (3.9)$$

3.3.3 Bending Test

The flexural strength σ_f indicates the ability of the specimen to withstand bending forces applied perpendicular to their longitudinal axes. The normal stress is linearly distributed over the cross-section of the specimen. Due to the more appropriate force distribution this test is better suited for brittle materials than tension testing. [99]

The three-point bending test is used to determine the flexural properties of homogenous plastics; whereas for FRPs, which is a more heterogenous material due to small internal defects, the four-point bending test where two loading pins instead of one are used is preferred. Otherwise, the bending strength is overestimated due to lever arm effects. Both test setups are shown in Figure 3.3.

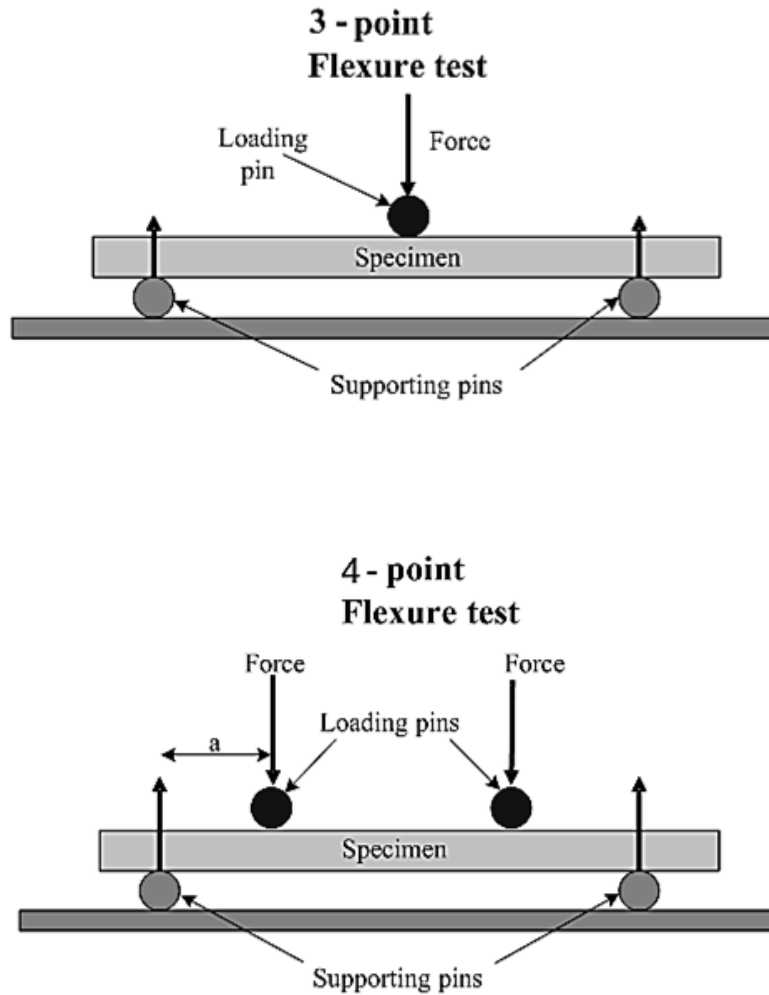


Figure 3.3: Schematic 3-point and 4-point setup for bending test [101]

Consequently, the material properties for three-point testing are calculated by the following equations (3.10, 3.11) according to the DIN EN ISO 178 standard:

$$\sigma_f = \frac{3FL}{2bh^2} \quad (3.10)$$

$$E_f = \frac{\sigma_{f2} - \sigma_{f1}}{\varepsilon_{f2} - \varepsilon_{f1}} = \frac{\Delta\sigma_f}{0.0025 - 0.0005} \quad (3.11)$$

The material properties for four-point testing are calculated by the following equations (3.12, 3.13) according to the DIN EN ISO 14125 standard:

$$\sigma_f = \frac{FL}{bh^2} \quad (3.12)$$

$$E_f = \frac{0,21E^3}{bh^3} \quad (3.13)$$

The occurring forces are a mix of compression loading on the upper side and tension loading on the bottom side of the specimen. In the middle of its thickness, there is a neutral plane which is stress and strain free. [98]

The advantage of the four-point over the three-point flexural test is the constant bending moment between the two loading pins and the absence of lateral forces. Therefore, this method is less sensitive to specimen and loading geometry as well as strain rate. Its results are more precise and reproducible as they exhibit lower dispersion, compared to the results of three-point bending test. [98] A Zwick 1474 testing machine was used.

3.3.4 Butt-Joint Test

In the butt-joint test, a geometry-dependent adhesive strength is tested. A round CFRP sample with a diameter of 30 mm is glued between two metal stamps. The sample preparation described in chapter 4.4.2 results in a defined round connecting area with a diameter of 20 mm. This procedure is intended to create a defined test area that is the same for all samples and to ensure that failure occurs within the sample itself and not between sample and metal stamp. The metal stamps are clamped in the testing machine and subjected to a continuously increasing load.

3.3.5 Shear Tests

3.3.5.1 Apparent Interlaminar Shear Strength (ILSS) Test

The apparent interlaminar shear strength τ_{ILSS} (3.14) is determined by the short beam shear test and calculated according to DIN EN ISO 14130 standard:

$$\tau_{ILSS} = \frac{3F}{4bh} \quad (3.14)$$

This test is similar to the three-point bending test, but a smaller span to thickness ratio is used to increase the shear stress over the bending stress inside the test specimen to promote interlaminar shear failure. [102] The shear stress distribution is shown Figure 3.4.

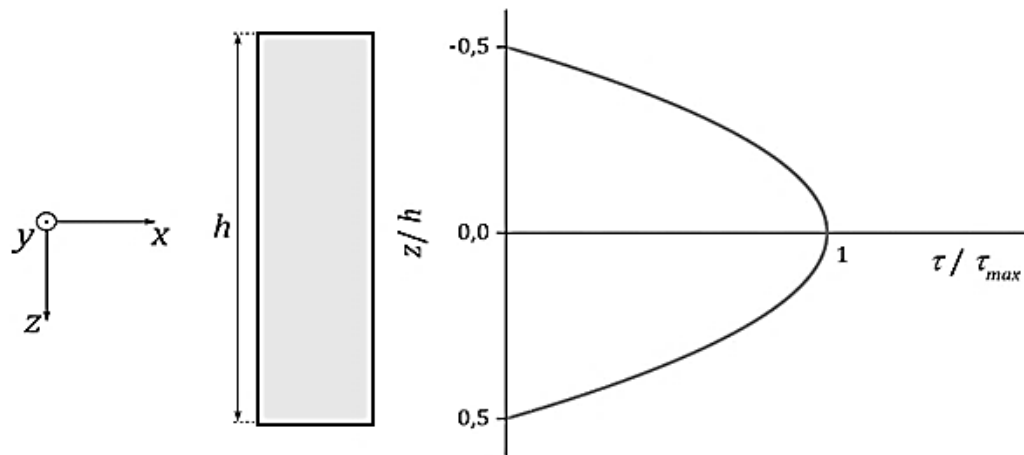


Figure 3.4: Schematic ILS stress distribution [103]

A Zwick/Roell Z250 testing machine was used. The data obtained is not suitable for determining design parameters, but it can be used for screening materials or for quality control. With various test samples there is also a variation on the failure mode.

3.3.5.2 Tensile Test of $\pm 45^\circ$ Laminates

The $\pm 45^\circ$ tensile test method on cross-ply $[0^\circ/90^\circ]$ CFRP material is a pseudo-shear test. The in-plane shear stress/shear strain response including the in-plane shear modulus and strength is determined, which is mainly influenced by the matrix properties and the fiber matrix adhesion. An uniaxial tension loading results in biaxial stress states in each $+45^\circ$ and -45° layer. [98] Therefore, a strip-shaped sample with a rectangular cross-section is loaded in tension in $\pm 45^\circ$ orientation to fiber direction. The test is finished when the ultimate failure occurred. Otherwise, it is stopped at

a shear deformation of $\gamma_{12} = 0.05$. The shear strength $\tau_{12 M}$ and the shear modulus G_{12} are calculated according to the equations (3.15-3.17) in the DIN EN ISO 14129 standard:

$$\tau_{12 M} = \frac{F_m}{2bh} \quad (3.15)$$

$$G_{12} = \frac{\tau''_{12} - \tau'_{12}}{\gamma''_{12} - \gamma'_{12}} = \frac{\tau''_{12} - \tau'_{12}}{0.005 - 0.001} \quad (3.16)$$

$$\gamma_{12} = \varepsilon_{11} - \varepsilon_{12} \quad (3.17)$$

This test configuration does not produce pure shear stress state and is therefore only an approximation to the real shear properties. It is useable to determine the shear modulus but not the shear strength. F_m is the maximum force or force at failure. A Zwick Z250 testing machine was used.

3.3.5.3 V-Notched Rail Shear Test

As a real shear test the V-notched Rail Shear Test according to the ASTM D7078 was chosen, which allows for consistent in-plane shear testing. This test determines the shear properties of fiber-reinforced composite materials, the maximum shear strength and the shear elastic modulus by face loading a V-notched specimen without holes between two pairs of loading rails. Tensile loads at $\pm 45^\circ$ are induced using the following test setup illustrated in Figure 3.5:

Methods

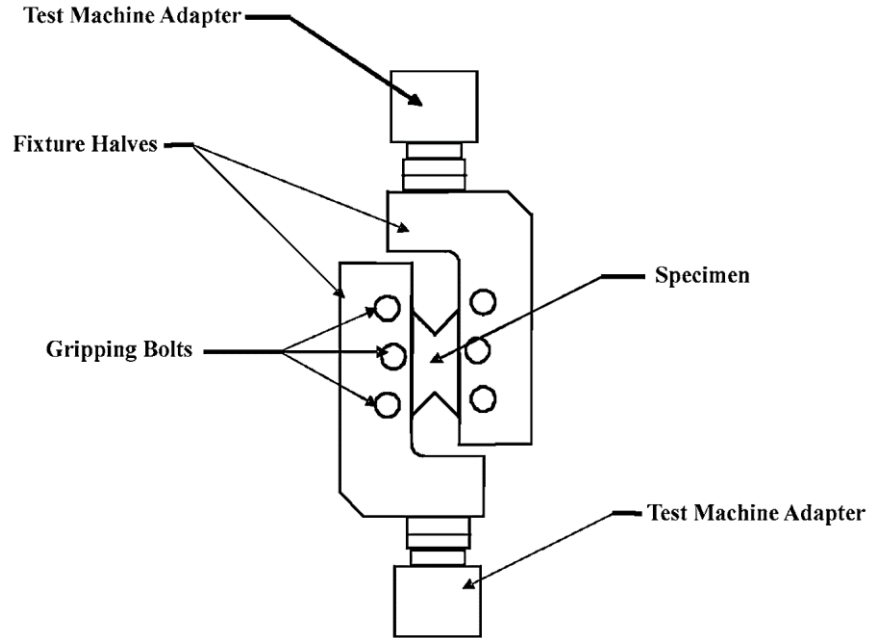


Figure 3.5: V-notched rail shear test setup [104]

Its advantages compared to the losipescu shear test are the larger gage section and the face loading instead of the force application through the top and the bottom edges of the specimen. The specimen size is larger than for the losipescu shear test. The V-notches increase the gage section shear stresses in relation to the shear stresses near the grips. Therefore, the failure more likely occurs within the gage section and a more uniform shear stress distribution is generated. From the notches a local stress concentration results during deformation, which finally causes the failure of the specimen. As testing machine, a Zwick Kappa 050DS was used. The shear stress τ_i is calculated using the following formula (3.8):

$$\tau_i = P_i/A \quad (3.18)$$

Where:

τ_i = shear stress at i th data point [MPa]

P_i = force at i th data point [N]

A = shear cross-sectional area between the notch ends [mm²]

For measuring the shear deformation, Digital Image Correlation (DIC) Analysis was used, which is much more precise than strain gages. The software used was ARAMIS. The strains are used to calculate the shear chord modulus according to the following formula (3.19):

$$G^{chord} = \Delta\tau/\Delta\gamma \quad (3.19)$$

Where:

$\Delta\tau$ = difference in applied shear stress between the two strain points

$\Delta\gamma$ = difference between the two engineering shear strain points

This formula is applied over a $4000 \pm 100 \mu\epsilon$ engineering shear strain range. The lower strain point starts in the range of 1500 to 2500 $\mu\epsilon$ inclusive. In cases where data was not available at these strain range end points, the closest available data point was used. The strain range used in the calculation was reported.

This test method is sensitive to notch preparation. Preliminary crack growth can occur at the tapered area and there is an influence of normal load components.

3.4 Fracture Mechanics - Double Cantilever Beam (DCB) Test

The double cantilever beam (DCB) test was used to determine the interlaminar fracture toughness of CFRP materials in mode I (transverse to crack growth plane). A scheme of the test specimen is shown in Figure 3.6. The fiber direction of unidirectional laminates is longitudinal to the specimen length. A separating foil is laminated within the middle of the prepreg layers to introduce a defined pre-crack with the length a_0 .

Methods

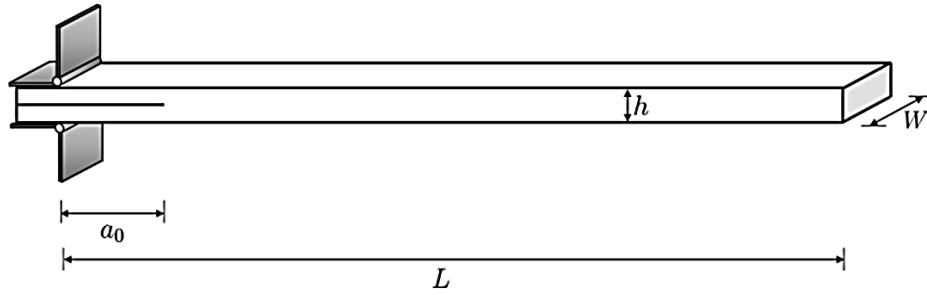


Figure 3.6: Scheme of DCB specimen with hinges [105]

The test is performed by loading the pre-cracked specimen with peeling forces, until the crack has a total length of 50 mm. Then the specimen is unloaded. The loads and traverse path of the testing machine is recorded during crack growth.

A Zwick universal testing machine was used. The applied standard was ASTM D 5528, where different evaluation methods for strain energy release rate G_I are listed. The simplest, but most inaccurate method, since it neglects the rotation of the beams, is the Beam Theory [106], which uses the following formula (3.20):

$$G_{Ic} = \frac{3F\delta}{2ba} \quad (3.20)$$

Here, F is the force when the distance between the beams is δ . To calculate the critical strain energy release rate G_{Ic} , the critical force F_c which occurs at the first delamination is used. The definition of crack length a is $a_0 + \Delta a$.

The Modified Beam Theory takes the rotation of the beams into account. Therefore, a virtual amount $|\Delta|$ is added to the crack length, which results in the following formula (3.21):

$$G_{Ic} = \frac{3F\delta}{2b(a + |\Delta|)} \quad (3.21)$$

$|\Delta|$ is determined by the regression line of the compliance C (here $C^{1/3}$) and the crack length a . C is calculated by (3.22)

$$C = \delta/F \quad (3.22)$$

In Figure 3.7 the diagram to obtain $|\Delta|$ is shown exemplarily for the E420 FML specimen.

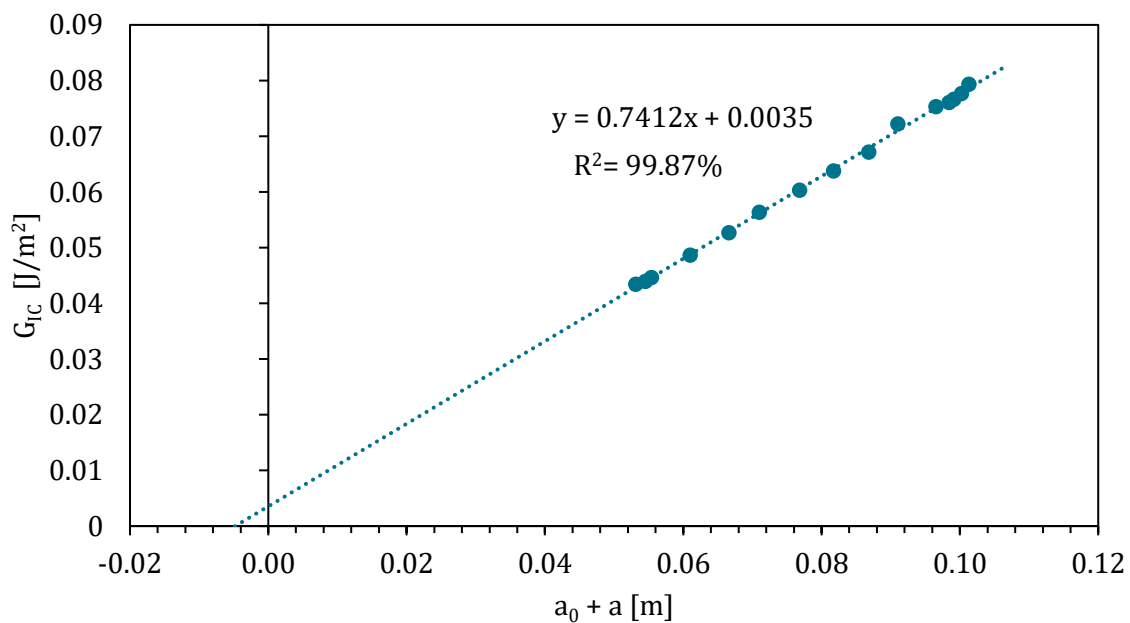


Figure 3.7: $C^{1/3}$ over crack propagation a to determine $|\Delta|$

Using the Modified Beam Theory for evaluation, generally similar results are obtained when using the compliance calibration or modified compliance calibration method, whereas using the beam theory, the G values are mostly overrated. [107, 108]

For specimens with low bending strength or high fracture toughness another correction factor shall be applied when the condition $\delta/a > 0.4$ is fulfilled. For this thesis, tabs were used for loading the specimen. Although the distance between the rotation point of the midplane of the

Methods

specimen is not as large as when load blocks are used, nevertheless, the following formula (3.23) can be considered:

$$S = 1 - \frac{3}{10} (\delta/a)^2 - \frac{3}{2} (\delta t/a^2) \quad (3.23)$$

The correction factor S considers the effective shortening of the beams due to the propagating opening of the specimen. To use this correction, the $G_{I,MBT}$ values are multiplied with S .

3.5 High Strain-Rate Test – Charpy Impact

To determine the impact toughness of plastics, Charpy impact test was performed. Therefore, a specimen is impacted by a pendulum and the amount of energy absorbed during fracture is measured. For this thesis, unnotched specimens and a Zwick pendulum with four joules was used. The schematic test setup is shown in Figure 3.8.

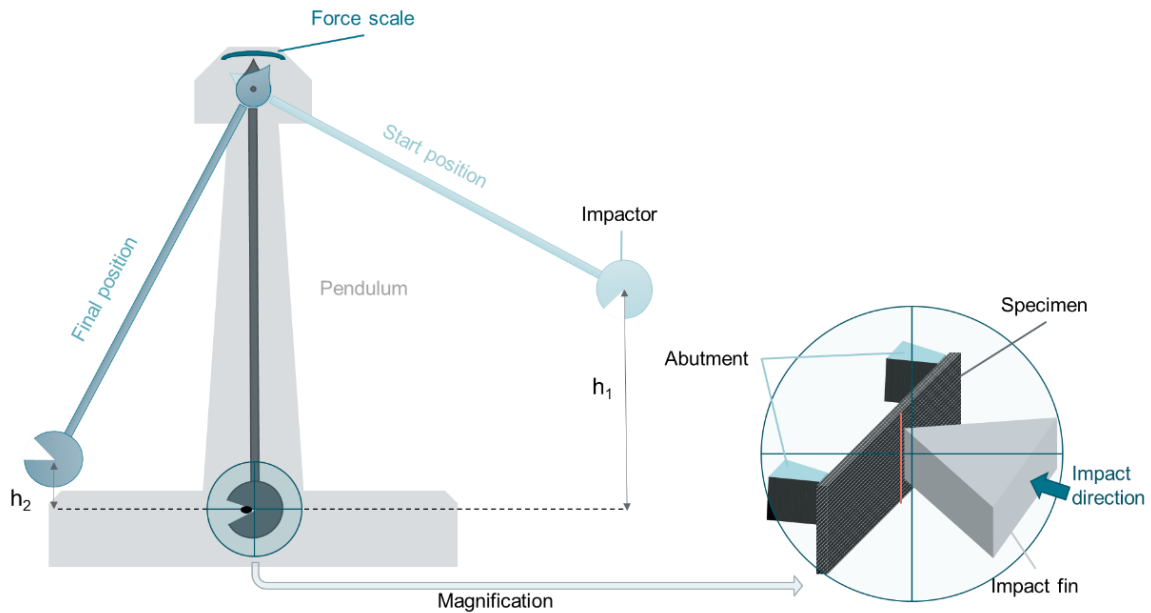


Figure 3.8: Schematic charpy impact test setup

To obtain the impact toughness, impact energy W required to destroy the specimen is measured. W is the difference between h_1 and h_2 , multiplied with the pendulum mass m and gravity constant g according to equation (3.24).

$$W = W_1 - W_2 = m * g (h_1 - h_2) \quad (3.24)$$

For Charpy impact toughness a_{cU} the consumed impact energy W is related to the original cross-section of the specimen according to equation (3.25).

$$a_{cU} = \frac{W}{b * h} \quad (3.25)$$

DIN EN ISO 179-1 standard was applied for evaluation. The specimens were impacted broadside in transverse direction to fiber orientation.

4 Materials and Sample Preparation

4.1 Base Materials

4.1.1 Resin Components

For this study, different resin and hardener components were mixed stoichiometrically to produce vitrimer epoxy resins. They differ in molecular weight, disulfide content and number of reactive groups. The disulfide bonds in the molecules used are either linked aliphatically or aromatically. For the resin materials the epoxy equivalent weight (EEW) is given. For the hardener materials the amine equivalent weight (AHEW) is given. SSEW is the disulfide equivalent weight, which means the weight of this chemical to obtain one mole of disulfide groups (analogous to the EEW and AHEW parameter definition).

In Figure 4.1 the chemical structures of the resin components are illustrated. In this thesis, based on the network structure of the created vitrimer epoxy polymer, the dynamic material behavior was deduced.

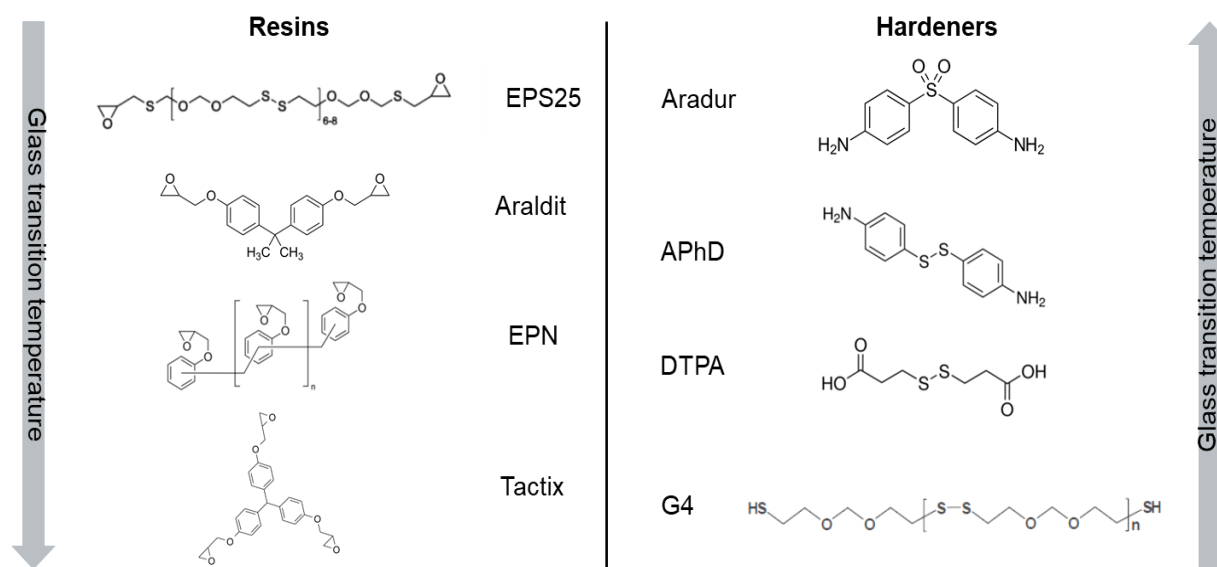


Figure 4.1: Molecular structure of single resin components used [109–115]

Furthermore, a commercially available resin mixture Thioplast EPS70 was used. EPS70 contains four resin components, whereof one contains disulfide bonds. Its composition can be found in Table 4.1.

Table 4.1: Composition of resin mixture EPS70 [116]

No	Designation of component	Category	Aromatic/aliphatic	Concentration [%]	M _w [g/mol]	EEW [g/eq]
1	Epichlorohydrin bisphenol A epoxy resin	DGEBA	aromatic	30-40	350-370	/
2	Long chain prepolymer	Epoxy resin	aromatic	30-40	1520-1720	810
3	Formaldehyde, oligomeric reaction products with 1-chloro-2,3-epoxypropane and phenol	Epoxidized Novolac	aromatic	15-20	350-370	/
4	1,6-Hexanediol diglycidyl ether	Reactive Diluent	aliphatic	10-15	300	140-160

Component No two has a remarkably high chain length and high molecular weight. Component No four is aliphatic and responsible for lowering of T_g values. The molecular structure of component No two (dynamic) is shown in Figure 4.2.

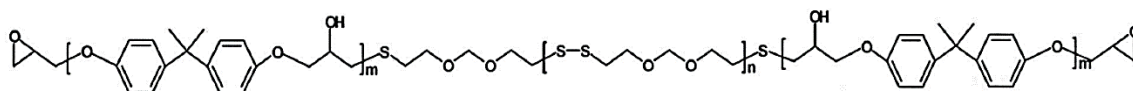


Figure 4.2: Molecular structure of the disulfide containing component of the commercially available resin mixture Thioplast EPS70 [111]

Table 4.2 lists the parameters of the resin components for calculation of resin formulations.

Materials and Sample Preparation

Table 4.2: Parameters of resins and hardeners from the respective product data sheets for calculation of resin formulations [109–118]

		Base resins					Hardeners			
Parameter	Unit	EPS70	EPS25	Araldite	EPN	Tactix	Aradur	DTPA	APhD	G4
M _w	g/mol	-	1356	370	357	480	248	210	248	1100
EEW	g	315	678	185	178.5	160	0	0	0	0
AHEW	g	0	0	0	0	0	62	105	62	550
SSEW	g	126	248	0	0	0	0	210	248	169
n(SS)	1	1.75*	6.5	0	0	0	0	1	1	6.5
aliphatic/ aromatic	/	aliphatic/ aromatic	aliphatic	aromatic	aromatic	aromatic	aromatic	aliphatic	aromatic	aliphatic

*for component № 2 of EPS70: $n(SS) = 5$

The chemicals were purchased from Nouryon, Sigma Aldrich, BrunoBock and JHECHEM. The full commercial names of the listed chemicals are Thioplast EPS70, Thioplast EPS25, Araldite LY 1564, EPN 1180, Tactix 742, Aradur 9664-1 and Thioplast G4.

The proportion of dynamic bonds (4.1) for the disulfide vitrimer epoxy resin formulations was calculated as follows:

$$\text{proportion of dynamic bonds (\%)} = \frac{\text{number of dynamic bonds}}{\text{sum of dynamic and static bonds}} \quad (4.1)$$

Dynamic bonds are the reversibly cleavable disulfide groups and static bonds are the irreversible crosslinking points of the hardeners with the epoxy.

Table 4.3 and Table 4.4 show information about the molecular structure of the base resins and hardeners.

Table 4.3: Base resin components in comparison [111, 116, 118]

	Base resins				
Property	EPS25	EPS70	Araldite	EPN	Tactix
Proportion of dynamic bonds [%]	76.5	(≈42.7)	0	0	0
Sulfur mass percentage [%]	30.7	13*	0	0	0
Aliphatic/ Aromatic	aliphatic	aliphatic/ aromatic	aromatic	aromatic	aromatic

*information of the manufacturer Nouryon, calculated from GPC

The proportion of dynamic bonds of EPS70 could only be calculated approximately, because it is not known how many epoxy groups per molecule the contained novolak (component № 3) has. The number of functional groups of an epoxy novolak usually ranges between two and six. [119] The epoxy functionalities of the other three components of EPS70 are mainly end groups, which means that approximately two static bonds per molecule can be formed. Therefore, an average number of four epoxy groups per novolak molecule is assumed and the value was calculated depending on the concentration of the individual components.

Table 4.4: Hardener components in comparison [111, 114, 115, 117]

	Hardeners			
Property	Aradur	APhD	DTPA	G4
Proportion of dynamic bonds [%]	0	20.0	33.3	76.4
Sulfur mass percentage [%]	0	25.8	30.5	37.8
Aliphatic/ Aromatic	aromatic	aromatic	aliphatic	aliphatic

4.1.2 Type of Carbon Fiber Material

The carbon fiber type used was the C T50-4.4/255-E100 of the SGL portfolio. This fiber is characterized by a good stiffness and especially a remarkably high strength [115]. It is a so-called high tenacity (HT) fiber, whose mechanical properties are listed in Table 4.5.

Table 4.5: Material properties of the employed carbon fiber type [120]

Property	Symbol	Value	Unit
Tensile strength	σ	4.4	GPa
Tensile modulus	E	255	GPa
Elongation at break	ε	1.65	%
Number of filaments		50k	1
Diameter		7	μm

The elongation at break of carbon fibers is sometimes less than 1% at high stiffness, while it can be up to 2% at low stiffness combined with higher strength. [121] This fiber type is a continuous carbon fiber heavy tow. The diameter of a single filament is in the medium range.

4.2 Overview of Resin Formulations

The first resin series was based on the E420 SGL resin as reference with a latent hardening system. The second resin series was based on a reference resin with a standard DGEBA and a dynamic primary diamine hardener, which was also used and tested by the Spanish company CIDETEC. [1] By changing the composition of the component A of the resin mixtures by increasing the proportion of dynamic base resin Thioplast EPS70 a color change could be observed. This is shown in Figure 4.3 for the respective components A of the second resin series (2a-2i) whose blends changed its appearance from white and opaque to yellowish tint and transparent. This picture was taken before the brown hardener powder APhD was added in stoichiometric amount to the respective component A.

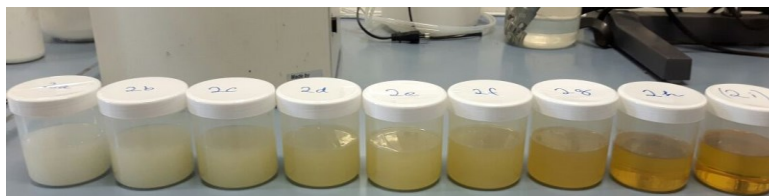


Figure 4.3: A Components of second resin series

By increasing the proportion of EPS70 in component A of the resin, an increase in the proportion of dynamic bonds was achieved. This procedure was chosen to test the influence of the dynamic base resin EPS70 and especially the influence of the proportion of dynamic bonds on the resin properties. By combining EPS70 with different resin components for creating the first and the second resin series, polymers with different network structures were obtained. With the prepared resin mixtures, the influence of the characteristics of the polymer network on the properties of the vitrimers was investigated. The formulations of first and second resin series are shown in Table 4.6.

Table 4.6: Resin formulations of first and second resin series

Resin	Base resins [m% in component A]			Hardeners [m% in component B]		Proportion of dyn. bonds
	E420 base resins	Araldite (SB1)	EPS70 (DB1)	E420 hardeners	APhD (DH1)	
1=E420	100%		0%	100%		0%
1a	93%		7%	100%		10%
1b	85%		15%	100%		20%
1c	75%		25%	100%		30%
1d	64%		36%	100%		40%
1e	49%		51%	100%		50%
1f	30%		70%	100%		60%
1g	0%		100%	100%		71%
2=VME02		100%	0%		100%	20%
2a		95%	5%		100%	25%
2b		89%	11%		100%	30%
2c		83%	17%		100%	35%
2d		75%	25%		100%	40%
2e		67%	33%		100%	45%
2f		58%	42%		100%	50%
2g		37%	63%		100%	60%
2h		11%	89%		100%	70%
2i		0%	100%		100%	73%

Comparing the two resin series, the first series starts with a completely static network (E420) and ends with a polymer network where the dynamic bonds are only contained in the polymer chains (1g). The second resin series already starts with a dynamic network (VME02), where dynamic bonds are contained in the hardener which connects the static base resin molecules and ends with a completely dynamic network where disulfide bridges are contained in the polymer chains as well as in the linkage between the chains via the dynamic hardener.

Several resin formulations were tested to evaluate the influence of further single (static and dynamic) resin components. Some mixtures were formulated to achieve a uniform proportion of dynamic bonds to be comparable regarding other differences of the resins. Afterwards, with the gained knowledge from the pretests, “optimized” resin mixtures were formulated with the aim to achieve the desired properties.

These mixtures were formulated to get closer to an ideal solution. For example, the expensive dynamic hardener APhD was mixed with cheaper dynamic components or dynamic components which strongly lower the T_g value and was then combined with static resin components which

raise or maintain a suitable T_g value. Also, slow or low reactive components can be combined with more reactive ones.

In Table 4.7, the percentage values resemble the stoichiometric fraction of resin, which was reacted with hardener and vice versa. Hence, the sum of the percentage resin and the sum of the percentage hardener was 100% each. This way of calculating the formulations was chosen to achieve comparability without the effect of the molecular mass of the components.

Materials and Sample Preparation

Table 4.7: Resin formulations of mixtures to test component influences, of mixtures with 20% proportion of dynamic bonds and of mixtures to optimize resin properties

Resin	Base resins				Hardeners				Proportion of dyn. bonds
	EPS25 (DB2)	Araldite (SB1)	EPN (SB2)	Tactix (SB3)	Aradur (SH2)	DTPA (DH2)	APhD (DH1)	G4 (DH3)	
Influence of EPS25									
11	0%	100%			100%				0%
12	15%	85%			100%				13%
13	30%	70%			100%				25%
Influence of DTPA									
21=11	0%	100%			100%	0%			0%
22		100%			85%	15%			7%
23		100%			70%	30%			13%
Influence of static base resins (literature)									
21=11	0%	100%			100%	0%			0%
50			100%		100%				0%
70				100%	100%				0%
Influence of static base resins									
13	30%	70%			100%				25%
51	30%		70%		100%				25%
M2.1	30%			70%	100%				20%
Influence of dynamic hardeners									
22		100%			85%	15%			7%
23		100%			70%	30%			13%
M2.2		100%			70%		30%		7%
M2.3		100%			85%			15%	33%
Mixtures with 20% proportion of dynamic bonds set									
VME02		100%					100%		20%
M1.6		100%			50%	50%			20%
M1.7	27%	73%			100%				20%
M2.4		100.0%			92.7%			7.7%	20%
M2.5	16.4%	83.6%			55.5%	44.5%			20%
M2.6	16.4%	83.6%			77.5%		22.5%		20%
M2.7	16.4%	83.6%			96.6%			3.4%	20%
Optimized Mixtures									
52	33%	33%	33%		100%				28%
53	50%	50%			50%		50%		45%
56	70%		30%		100%				55%
71	50%			50%	100%				34%
M1.1	40%			60%	70%	30%			34%
M1.2	40%			60%	90%		10%		28%
M1.3	50%		50%		80%		20%		38%
M1.4				100%	60%			40%	57%
M1.5		100%			50%		50%		11%

To compare the influence of EPS70, which was only used in the first resin series shown in Table 4.6, (in combination with different base resins and hardeners than the resin formulations shown in Table 4.7) with the influence of the other components, a reference mixture EPS70-REF was formulated (see Table 4.8).

Table 4.8: Resin formulation of EPS70-REF

Resin	Base resins		Hardeners	Proportion of dyn. bonds
	EPS70 (DB2)	Araldite (SB1)	Aradur (SH2)	
EPS70-REF	30%	70%	100%	43%

4.3 Prepreg Materials

Four resins of the two resin series each were used to manufacture prepreg material: 1c, 1e, 1f, 1g and 2b, 2h, 2g, 2i. These prepreg materials were used to perform several tests (mechanical performance of CFRP and FML, repair, recycling, fracture toughness, impact resistance). Several random samples were taken from the material during prepreg production and weighed to ensure a constant quality of the material. The average fiber weight per unit area of the prepreg was about 215 g/m². This value was set in advance as the target value to achieve a good workability of the material and a reasonable fiber volume content. Table 4.9 summarizes the main material parameters of the vitrimer prepreps produced.

Table 4.9: Main properties of vitrimer prepreg materials of first and second resin series

Resin		Press time @ 150 °C [min]	T _g [°C]	T _d [°C]	Proportion of dynamic bonds [%]
			(DSC, 10 K/min, N ₂)	(TGA, 10 K/min, N ₂) Criterion: 98% residual mass	
1c		10	133	287	30
1e		10	99	248	50
1f		10	71	212	60
1g		10	23	205	70
2b		45	131	280	30
2f		60	96	275	50
2g		65	72	277	60
2i		85	16	271	70

4.4 General Sample Preparation

4.4.1 Neat Resin Specimens

For producing neat resin specimens, a mold was used. The mold was wetted with release agent and then filled with resin. For high-viscous resins, both the resin mixture and the mold were preheated to lower the resin viscosity and facilitate the filling of the mold. The filled mold was put in an oven, heated, and vacuum was sucked to avoid pores in the specimens.

Especially fast-curing resin mixtures must be cured very carefully. In general, due to the generation of exothermic energy during the curing reaction the resin was only heated until it gelled (certain time at 80-110 °C depending on the mixture) and then taken out of the oven. The initiated curing reaction proceeded overnight and the next day solid resin specimens were obtained. To reach the final material properties a post-curing step was performed by heating the specimens to 150 °C for a certain time depending on the mixture. After cooling to room temperature, the specimens were carefully demolded.

Before testing, the neat resin specimens shown in Figure 4.4 were dried to constant weight to obtain a defined condition of the material tested.

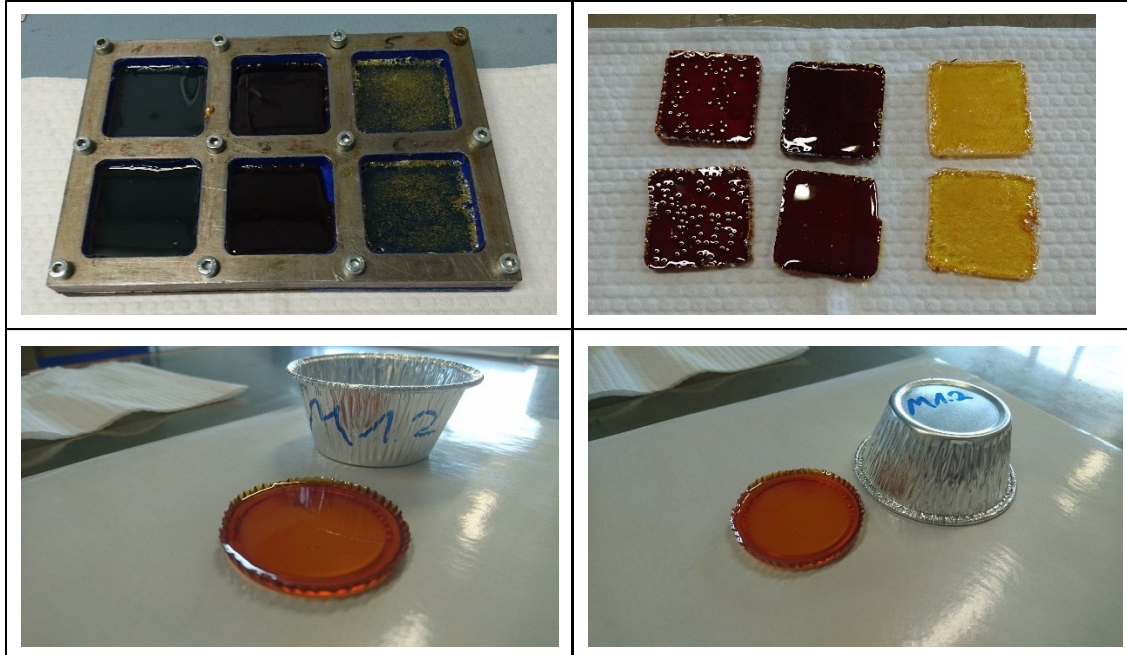


Figure 4.4: Neat resin specimens for flow tests

4.4.2 CFRP Specimens

To manufacture CFRP specimens, the refrigerated prepregs were defrosted to room temperature, cut to the required sizes and stacked onto each other to achieve a plate thickness depending on the intended test method. The laminated plates were pressed at 150 °C with 10 bar and for a specific pressing time required by the resin contained in the CFRP. For pressing release agent, coated aluminum foil was used to fix the layers and fibers in a defined form. The C T50-4.4/255-E100 Carbon fiber specified in chapter 4.1.2 was used.

Materials and Sample Preparation

Furthermore, hand laminated woven plates were produced. Therefore, woven carbon fabric cuts were coated with resin and stacked onto each other as depicted in Figure 4.5.

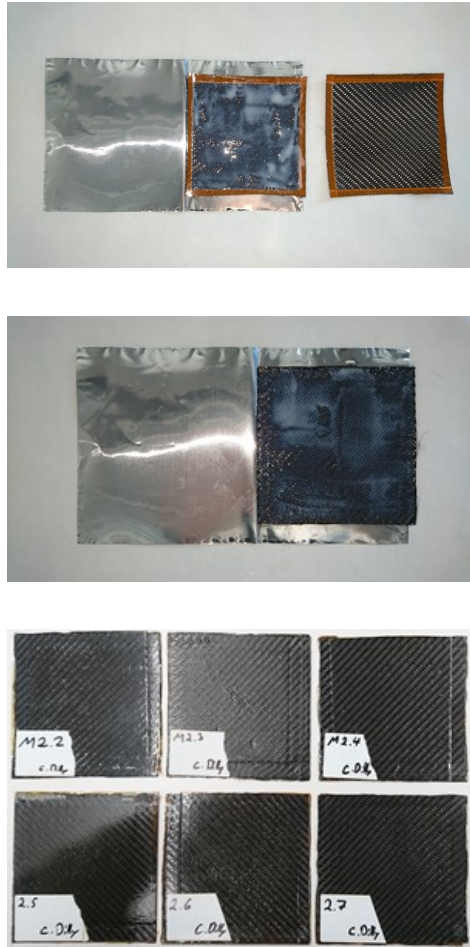


Figure 4.5: Hand laminating of plates with woven carbon fiber fabric

For butt-joint test, separating foil was used to get a defined circular area for the specimens with a 30 mm diameter as shown in Figure 4.6.

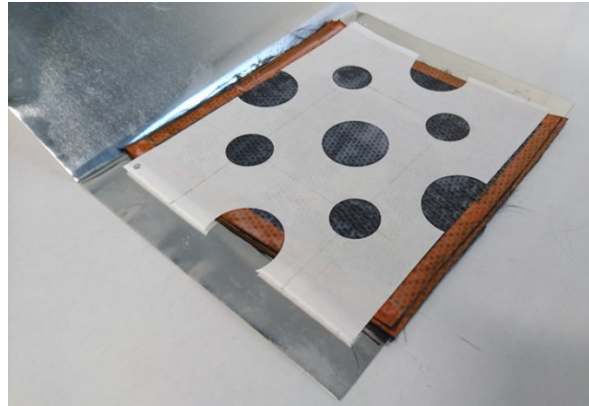


Figure 4.6: Preparation of CFRP plates for butt-joint test with separating foil

4.4.3 FML Specimens

The FML specimens as exemplarily shown in Figure 4.7 were produced analogously to the CFRP specimens, with the only difference that aluminum metal layers were used together with prepreg layers. The aluminum metal layers were cleaned by simple acetone wiping to remove any grease or dirt which might lower the adhesion of CFRP layers. Aluminum 1050 type was used.

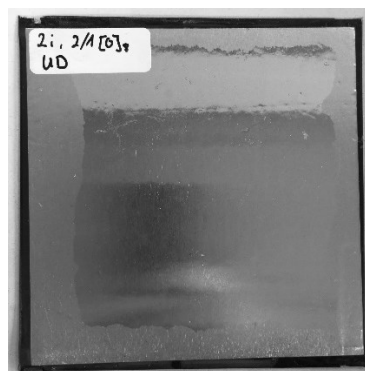


Figure 4.7: FML plate with outer aluminum layers

Materials and Sample Preparation

The layer structure of FML was 3/2 for tensile, bending, compression and $\pm 45^\circ$ -shear test and 2/1 for impact test.

5 Results and Discussion

First, the reactivity (gelation and curing) of the resins was evaluated, which is essential to adequately manufacture the material (curing/pressing time and temperature). Second, the thermal behavior (glass transition and decomposition) of the resins was characterized. This information is essential for processing the material at reasonable temperatures (forming temperature, repair temperature) and to define a temperature range of use. The focus was laid on the influence of the single resin components, to get the knowledge how to adjust the resin properties according to specific requirements and applications. Third, the mechanical performance of vitrimer neat resin, CFRP and FLM was tested to ensure or assess the competitiveness of vitrimer materials compared to established polymer and composite materials. Last, the dynamic properties (formability, reparability, recyclability) of the vitrimer resin materials were tested, which represent the added value of the material compared to established polymers.

5.1 Curing Behavior

The curing behavior was investigated by rheological measurements, DSC measurements and thermokinetic modelling. To exclude interactions between hardener components with each other and resin components with each other, DSC measurements were performed on mixtures with only hardener and only resin components together. No enthalpy appeared in the DSC measurements for the temperature range used to cure the resin mixtures. Therefore, it can be assumed that no interactions between components of the same kind took place. Though not further tested in the scope of this thesis, there is the possibility to use catalysts e.g., BF_3 to decrease the cure time.

5.1.1 Gel Time Measurements (t_{gel})

The gel time was measured by rheology. The refrigerated resin was stored at ambient temperature and put onto the pre-heated plate geometry of the rheometer. Gel time was measured as modulus cross over of an isothermal curing step at 150 °C. Before the oscillation step started, the sample was conditioned by a preshear of 30 s @ 150 °C and an equilibration of 60 s @ 150 °C. Figure 5.1 represents an example of a rheometer measurement curve, which shows the modulus crossover during the isothermal curing step.

Results and Discussion

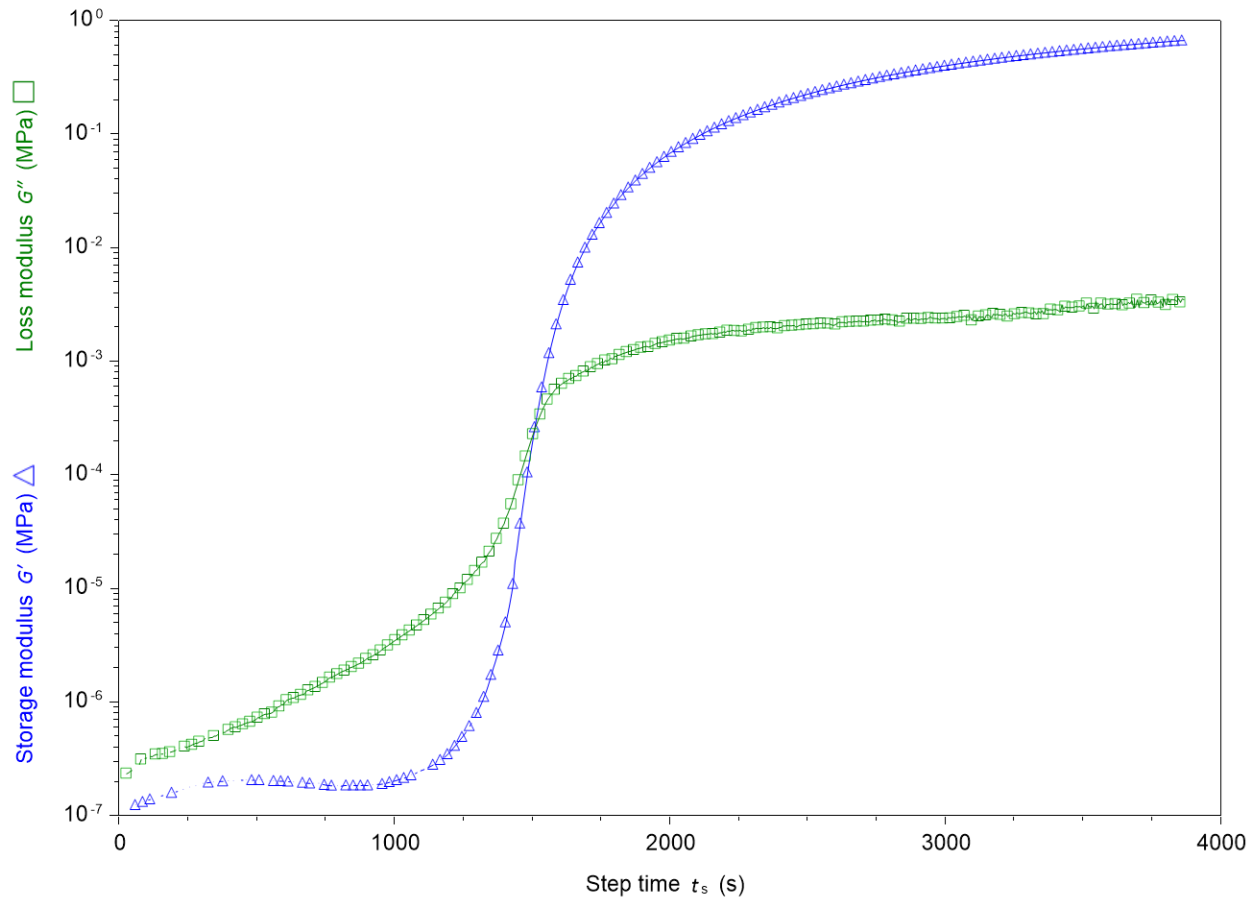


Figure 5.1: Example of modulus crossover at DMA during isothermal curing

The gel time varied depending on the resin and hardener used. First, the influence of the single components on the gel time was tested. Second, the gel time of multi-component mixtures was determined. The reactivity was mainly influenced by the chain length of the molecules, the molecular structure (aliphatic or aromatic) and the functional group. The higher the chain length, the slower the reaction, because diffusion is hindered and the probability of two reactive groups finding each other is lower.

Influence of EPS70 (DB1)

The concrete values of the gel times for the first and second resin series can be found in Table 6.1 and Table 6.2 in the Appendix. As it can be seen from Figure 5.2 (first resin series) and Figure 5.3 (second resin series), Thioplast EPS70 had an increasing effect on the gel time.

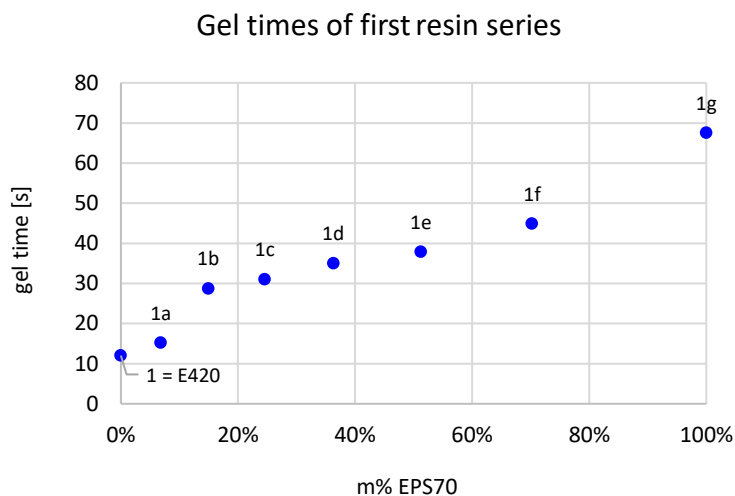


Figure 5.2: Gel times of first resin series

The addition of small quantities of EPS70 led to a significant increase in gel time. As long as the original base resins of E420 were still present, a further increase in concentration of EPS70 led only to a slight increase in gel time. If the E420 base resins were completely replaced by EPS70, the gel time again increased very much. Due to the very reactive hardener system of the E420, resin 1g still had a relatively short gel time.

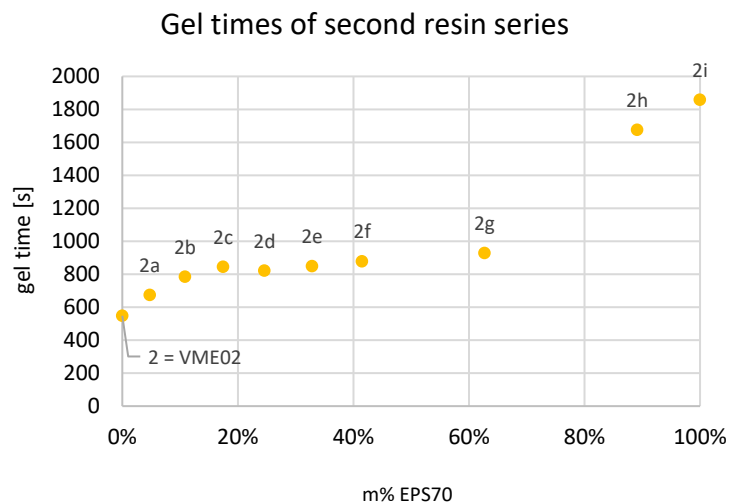


Figure 5.3: Gel time of second resin series

Looking at the second resin series, a slightly stronger increase of the gel time was observed when small amounts of EPS70 were added, which then reached saturation up to resin 2g. The complete replacement of the base resin of VME02 by EPS70 led here again to a strong increase of the gel time.

Although no specific gel time or cure time was set as a target value for this work, it would probably be useful to combine EPS70 or slow reacting vitrimer base resins in general with other resins to make curing more time efficient.

An extra study was performed to understand the influence of the Thioplast EPS70, which is, as already mentioned, composed of four resin components (Table 4.1, chapter 4.1.1). Thioplast EPS 70 contains a static aliphatic reactive diluent (№ 4), which reduces the viscosity but has no significant effect on the reactivity or respectively the gel time. The sulfur-containing and thus dynamic component of Thioplast EPS70 (№ 2) is an epoxy prepolymer with a relatively long chain length and a high molecular weight. This component is responsible for the prolonging effect of Thioplast EPS70 on the gel time. Thus, for longer chain lengths, the distance between the reactive groups is higher, the probability that two reactive groups find each other is lower, the concentration of reactive groups per mass is lower, and, once crosslinked, the diffusion of bigger molecules to find reaction partners is hindered.

Furthermore, EPS70 contains two standard resin components – a DGEBA and a novolak. From the EEW values it can be assumed that the DGEBA has little to no effect on the gel time compared to the reference resin component Araldite (SB1) which is also a DGEBA. A novolak generally increases the reactivity of the resin in comparison to standard DGEBA prepolymers.

The concrete values of the gel times for all other resins are listed in Table 6.3 in the Appendix.

Influence of EPS25 (DB2)

EPS25 had an increasing effect on the gel time because the chain length of the molecule is higher compared to Araldite (DGEBA) and the reactivity of aliphatic epoxies is lower than of aromatic epoxies. Using EPS25 or EPS70 in the same stoichiometric ratio to the same hardener the gel times of both mixtures were quite similar.

Influence of DTPA (DH2)

DTPA (Dithiopropionic acid) is more reactive than Aradur (4,4'-Diaminodiphenyl sulfone, DDS) and thus reduced the gel time. Reasons may be the shorter molecule size of DTPA and the higher reactivity of the carboxylic acid groups of DTPA compared to the amine groups of Aradur.

Influence of Static Base Resins

No gel times were available for resin mixture 50 and 70 in the literature scope. Therefore, the influence of the static base resins was tested experimentally. Comparing the static base resins in each case when mixed with the dynamic base resin EPS25, EPN (51) reduced the gel time and Tactix (2.1) increased the gel time compared to Araldite (13).

Influence of APhD

When resin mixture 2=VME02 and 11 were compared, APhD led to faster gelation than Aradur. APhD and Aradur are similar molecules. They differ in the connection of the two benzene rings. The sulfone group (of Aradur) has a stronger -I-effect than the disulfide bridge (of APhD) and thus the H-atoms of the amines of Aradur are less nucleophilic than of APhD. The stronger the nucleophile, the faster the epoxy-amine reaction.

Results and Discussion

Influence of Dynamic Hardeners

Comparing the three dynamic hardeners in terms of their influence on the gel time, DTPA (22, 23) led to the shortest gel times. As mentioned before, the carboxylic acid group is more reactive than amine group or thiol groups. The molecule size of DTPA is the smallest.

APhD was slower than DTPA (and Aradur was again slower than APhD). G4 was the slowest hardener because it has the highest chain length and has the thiol group which is less reactive than amines. Thus, the reactive groups are far away from each other and the probability that they meet is rather low.

Mixtures with 20% Proportion of Dynamic Bonds set

The gel times of the mixtures with 20% proportion of dynamic bonds ranged from six to 47 minutes.

Optimized/Multi-Component Mixtures

M1, M3, M4 and M5 had shorter gel times than the other resin mixtures. Short gel times are favorable because they normally lead to short or moderate cure times and are thus preferred for mass production.

5.1.2 Cure Time

In the following section the press times refer to the vitrimer CFRP and FML respectively. The concrete values of the cure times of all resin mixtures are listed in Table 6.4 in the Appendix. Those times are not valid for the manufacturing of neat resin specimens, which must be cured more cautiously (slower and at lower temperature) and in most cases using a multi-stage process as well. The times were obtained from isothermal rheology measurements when the viscosity no longer changed significantly, then a buffer was added to ensure complete as possible curing.

The press times for prepreg materials of first and second resin series was double checked by thermokinetic modelling. Therefore, DSC measurements with different heating rates (0.5, 1, 2, 4 and 8 K/min) were used to calculate isothermal cure times with the software NETZSCH Thermokinetics. This software fits a mathematical model to the DSC curves which enables it to predict cure times for certain temperatures. A two-stage model with first step autocatalyzed reaction Prout-Tompkins of n-th order and second step n-th order reaction (BnaFn) had the

highest fitting score of over 99%. A fractional reaction of 98% was set as condition and a buffer was added to get cure times rounded up to steps of five minutes.

The gel time is not always proportional to the cure time, thus, depending on the functionality of the components and according to the Flory-Stockmayer theory, gelation occurs at different percentage of monomer conversion (fractional reaction). [122] Here, in most cases the effect of the components on gel time resembled their effect on cure time.

The press times of the first resin series were ten minutes for each mixture. The press times of the second resin series ranged between 45 and 85 minutes. The achieved cure times of the other mixtures ranged from a few minutes to several hours.

5.1.3 Discussion

The effect of a reactive molecule (resin or hardener) on gel time is influenced by its chain length, the aromaticity and the accompanying mesomeric effect on its reactive site and the reactive group itself. Higher chain length leads to slower gelation. Here, the carboxylic acid group is more reactive than the aromatic amine. The thiol has the weakest reactivity. Aromatic epoxies have a higher reactivity than aliphatic ones.

Based on the knowledge of the single component influence, it is possible to formulate mixtures with the target properties e.g., for specific applications. Effects can be balanced and in general there is a great range of possible variations. In Table 5.1 and Table 5.2, the influence of the resin and hardener components on gel time and cure time is presented in simplified form. The “o” means reference and “-” means quite similar. The arrows up (↑) resemble an increase of the property, whereas the arrows down (↓) resemble a decrease. The number of the arrows reflects the strength of the effect.

Table 5.1: Influence of resin components on gel time and cure time

Property	Base resins				
	EPS25	EPS70	Araldite	EPN	Tactix
Gel time	o	-	↓↓	↓	↑
Cure time	o	-	↑	↓	↑

Table 5.2: Influence of hardener components on gel time and cure time

Property	Hardeners			
	Aradur	APhD	DTAP	G4
Gel time	o	↓	↓↓	↑↑
Cure time	o	↓	↓↓	↑↑

Most of the mixtures cured after one to two hours. Furthermore, there would also be the possibility of catalysis to reduce cure time. Even if the resin has longer cure time, the added value due to dynamic properties possibly puts this disadvantage into perspective.

5.2 Glass Transition Temperature (T_g)

T_g values were obtained from DSC and rheometry measurements on neat resin material. At first, the influence of the single base resin and hardener components was investigated and the T_g values of all the other resin formulations as well. Afterwards, the results from both methods are discussed and compared to each other and the findings of this chapter are summarized. Rheometry measurements also provide information about the degree of softening due to glass transition when looking at the change of storage modulus.

5.2.1 DSC

First and second resin series were each based on a reference resin system as explained in chapter 4.2. The results of DSC measurements presented in Figure 6.1 and Figure 6.2 in the Appendix show that T_g decreased with increasing content of Thioplast EPS70 from 159 °C to 23 °C for the first resin series and from 142 °C to 16 °C for the second resin series. Thus, Thioplast EPS70 is a dynamic component and contains disulfide bridges, the proportion of dynamic bonds was increased simultaneously. An approximately linear trend could be observed. DSC was measured with 10 K/min heating rate under N_2 atmosphere. The resins 1e and 2f with a proportion of dynamic bonds of 50% each marked the border to the target T_g of 100 °C.

5.2.2 Rheological Measurements

As explained in chapter 3.1.3.1, the T_g value obtained from rheometry measurement depends on the criterion. For this thesis, the maximum of the loss modulus curve G'' was chosen, which resembles the midpoint of the mechanical glass transition.

Influence of EPS70

The decreasing effect of base resin EPS70 on the T_g value measured with rheometry is shown in Figure 6.3 and Figure 6.4 in the Appendix and was analogous to the DSC measurement results. The selected criterion for the DMA represents the midpoint of the glass transition. The T_g values were slightly higher than in the DSC measurement.

The T_g values from rheological measurement with the max. G'' criterion of all resins are listed in Table 6.5 in the Appendix. Table 6.6 shows four values obtained from rheological measurement (onset, midpoint, endset and ΔT) to describe the entire glass transition of all resins.

Influence of EPS25 (DB2)

EPS25 had a decreasing effect on the T_g value. Due to the aliphaticity and the relatively long chain length, the network is rather flexible and wide-meshed. This means that the cross-linking density is lowered. When EPS25 was used instead of EPS70, the decrease of T_g was stronger.

Influence of DTPA (DH2)

DTPA had a decreasing effect on T_g as well, but the effect was less pronounced compared to EPS25. Though DTPA is aliphatic as well, its chain length is much shorter than that of EPS25. Thus, the crosslinking density of the network is higher, which results in higher T_g values.

Influence of Static Base Resins

From literature, the T_g values for 100% of the static base resins each mixed with 100% Aradur hardener were available and consistent with the measurement results. Comparing the measured T_g values, Tactix (M2.1) also led to the highest T_g , followed by EPN (51) and Araldite (13).

Results and Discussion

Influence of Dynamic Hardeners

Among the tested hardeners, APhD led to the highest T_g values. Comparing the dynamic hardeners, due to its aromatic structure, APhD led to comparatively high T_g values. DTPA lowered the T_g value only slightly, but due to its high cost and high reactivity its usable amount in the resin is limited. Using G4 resulted in the lowest T_g value because the molecule is purely aliphatic and has a relatively long chain length. Thus, the network is quite wide-meshed.

Influence of APhD

The T_g value of the APhD-containing resin mixture was lower than that of the reference because the molecule is more flexible compared to Aradur and the rotation barrier of the disulfide bridge is rather low. Thus, the polymer network is more flexible.

Mixtures with 20% Proportion of Dynamic Bonds set

The T_g values of the mixtures with 20% proportion of dynamic bonds were all above the target value of 100 °C.

Optimized/Multi-Component Mixtures

As already explained in chapter 5.1.1, these mixtures were formulated to get closer to an ideal solution. Considering the T_g value, resin mixture 52 was close to meeting the target value with T_g being only slightly below 100 °C. Mixture 71, M1.1, M1.2 and M1.5 fulfilled the criterion with T_g being equivalent to 100 °C or even higher.

5.2.3 Discussion

T_g of the resin mixtures was measured with DSC and Rheometry. When the maximum of G'' was used as criterion in rheometry, the T_g value tended to be detected later than in DSC, although a lower heating rate was used. It is noticeable that the resin mixtures had different broadness of glass transition. Most of the mixtures with an expected sufficient proportion of dynamic bonds regarding dynamic behavior had a T_g of at least 100 °C. T_g is influenced by the network structure of the polymer, where chain length or respectively mesh width, aromaticity and steric factors play a major role. The shorter the chains and meshes, the more aromatic rings and a high degree of

branching lead to high T_g values. The influence of single components was evaluated and given in Table 5.3 and Table 5.4 of which the legend is already given in chapter 5.1.3.

Table 5.3: Influence of base resin components on T_g

Property	Base resins				
	EPS25	EPS70	Araldite	EPN	Tactix
T_g	-	↑	↑	↑↑	↑↑↑

Table 5.4: Influence of hardener components on T_g

Property	Hardeners			
	Aradur	APhD	DTAP	G4
T_g	-	↓	↓↓	↓↓↓

The introduction of disulfide bonds was accompanied with a decrease of T_g by all components except the expensive hardener APhD. Therefore, the more cost-efficient dynamic components should only be used up to a reasonable share to balance the decrease of T_g and the increase of dynamics. Only in this way, the mechanical properties of the material can be maintained, and the dynamic behavior can be ensured simultaneously, which means there is a trade-off between mechanical properties and dynamic properties.

5.3 Degradation Temperature (T_d)

The temperature stability of the vitrimers is crucial for the appropriate curing temperature of the neat resin, the operating temperature of the final product and for the upper temperature limit of the repair process. Therefore, TGA measurements were performed to monitor the mass loss during curing of the resin and during heating of the cured resin. Heating rate was 10 K/min in an N_2 atmosphere and the criterion for T_d was set to the temperature at 95% residual mass. 1-2% mass loss can be related to the evaporation of moisture. Most resins cured during heating which was verified with Thermokinetic Modelling. When the degree of cure was below the calculated 99%, an extra isothermal curing step was performed before the heating step. The mass loss

Results and Discussion

during isothermal curing should be relatively low. Otherwise, it indicates that the resin must be cured at lower temperature. When the TGA was performed in two steps, the mass loss was summed up.

In general, polymers or any material can withstand higher temperatures for shorter time. When the polymer is exposed to elevated temperatures for longer periods of time (repair process, in-service temperature), this temperature must be much lower than the degradation temperature given here. The temperature considered in the following is not the decomposition temperature but the temperature where the material undergoes embrittlement, the elongation of break is reduced, and where the polymer generally starts to lose mechanical performance, and, in the case of vitrimers, also dynamic performance, which should be prevented.

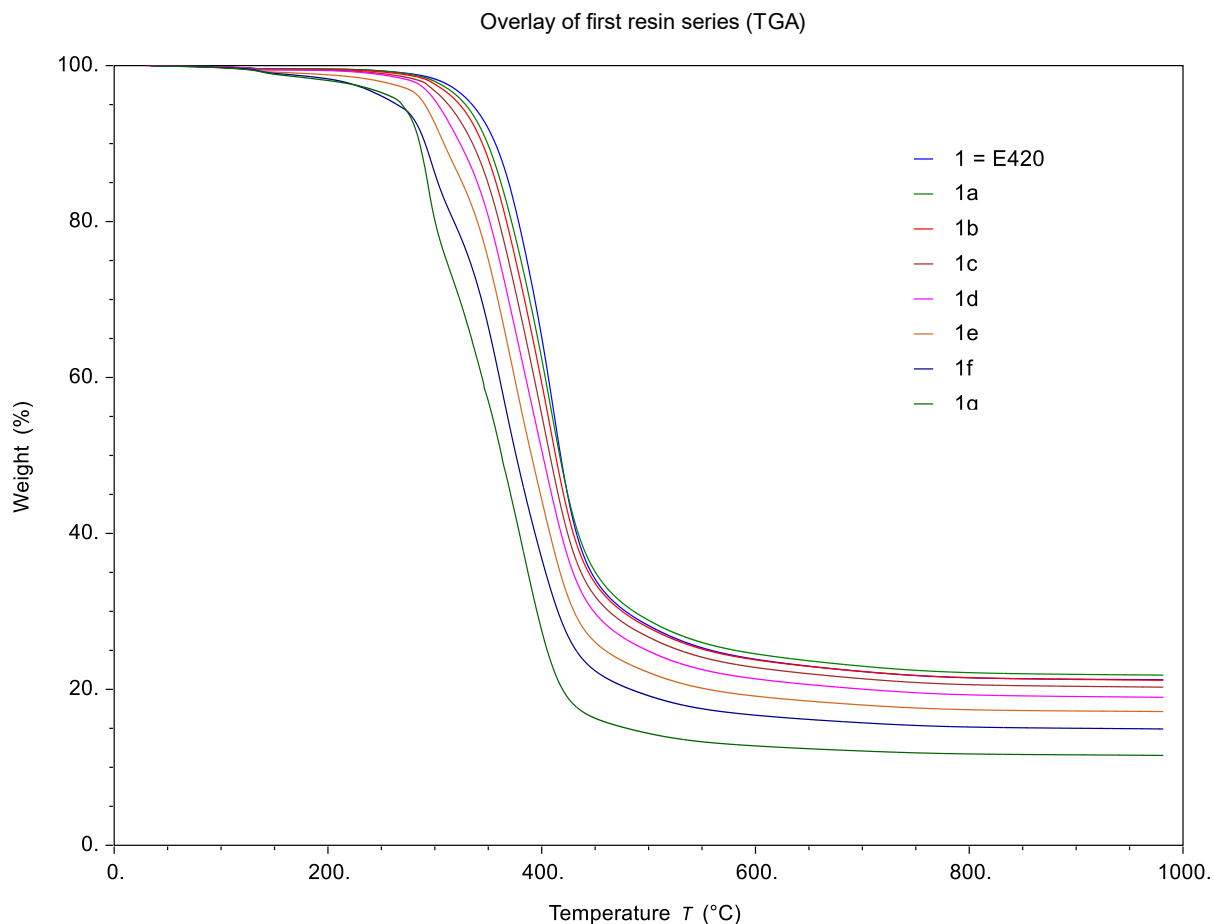
Influence of Thioplast EPS70 in the First Resin Series

Figure 5.4: Overlay of TGA curves of first resin series

As can be seen from Figure 5.4, the TGA curve shapes of the first resin series inclusive E420=1 were quite similar. The more Thioplast EPS70 was added, the earlier the curve started to drop.

The degradation temperature as a function of the EPS70 content for the first resin series is shown in Figure 6.5 in the Appendix. It seemed that combined with the E420 base resins and the E420 hardener system, the increasing amount of EPS70 in the resin mixture lowered the degradation temperature. Further TGA measurements on pure EPS70 were performed to investigate its

Results and Discussion

degradation behavior which confirmed the lower temperature stability of the EPS70 compared to the E420 base resins.

Influence of Thioplast EPS70 in the Second Resin Series

When EPS70 was combined with Araldite (DGEBA) and APhD, the degradation temperature of the original VME02 was not much affected until a certain amount of EPS70 was present (see Figure 6.6 in the Appendix). Comparing the absolute values, the degradation temperature of VME02 was lower than that of E420, which partly explains the difference to the observations on the first resin series.

Temperature Stability of pure Thioplast EPS70

The $T_{d,95\%}$ of EPS70 was 205 °C. When exposed to isothermal conditions, the residual mass of EPS70 after one hour at different temperatures is shown in Table 5.5.

Table 5.5: Residual mass of EPS70 at isothermal temperatures measured by TGA

Isothermal temperature [°C]	Atmosphere	Residual mass [%]
140	N ₂	94.8
150	N ₂	92.9
150	Air/O ₂	93.6
160	N ₂	90.5

Therefore, the curing temperature (depending on the required time) should be chosen high enough to achieve a cure time not unnecessarily long, but low enough to not degrade the material. At around 150 °C disulfide bonds break and the molecule fragments reform to volatile, ring-shaped molecules which are split off. Thus, this is the temperature limit for curing of EPS70 containing resin mixtures. When the residual mass of a resin is higher when in contact with air, this can be explained by mass gain reactions due to uptake of oxygen.

Degradation under Air

When the TGA is performed under oxygen-containing atmosphere (air), the degradation temperature is usually lower than under N₂ atmosphere. To make a comparison, four resins were

measured under both atmospheres each. As can be seen from Table 5.6, the $T_{d,95\%}$ under air were only slightly lower than under N_2 each.

Table 5.6: Comparison of degradation temperature $T_{d,95\%}$ under N_2 and under air

Resin		$T_{d,95\%} (N_2) [^{\circ}C]$	$T_{d,95\%} (air) [^{\circ}C]$
E420		335	333
1g		269	261
2a		301	295
2i		241	232

Degradation Temperatures of the other Resins

Furthermore, resins with their T_g near 100 °C and with expected good dynamic properties were tested with TGA to primarily obtain the upper temperature limit for repair tests. T_d was determined by the criterion when the mass loss in total reaches 5%. When the mass loss during isothermal cure at 180 °C is significantly higher than 2%, the resin must be cured at lower temperatures. In this case, a second criterion was applied, and T_d was determined as the temperature when the mass loss in the second step reached 2%. These values must be regarded as provisional. To obtain temperature stability under isothermal conditions, further measurements would need to be carried out.

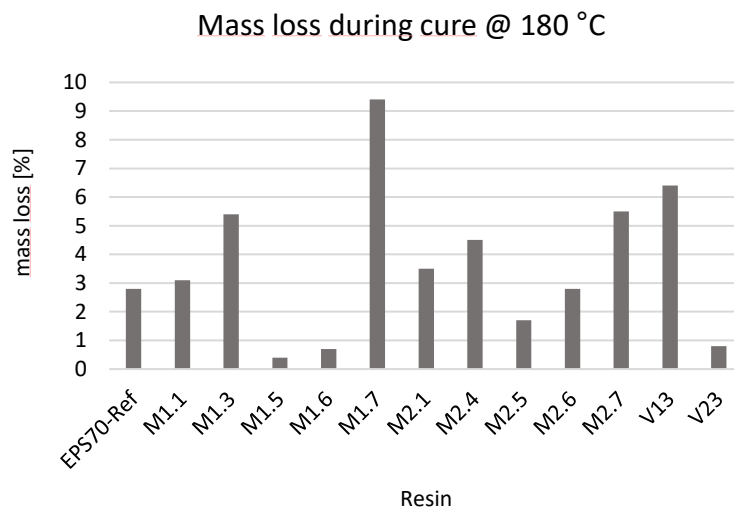


Figure 5.5: Mass loss during cure at 180 °C

The degradation temperatures of these resins can be found in Table 6.7 in the Appendix. There was no direct relation between mass loss and degradation temperature. The lowest degradation temperature was 253 °C, so it could be assumed that all the resins can withstand temperatures up to 200 °C, depending on the time, for repairing.

Influence of Resin Components in terms of Mass Loss

When EPS70, EPS25 or G4 were used, the mass loss increased. APhD and DTPA had no particularly negative influence on mass loss.

Influence of Resin Components in terms of Degradation Temperature

From the measurements performed and the components contained in the resins being considered, it was observed that EPS70, EPS25 and G4 reduced T_d . APhD and DTPA had no significantly negative effect on T_d .

5.4 Mechanical Performance at Room Temperature

The mechanical properties of the vitrimer materials at room temperature were tested on three levels: the pure vitrimer resin, CFRP and FML with vitrimer epoxy matrix. The first (1a-1g) and second (2a-2i) resin series and their respective four prepreg materials (1c, 1e, 1f, 1g and 2b, 2f, 2g, 2i) were tested the most. Thereof, the influence of the resin structure and especially the

amount of the component EPS70 was tested. The focus was laid on the influence of the resin properties such as T_g on the corresponding composite properties. Due to the influence of fiber volume fraction, the measured values were normalized where possible. Benchmarking was conducted as well. The mechanical values of vitrimer material obtained were compared to standard and commercially available reference materials (mainly E420, PA6). The Benchmarking can be found in chapter 5.4.4. Finally, bending values of three vitrimer resin mixtures promising regarding their dynamic properties were tested to prove their competitiveness as engineering materials for structural applications and composite industry.

5.4.1 Neat Resin

Neat resin specimens of first and second resin series were tested in tension and bending. Due to the manufacturing process the neat resin specimens are, despite degassing, prone to defects such as small voids and, although curing was performed carefully, in some samples the exothermic reaction led to regions in the material which were cured faster than others. This led to a not completely homogenous material. Overall, the strength values decreased with increasing amount of EPS70 for both resin series, but they widely varied, did not show the clear trend of the modulus and had a very large spread. Therefore, primarily the tensile and bending modulus were used here to explain the effect of the dynamic base resin EPS70. Both resin series showed the same trend, therefore the stress-strain diagrams are only shown for one resin series.

As can be seen from Figure 5.6 and Figure 5.7, the more EPS70 was contained, the lower was the strength and the higher was the elongation at break. EPS70 decreased the stiffness of the polymer and increased its ductility.

Results and Discussion

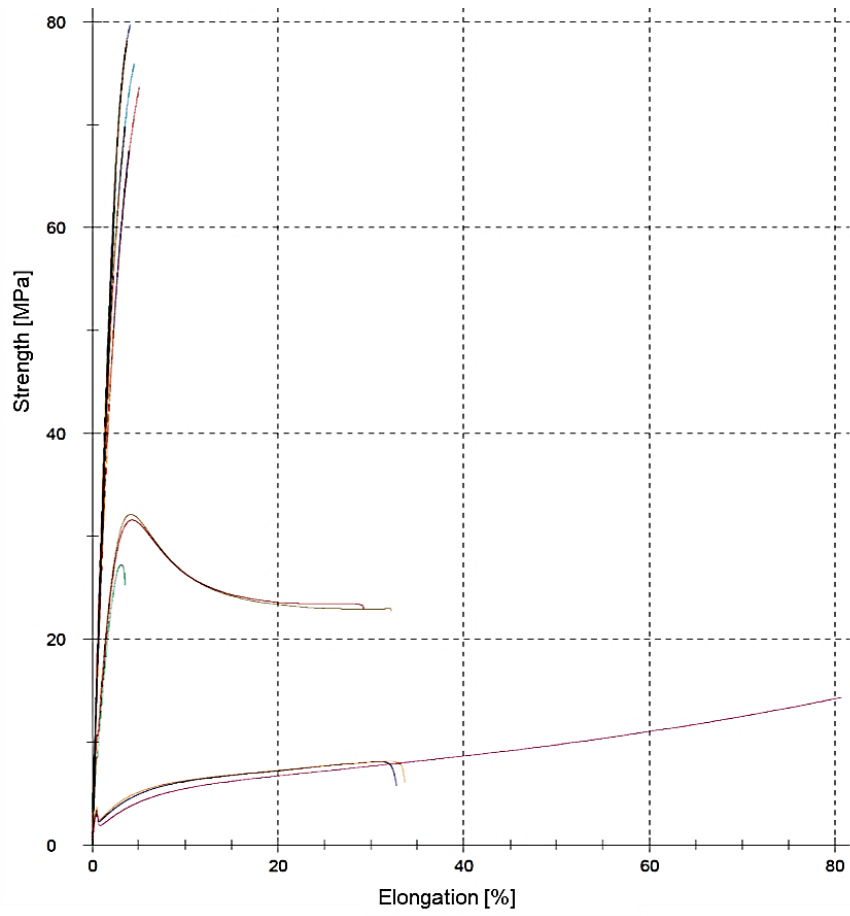


Figure 5.6: Stress-strain diagram of tensile test of second resin series polymers

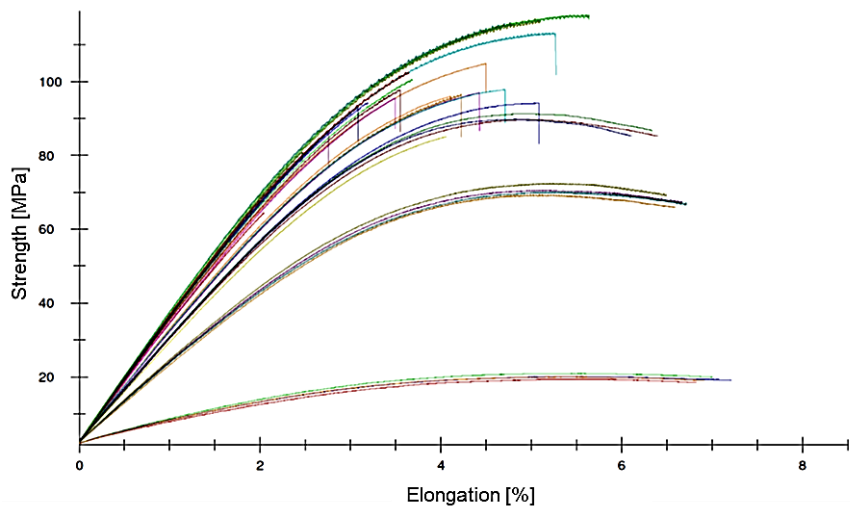


Figure 5.7: Stress-strain diagram of bending test of first resin series polymers

The values of the modules as a function of the mass percent of EPS70 used in the component A of the resin are shown in Figure 5.8 and Figure 5.9.

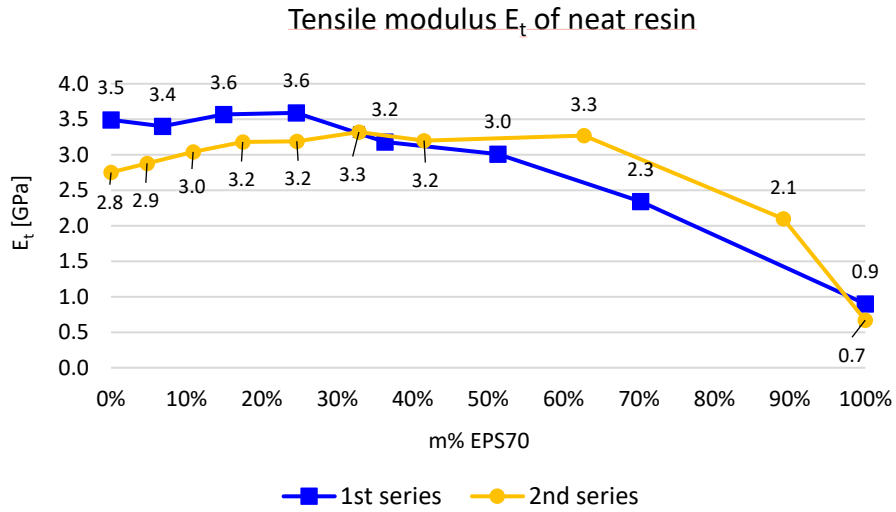


Figure 5.8: Influence of mass percent of EPS70 in component A of the resin on tensile stiffness E_t

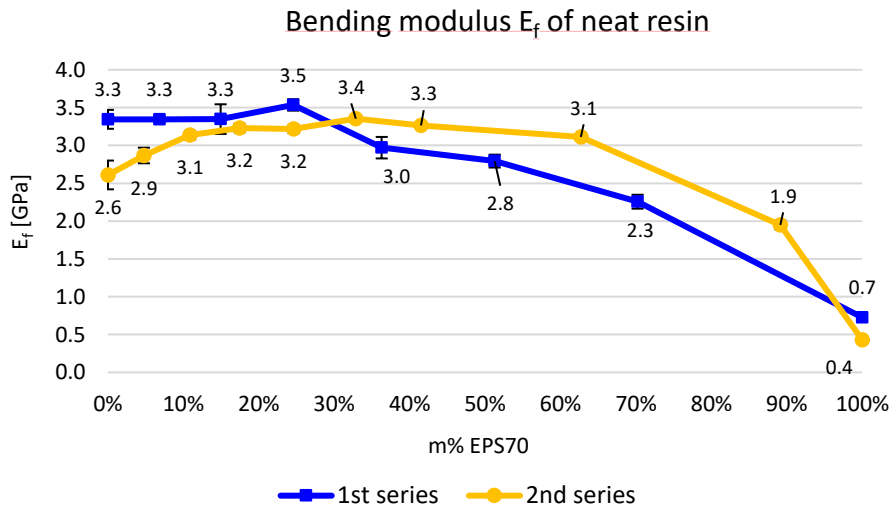


Figure 5.9: Influence of mass percent of EPS70 in component A of the resin on bending stiffness E_f

5.4.2 CFRP

For vitrimer CFRP materials the influences of increasing the amount of EPS70 and the corresponding rise of the proportion of dynamic bonds as well as the decrease in T_g on the mechanical properties were investigated using prepreg material produced on the SGL prepreg line. The four prepregs of the first resin series (on the basis of E420) with vitrimer resin matrices 1c, 1e, 1f, 1g and the four prepregs of the second resin series (on the basis of VME02) with 2b, 2f, 2g and 2i which each had 30%, 50%, 60% and 70% proportion of dynamic bonds were used.

Tensile, bending and compression tests were all performed in 0° and 90° direction to fiber orientation. Quasi-shear (tensile test in $\pm 45^\circ$), V-notched rail shear test and ILSS test was conducted. Fiber volume fractions were measured as well to be able to better evaluate the pure resin influence. For this purpose, a normalization of the mechanical values can also be carried out. Furthermore, impact testing was performed to evaluate the material behavior and influencing factors under suddenly applied load.

In addition, bending values of hand laminated woven fabric CFRP with three vitrimer resins promising regarding their dynamic properties were determined.

Table 5.7 lists the values of all EPS70 containing CFRP plates (of first and second resin series) for almost all tests performed. For all tested parameters, the fiber volume fraction (see Table 6.8 in the Appendix) must be considered.

Table 5.7: Mechanical testing results of first and second resin series CFRP materials

Parameter	Standard	1c	1e	1f	1g	2b	2f	2g	2i	Unit
Tensile strength 0°	ISO 527-5	1833	1819	1761	1546	2045	1921	2028	1777	MPa
Tensile modulus 0°		125	123	126	136	132	127	127	142	GPa
4P-bending-strength 0°	ISO 14125	1380	1230	1093	460	1499	1467	1271	509	MPa
4P-bending modulus 0°		128	126	123	117	155	156	138	109	GPa
4P-bending-strength 90°	ISO 14125	81	77	71	21	26	33	54	24	MPa
4P-bending modulus 90°		8	7	6	2	10	10	8	2	GPa
Compression strength 0°	ISO 14126	997	892	734	244	1283	1260	941	369	MPa
Compression strength 90°		173	138	114	35	146	145	113	51	MPa
±45-shear strength	ISO 14129	59	45	34	13	60	51	46	7	MPa
±45-shear modulus		4	3	3	1	5	5	4	0.3	GPa
ILS strength	ISO 14130	77	68	58	31	45	53	58	36	MPa

Further values which would enable a normalization of the results of 1e and 1f above can be found in Table 6.9 in the Appendix. Since tensile test in 0° direction is dominated by the fiber, the different resins as matrix in CFRP showed only slight effect on the strength and no real influence on the modulus values. The strength values of the first resin series were higher than of the second series. According to the rule of mixture, the resin effect hardly affects the values. According to literature, the T_g effect is also low to non-existent. [123] One-way analysis of variance revealed that only the last prepreg of the second series was statistically distinguishable from the others.

Changing the amount of EPS70 in the bending test in 0° direction there was a strong influence of the matrix resin on the strength values, but almost no influence on the modulus except for the prepregs with 100% EPS70 in component A. The second series had better performance. In this test, compressive and tensile stresses exist. Due to the compressive stresses, the resin effect is strongly present.

Results and Discussion

For bending in 90° direction, the matrix and fiber-matrix adhesion play a role, but also the density of defects. The strength is rather influenced by the defect density due to manufacturing. The modulus of the second series were higher. Considering the strength, there is only a slight effect or rather a T_g effect observed for the first series and no real trend in the second series. There was a strong influence of the EPS70 content on the modulus.

Compression strength in 0° and 90° is strongly dominated by the matrix which supports the fibers against kinking. The softer the matrix, the worse is the performance. The more EPS70 was added, the lower the values of 0° and 90° compression strength. This means that there was a very strong effect of the matrix and clear decreasing trend observable. The compression strength values of the second series were significantly higher.

On the ±45° tensile test (pseudo-shear), there is a strong effect of the matrix on the strength and modulus. This test is dominated by matrix properties and fiber-matrix adhesion; both properties decreased.

For ILSS test, a trend could be observed for the first resin series. The more EPS70 was contained and the lower the T_g was, the lower the measured τ_{ILSS} value.

Fracture Toughness G_{Ic}

For the G_{Ic} values it must be mentioned that the initial crack length was shorter than the 50 mm demanded by the standard. Thus, the values can only be compared with each other.

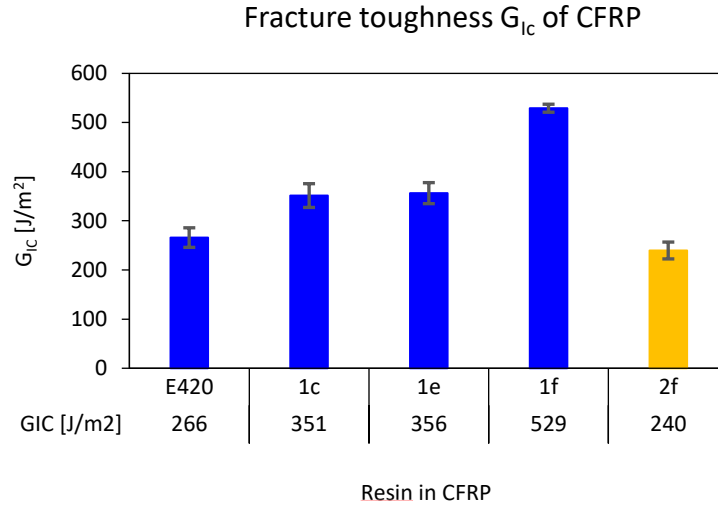


Figure 5.10: G_{Ic} values for different resin systems used in CFRP

As shown in Figure 5.10 the more EPS70 was added from E420 to 1f, the higher the crack resistance and respectively the fracture toughness. 2f had the same proportion of dynamic bonds as 1e, but for 2f a lower amount of EPS70 was used, because the hardener APhD also contains dynamic bonds. The aromatic hardener APhD made the polymer network more rigid and the amount of EPS70 contained was less than in 1e. Hence, the fracture toughness of 2f was lower than of 1e. The fracture toughness of 1g was tested as well but could not be determined by DCB test. The stiffness of the beams was lower than the adhesion between the CFRP layers and thus the specimen failed in bending. This means that the resin 1g, which exhibits the highest amount of EPS70, was even more ductile and flexible than 1f, but due to its low T_g the dynamic bonds were active as well, which increased these properties even more.

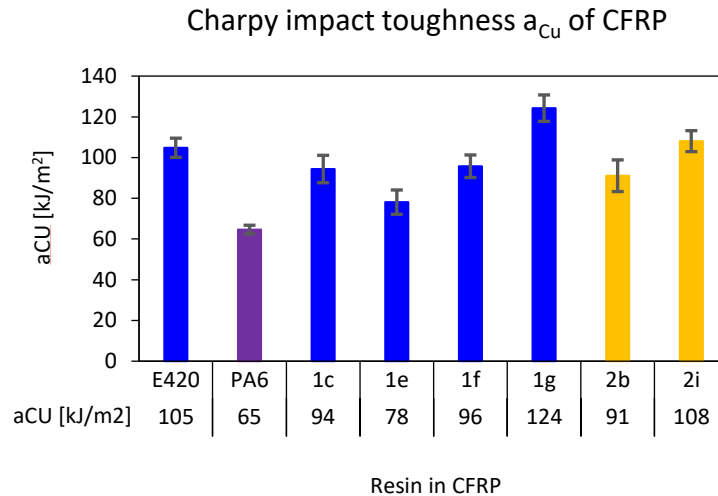
Impact Resistance of CFRP

Figure 5.11: Influence of resin system on impact resistance of CFRP

The Charpy values seen in Figure 5.11 showed that with increasing content of EPS70, the ductility and flexibility of the resin increased and subsequently the impact resistance as well. Compared to the reference values, the vitrimers were more resistant to impact than PA6. E420 is a tough resin. When the T_g was low and EPS70 content was maximum as it was the case for 1g, then the highest amount of energy was absorbed. 2b and 1c had the same proportion of dynamic bonds, as do 1g and 2i. The impact resistance of the corresponding resin of the second resin series was slightly lower because less EPS70 was contained as a part of the dynamic bonds was provided by the aromatic hardener APhD which does not contribute to toughness or impact properties.

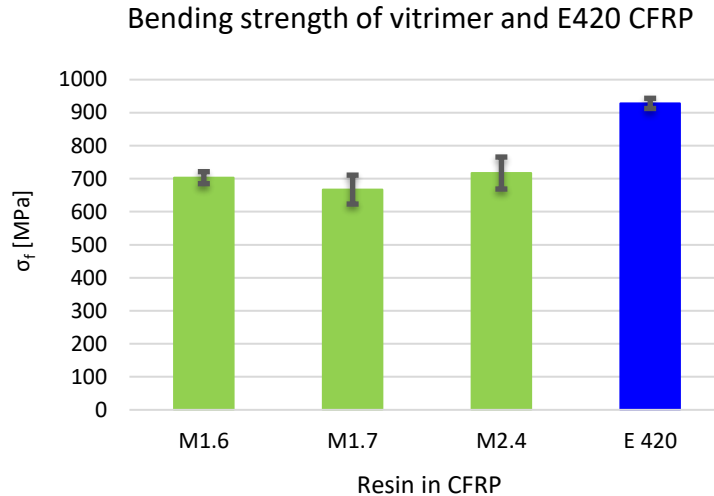
Mechanical Performance of Woven Fabric CFRP with the three Resin Mixtures M1.6, M1.7, M2.4

Figure 5.12: Comparison of bending strength of woven fabric CFRP with M1.6, M1.7, M2.4 and E420 reference as matrix

The bending strength of the CFRP with the three vitrimer resin mixtures was significantly lower than that of the E420 reference. It must be taken into account that these three CFRP plates were hand-laminated and that this also contributed to the lower values. The values of the three vitrimer composites were statistically not distinguishable. Comparing the mean values, M2.4 had the highest strength, followed by M1.6 and M1.7.

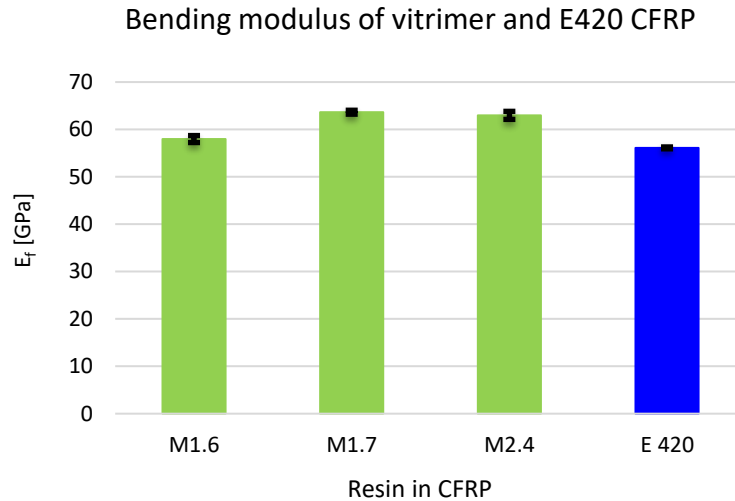


Figure 5.13: Bending modulus values of woven fabric CFRP with M1.6, M1.7, M2.4 and E420 reference as matrix

The bending modulus of the CFRP with the three vitrimer resin mixtures was higher than that of the CFRP with E420. The highest value was reached when M1.7 was used, followed by M2.4 and M1.6.

5.4.3 FML

For vitrimer FML materials the influences of increasing the amount of EPS70 and the corresponding rise of the proportion of dynamic bonds as well as the decrease in T_g on the mechanical properties were investigated using prepreg material produced on the SGL prepreg line and 1050 aluminum foil in 0.2 mm thickness. Tensile tests in 0° direction and bending and compression tests in 0° and 90° direction to fiber orientation were performed. A quasi-shear (tensile test in $\pm 45^\circ$) and ILSS test was conducted. Furthermore, impact testing was performed to evaluate the material behavior and influencing factors under suddenly applied load.

In addition, bending values of hand laminated woven fabric FML with three vitrimer resins promising regarding their dynamic properties were determined.

Table 5.8: Mechanical testing results of first and second resin series FML materials (layer structure 3/2)

Parameter	Standard	1c	1e	1f	1g	2b	2f	2g	2i	Unit
		FML	FML	FML	FML	FML	FML	FML	FML	
Tensile strength 0°	ISO 527-5	1588	1367	1440	1154	1828	1557	1610	1208	MPa
Tensile modulus 0°		99	91	90	97	107	104	99	98	GPa
4P-bending strength 0°	ISO 14125 A	1306	1193	967	627	1591	1364	1157	591	MPa
4P-bending modulus 0°		79	75	74	76	82	81	78	79	GPa
4P-bending strength 90°	ISO 14125 A	78	92	71	56	64	56	54	64	MPa
4P-bending modulus 90°		26	25	24	25	28	29	28	21	GPa
Compression strength 0°	ISO 14126	797	750	586	384	974	908	765	350	MPa
Compression strength 90°		140	126	102	59	127	103	103	60	MPa
±45-shear strength	ISO 14129	54	46	35	14	52	47	43	23	MPa
±45-shear modulus		3.4	3.1	2.3	0.5	3.9	3.8	3.4	1.5	GPa

Tested in 0° tension, CFRP and FML followed the same trend while the FML values were lower. The resin did not show an effect on the difference which was relatively constant. The bending strength in 0° direction was only slightly lower for FML than for CFRP. For the last prepreg there was a reversal of trend in each due to T_g effect. Bending modulus 0° was significantly lower for FML than for CFRP. For bending strength 90° there was no trend observable. A slight trend seemed to be present for the modulus. The FML of first series had higher bending strength than of second series, but a lower bending modulus. For the first series, no trend appeared for bending strength in 90° direction, the bending modulus in 90° direction remained constant. For the second series, bending strength and modulus remained unchanged when the amount of EPS70 was increased.

Tensile strength and modulus 0° and bending modulus 0° are dominated by the fiber. Bending strength 0°, compression strength 0°, compression strength 90° and ±45-shear strength showed a strong influence of matrix. Bending modulus 90° is dominated by the metal.

Results and Discussion

Comparing the ILSS values for FML and CFRP with 1g as matrix resin, the T_g effect led to delamination of CFRP from metal in FML material before the CFRP material failed.

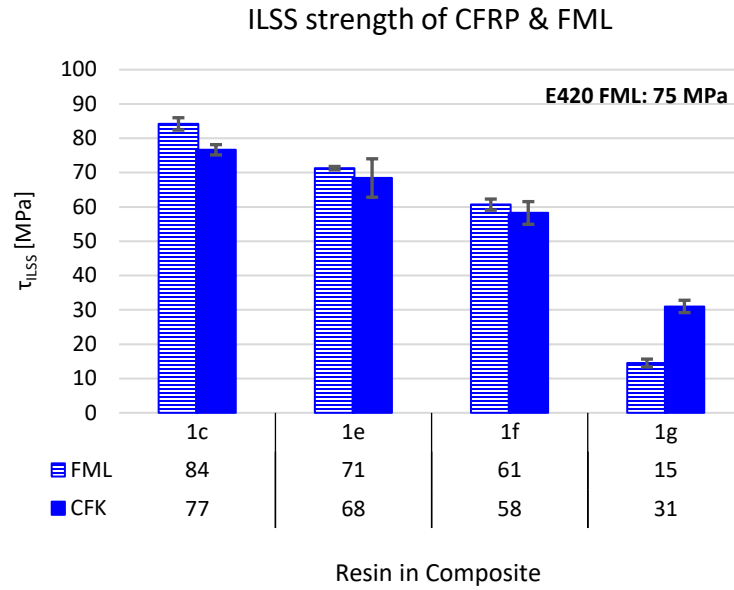


Figure 5.14: Comparison of the ILSS strength of CFRP and FML with resin 1c, 1e, 1f, 1g

Fracture Toughness of FML

The influence of different resin systems on the fracture toughness and adhesion of metal to CFRP in FML was tested by DCB test. The results are shown in Figure 5.15.

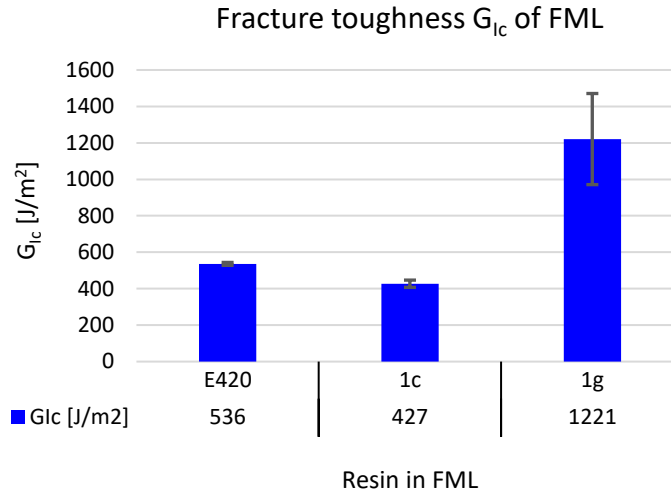


Figure 5.15: G_{Ic} values for FML with different resin systems

When comparing 1c and 1g, the ductility added by Thioplast EPS70 had a positive influence on the fracture toughness of FML material. The decrease of fracture toughness of 1c compared to E420 may be explained by the higher average EEW of the base resins in 1c compared to E420. This means that less reactive groups existed to covalently bond to the metal which apparently could not be compensated by higher ductility of the resin. The assumed worse adhesion of 1g to the metal seemed to be no disadvantage in FML when tested by DCB in contrast to when the 1g FML material was tested by Charpy. In a high-velocity impact test the bad adhesion of 1g would be disadvantageous, whereas when the material was loaded slowly and continuously in DCB mode I the resin properties were beneficial.

Microscopic investigation of the fracture area was conducted. The E420 FML showed adhesive failure. Almost no CFRP material stuck to the metal, which means that the cohesion within the E420 CFRP was stronger than the adhesion to the metal. The cohesion in 1c CFRP was lower and thus the 1c FML showed partly cohesive failure on the interface between metal and CFRP. 1g FML showed adhesive failure. Those results correlated with the ILSS results (Figure 5.16) of the same materials. Therefore, 1g showed the worst adhesion to metal.

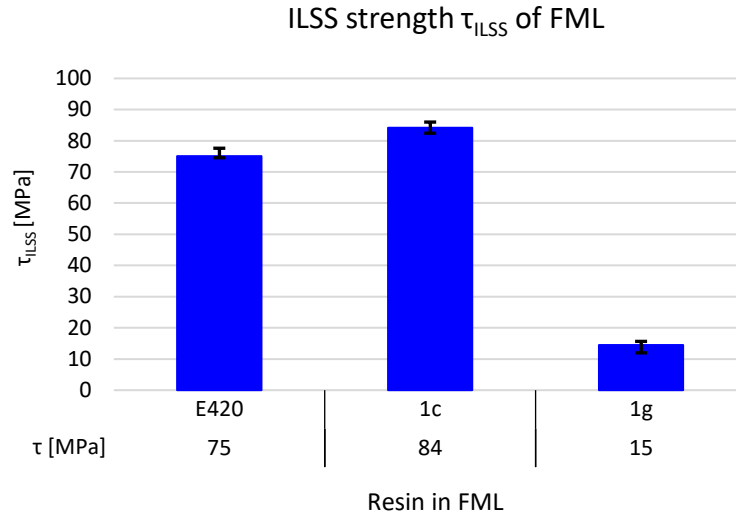


Figure 5.16: ILSS strength τ_{ILSS} of FML with different resins

Impact Resistance of FML

The FML specimens for Charpy test were made of prepreg material of the designated resin and 1050 aluminum in 0.2 mm thickness additionally. The configuration chosen was 2/1, which means that aluminum was bonded on the lower and upper side of the CFRP layer.

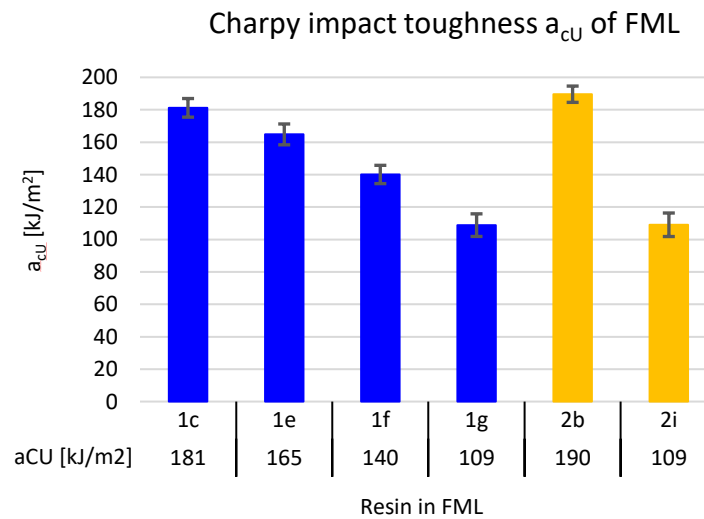


Figure 5.17: Influence of resin system on Charpy impact resistance of FML

The impact resistance decreased when more EPS70 was used. This resulted from the reduction of the adhesion to the metal surface, which has a negative effect under high-velocity impact load.

Dynamic adhesion promoter was tested with 1f and static adhesion promoter with 1e, which both did not enhance Charpy impact properties of the overall FML material.

Mechanical Performance of Woven Fabric FML with the three Resin Mixtures M1.6, M1.7 and M2.4

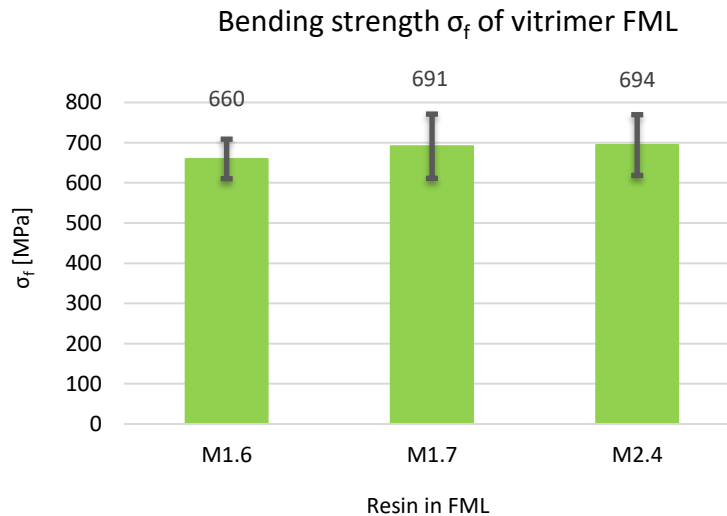


Figure 5.18: Bending strength σ_f values of woven fabric FML with M1.6, M1.7, M2.4

As can be deduced from Figure 5.18, the bending strength was similar for all three vitrimer FMLs. M1.7 led to the highest values, followed by M2.4 and M1.6. The bending strength value of FML with resin M1.6 and M2.4 was lower than that of the corresponding CFRP, and higher with resin M1.7. The statistical spread here was relatively high and taking it into account, the three materials were statistically not distinguishable.

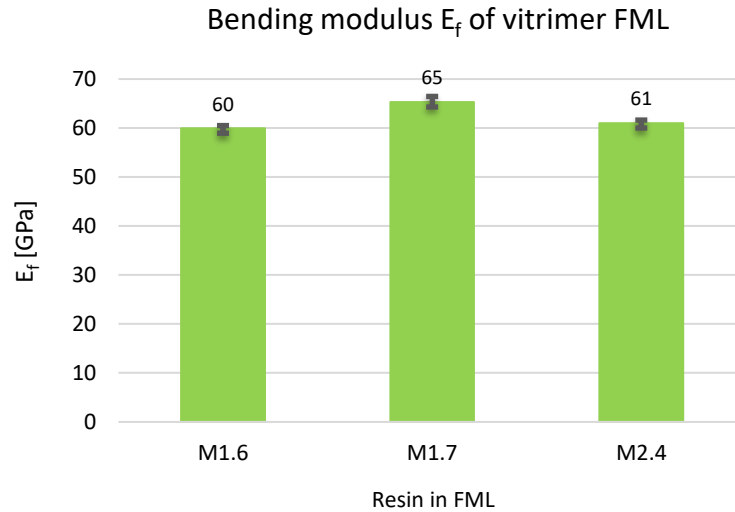


Figure 5.19: Bending modulus E_f values of woven fabric FML with M1.6, M1.7, M2.4

The bending values (Figure 5.19) of the three FMLs showed the same trend as for CFRP. The bending modulus of the FML with M1.6 and with M1.7 was about 2000 MPa higher and with M2.4 about 2000 MPa lower than those of the corresponding CFRPs. Using M1.7 as matrix, compared to CFRP the modulus increased due to the introduction of a metal layer in the middle. Using M2.4, compared to the modulus of CFRP the material lost performance due to the introduction of metal.

5.4.4 Benchmarking

Thermosetting, Thermoplastic and Vitrimer Polymers

Table 5.9 shows mechanical values for different polymers and where the vitrimers ranged.

Table 5.9: Benchmarking of polymer materials (source for values of thermoplastics: [87])

Polymer	σ_t [MPa]	E_t [GPa]	T_g [°C]	T_m [°C]	crystallinity	cost (range) [€/kg]
PP	20...40	1.1...1,6	-10...-10	168...173	semi-crystalline	1...2
PA6	50...95 (SGL: 58)	0.8...2	50...60	215...220 (SGL: 220)	semi-crystalline	2...4
PPS	50...80	3.3...4	88...93	275...290	semi-crystalline	7...13
PEEK	70...100	3.6...3.9	143...143	334...334	semi-crystalline	50-75
PESulphone	70...95	2.3...2.8	210...230		amorphous	7...13
PEI	90...100	3...3	215...215		amorphous	10...15
Phenolic resin	30-50	6-8	180-250			2...10
Epoxy resin	60-160	2.8...3.5	80-180			10...20, *, **
Benzoxazine	127	2.8...4.5	160...210			10...20
Epoxy E420	51°	3.5	159			
Epoxy VME02	76	2.8	142			
1 st resin series	18...67	0.9...3.6	23...160			
2 nd resin series	8...79	2.1...3.3	16...142			

°No higher values achievable due to the manufacturing procedure

*Automotive application: EUR 5-10/kg

**Aerospace application: EUR 10-30/kg

***VDI2536

Compared to the values of the other polymers listed, the vitrimer neat resin specimens of the first and second resin series showed medium to good tensile values depending on the amount of EPS70 used. The mechanical performance of these vitrimer neat resin specimens is discussed in detail in chapter 5.4.1.

Results and Discussion

Thermoplastic, Thermosetting and Vitrimer CFRP

Table 5.10: Benchmarking of CFRP with PP, PA6, E420 and VME02 as matrix material

Parameter	Unit	Standard	PP-CFRP	PA6-CFRP dried	E420-CFRP	VME02-CFRP
Fiber volume fraction	%	EN 2564	41	42	55	71
T_g (DSC Midpoint)	°C				159	142
Tensile strength 0°	MPa	ISO 527-5	1481	1631	1963	/
Young's Modulus 0°	GPa		98	103	127	/
3P bending strength 0°	MPa	ISO 14125 A	671	1059	1503	1726 (4P)
3P-bending modulus 0°	GPa		89	96	121	143 (4P)
3P bending strength 90°	MPa	ISO 14125 A	23	110	82	60 (4P)
3P-bending modulus 90°	GPa		4	6.3	7.4	8.9 (4P)

When the expensive VME02 resin was used as matrix material in CFRP, high mechanical performance was achieved.

Table 5.11: Benchmarking of CFRP with vitrimer epoxy matrix 1c and 1f in comparison to SGL epoxy resin E420 and SGL PA6 as matrix material

Property	Standard	Unit	E420	1c	1f	PA6
Fiber volume fraction	DIN EN 2564	%	55	55	55	45
T_g (DSC Midpoint)	ISO 11357	°C	150	135	70	54
Tensile strength 0°	ISO 527-5	MPa	1970	1830	1760	1720
Young's Modulus 0°		GPa	130	130	130	110
Compression strength 0°	ISO 14126	MPa	1430	1000	730	670
Compression strength 90°			170	170	110	120
Fracture toughness G_{Ic}	ASTM 5528	J/m ²	270	350	530	1190

As can be seen from Table 5.11, the mechanical properties of vitrimer-CFRP with resin 1c or 1f as matrix material ranged between E420 and PA6. The mechanical performance strongly depends on the polymer network. The lower the T_g and the wider the network meshes, the lower the tensile and compression performance, but the higher the fracture toughness. Using the aliphatic and long-chain disulfide components, except APhD, the T_g was lowered. Therefore, there is a trade-off between mechanical performance and dynamic properties. A reasonable T_g to maintain material performance for structural applications and ensure dynamic behavior as well might be around 100 °C.

5.4.5 Discussion

Mechanical performance at room temperature was tested on three levels: neat resin, CFRP and FML. Most tests were conducted on first and second resin series and respectively their prepreg material. Thus, the influence of EPS70 was intensively investigated in relation to different tests and types of loading. A benchmarking was conducted as well to classify the vitrimer materials in comparison to standardized polymer and composite materials. E420 and PA6 were used as reference (matrix) polymers. In addition, the mechanical performance of composite materials (CFRP and FML) with the three vitrimer resins as matrix material which showed good dynamic behavior and fulfilled the target criteria of this thesis was evaluated.

Results and Discussion

Testing the neat resin performance of first and second resin series, an increasing amount of EPS70 led to a more ductile behavior. For both resin series, the tensile and bending modulus first slightly increased and then significantly decreased with increasing amount of EPS70.

Evaluating the performance of CFRP, of course, the influence of a changed amount of EPS70 was particularly evident in matrix dominated tests. For those quasi-static tests, an increasing amount of EPS70 decreased the strength and stiffness values. When the T_g of the material was close to room temperature (testing temperature), then the effect was particularly strong. The performance of the second resin series in quasi-static tests was slightly better because when comparing materials with the same proportion of dynamic bonds, the amount of EPS70 was lower for the second series because a share of dynamic bonds resulted from the aromatic dynamic hardener APhD.

Regarding fracture toughness, EPS70 increased the G_{Ic} value of CFRP in comparison to the E420 reference. Here, when materials with same proportion of dynamic bonds were compared, the second resin series showed worse performance than the first series because its EPS70 content was lower. EPS70 had a positive influence on impact properties of CFRP.

Bending strength of hand-laminated woven fabric CFRP of the three mixtures M1.6, M1.7 and M2.4 was by about a quarter less than the bending strength of the reference material E420. The difference in performance was probably also lower because the CFRP with the three vitrimer resins was hand-laminated and the E420 woven fabric reference material was machine-made. The modulus of the three vitrimer CFRPs was approximately slightly higher compared to the value of E420 CFRP.

Evaluating the performance of FML, the values in comparison to CFRP of course were lower when the test was dominated by fiber, because the fiber content related to the entire composite is lower of FML than of CFRP due to the inserted metal. For bending in 0° , a trend reversal was observed when the T_g of the material was reached (for prepreg with 2i and 1g). Then, the value of FML was higher than of CFRP. In general, a T_g close to room temperature is problematic for the adhesion of CFRP to metal and the FML is more prone to delamination. Fracture toughness of FML was positively influenced by EPS70. There it strongly depends on whether the resin leads to higher or lower cohesion in CFRP than adhesion of CFRP to metal. In contrast to its positive influence on the impact properties of CFRP, EPS70 negatively influenced the impact properties of FML due to the negative influence of EPS70 on adhesion of CFRP to metal.

The bending strength of FMLs with the three mixtures M1.6, M1.7 and M2.4 were in the same range. M1.7 led to the highest bending strength when used in FML, followed by M2.4 and M1.6. The values of M1.6 FML and M2.4 FML were lower and the value of M1.7 FML was higher than the strength value of the corresponding FML. Regarding modulus, the insertion of metal led to an increase of stiffness compared to CFRP when M1.6 and M1.7 was used and to a decrease when M2.4 was used.

CFRP with VME02 showed mechanical performance in the upper range regarding quasi-static mechanical tests. From the prepregs of the first and second resin series, where EPS70 was used, 1e and 2f composites exhibited good mechanical values with high proportion of dynamic bonds. In the mechanical tests considered above, the performance of 1e and 2f ranged between that of the two references E420 which had the highest performance and PA6 which had the lowest performance. This also applied to the composite materials with resin mixtures M1.6, M1.7 and M2.4 where DTPA, EPS25 and G4 was used as dynamic component each.

Using the dynamic resin components in an appropriate amount, the vitrimer polymers are competitive to standard polymers as matrix material for composites. Adjusting a suitable T_g of minimum 100 °C, the network structure had sufficient mechanical properties in CFRP and an adequate adhesion to the metal component in FML.

The benchmarking showed that the pure resins with medium to high T_g of the first and second resin series achieved comparable tensile performance to established or commercially available polymers. When comparing the flexural performance of CFRP with PP, PA6, E420 and VME02, the vitrimer VME02 achieved similar or even better values than the reference epoxy resin E420. However, the higher fiber volume content in this VME02 CFRP must also be included in the evaluation. Comparing the tensile and flexural performance of 1c and 1f CFRP with the thermosetting reference E420 and the thermoplastic reference PA6, the performance of these vitrimer resins ranged between E420 and PA6. Thus, it could be concluded that these vitrimer resins would be competitive to established resins for use in CFRP.

5.5 Mechanical Performance at Elevated Temperatures

In addition to the mechanical performance at room temperature, DMA measurements were performed to identify the temperature range, where the mechanical properties do not change, and

where the material could be used in-service and respectively to get an idea at which temperature the material may be formable. For CFRP mainly the stiffness of the material changes in dependence on temperature. For FML in particular the interfacial adhesion is affected as well, and the evaluated temperatures can also be used to determine a sufficient temperature for thermal delamination (separation of CFRP and metal) for a recycling step of vitrimer FML.

5.5.1 Mechanical Stability of the CFRP (DMA Measurements)

With DMA in single-cantilever mode and heating rate of 4 K/min, the T_g of CFRP material was measured on all prepreps of the first and second resin series and on VME02 CFRP. In Figure 5.20, an exemplary DMA curve is shown.

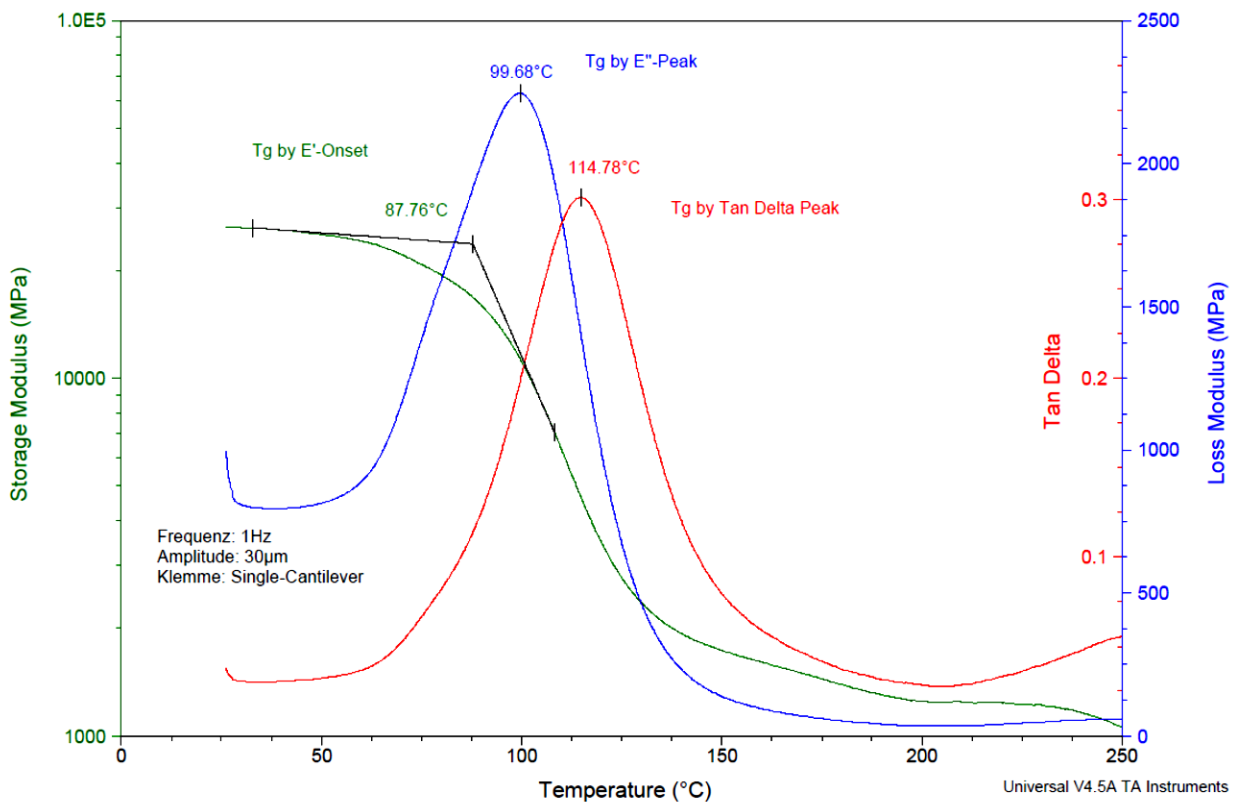


Figure 5.20: Exemplary DMA curve for 1e CFRP

The values characteristic for glass transition were evaluated and are listed in Table 6.10 in the Appendix. Depending on the resin, the broadness of the glass transition and the drop of storage modulus was different.

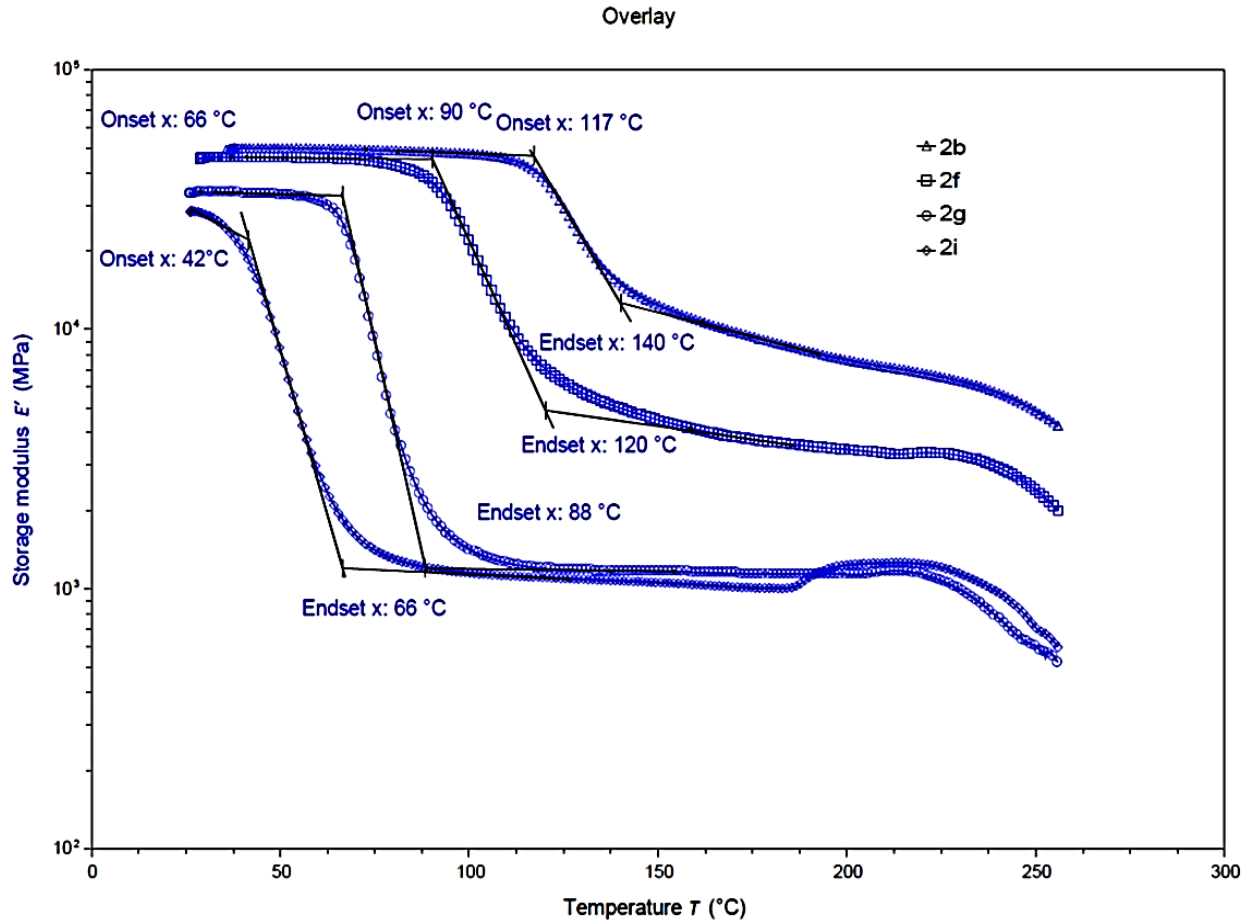


Figure 5.21: Glass transition of vitrimer CFRP of second resin series measured by DMA

As can be seen in Figure 5.21, the more EPS70 was added, the stronger was the drop of the storage modulus (lower value according to the criterion onset of storage modulus drop) and the softening of the material (stronger drop of storage modulus curve regarding their height). This means that with higher proportion of dynamic bonds and lower T_g the material becomes more flexible and thus formable, but the upper temperature limit for usage is lowered. The same trend was observed for the first resin series.

5.5.2 Mechanical Stability of the FML (DMA Measurements)

DMA is measured on FML containing resin 1c, 1g and 2i (see Figure 6.7, Figure 6.8 and Figure 6.9 in the Appendix). Due to the low T_g value of resin 1g and 2i, delamination probably already started around room temperature.

The adhesion in FML with higher T_g was stable for higher temperatures, which means in turn that for thermal delamination for recycling a higher temperature must be applied to remove the aluminum foil.

5.5.3 Discussion

The change of mechanical properties of vitrimer CFRP made of prepregs of first and second resin series was measured. Elevated temperature influenced the stiffness and adhesion of the composite materials. This information is relevant to determine the upper temperature of usage, where the mechanical performance of the material is ensured and in the case of FML to get the temperature where separation of CFRP and metal layer is easily possible. Considering CFRP, an increasing amount of EPS70 led to a more substantial drop of the storage modulus due to glass transition. The softening of the material was stronger which probably resulted from the increasing amount of disulfide groups in the material and therefore a stronger formability. As already discovered, EPS70 decreases the T_g , which means a reduction of the upper limit of in-service temperature. In terms of recycling, then separation of metal and CFRP layer is possible at lower temperatures.

5.6 Water Absorption and Media Resistivity of the CFRP and FML

Vitrimer composite materials as well as E420 epoxy thermosetting and PA6 thermoplastic composite reference materials were conditioned in different media (water/humidity, salt spray, chemicals). Mass gain was recorded and evaluated. The change of mechanical properties was measured with four-point bending test. Some DMA measurements were performed as well to determine a possible change of T_g of the polymers. In this chapter, it shall be shown that vitrimer polymers are durable in various environments, their performance shall be compared to standard polymer materials and factors of influence of their media resistivity shall be analyzed.

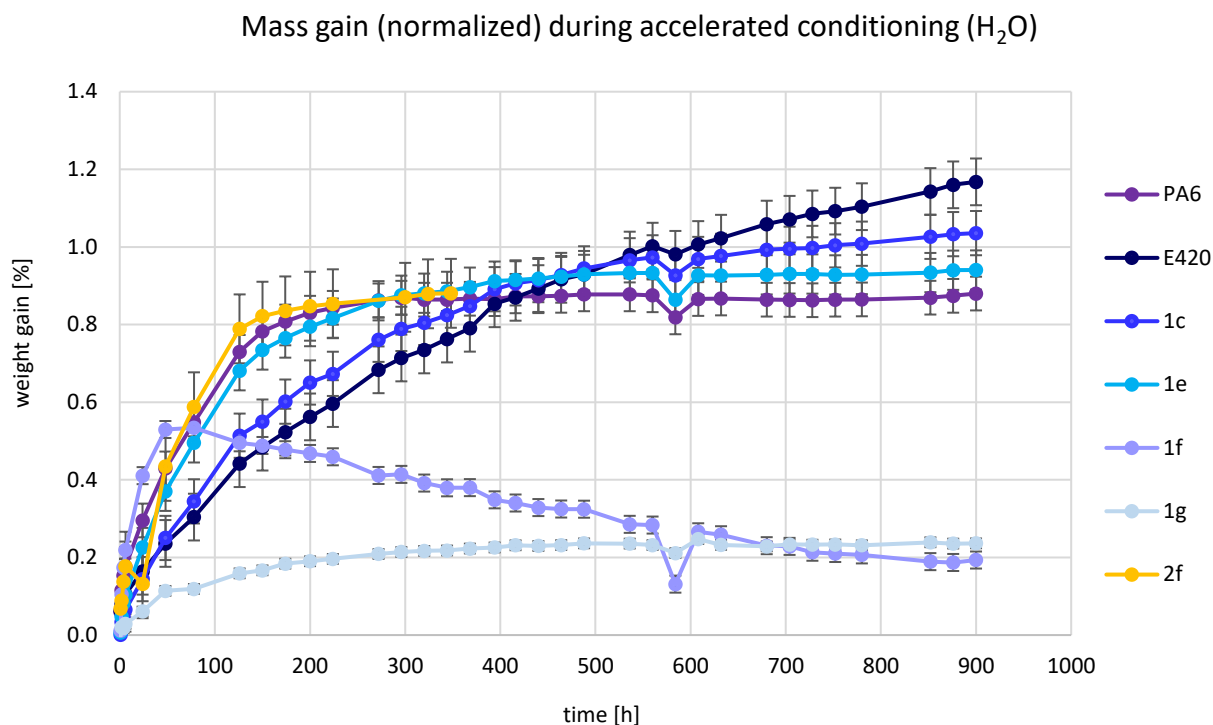
5.6.1 Accelerated Conditioning (H_2O)

Accelerated conditioning was performed based on ISO 1110. The specimens were placed in a climate chamber. After conditioning for a period of t_1 the samples were weighed, put back into the chamber and afterwards regularly weighed after a period of t_2 . When three consecutive weighing laid within a tolerance of 0.1%, the conditioning was assumed to be completed. According to the standard, under these conditions, the specimens will have acquired a moisture content equal to at least 95% of the equilibrium value. A prolonged of conditioning beyond this point would have no noticeable effect on the properties of the specimens.

Temperature was set to 70 °C to accelerate the conditioning. Relative humidity was set to 60%. Since the first 24 hours are most interesting in terms of mass change, the specimens were weighed after 1, 2, 4, 6 hours and afterwards daily (every 24 hours). The samples were taken out of the oven, dry wiped and weighed.

Normalization

Since only the resin is involved in absorption and fiber volume fraction influences the mass change of the specimen, resin mass fractions were calculated with given densities of fiber and resin. Then the average resin mass fraction was calculated, and all values were normalized to this value to be comparable. The corresponding values of the samples tested can be found in Table 6.11 in the Appendix.

Weight ProgressFigure 5.22: Mass gain of vitrimer CFRP due to accelerated conditioning (H_2O)

It seemed that when T_g decreased, the absorption rate increased (Figure 5.22). The wider the network meshes are, the more water is taken up in the material. In contrast, the saturation level does not follow the same trend. 1e and 2f had the same T_g (and proportion of dynamic bonds), but when APhD was used as hardener combined with EPS70 instead of the E420 resin system with EPS70, the network was more aromatic, and less water was taken up. Thus, aromatic rings in the polymer network probably led to less water uptake.

Different mechanisms of diffusion were observed. Most of the resins approximately followed Fick's law of absorption. However, the curve of 1g looks significantly different because the conditioning temperature was far above the T_g of the resin. After swelling like the other samples, 1g probably irreversibly degraded due to breakage of bonds, which permanently changed its absorption characteristics.

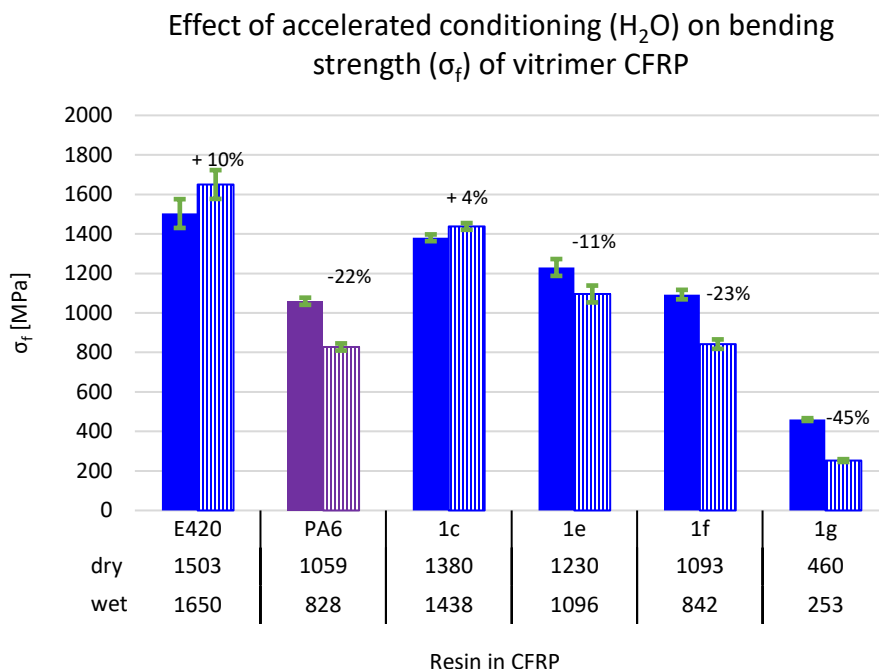
Bending Values

Figure 5.23: Effect of accelerated conditioning on bending strength of vitrimer CFRP

As seen in Figure 5.23 for the two resins with the highest mechanical performance E420 and 1c, the percentage change of bending strength from dry to wet condition was positive, which indicated plasticization phenomenon. This generally results from the interruption of Van-der-Waals bonds between polymer chains by moisture. The spaces between polymer molecules are enlarged. When the original T_g of the resin was higher than the conditioning temperature, which was the case for 1e, the strength drop was moderate. The T_g of PA6 and 1f was close to the conditioning temperature and thus the effect of water uptake on bending strength was stronger. 1g had the highest strength drop, which was consistent with the progression of mass recorded. Moisture absorption is usually accompanied by a reduction of T_g , which was confirmed for the vitrimer resins under consideration by comparing DMA measurements before and after conditioning. The

Results and Discussion

difference in T_g was about 20-30 °C. In Figure 5.24 the DMA curves of 1c before and after moisture uptake are shown as an example.

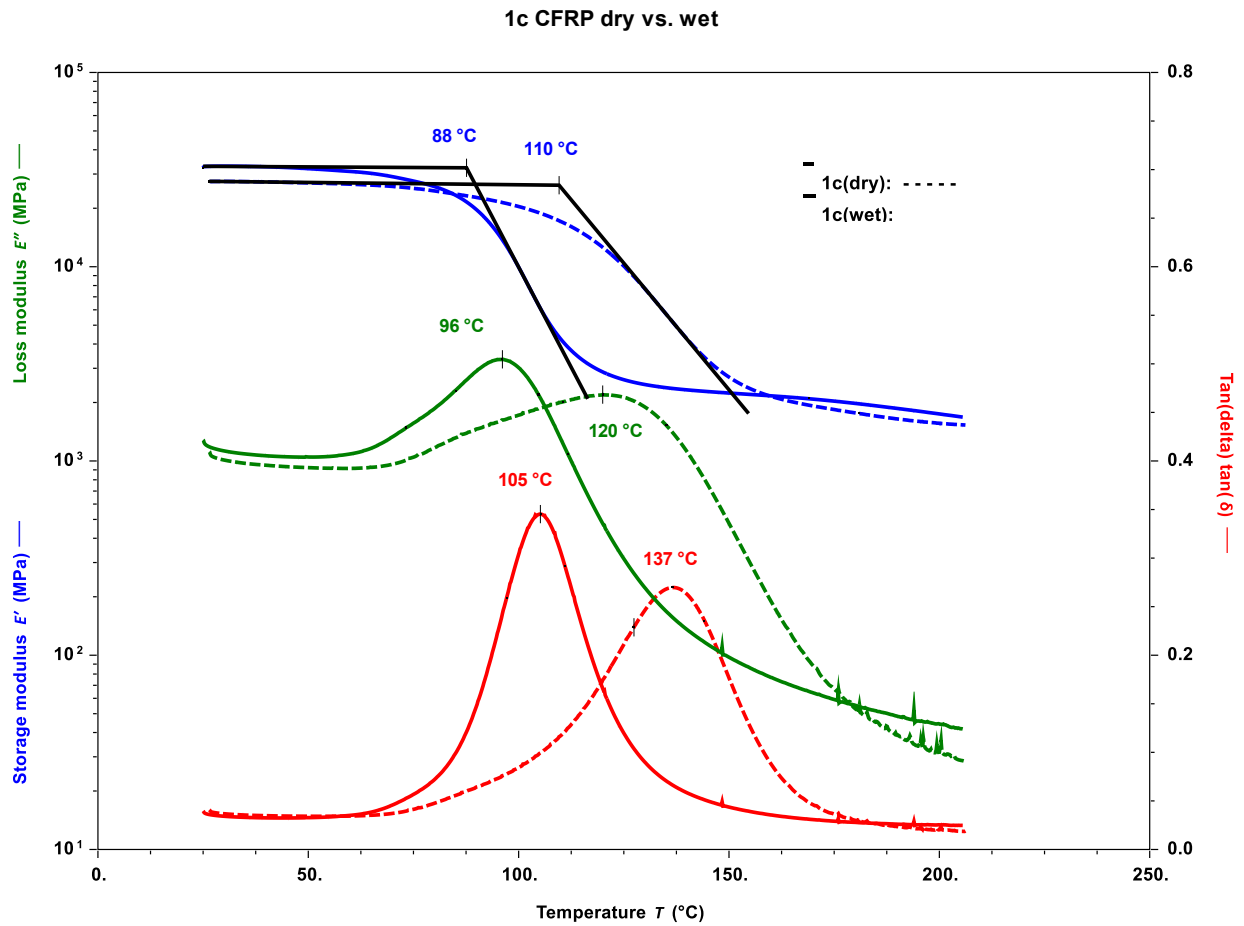


Figure 5.24: Decrease of T_g of epoxy resin 1c due to moisture uptake measured by DMA

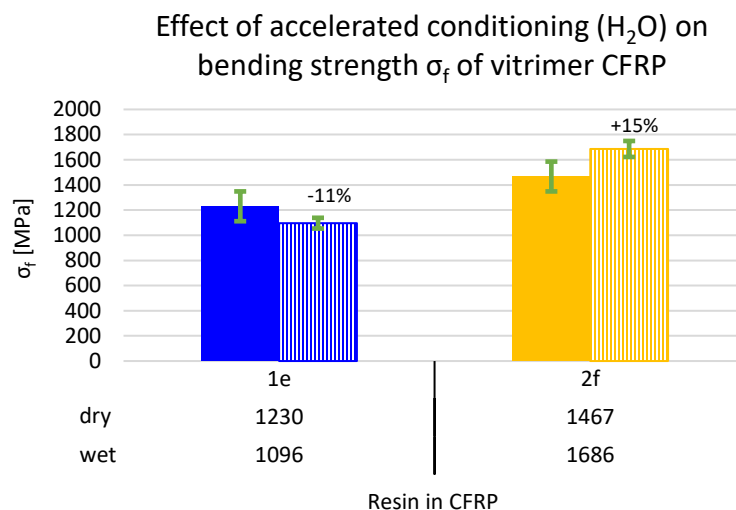


Figure 5.25: Effect of accelerated conditioning on bending strength σ_f of vitrimer CFRP

An important influencing factor is the aromaticity of the network. 2f took up much less moisture than 1e. Both resins had approximately the same T_g value and the same proportion of dynamic bonds. As seen in Figure 5.25, considering the statistical error, the strength values of the two resins before and after conditioning could not be distinguished. Considering only the mean values, 2f seemed to have undergone plasticization, as did E420 and 1c.

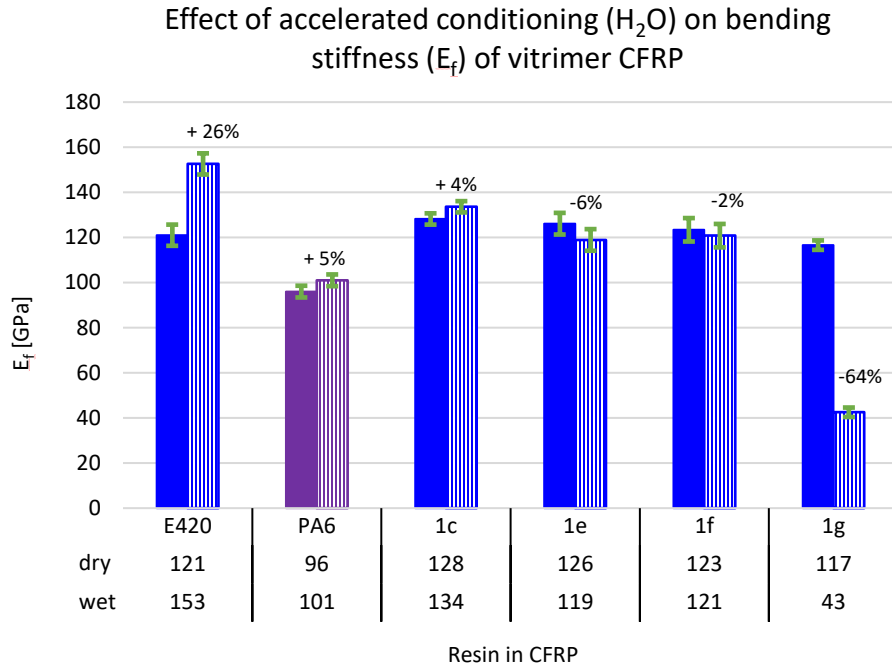


Figure 5.26: Effect of accelerated conditioning on bending stiffness of vitrimer CFRP

The change of stiffness (Figure 5.26) followed the same trend as the change of strength. The decrease of bending modulus of 1g from the dry compared to the wet condition was even more pronounced than the increase of bending modulus of E420. The values of the other resins could not be distinguished from a statistical point of view and nearly remained constant, as they did in the case of PA6.

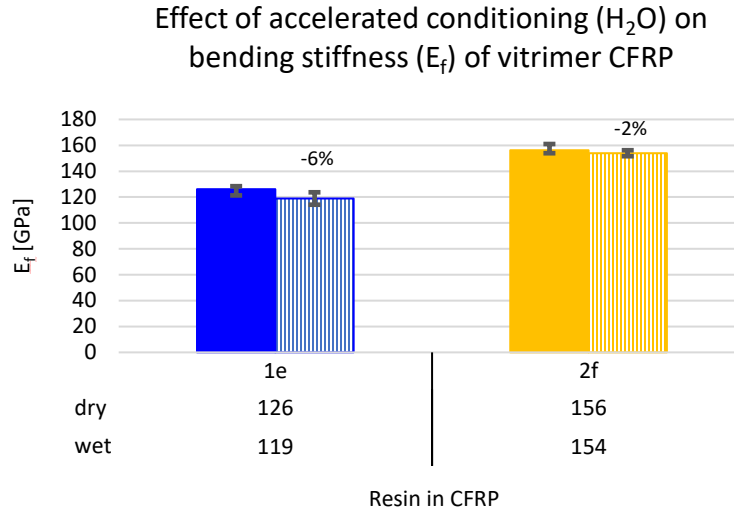


Figure 5.27: Effect of accelerated conditioning on bending stiffness E_f of vitrimer CFRP

The bending modulus of resin 2f was practically not affected by the little amount of moisture taken up (Figure 5.27).

5.6.2 Salt Spray Test ($NaCl$)

Neutral salt spray (NSS) test following DIN EN ISO 9227 was performed at 35 °C to test the durability of the material in salty and moist environments and attendant metal corrosion. CFRP specimens were tested after ten, 20 and 30 days. FML specimens were only exposed to salt for ten days because a stronger effect was expected due to the aluminum layer. After exposure, the specimens were rinsed with water and dried with compressed air. Again, the change of flexural properties was tested.

Effect on CFRP

Three sets of CFRP samples were tested each after 10, 20 and 30 days of NSS test.

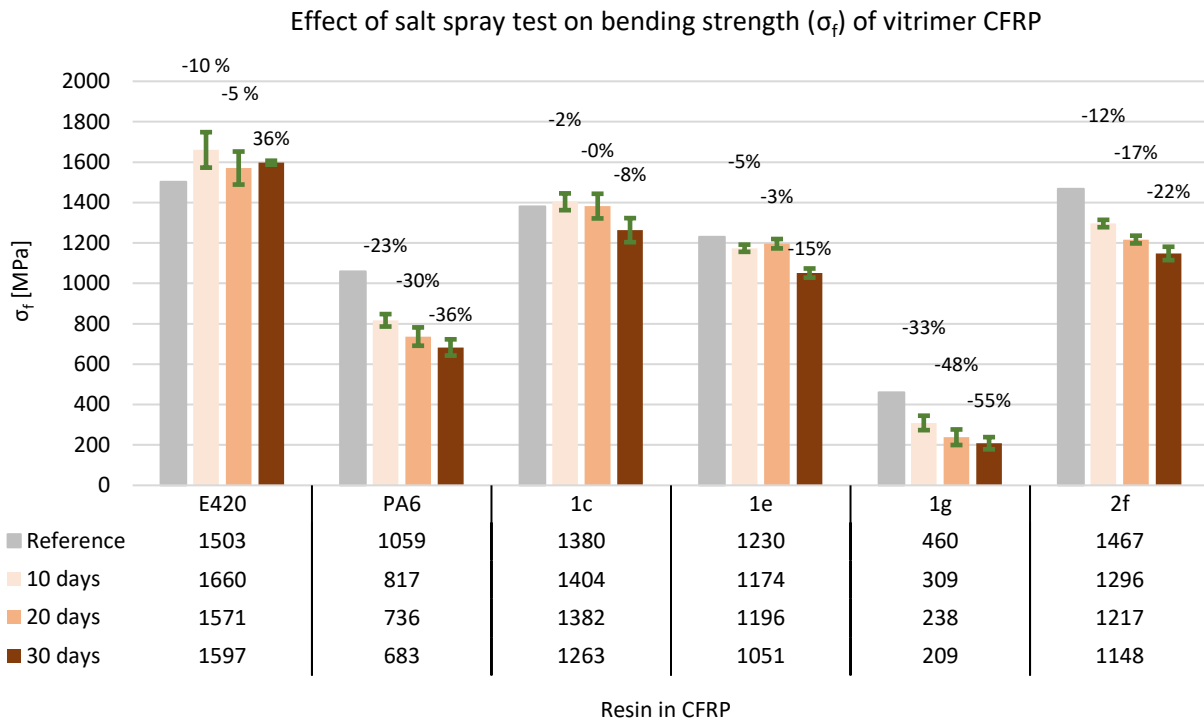


Figure 5.28: Effect of salt spray test on bending strength σ_f of vitrimer CFRP after 10, 20 and 30 days of conditioning

As shown in Figure 5.28, it was observed that the material degradation depended on the exposure time. The E420 CRRP seemed not to be affected by salt spray. The materials with low T_g (PA6 and 1g) showed the greatest strength drop. The other CFRP materials fairly maintained their strength over the tested time interval.

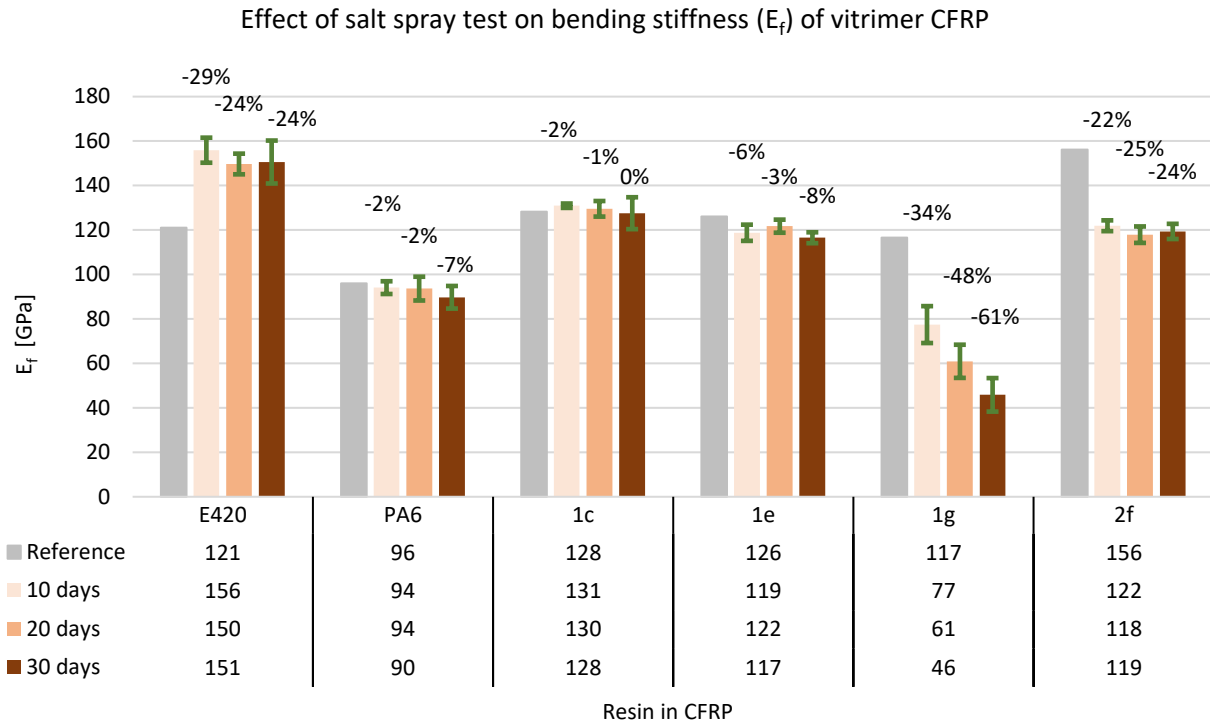


Figure 5.29: Effect of salt spray test on bending stiffness E_f of vitrimer CFRP after 10, 20 and 30 days of conditioning

Aside from E420 CFRP, whose stiffness increased due to salt spray exposure, as well as PA6 and 1c which fairly maintained their stiffness properties, the other CFRP materials showed the same decreasing trend concerning bending stiffness as for bending strength (Figure 5.29).

Effect on FML

The FML samples were much more affected than the CFRP samples, even though they were exposed to the salt spray for a much shorter time. This means that the interface between metal and CFRP was weakened more than the polymer or respectively the CFRP material itself.

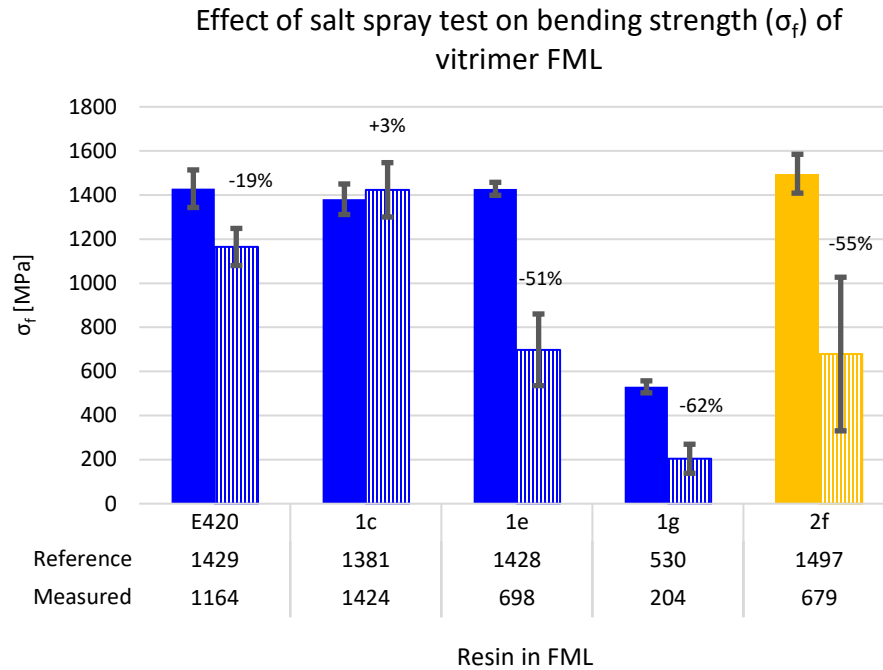


Figure 5.30: Effect of salt spray test on bending strength σ_f of vitrimer FML

As can be seen from Figure 5.30, the salt spray had a negative effect on the strength of almost all tested FML materials. Due to the moisture absorption the salt diffused into the polymer network and weakened the material. On the interface between CFRP and aluminum foil the adhesion was weakened as well. Compared to E420, the average EEW decreased when EPS70 was added. This means that less reactive groups could form covalent bonds to the metal and thus adhesive strength decreased. Hence, more water was incorporated between metal and polymer.

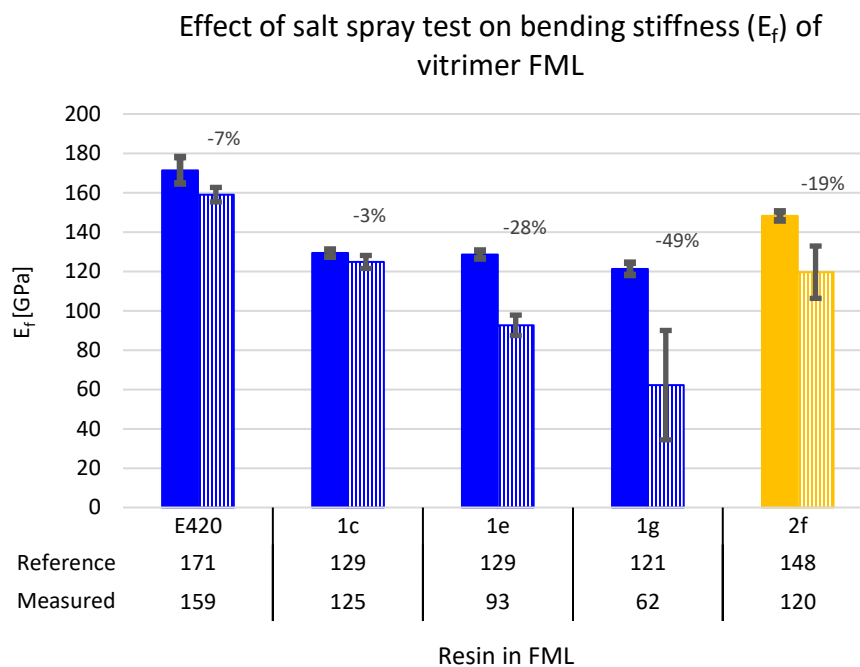
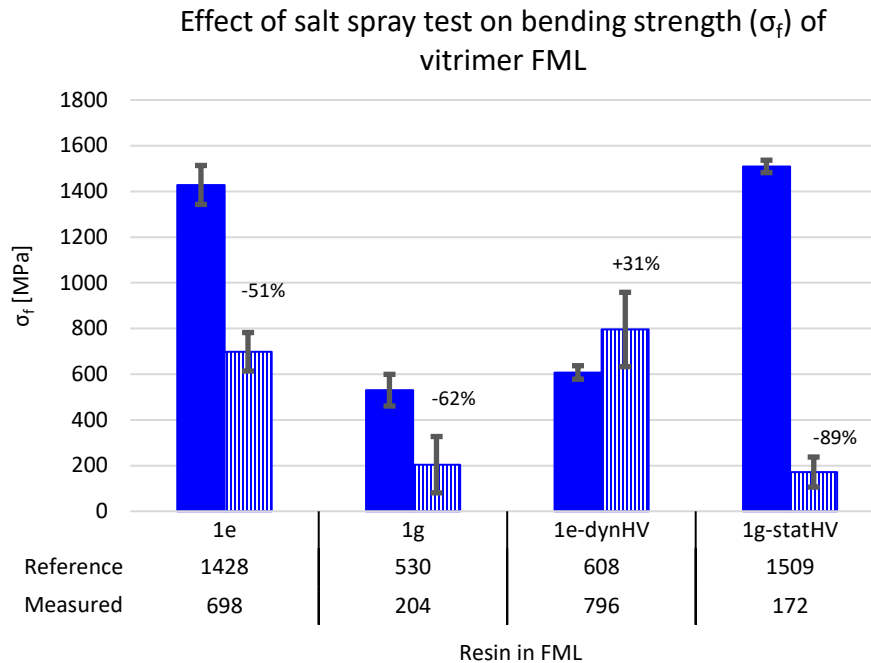


Figure 5.31: Effect of salt spray test on bending stiffness E_f of vitrimer FML

The drop in bending stiffness increased with increasing proportion of dynamic bonds (decreasing EEW), looser polymer network and decreasing T_g value of the material. The aromatic polymer 2f did not have a significant advantage over the more aliphatic 1e (Figure 5.31).

Effect of Adhesion Promoters on FMLFigure 5.32: Effect of salt spray test on bending strength σ_f of vitrimer FML

The idea to enhance the interfacial adhesion arised and therefore, dynamic and static adhesion promoters were tested (see Figure 5.32). The dynamic one contained tetrasulfides ($R - S - S - S - S - R$) which can bond to the disulfides in the polymer and silane groups which bond to the metal. The static one contained amine groups which react with the epoxy groups of the polymer and silane groups as well which react with the metal site. Comparing the reference values before NSS, the dynamic adhesion promoters even had a negative effect on the adhesion and respectively the bending strength. Considering statistical errors, no statement could be made about the effectivity of the dynamic adhesion promoter on the resistance against salt spray, whereas the static adhesion promoter strongly compensated the adhesion problem of 1g resulting from the low T_g of the material. The flexural strength was almost tripled. However, the static adhesion promoter was not sufficient for resistance against salt spray.

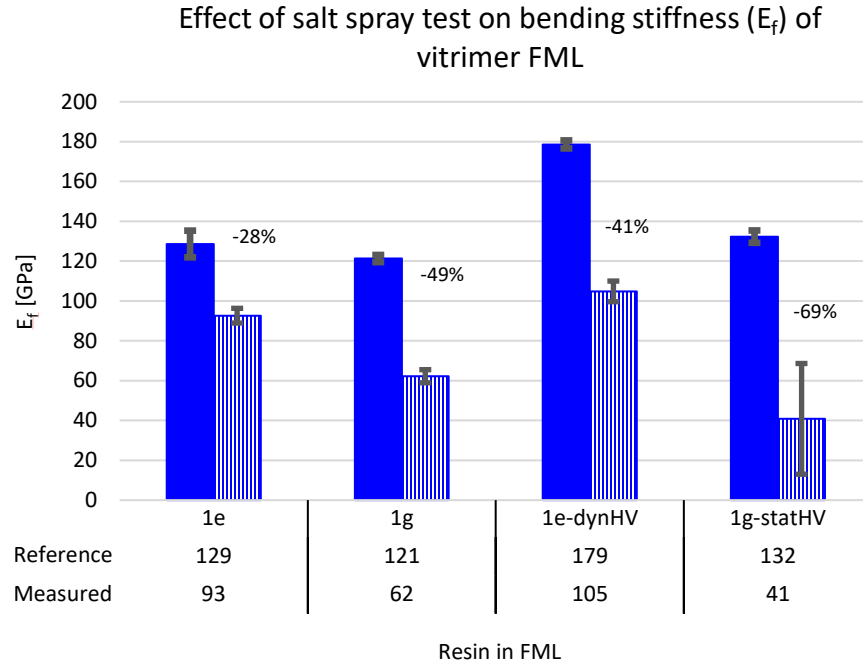


Figure 5.33: Effect of salt spray test on bending stiffness E_f of vitrimer FML

As with the bending strength, the dynamic adhesion promoter improved the bending stiffness of the 1e FML (see Figure 5.32). Here, the static adhesion promoter seemed to have a positive influence on the bending stiffness of 1g FML.

5.6.3 Media Resistivity (HCl , $NaOH$, $Ca(OH)_2$, $CaCl_2$)

CFRP specimens (of E420, PA6, 1e, 1g, 2f) were exposed to four chemicals for 30 days. The procedure was based on DIN EN ISO175:2010. Samples were placed in containers with HCl 1M (acid solution), $NaOH$ 1M (alkaline solution), $Ca(OH)_2$ (alkaline solution) and $CaCl_2$ 1 M (salt solution) which again were put in an oven at 60 °C. The chemicals were selected for the following purposes: HCl to simulate low pH environments such as in sewer pipes and acid rain infiltration, $NaOH$ to simulate corrosion damage, $Ca(OH)_2$ to simulate corrosion damage such as hydrating cement and $CaCl_2$ which is used as road salt in winter.

Mass change was recorded regularly. The temperature and duration of the test were set following EN 2489 standard.

Results and Discussion

Progression of Mass

Before weighing, the excess chemical on the surface of the sample was wiped off. The progression of mass during media exposure was measured every three days and can be found in the Appendix for all chemicals used (see Figure 6.10, Figure 6.11, Figure 6.12 and Figure 6.13).

Bending Values

The change of mechanical properties due to chemical exposure (Figure 5.34) correlated with the progression of mass recorded.

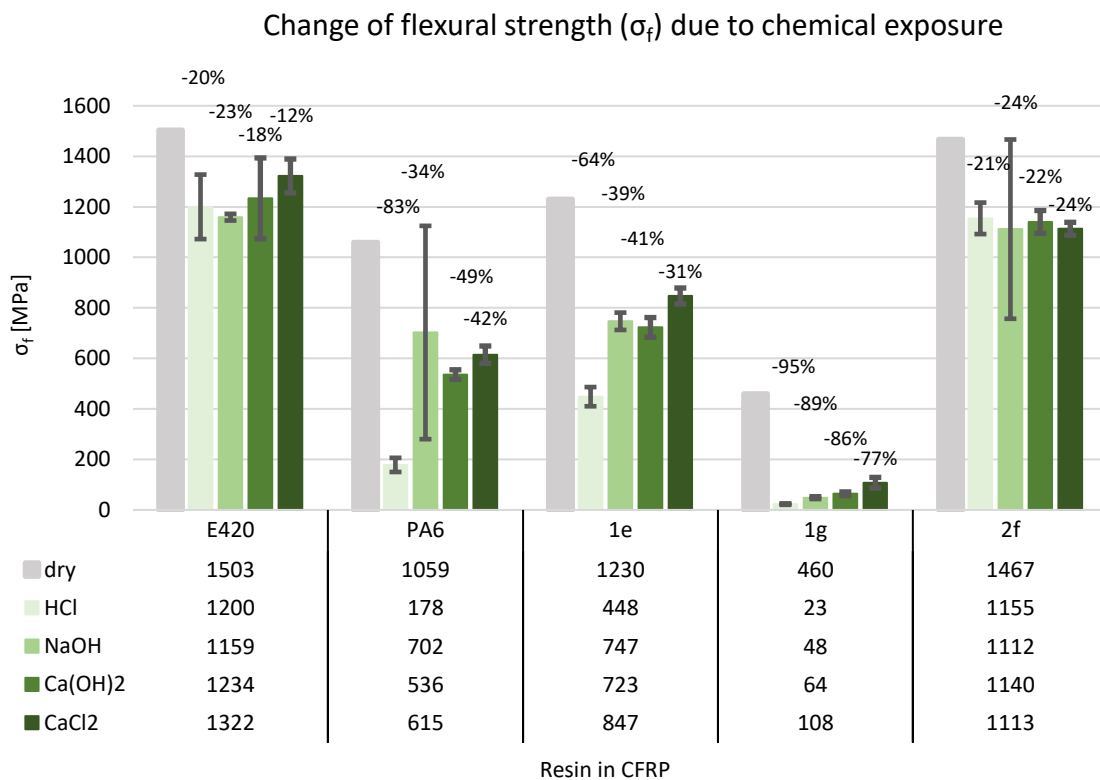


Figure 5.34: Change of flexural strength σ_f of CFRP samples due to chemical exposure

HCl seemed to be the most harmful agent for the mechanical performance of the CFRP samples tested. *NaOH* had a strong effect as well. As observed from the previous tests, when the T_g of the material decreased, the material was more affected. When the T_g of the material was below the

conditioning temperature, as in the case of 1g, the material was severely degraded by any of the chemicals. E420 had the highest resistance against the chemicals used. 1e was slightly better than PA6. The media resistivity of 2f, which had a similar T_g and the same proportion of dynamic bonds as 1e, was almost as good as that of E420. This again may mean the more aromatic the polymer network, the better the media resistivity.

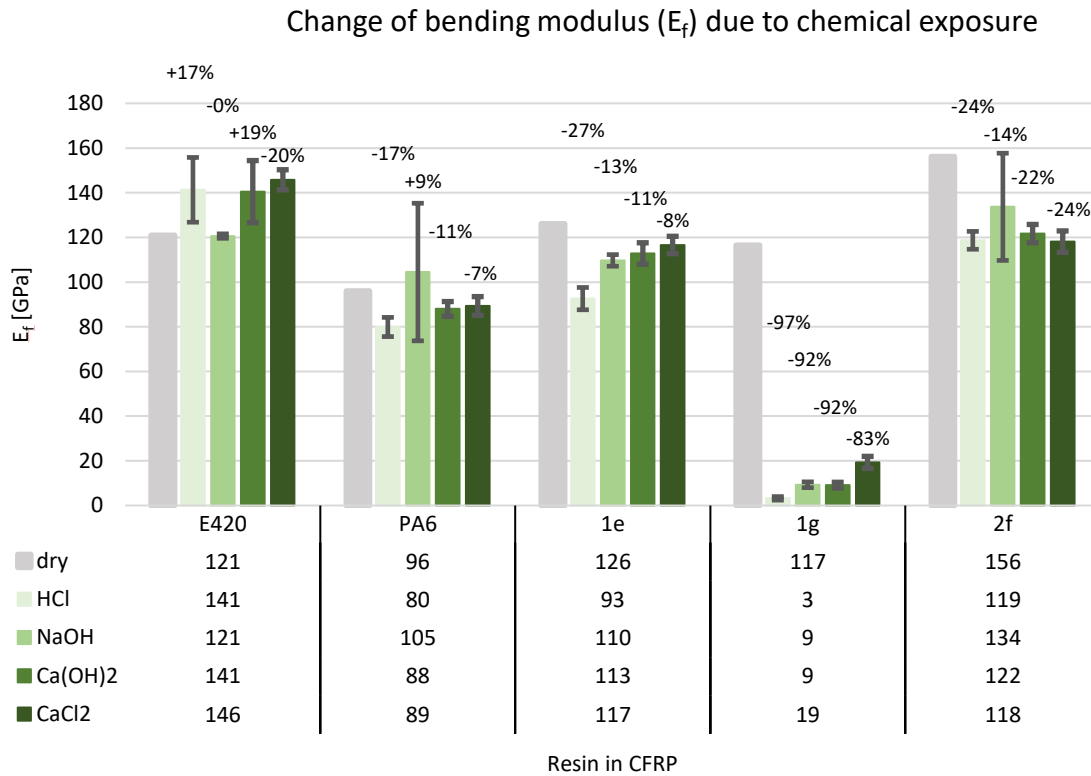


Figure 5.35: Change of bending modulus E_f of CFRP samples due to chemical exposure

Similar trends were observed concerning the bending modulus (Figure 5.35). Looking at the mean values, E420 showed anomalous behavior, but this could be relativized taking into account the statistical error.

5.6.4 Discussion

Water absorption and media resistivity of vitrimer CFRP and FML was tested and compared to reference materials with PA6 and E420. Influencing factors were investigated. Exposure to humid

Results and Discussion

environment (H_2O) led to mass gain due to swelling of the vitrimer polymers and the reference materials. Least water was taken up by 2f. After swelling, 1g showed degradation behavior by mass loss. This means that the T_g of the material must be sufficiently high (well above the temperature of use in this medium), thus especially when T_g is exceeded it also has an influence on resistivity of the material to water uptake. The mass gain did not correlate with the change of mechanical performance. E420 took up the most water. PA6 ranged in the middle. The vitrimer materials took up more water the more EPS70 was used.

Evaluating the bending test of the conditioned material compared to dry reference, E420, 1c and 2f showed a plasticization effect due to water uptake and the strength was increased. For the other materials, the strength drop was stronger the more EPS70 was used. The reduction of T_g due to water uptake was proven. The aromatic hardener APhD which was contained in 2f led to low water absorption. The bending modulus of E420 material increased; of PA6 and 1c it increased only slightly or respectively remained quite constant; of 4e and 4f it slightly decreased; and of 1g it showed a significant decrease due to T_g effect. Change of strength and modulus showed quite the same trend.

The effect of salty environment on the CFRP (10, 20, 30 days exposure) and FML (10 days exposure) composite materials was tested. Testing CFRP material after every 10 days showed a strong dependence on exposure time. PA6 and 1g CFRP showed the greatest strength drop. Due to their low T_g value they were most affected. The strength of 1e and 2f decreased as well. The other materials fairly maintained their strength or showed only small decreasing effect wherefore a good resistivity to salt could be assumed. The modulus of E420 increased, PA6 and 1c fairly maintained their stiffness and the other materials showed the same trend as for change of strength.

Although the FML materials were only exposed to salt for 10 days, they were more affected than the CFRP because the interface was significantly weakened. EPS70 led to wider meshed and less covalent bonds between CFRP and metal due to a lower EEW. Thus, more water was incorporated, and the adhesion was strongly weakened. Amine (static) adhesion promoter was tested on 1g FML to compensate the T_g effect (weak adhesion of polymer to metal). Thereby, the adhesion of dry FML was significantly improved, but no effect on resistivity of FML against salty environment was observed. The effect of tetrasulfide (dynamic) adhesion promoter was tested on 1e FML. A negative effect on bending strength of dry material was observed and no effect was ascertainable on the resistivity to salt.

Bending modulus of the vitrimer FML showed that the more EPS70 was contained, the stronger the drop of stiffness. The modulus of 2f and 1e decreased. The modulus of dry 1e FML increased when dynamic adhesion promoter was applied and the modulus of dry 1g FML increased when static adhesion promoter was used. No effect of the adhesion promoters was seen on resistivity to salt.

Chemicals $NaOH$, HCl , $Ca(OH)_2$ and $CaCl_2$ were used to evaluate media resistivity of vitrimer composite in comparison to reference materials. The change of mechanical properties correlated with the progression of mass. HCl was most harmful for the bending strength as well as $NaOH$ which showed a strong effect. When the T_g of the material was close to the conditioning temperature, the material was even more affected than already observed for H_2O and salt. E420 had the highest resistivity to the chemicals tested. The more EPS70 was used, the lower was the media resistivity. The resistivity of 2f was almost as high as of E420. The change of modulus showed the same trend as the change of strength.

5.7 Dynamic Properties

This chapter shall highlight the added value of vitrimers over standard materials. Several resin formulations were tested and compared according to their dynamic properties. First, the resin structures are explained, and their respective characteristics are discussed. An attempt is made to make a connection between network structure and dynamic properties of the polymer. Knowledge about the influence of the single component on dynamic efficiency and about how to design vitrimer resins with good dynamic properties is gained as well. The relaxation behavior, repair potential and recyclability of the resins was tested. In the end, three resins most efficient regarding their dynamic properties, which also meet the other criteria set, are evaluated. Then, bending properties of CFRP and FML of these three resins were tested to ensure their competitiveness compared to standard material regarding mechanical properties and respectively their suitability for structural composite applications.

5.7.1 Network Structure

The network structure of the vitrimer polymer influences static mechanical properties and the dynamic behavior. Depending on the static and dynamic resin components and its concentration used, the network had different characteristics. As explained in chapter 2.1.3.3, the disulfide bond and thus disulfide exchange is influenced by the substituent. Aromatic disulfide exchange is more

Results and Discussion

effective than aliphatic one. T_g is a good indicator for the aromaticity and density and respectively mesh width of the network. The more aromatic, the more rigid and less flexible is the network. Resin components with high chain length and especially aliphatic chains lead to wide meshes and low T_g values.

To characterize the vitrimer polymer network, some information or several parameters are required. A high proportion of dynamic bonds promotes the bond exchange. However, the relation between static and dynamic bonds is not meaningful alone. The distribution of dynamic bonds over the entire network and the steric conditions play an important role. Remembering Figure 4.1 and Figure 4.2 of the resin components, DTPA and APhD have only one disulfide bond in their molecular structure. In the molecular structure of G4, EPS25, and in the dynamic component of EPS70 the disulfide bridges are in the repeat unit of the molecule each and thus, those dynamic components exhibit several disulfides each. The disulfide bonds can be only in the hardener or in the resin component or in both. There are both resin mixtures with only aromatic or only aliphatic disulfide and with aromatic and aliphatic ones. The sulfur content can also be related to the total mass of the vitrimer polymer.

When the disulfides are broken up with thiol chemicals as if for recycling, the network is fragmented into smaller pieces. For this procedure, the disulfides must be accessible for the thiol chemical and the network must have a critical proportion of dynamic bonds so that the recycling of the polymer is effective. The fragment size distribution gives important information about the network structure and was measured by GPC.

5.7.2 Relaxation Behavior

Relaxation behavior was measured using DMA in three-point bending mode. This method was applied to quantify the dynamic behavior of the material and to get an idea of the time frame of forming processes. The decrease of storage modulus G was measured over time under isothermal temperature condition. The relaxation time is defined as the time when the normalized modulus G/G_0 reaches the value $1/e$.

Influence of Fiber

The first phenomenon observed was the influence of fiber (content) on relaxation time. The relaxation time of the pure resin VME02 was found in literature with a value of 0.52 minutes at 180 °C. [1] In contrast, UD-CFRP with VME02 as matrix is said to have a relaxation time of 12.50

minutes at 180 °C. The added fiber effectively lowers the content of dynamic material in total and acts as a physical barrier for dynamic bond exchange.

When the same resin 2f was used once in UD-CFRP and then in comparison in woven fabric CFRP, the influence of the different fiber geometries could be observed. There was a huge difference as can be seen from Table 5.12.

Table 5.12 Influence of fiber geometries on relaxation (with resin 2f)

Resin 2f	UD-CFRP	woven fabric
Proportion of dynamic bonds	50%	50%
Residual Modulus 10 min @ 180 °C	7%	45%
Residual Modulus 1 h @ 180 °C	2%	33%

Influence of EPS70

The influence of EPS70 on the relaxation time was measured as well (see Figure 5.36). For UD-CFRP made of prepreg, the material was tested in 90 °C direction to fiber orientation.

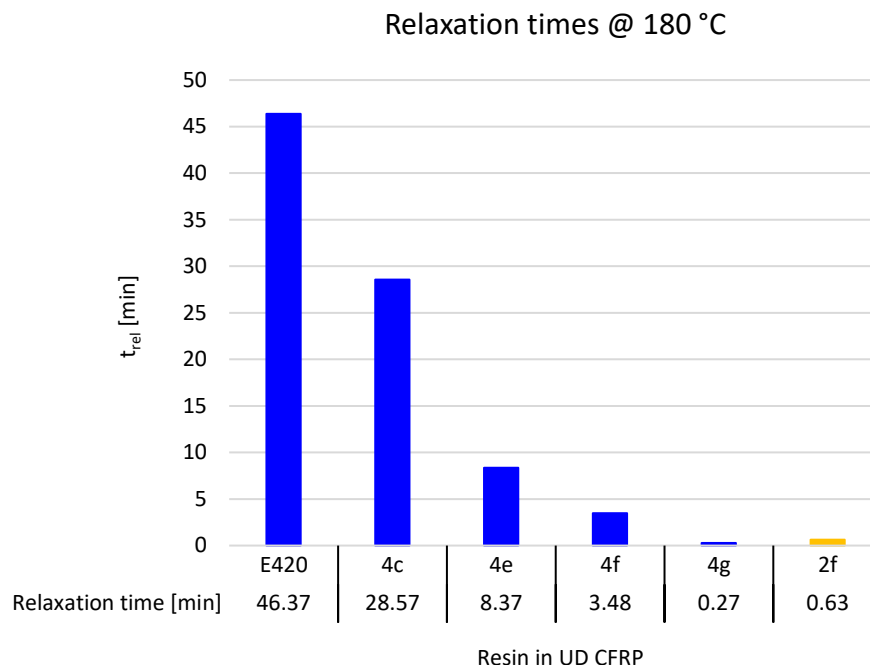


Figure 5.36: Relaxation times of UD CFRP of first and second resin series

From resin E420 ($T_g \approx 150$ °C) without EPS70 to 1g ($T_g \approx$ RT) with 100% EPS70 as component A, the relaxation time significantly decreased, and the proportion of dynamic bonds increased. 1c and VME02 had approximately the same T_g around 130 °C. 2f contained aromatic and aliphatic disulfides due to the combination of EPS70 and APhD. 2f and 1e had a similar T_g (≈ 100 °C) and the same proportion of dynamic bonds (50%). However, the relaxation of 2f was much faster. Comparing the first and second resin series, concerning relaxation behavior of vitrimer CFRP, EPS70, which is much cheaper than APhD, can be used as an alternative when a slightly lower T_g value is accepted; or a longer time range for relaxation for a similar T_g . It should be noted that the increase of temperature is limited by the degradation temperature.

When EPS70 was used with Araldite and Aradur in mixture 4c in the same stoichiometric amount (30%) as EPS25 in mixture 13, both as matrix in woven fabric CFRP to be comparable, both resins had nearly the same ΔT (55 °C, 56 °C); EPS25 led to stronger relaxation than EPS70.

Influence of Temperature

Depending on the T_g , the difference to the measurement temperature varied. Here, ΔT was defined as the difference between measurement temperature and endset of glass transition. When ΔT was increased, the relaxation accelerated. When 1e for example was measured at 180 °C ($t_{rel} = 8.37 \text{ min}$) and at 200 °C ($t_{rel} = 4.93 \text{ min}$), the relaxation time was lowered significantly.

The influence of the other components on relaxation was measured as well. The progression of the curves varied widely. The materials had either faster or slower relaxation and higher or lower residual modulus after the total measurement time of 60 min. Since a fast relaxation was favored and the relaxation time $t(G/G_0 = 1/e)$ was not reached by all specimens, focus was laid on the relaxation ability after 10 min.

The residual modules of all other resin mixtures after 10 and 60 minutes at 180 °C are shown in Table 6.12 in the Appendix. In Table 6.13 in the Appendix relaxation measurement results at further temperatures including also the minimum and maximum storage modulus and the difference of the measuring temperature to the T_g endset of the respective resin are represented.

Influence of EPS25 (DB2)

The higher the content of EPS25 was, the stronger the relaxation (lower residual modulus after 10 min). This makes sense, since both a higher proportion of disulfide bonds and a widened network favour relaxation.

Influence of DTPA (DH2)

The higher the content of DTPA was, the stronger the relaxation. With 30% DTPA (resin 23) as hardener, the proportion of dynamic bonds was lower than with 30% EPS25 (resin 13), whereas the relaxation was stronger although T_g of mixture 23 was higher than of mixture 13. This may indicate, for example, that the distribution of dynamic bonds may have been better, or the steric condition may have been more suitable for disulfide exchange.

Influence of Static Base Resins

Comparing the influence of static base resins on relaxation, Tactix (M2.1) had the slowest relaxation, followed by EPN (51) and Araldite (13). The explanation can be found in the T_g value

Results and Discussion

which showed a correlating trend (highest for M2.1 and lowest for M13). The endset of glass transition of the resin with the highest T_g value (M2.1) here was 170 °C. This means the measurement temperature of 180 °C was above the glass transition for all materials.

Influence of Dynamic Hardeners

Comparing mixture 22 (15% DTPA) and M2.3 (15% G4), the same stoichiometric amount of G4 had a much stronger effect on relaxation compared to DTPA. Comparing mixture 23 (30% DTPA) and M2.2 (30% G4), the same stoichiometric amount of DTPA led to much stronger relaxation than APhD. This means that G4 had the strongest effect on relaxation, followed by DTPA and APhD.

Taking the ΔT into account, the difference from the endset to the measurement temperature was much higher for M2.3 (95 °C) than for 22 (23 °C), which, again, indicates that when evaluating the relaxation effects, ΔT plays a major role. ΔT for 23 (47 °C) was only slightly higher than ΔT for M2.2 (35 °C), but here also the mixture with the higher ΔT had the significantly stronger relaxation.

Influence of APhD

As expected, APhD led to significantly stronger relaxation than Aradur due to its dynamic nature.

Mixtures with 20% Proportion of Dynamic Bonds set

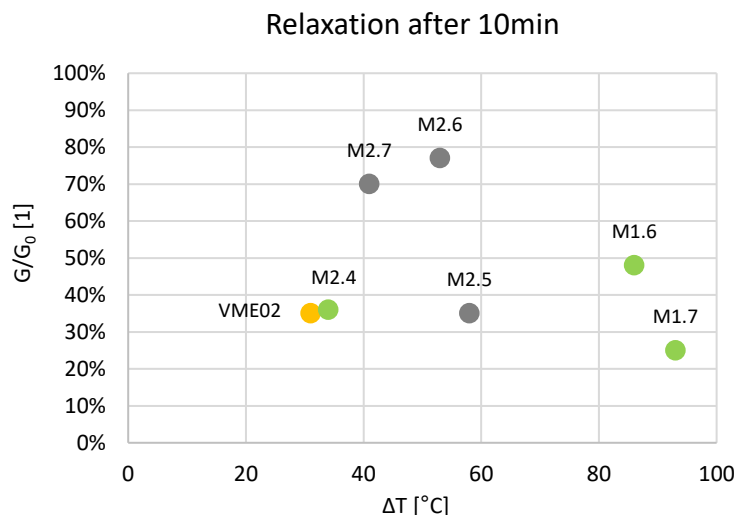


Figure 5.37: Relaxation after 10 minutes over ΔT for mixtures with 20% proportion of dynamic bonds

Although it had been noted in some cases before in this thesis, the relation ‘the higher ΔT , the stronger the relaxation’ did not apply when different resins were compared with each other as can be seen in Figure 5.37. Apparently, the network structure regarding the distribution of the disulfide bonds and the steric conditions (e.g., mesh widths, aromaticity) are contributing factors to relaxation ability or speed.

Multi-Component Mixtures

Taking the target properties into account, only resin mixture M1.7 with 27% EPS25 and M2.4 with 8% G4 led to stronger relaxation than the reference material VME02 with 100% APhD.

5.7.3 Flow Tests on Vitrimer Neat Resin to Assess Reparability

The flow tests were conducted on neat resin to assess their flow and repair properties. The better the resin flows, the better the reparability is expected especially of vitrimer CFRP. Two pieces of cured resin were put onto each other, bonded together and pressed into a thaler shape. Temperature, pressure and time were increased stepwise to approach a suitable parameter combination for each resin mixture. The thalers were cooled down below T_g under pressure. The

Results and Discussion

polymers with DTPA and APhD generally required higher temperature and pressure than the polymers with EPS25 and G4. The thalers were evaluated by their diameter, thickness, homogeneity and surface smoothness.

First, the influence of the static base resins was tested by comparing the mixtures shown in Figure 5.38 (each containing EPS25 as dynamic component).

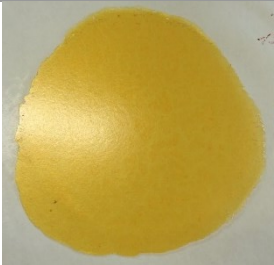


13 (70% Araldite)	51 (70% EPN)	M2.1 (70% Tactix)
150 °C	190 °C	200 °C
2 bar	5 bar	5 bar
20 min	25 min	50 min
		

Figure 5.38: Influence of static base resins on flow behavior tested with mixture 13, 51 and M2.1

The best result was achieved by Araldite. Its thaler had the biggest diameter, a good homogeneity and smooth surface, which indicates good flowability. For EPN and Tactix, the result was quite bad. Their thalers were crumbly and no good cohesion was observed. The surface was quite rough. The latter two resins probably negatively influenced the steric conditions for disulfide exchange in the polymer network.

Then, the influence of the dynamic hardeners was tested on flowability. For this purpose, mixtures VME02, M1.6 and M2.4 with 20% share of dynamic hardener each were used and the results are presented in Figure 5.39.









VME02 (APhD)	M1.6 (DTPA)	M2.4 (G4)
200 °C	180 °C	150 °C
5 bar	5 bar	3.5 bar
45 min	35 min	25 min
		

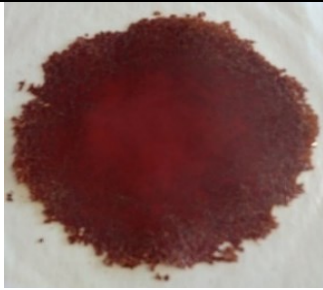


Figure 5.39: Influence of dynamic hardeners on flow behavior tested with mixtures VME02, M1.6 and M2.4

Looking at the thalers, APhD offered the greatest resistance against forming. The aromaticity of the network was quite high. VME02 remained relatively solid and stiff even at high temperature (well above T_g) and pressure. If fibers would be added to create CFRP material, the reparability would be expected to be quite bad. The thaler was quite thick but at least the two pieces of neat resin were fully bonded to one piece. DTPA and G4 led to better flowability.

Furthermore, flow test was conducted for all optimized mixtures; except for M1.4 and M2.3 because their T_g value was far too low compared to the target value set. The results are presented in Table 5.13. Satisfactory results were achieved by M1.6, M 1.7, M 2.4, M 2.6 and M 2.7. The bad flow properties due to EPN and Tactix resembled their negative influence on relaxation. The positive influence of APhD on relaxation did not correlate with its (negative) influence on flowability. The very low viscosity of M2.6 at the temperature set for flow test must be emphasized.

Table 5.13: Flowability of optimized resin mixtures

Resin	Composition	Parameters	Resulting thaler
M 1.1	EPS25 (40%) + Tactix (60%) / Aradur (70%) + DTPA (30%)	150 °C 3 bar 50 min	
M 1.2	EPS25 (40%) + Tactix (60%) / Aradur (90%) + APhD (10%)	200 °C 5 bar 45 min	
M 1.3	EPS25 (50%) + EPN (50%) / Aradur (80%) + APhD (20%)	150 °C 5 bar 30 min	
M 1.5	Araldite (100%) / Aradur (50%) + APhD (50%)	180 °C 3 bar 30 min	
M 1.7	EPS25 (27%) + Araldite (73%) / Aradur (100%)	150 °C 2 bar 10 min	

M 2.5	EPS25 (16%) + Araldite (84%) / Aradur (55%) + APhD (45%)	180 °C 50 bar 5 min	
M 2.6	EPS25 (16%) + Araldite (84%) / Aradur (77%) + DTPA (23%)	150 °C 1.5 bar 10 min	
M 2.7	EPS25 (16%) + Araldite (84%) / Aradur (97%) + G4 (3%)	150 °C 2.5 bar 15 min	

5.7.4 Recycling of Vitrimer Neat Resin

By means of pre-testing, several recycling agents were tested concerning their effectivity. The aim was to find an alternative to harmful chemicals previously used in literature such as 2-ME, in addition to hazardous solvents such as DMF, and also to create resins which are recyclable using less harmful Thiols (which are less toxic to the environment and to human health). Therefore, the following chemicals with $-SH$ functionality were compared.

Ethylene glycol bis(3-mercaptopropionate), glycol dimercaptoacetate (Evabopol[®] 120) (Figure 5.40), 2-ethylhexyl mercaptoacetate, 2-aminoethanol and dithiotreitol (DTT) were dissolved in *NaOH* and water because the thiol-disulfide exchange prefers alkaline conditions. The most effective chemicals were DTT and glycol dimercaptoacetate purchased from Bruno Bock, but the former one has extremely high cost and has therefore not been further considered. The pH value was set at 10-12.

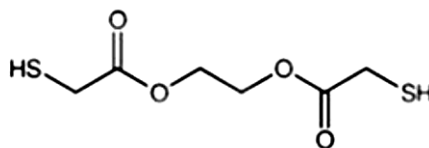


Figure 5.40: Molecular structure of recycling chemical glycol dimercaptoacetate [124]

Recycling of Mixtures with EPS70

From the first and second resin series with EPS70, recycling was tested for the neat resin specimens 1c, 1e, 1f, 1g, 2b, 2f, 2g, 2i and E420 as reference. The resin specimens were put in the recycling solution in a beaker each, which was heated in an oven. The temperature for recycling was limited due to the evaporation of the recycling solution. By testing at different temperatures, it was found out that the resin material has only significantly been affected by the chemical when the temperature was above T_g . Consequentially, recycling was possible for 1f, 1g, 2g and 2i whose T_g (around room temperature for 60% proportion of dynamic bonds and 70 °C for 70% proportion of dynamic bonds) was sufficiently low. The maximum temperature the oven was set to was 120 °C. The reference material E420 did not show dissolution. The dissolution times are shown in Table 5.14.

Table 5.14: Dissolution times (recycling) of resins of first and second series and E420

Resin		Time of dissolution [h]
2i		6 < t < 8
2g		6 < t < 12
1g		t > 48
1f		t > 48
1e		No dissolution
E420		No dissolution

It was observed that the resin materials of the second series were more prone to dissolve or dissolve faster than those of the first series. This phenomenon was investigated further. After exposure to the recycling solution for some hours, polymer 1g could be broken down into crumbs

by crushing the material with a spatula. The dimensions and weight of specimen 1g and 2i were measured and compared (see Figure 5.41).

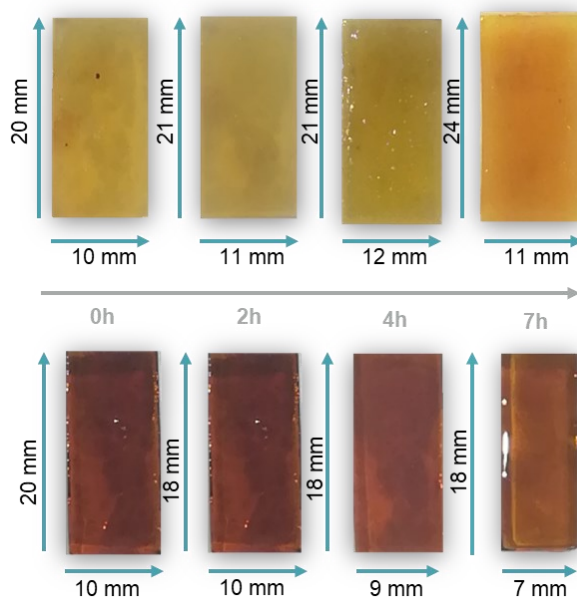


Figure 5.41: Dimensional changes of resin specimen 1g (upper, yellow) and 2i (lower, brown) during recycling

From Figure 5.41 and Figure 5.42, the same trend can be observed. While specimen 1g swelled and gained mass, specimen 2i dissolved.

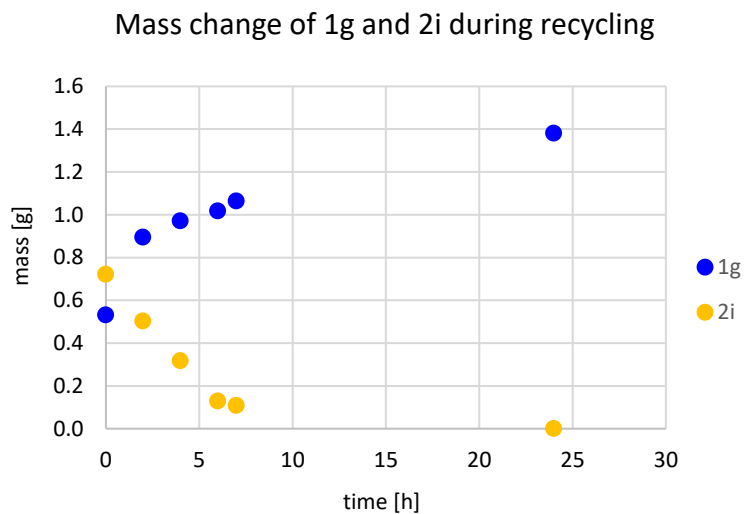


Figure 5.42: Mass change of resin specimen 1g and 2i during recycling

This experiment was repeated for the polymers 1f and 1g with magnetic stirring at 70 °C (Figure 5.42). It was observed that in approximately 12 h both polymers first swelled and only dissolved afterwards. The reason is the different network structure of the first and second resin series. It seems that the steric condition for penetration of recycling agent and reduction of disulfide by the thiol chemical was more favorable for the resins of second series. GPC measurement was conducted for the dissolved polymers 1g (Figure 5.43) and 2i (Figure 5.44) to compare the distribution of molecular mass of the network fragments after recycling.

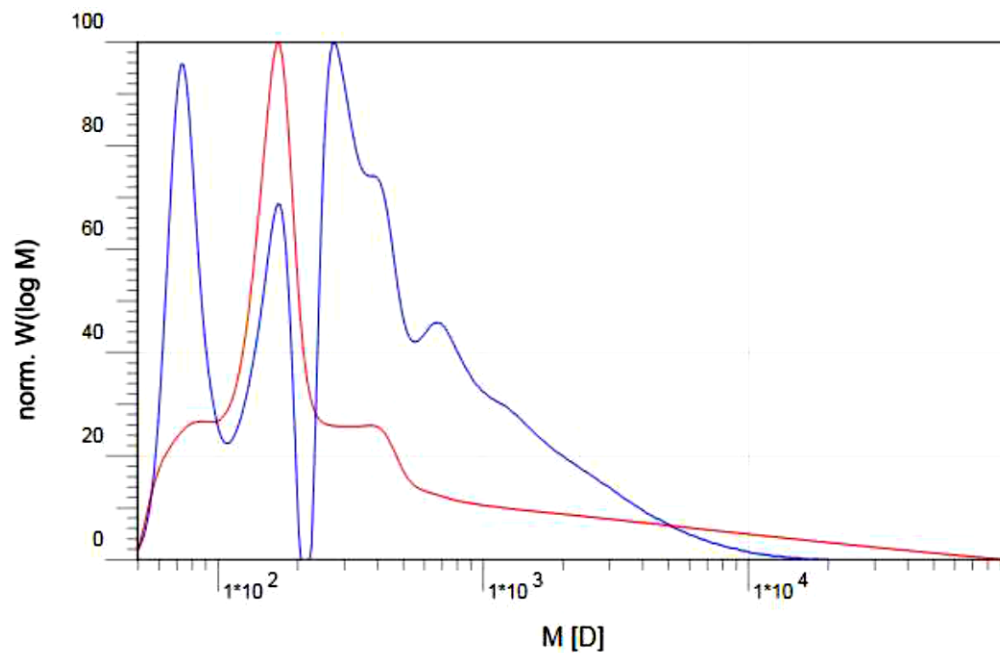


Figure 5.43: GPC measurement of dissolved resin 1g with RI detector (red) and UV detector (blue)

The GPC measurement shows that dissolving resin 1g results in fragments with different sizes. The first peak may be assigned to the THF eluent used. Both detectors record the same species.

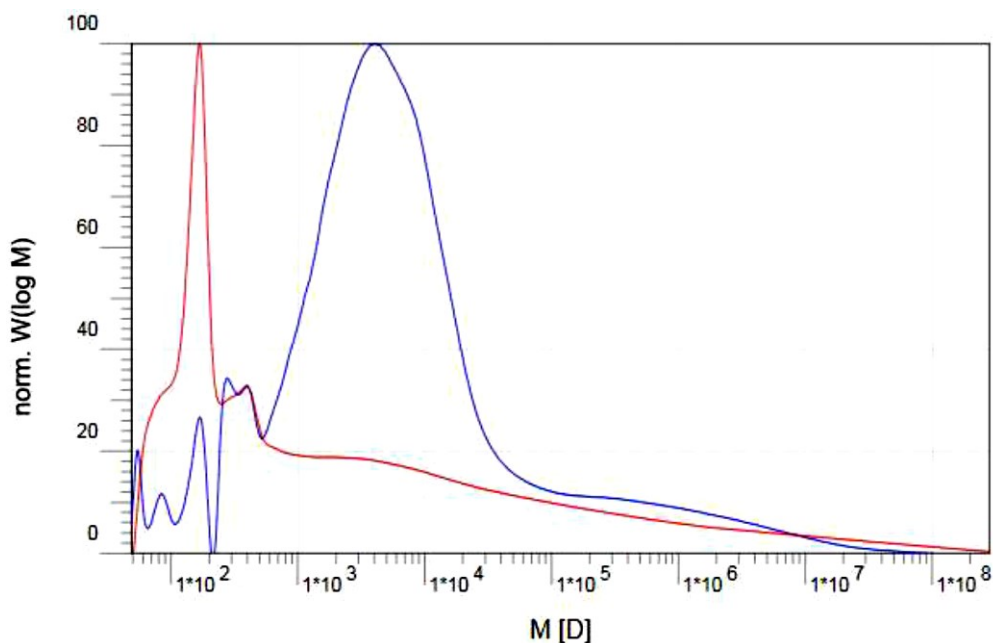


Figure 5.44: GPC measurement of dissolved resin 2i with RI detector (red line) and UV detector (blue line)

The fragments of 2i had a larger fragment size distribution. The UV signal was proportional to the number concentration, while the RI signal was proportional to the mass concentration of eluting chains. UV detectors show a signal when polymers containing unsaturated bonds, aromatic groups or functional groups with heteroatoms are present.

Calculating the value of polydispersity 3.52 was obtained for 1g and $3.04 \cdot 10^2$ for 2i. If the polydispersity $D > 2$, the fragments of the examined sample are widely distributed. In this case, both resins were dissolved into several species of polymers. 2i fragmented into a wider range of oligomers than 1g.

Recycling of Mixtures with EPS25, G4, APhD and DTPA

Mixtures M1.6, M 1.7, M 2.4, M 2.6 and M 2.7 were tested because of their good flow and presumed repair properties, and M1.1, M1.3 and M1.5 all under the same conditions. A small piece of cured resin was put into the recycling solution which then was heated to 90 °C on a heating plate (Figure 5.45).

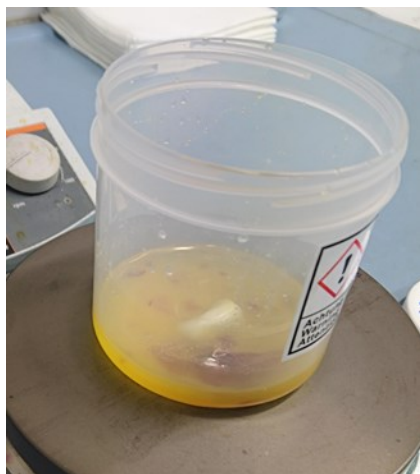


Figure 5.45: Dissolution of vitrimer resin on heating plate

The results were checked after time intervals of 24 hours where the solution was heated for 6 hours per day. M1.7 and 2.6 completely dissolved after one day. M1.5, M1.6, M2.4 and M2.7 took twice the time for dissolution. M1.1 and M1.3 did not fully dissolve even after 6 days.

For M1.5, M1.6, M1.7 and M2.4 containing one dynamic hardener component each a GPC analysis with two samples ($n=2$) was performed to obtain the fragment size distributions. The bigger the fragments, the smaller is the volume of elution. M1.5 and M1.6 have smaller mesh widths because APHD and DTPA have shorter chain lengths. M1.7 and M2.4 have bigger mesh width because EPS25 and G4 have longer chain length.

The GPC curves of both resins M1.5 and M1.6 shown in Figure 6.14 and Figure 6.15 in the Appendix are quite similar, from which it may be concluded that the fragment sizes might be similar, too. For both resins, there is a main peak which may indicate a quite homogenous distribution of disulfide groups in the network.

Using EPS25 and G4, the GPC signal shown in Figure 6.16 and Figure 6.17 in the Appendix indicated that smaller and bigger fragments than the main peak were present. This results from the small repeat unit present in G4 and EPS25 and from the comparatively high chain length of those two hardener molecules.

The RI detector is generally better able to detect fragments of different sizes but is not that sensitive if only a small amount of substance is present. The UV detector is more sensitive to the difference in molecular structure and can determine those more precisely but is not able to detect

any molecular structure. The results are only comparable to each other and to the reference substance polystyrene.

All resin mixtures showed a maximum at nearly the same volume of elution, which indicates that mainly one type or size of fragment was formed. The thiol chemical may have penetrated the network better and the disulfide bonds may have been more accessible for the reactive thiol group due to the wider meshes of M1.7 and M2.4. Comparing these results with the results from the relaxation test, it seems that rather the good flexibility due to a wide meshed network is decisive than the distribution of disulfide bonds. Altogether, all four dynamic hardeners lead to appropriate recycling efficiency.

5.7.5 Interim Conclusion

The selection of those three mixtures was made using an evaluation matrix (Table 5.15) containing qualitative criteria concerning the thaler appearance, T_g , cure time, relaxation in CFRP, required pressing parameters for flow test, cost and recycling effectivity. All criteria were scored with a score from one to five points and weighted resulting in a total score. The flow properties were given the highest weighting.

Cure time under 45 minutes was rated with five points. For every 15 minutes more, one point was subtracted. The residual modulus of relaxation after 10 minutes of CFRP was rated with five points if below 25%. For every 10% more, one point was subtracted. The flow properties were rated qualitatively. Cost of resin under EUR 15/kg were rated with five points, four points for \leq EUR 25/kg, three points for \leq EUR 50/kg, two points for \leq EUR 100/kg and one point for $>$ EUR 100/kg. Points for recycling were distributed depending on duration and effectiveness. M1.6 and M2.7 reached the same score in third place.

Table 5.15: Evaluation matrix for selection of three vitrimer resin mixtures

Criterion/Resin	M 1.1	M1.3	M1.5	M1.6	M1.7	M2.4	M2.5	M2.6	M2.7
T_g	5	1	5	5	5	5	5	5	5
Cure time	4	4	3	4	1	1	4	1	1
Score	9	5	8	9	6	6	9	6	6
Relaxation of CFRP	1	1	2	2	5	3	1	1	1
Score	1	1	2	2	5	3	1	1	1
Flow properties									
Thickness	5	5	1	5	5	5	5	5	5
Homogeneity/ Surface	2	2	5	4	4	4	2	3	3
Pressing parameters	2	2	3	2	5	4	2	5	5
Score	9	9	9	11	14	13	9	13	13
Cost of pure resin	3	2	1	3	5	5	1	3	5
Score	3	2	1	3	5	5	1	3	5
Recycling duration/ effectivity	1	1	4	4	5	4	4	5	4
Score	1	1	4	4	5	4	4	5	4
Total score	23	18	24	29	35	31	24	28	29

The best results were achieved by mixture M1.7, followed by M2.4, M1.6, and M2.7. Since dynamic properties are in the foreground and M1.6 has the better relaxation behavior it is preferred over M2.7.

5.7.6 Repair Potential of Vitrimer Composites

The repair potential of the different resin systems was tested on CFRP and neat resin material.

Results and Discussion

1c, 1e, 1f, 1g CFRP

The DCB plates to test the reparability were produced in a similar way as to test the fracture toughness on the original plates. Two half plates were cured separately and then placed onto each other to bond. For first trials, the T_g values from DMA measurements were used and 60 °C were added to obtain a repair temperature, which might be reasonable. The repair time was set to 15 minutes and the pressure to 20 bar. Table 5.16 shows the resulting repair temperatures used.

Table 5.16: Temperatures set for repair tests of resin 1c, 1e, 1f and 1g

Resin		Repair temperature [°C]
1c		200
1e		175
1f		170
1g		130

Using these parameters, the G_{IC} values in Figure 5.46 were achieved.

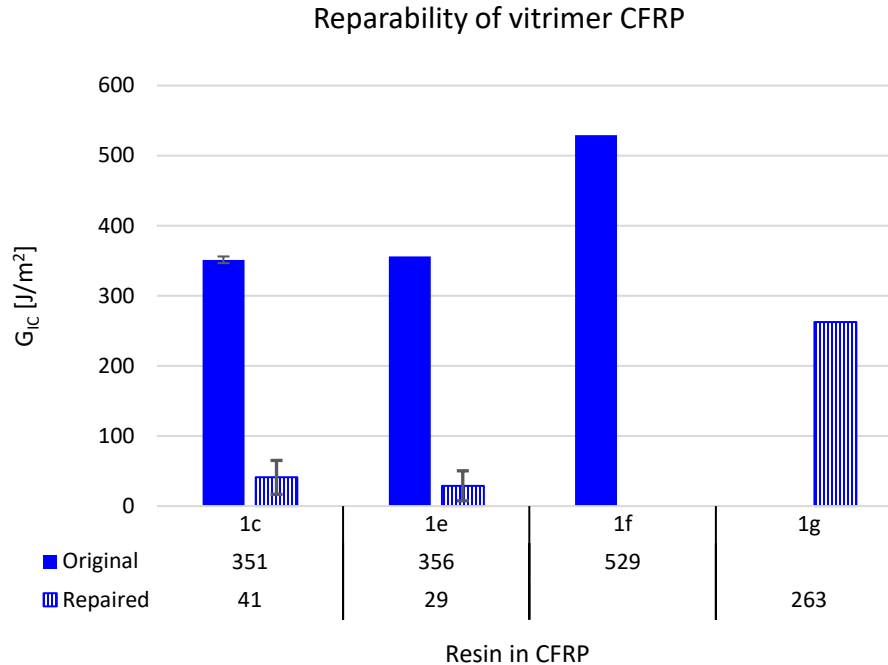


Figure 5.46: Comparison of fracture toughness of original and repaired CFRP with resins 1c, 1e, 1f and 1g

The adhesion of the 1f plate repaired with those parameters was insufficient and thus could not be evaluated. C-scans of the original and repaired plates were produced to show the difference in adhesion and the influence of the respective resin. Also, waviness of the plates, internal stress, slipping of the plates and insufficient repair parameters are possible explanations for the values obtained. As can be seen from Figure 6.18, Figure 6.19, Figure 6.20 and Figure 6.21 in the Appendix showing the C-Scan images, only resin 1g led to sufficient reparability of CFRP with the parameters used. The colors resemble the depth of defects as described by the color-code below each image.

1e FML

To test the reversibility of the adhesion between the resin and metal, a cured CFRP plate was pressed onto a metal foil and the ILSS value was compared to an FML cured in one step. The dynamic disulfide containing adhesion promoter was used on the metal foil.

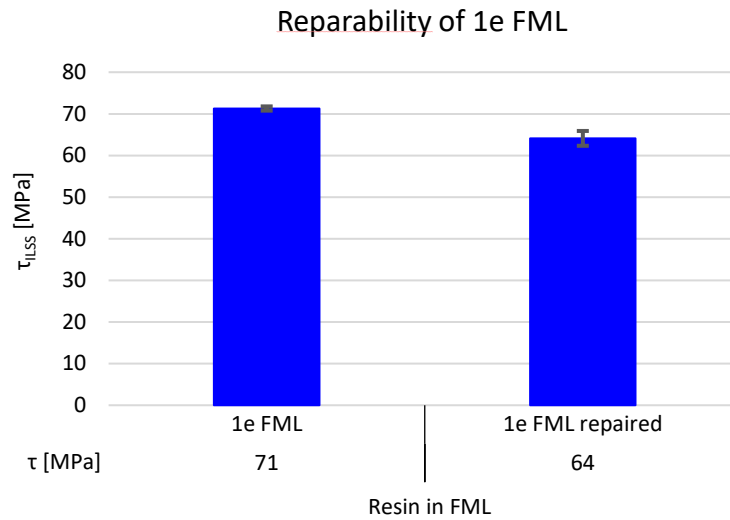


Figure 5.47: Reparability of 1e FML

The results in Figure 5.47 prove that it is possible to reconnect the surfaces of CFRP and metal and therefore to repair FML with vitrimer resin matrix. The efficiency here was about 90%.

Butt-Joint Test on M1.7

To test the reparability of vitrimer resin M1.7 in hand-laminated woven fabric CFRP butt-joint tests were conducted. This is a tensile test in direction perpendicular to plate plane. Therefore, plugs with circular shape and a diameter of 40 mm were glued onto the upper and bottom surface of the plate. A separating foil was inserted to reduce the diameter of the connected material inside to a circular area with 30 mm in diameter, to generate a failure inside the CFRP and avoid failure between CFRP and plug if possible. The values of originally pressed and repaired specimens are compared in Figure 5.48.

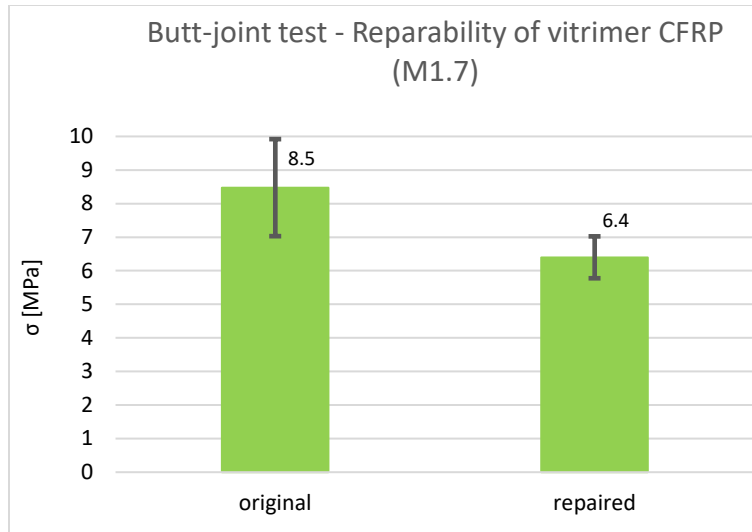


Figure 5.48: Butt-joint test results of pressed (original) and repaired CFRP specimen with M1.7 resin

Looking at the mean values, the repaired specimen did not reach the original value. Taking the standard deviation into account, both specimens are statistically not distinguishable. It is remarkable that the standard deviation of the repaired specimen was lower which may mean that a longer pressing time led to an improvement of the overall quality of the laminate.

5.7.7 Recyclability of Vitrimer Composites

Thermal Delamination

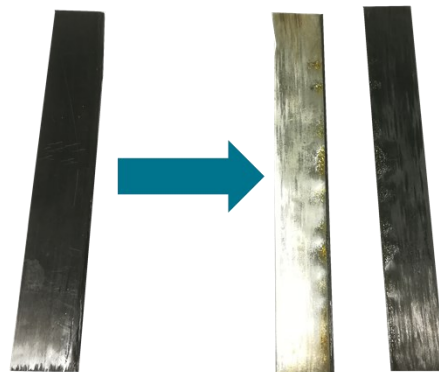


Figure 5.49: Thermal delamination of vitrimer FML to metal and CFRP

Results and Discussion

For thermal delamination (see Figure 5.49), an FML sample containing resin 1g was tested by being placed in an oven for 30 minutes at a temperature of 60 °C. Then the still hot sample was removed from the oven and manually delaminated. This test qualitatively proves the possibility of an easy thermal delamination step of vitrimer FML by heating the material above T_g . The surface of the aluminum was not as clean as after chemical recycling; traces of resin remained on the surface.

Chemical Recycling

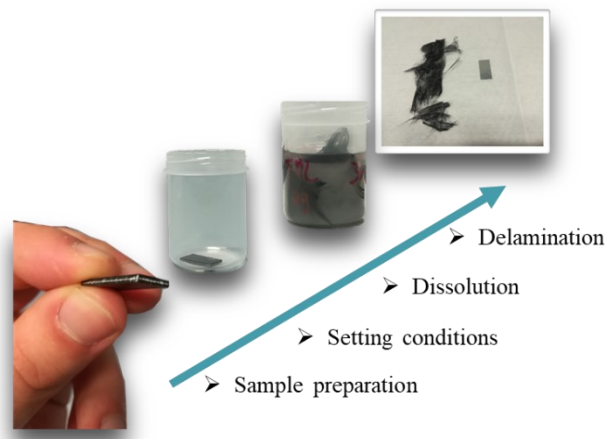


Figure 5.50: Steps of chemical delamination: separating fiber and metal layers as well as fiber and resin matrix of a vitrimer FML sample

Since the chemical recycling method proved to be successful for CFRP samples, its application was also tested in the case of FML samples (see Figure 5.50). An FML sample with 1g resin was put in a basic solution containing glycol dimercaptoacetate and the resin was completely dissolved. At this point the delamination of the piece simply consisted of removing the fibers and aluminum foil from the solution. For chemical conditioning, the recycling solution containing the FML specimen was placed in an oven at a temperature of 60 °C.

5.7.8 Discussion

In this thesis the dynamic properties of vitrimer epoxy materials were investigated and of special interest. The static (mechanical) properties as well as the dynamic properties are strongly influenced by the network structure of the vitrimer polymers. The flexibility, steric conditions and disulfide concentration of the network, of which either the mass percent of sulfur or the proportion of dynamic bonds can be a measure, are decisive for efficiency of disulfide bond exchange. T_g is a key parameter for the network structure. It depends on the mesh width and on the proportion of aromatic and aliphatic parts of the network. For recycling, the disulfide groups must be accessible for the thiol chemical. The thiol-disulfide exchange is influenced by similar factors. Therefore, disulfide groups must be present in a certain minimum concentration as well. For cost-efficient dynamic components, an increase of disulfide concentration is always accompanied with a decrease of T_g . This means a trade-off exists and the respective resin components must be combined in reasonable concentration.

Relaxation behavior of vitrimer materials was tested. The influence of single components was investigated and summarized in Table 5.17 and Table 5.18.

Table 5.17: Influence of base resin components on relaxation

Property	Base resins				
	EPS25	EPS70	Araldite	EPN	Tactix
Relaxation	-	-	↓	↓↓	↓↓

Table 5.18: Influence of hardener components on relaxation

Property	Hardeners			
	Aradur	APhD	DTAP	G4
Relaxation	-	↑	↑↑	↑↑↑

The addition of fiber to neat resin material to create CFRP led to a prolongation of the relaxation times. The fiber material was a mechanical barrier for disulfide bond exchange and fiber geometry influenced the stiffness and softening behavior of the vitrimer composite. Increasing amounts of

Results and Discussion

dynamic components in resin mixture led to better relaxation. The static base resins EPN and Tactix showed negative influence on relaxation. The higher the temperature was above the endset of the glass transition, the faster the relaxation. The relaxation behavior of VME02 from literature was used as reference or target value respectively. Mixture M1.7 with EPS25 and M2.4 with G4 showed better relaxation than VME02.

Flow tests were conducted on neat resin to estimate the reparability of the vitrimers and to investigate the effect of the single resin and hardener components again. Static base resins EPN and Tactix showed a negative influence as already identified for relaxation. When APhD was used as dynamic hardener, the resin still had a very high viscosity at elevated temperatures. Hence, repair of the corresponding CFRP is considered to be difficult. For relaxation and reparability, it can be stated that it is possible to formulate mixtures with T_g of minimum 100 °C and simultaneously ensure sufficient dynamic properties. Reparability (flow properties) was evaluated qualitatively and used for valuation purposes together with the criteria T_g , cure time, relaxation, cost and recyclability to score a selection of resin mixtures. Based on the target criteria defined at the beginning of the thesis, three resin mixtures M1.6 with DTPA (Table 5.21), M1.7 with EPS25 (Table 5.19) and M2.4 with G4 (Table 5.20) gave the best overall results. Although M2.4 did not exactly fulfill the relaxation and cost criteria, it had remarkable reparability.

M1.7

Table 5.19: Key values of mixture M1.7

EPS25	Araldite	Aradur	T_g	Relaxation	Cost	Recycling
27%	73%	100%	122 °C ✓	25% ✓	EUR 13/kg ✓	Yes ✓

M2.4

Table 5.20: Key values of mixture M2.4

Araldite	Aradur	G4	T_g	Relaxation	Kosten	Recycling
100%	92%	8%	134 °C ✓	34% ✓	EUR 13/kg ✓	Yes ✓

M1.6

Table 5.21: Key values of mixture M1.6

Araldite	Aradur	DTPA	T_g	Relaxation	Kosten	Recycling
100%	50%	100%	111 °C ✓	46% ✗	EUR 48/kg ✗	Yes ✓

Recycling of vitrimer neat resin was conducted with glycol dimercaptoacetate which is less toxic and less harmful than chemicals commonly used for recycling of disulfide vitrimers in literature. Alkaline conditions in aqueous solution with the recycling agent and a temperature above T_g were set. The evaporation of the recycling solution at a certain temperature limits the selection of resin which can be recycled this way. Comparing the first and second resin series, the resin components of VME02 (used for the second series) were more suitable in context of recycling than those of E420 (used for the first series) when combined with EPS70. GPC was conducted to compare the fragment size distribution of dissolved resins. 2i had a larger fragment size distribution than 1g. GPC of M1.5, M1.6, M1.7 and M2.4 showed quite similar results. This may mean that mainly one fragment size resulted from breaking disulfides with thiol and the disulfide bonds in those recyclable mixtures are distributed quite homogeneously.

Repair potential of vitrimer composites was tested. The prepregs of the first resin series were used for repair tests and DCB test was conducted for this purpose. The temperature was set above the endset of the glass transition. Probably the 15 minutes repair time was not sufficient for repairing CFRP with resin 1c, 1e and 1f. 1g showed quite good results. When cured vitrimer

CFRP and metal was pressed together, the efficiency of reconnection (resembling repair case of FML) was about 90%. Butt-joint test of repaired and originally pressed woven fabric CFRP with resin M1.7 was conducted. The repair efficiency was about 75% when both the original and repaired materials are compared.

Recycling experiments were conducted on vitrimer composite as well. When 1g FML was heated to 60 °C, the metal layer could easily be removed manually from the CFRP. Little resin residuals remained on the metal. When FML was recycled chemically, the metal surface was cleaner. Therefore, a piece of vitrimer FML was put in recycling solution and heated to 60 °C, and the metal and CFRP easily separated.

5.8 Summary

Initially, the target properties for the resin development shown again in Figure 5.51 were defined. The glass transition temperature should be at least 100 °C. The vitrimer resin shall relax stress faster than the reference resin VME02 from literature. The cost of pure resin should be a maximum of EUR 20 per kg to be competitive with commercially available standard materials and therefore applicable for automotive and aerospace industry as well as for several other fields. Sustainability in terms of recyclability was also set as condition.

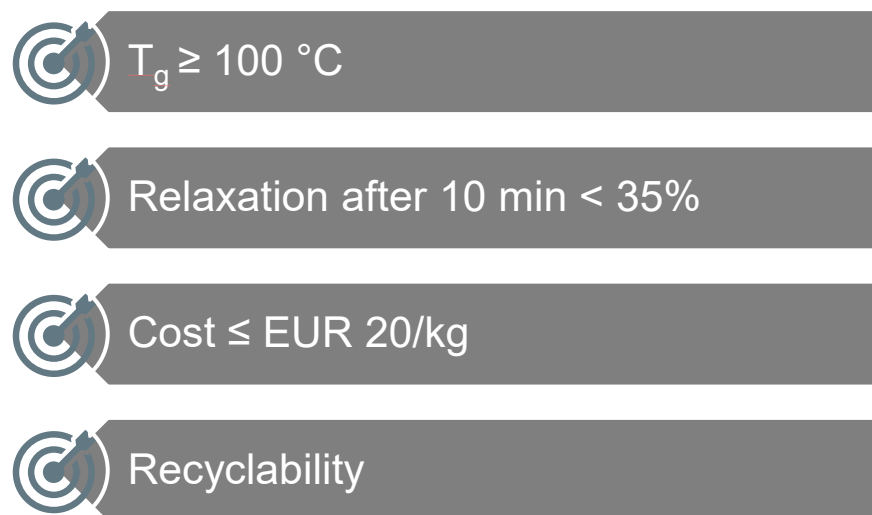


Figure 5.51: Target properties for resin development

For combining the resin and hardener components, their single effects on the target resin properties were investigated and are summarized in Table 5.22 and Table 5.23.

Table 5.22: Influence of base resin components on resin properties

Property	Base resins				
	EPS25	EPS70	Araldite	EPN	Tactix
Gel time	-	-	↓↓	↓	↑
Cure time	-	-	↑	↓	↑
T _g	-	↑	↑	↑↑	↑↑↑
Relaxation	-	-	↓	↓↓	↓↓
Cost [€/kg]	15	12	10	7	45
Recycling	↑↑	↑	-	↓↓	↓↓

Table 5.23: Influence of base hardener components on resin properties

Property	Hardeners			
	Aradur	APhD	DTPA	G4
Gel Time	-	↓	↓↓	↑↑
Cure Time	-	↓	↓↓	↑↑
T _g	-	↓	↓↓	↓↓↓
Relaxation	-	↑	↑↑	↑↑↑
Cost [€/kg]	18	1180	200	5
Recycling	-	↑	↑↑	↑↑

The influence of the molecular structure of the base resin and hardener components as well as of the different functional groups of the hardeners on curing behavior was investigated. Aromatic and branched molecules as well as molecules with higher chain length led to long gel times. Aliphatic and linear molecules as well as molecules with shorter chain length led to shorter gel times. When it comes to the different hardeners, the carboxylic acid group of DTPA was more

Results and Discussion

reactive than the aromatic amine group of Aradur and APhD. The thiol present in G4 had the weakest reactivity. Aromatic epoxies have a higher reactivity than aliphatic ones. EPS25, EPS70, Tactix and G4 led to rather longer gel times and Araldite, EPN, APhD and DTPA led to rather shorter gel times. Knowing the influence of the molecular structure or the single components, it is possible to formulate vitrimer resins with gel times reasonable for industrial applications. Cost-efficient dynamic resin components such as EPS70, EPS25 and G4 with long aliphatic molecules were best combined with static resin and hardener components such as Araldite and Aradur with short aromatic molecular structure. Most of these mixtures cured after one to two hours. Furthermore, there would also be the possibility of catalysis to reduce cure time. Considering the added value due to the dynamic properties of vitrimers, longer cure times for vitrimer resins might be acceptable.

T_g is influenced by the network structure of the polymer, where chain length or respectively mesh width, aromaticity and steric factors play a major role. The shorter the chains and meshes, the more aromatic rings and a high degree of branching lead to high T_g values. The influence of the single components was as follows: in view of the target value of 100 °C, EPS25, EPS70, DTPA and G4 had a decreasing or negative effect and Araldite, EPN, Tactix, Aradur and APhD had a positive effect on T_g . Most of the mixtures with a sufficient proportion of dynamic bonds regarding dynamic behavior achieved a T_g of at least 100 °C. The introduction of disulfide bonds was accompanied with a decrease of T_g by all dynamic components except the expensive hardener APhD. The more cost-effective dynamic components EPS70, EPS25 and G4 should be used up to a reasonable share to balance the decrease of T_g and the increase of dynamics. Only in this way, the mechanical properties of the material can be maintained, and the cost-efficiency as well as dynamic behavior can be ensured simultaneously, which means there is a trade-off between mechanical properties, cost and dynamic properties.

Determining the temperature stability is crucial to define the upper limit of the curing temperature of the neat resin, of the operating temperature and in the case of the vitrimers also of the repair temperature. The more EPS70 was used in the first resin series, the lower was T_d . Increasing the concentration of EPS70 in the second resin series did not show a significant decrease in T_d . This resulted from the fact that the base resin of the VME02 does not inherently have such a high temperature stability as the base resins of E420. The pure EPS70 is only thermally stable below 150 °C, why it is the temperature limit for curing. For the resins meeting the T_g criterion, the T_d was also determined. The lowest T_d evaluated was 253 °C. To be safe, the upper limit of in-

service and repair temperature should be set significantly below T_d . Therefore, all resins tested should be safe to use and repair at temperatures up to 200 °C. EPS25, EPS70 and G4 tended to decrease the T_d , whereas APhD and DTPA did not show a negative effect. Tactix and EPN tended to increase the T_d as expected.

The mechanical performance of vitrimer neat resin and composite material was tested. Increasing the amount of EPS70 in the first and second resin series led to an increase of ductility of the polymers. The tensile and flexural modulus first slightly increased, but then significantly decreased with increasing amount of EPS70. When CFRP material was tested, for matrix dominated tests the same effect occurred. With increasing amount of EPS70, the strength and stiffness decreased, especially when the T_g was close to the test temperature. Thus, EPS70 had a rather negative effect on the mechanical performance of the CFRP in quasi-static tests. The results of the second resin series where APhD was used as hardener beside the EPS70 base resin to provide dynamic disulfides were slightly better. It could be concluded that an introduction of dynamics into the polymer by cost-efficient aliphatic dynamic components is accompanied by a decrease in T_g and a decrease in mechanical performance. Therefore, care should be taken to ensure that the T_g does not become too low or the negative effect on the T_g should be compensated by other components to maintain suitable mechanical properties. For impact strength and fracture toughness, rather the opposite effect was observed. EPS70 increased the fracture toughness and improved the impact properties of CFRP. The three best mixtures in terms of dynamic properties and target criteria were tested in bending as well and compared to the reference E420. The vitrimer CFRPs achieved about three quarters of the bending strength of E420, but it must be mentioned that these were laminated by hand, whereas the woven prepreg with E420 was produced by machine. The bending stiffness was even about 10% higher.

Besides CFRP, FML material with vitrimer resins was tested. Especially in fiber-dominated tests, the FML performed worse than the CFRP material, as expected. In FML, the interface between CFRP and metal plays a critical role. Due to a higher concentration of EPS70, the adhesion to the metal deteriorated, which is why the impact performance of the FMLs also deteriorated, in contrast to the trend of the impact performance of the CFRP. Fracture toughness of FML was positively influenced by EPS70. There it strongly depends on whether the resin leads to higher or lower cohesion in CFRP than adhesion of CFRP to metal. The flexural strength of the FML of the three optimum mixtures was within the range of the flexural strengths of the CFRP of those resins,

Results and Discussion

which was observed similar for the other materials. It could be concluded that these three mixtures might also have good adhesion to metal and might therefore be suitable for use in the FML.

The benchmarking showed that the pure resins with medium to high T_g of the first and second resin series achieved comparable tensile performance to established or commercially available polymers. When comparing the flexural performance of CFRP with PP, PA6, E420 and VME02, the vitrimer VME02 achieved similar or even better values than the reference epoxy resin E420. However, the higher fiber volume content in this VME02 CFRP must also be included in the evaluation. Comparing the tensile and flexural performance of 1c and 1f CFRP with the thermosetting reference E420 and the thermoplastic reference PA6, the performance of these vitrimer resins ranged between E420 and PA6. Thus, it could be concluded that these vitrimer resins would be competitive to established resins for use in CFRP.

DMA measurements on vitrimer CFRP with the first and second resin series prepregs were performed. The T_g values of the CFRP were in some cases slightly higher than those of the pure resin. The fiber serves as a mechanical barrier to disulfide exchange and the fiber matrix adhesion stabilizes the material a bit under the elevated temperature. T_g values were also measured on FML material to find out at what temperature the adhesion to the metal is weakened. Thus, a suitable temperature for thermal recycling (delamination of CFRP from metal) can be found. As in the previous experiments, an increased amount of EPS70 reduced the T_g . The width of the glass transition was similar for the tested materials with different proportions of dynamic bonds but showed a correlation to the level of the modulus drop.

Water absorption and media resistivity of vitrimer CFRP and FML was tested and compared to reference materials with PA6 and E420. Prepregs of the first and second resin series were used for this purpose. Accelerated conditioning showed a plasticizing effect on E420 and 1c due to water absorption, which slightly increased the flexural performance. For the remaining materials, strength and stiffness decreased with increasing amount of EPS70. Water absorption also resulted in a decrease in T_g . Materials whose T_g was close to or below the conditioning temperature were even more negatively affected. When comparing 2f and 1e, which both had the same proportion of dynamic bonds, the second resin series performed better. The materials' resistance against salty environment was also tested. E420, PA6 and 1c performed well. For the other materials, a decreasing performance with increasing amount of EPS70 was again observed. The results showed a strong dependence on the exposure time of 10, 20 and 30 days. The FML materials overall degraded more in salty environment, due to the weakening of the interface to

the metal and corrosion issues. In contrast to the water resistance, the chemical resistance showed a correlation with the change in mass. HCl was the most harmful chemical, NaOH also had a strong negative effect. As well as in the tests before, a lower T_g again resulted in more damage. The more EPS70 was used, the more the flexural strength and modulus decreased. In summary, it can be said that the vitrimer materials, with a moderate proportion of dynamic bonds, exhibit media resistivity comparable to the reference or standard materials.

As known from literature and explained in chapter 2.1.3.3, the efficiency of disulfide exchange depends on the molecular structure surrounding the disulfide bridge as well as on the network structure, which was investigated in more detail in chapter 5.7. Flexibility, steric conditions and the proportion of dynamic bonds play a central role. The T_g is a key parameter, which also reflects the mesh size and the proportion of aromatic and aliphatic network regions. For the thiol disulfide exchange the accessibility of the disulfide bonds is crucial. For both mechanisms, a sufficient concentration of disulfides must be present. The influence of the single components on relaxation was tested. The dynamic components showed a positive influence on relaxation as expected. Araldite and Aradur did not show a negative effect on relaxation. However, EPN and Tactix, which positively affected T_g , showed negative effects, because of their branched and rigid aromatic molecular structure. In studying the relaxation behavior of CFRP material, the fiber acted as a mechanical barrier to disulfide exchange and the fiber geometry also showed an influence on the softening behavior. The more amount of dynamic component was used, the better the relaxation was, as expected. A temperature above the T_g endset was chosen for the relaxation experiments and proved to be useful. The further the temperature was above, the more effective. M1.7 with EPS25 and M2.4 with G4 showed a better relaxation behavior than the VME02 reference from literature. Flow tests were used to estimate the repair capability of the material. EPN and Tactix also showed a negative effect here. When APhD was used, the material maintained a remarkably high viscosity even at high temperatures, which would probably lead to problems with the repair capability especially in CFRP, due to the low flow tendency of the resin. Based on the target criteria and a decision matrix, the three optimum mixtures selected in chapter 5.7.5 and their key values are shown again in Table 5.24.

Table 5.24: Key values of the three mixtures selected

Resin	T_g	Relaxation	Cost	Recycling
M1.7	122 °C ✓	25% ✓	EUR 13/kg ✓	Yes ✓
M2.4	134 °C ✓	34% ✓	EUR 13/kg ✓	Yes ✓
M1.6	111 °C ✓	46% ✗	EUR 48/kg ✗	Yes ✓

Chemical recycling of disulfide epoxy vitrimers is effective under alkaline conditions in aqueous solution. In this work, a process using a less harmful chemical than commonly used in literature was proven to be effective on several vitrimer resins. The temperature must be set above the T_g . The first resin series proved to be more effective in terms of recycling, since the base resins of E420 cause a branched or stiff and aromatic network structure, making it difficult to access the disulfide bridges. A homogeneous distribution of the disulfide bridges with sufficient concentration of the same proved to be advantageous. Feasibility tests regarding the repair were also carried out on CFRP specimens. There is still potential for optimization regarding the parameters. The time and temperature set were only effective for resin 1g. For resins 1c, 1e, 1f the time was probably too short and maybe the temperature too low, or there was not enough dynamic component in the resins. The rebonding of vitrimer CFRP to metal also proved to be possible, whereby vitrimers also provide repair potential for FML. When vitrimer FML was heated, the metal could be easily removed from the CFRP. This process is a simple way to thermally recycle FML, which is not possible with static epoxy resins this way. Chemical recycling with the mild recycling agent also worked for vitrimer FML, producing an even cleaner surface without resin residues than thermal FML recycling.

Table 5.25 contains the gel time, cure time, T_g , decomposition temperature (T_d) and the normalized modulus of relaxation G/G_0 after 10 min for the comprehensive characterization of the resins.

Table 5.25: Gel time, cure time, T_g from DMA, decomposition temperature and normalized modulus after 10 minutes of all resins tested

Resin	Gel Time [min]	Cure Time [min]	$T_{g,maxG''}$ [°C]	T_D [°C]	G/G ₀ after 10 min [%]
1c	0.5	10	121	313	-
1e	0.6	10	100	291	-
1f	0.75	10	91	265	-
1g	1.1	10	54	269	-
2b	13	45	126	296	-
2f	15	60	99	297	-
2g	16	65	72	292	-
2i	31	85	43	241	-
11	27	108	193	-	-
12	30	85	132	-	82
13	35	70	110	<266	70
21	27	108	193	-	-
22	9	60	148	-	87
23	6	50	121	291	53
51	8	50	126	-	81
52	19	50	89	-	67
53	20	70	60	-	25
56	24	70	36	-	-
71	15	45	100	-	68
M1.1	13	55	104	257	76
M1.2	11	70	105	-	71
M1.3	11	55	76	<253	66
M1.4	4	40	≈20	-	-
M1.5	5	65	138	<281	53
M1.6	13	60	111	306	48
M1.7	48	95	122	<281	25
M2.1	16	75	139	270	85
M2.2	16	70	126	-	81
M2.3	51	120	68	-	35
M2.4	46	110	134	250	36
M2.5	14	60	107	285	35
M2.6	45	120	117	281	77
M2.7	47	110	126	<279	70
EPS70-Ref	32	85	104	290	80

6 Conclusions and Outlook

Several vitrimer epoxy resins were tested regarding their reactivity (gelation and curing), thermal behavior (glass transition and degradation temperature), mechanical properties (quasi-static and high-velocity loading) and especially their dynamic properties (relaxation, recycling and reparability). Furthermore, the costs of the vitrimer resins were given.

After determining the influences of the single components, general relations of network structure and material behavior regarding reactivity, processing time of the material, glass transition and decomposition, the mechanical performance of vitrimer material were quantified and analyzed. Therefore, neat resin, CFRP and FML materials of first and second resin series were intensively tested with respect to mechanical properties at room temperature and at elevated temperatures. A benchmarking was conducted. Water absorption and media resistivity of the material was quantified as well and compared to the standard reference materials E420 and PA6.

Most of interest was the dynamic behavior of the vitrimer resin materials. Therefore, characteristics of the network structure were analyzed, the relaxation behavior was quantified, flow tests were conducted to assess the reparability and recycling tests were performed. Based on the target criteria set and the characteristic values determined for all resins with a special focus on the flow properties, three most appropriate mixtures were evaluated: M1.6 with DTPA, M1.7 with EPS25 and M2.4 with G4.

For these three mixtures, bending test of CFRP and FML was performed as well, where they could achieve a flexural strength of about three quarters of the flexural strength of the reference material E420 and a flexural modulus about 10% higher than the flexural modulus of the reference material. However, the vitrimer prepreps were hand-laminated, while the E420 materials were machine-made which must be taken into account in the comparison at the expense of the potential of the vitrimer material. Since the dynamic properties were in the foreground in this work, the best mixture regarding the set target criteria but especially regarding the relaxation was M1.7. For mixture M1.7 also butt-joint test was conducted to quantify the reparability of its CFRP material and it achieved about 75% with the used parameters.

The structure of the polymer network must be designed to meet the desired properties. Steric conditions must be appropriate to enable disulfide and thiol-disulfide exchange. Resin components with branched aromatic structure such as EPN and Tactix show negative influence

Conclusions and Outlook

on dynamic properties and should be avoided. With the affordable or cost-efficient dynamic resin components currently existing on the market, there is a trade-off between static (mechanical) and dynamic properties of vitrimers. T_g is a key measure for the network structure and was it as well for the materials used for this thesis. A T_g of 100 °C was found to be a reasonable value for obtaining appropriate static and dynamic properties. Then, the applicability of the material for structural applications is maintained and the specific desired vitrimer functionalities (relaxation, repair, recycling) are achieved simultaneously.

Due to the variety of static resin components available on the market and due to the dynamic disulfide components tested, there is the possibility to tune resin properties tailored for different applications and a wide range of demanded properties. The advantages of vitrimers can especially be used for FML. As vitrimers are formable and have good adhesion to metal, it is possible to produce rolling stock. The material can be produced in plate geometry and afterwards pressed into part geometry. This saves process steps and cycle time, and therefore cost. To sum up, vitrimers represent an alternative matrix material for CFRP and FML composites and offer several functionalities in addition. Although feasibility of repairing CFRP was shown, the parameters therefore is one aspect which can be investigated in more detail and optimized for different resin mixtures. Considering the overall results of this thesis, combining static and dynamic resin properties in reasonable relation, it is possible to formulate vitrimer epoxy resins with a wide range of properties which are competitive to standard materials and offer added value with regard to sustainability.

This work can be used as a basis for further research. Both the sample and test scopes could be further expanded. Starting with reactivity, for example, accelerators or catalysts could be used for faster curing, which would shorten the cycle times for industrial applications and thus make them more profitable. However, it should be noted that such additives can influence not only the curing time but also the other material properties. The concentrations of the resin components could still be varied further as well as the components used to tune the properties of the vitrimer resins, plastics or matrix materials with respect to the intended applications.

Within the scope of this thesis, influencing factors, correlations and interactions were investigated, as well as the influence of the individual components. Some tests were only carried out as feasibility studies to investigate or demonstrate the general potential of vitrimers and especially vitrimers in composites, based on which more detailed tests with a larger sample and test scope

could be carried out. Especially for repairing and reshaping vitrimer CFRP and FML, parameter studies could still be performed to find out optimal time, pressure and temperature conditions.

Mainly the prepregs of the first and second resin series were characterized with regard to the mechanics in order to find out general correlations. Thus, also regarding mechanical tests on composites with different vitrimer matrix materials, various further tests could be carried out, also to in turn improve the resin. The tests on the composite material with the three optimum vitrimer resins were performed on hand-laminated material. Machine production of the prepreg, for example, would increase the homogeneity of the material and thus improve its performance. The performance of the FML composite can be improved by surface treatments of the metal. Furthermore, materials other than the pure aluminum and aerospace aluminum alloy can be used as metal foil.

Since the resins formulated in this work cover a wide range of properties, they could be used for various common applications. Extensive tests which would make it possible to define specific applications were only carried out on selected materials, which is why no recommendation for concrete applications is given here for every resin. However, a specific application would probably require even more precise optimization of the resin in question. The selection of the three optimum materials as the result of this work was based on the initially set target criteria. These resins, which met the criteria harmonize the static and dynamic properties, focusing on or prioritizing sustainability and affordable costs. Since the low-cost or at the moment cost-efficient dynamic components for example have the disadvantage of lowering T_g , it would be a great advance for the widespread use of vitrimers if aromatic dynamic components such as APhD and BGPDS were to be produced on an industrial scale, thus lowering their raw material cost.

Definitions and Parameter Conventions

Thermal Analysis

Storage modulus, Loss modulus, Tangens delta

$G', G'', \tan \delta$

Gel time

t_{gel}

Glass transition temperature

T_g

Degradation temperature

T_d

Mechanical Testing

Force, Area

F, A

Strength (tensile, compression, flexural, ILSS)

$\sigma_t, \sigma_c, \sigma_f, \tau_{ILSS}$

Modulus, Elongation

E, ε

Poisson ratios

ν_{ij}

GPC Analysis

Average molecular weights (weight, number)

M_w, M_n

References

- [1] R. de Luzuriaga, R. Martín, N. Markaide, A. Rekondo, G. Cabañero, J. Rodríguez, I. Odriozola, Epoxy resin with exchangeable disulfide crosslinks to obtain reprocessable, repairable and recyclable fiber-reinforced thermoset composites, *Materials Horizons* 3 (2016) 241–247.
- [2] G.W. Ehrenstein, *Polymeric materials: Structure - Properties - Applications*, Hanser, Munich, 2001.
- [3] J.D. Menczel, R.B. Prime, *Thermal Analysis of Polymers: Fundamentals and Applications*, Wiley, 2009.
- [4] G.W. Ehrenstein, *Härtung von Reaktionsharzen: Das Time-Temperature-Transition-Diagramm*, 2003.
- [5] L.M. Johnson, E. Ledet, N.D. Huffman, S.L. Swarner, S.D. Shepherd, P.G. Durham, G.D. Rothrock, Controlled degradation of disulfide-based epoxy thermosets for extreme environments, *Polymer* 64 (2015) 84–92.
- [6] B. Ellis, *Chemistry and Technology of Epoxy Resins*, Springer Netherlands, Dordrecht, 1993.
- [7] J.-E. Ehlers, N.G. Rondan, L.K. Huynh, T.N. Truong, H. Pham, M. Marks, Theoretical Study on Mechanism of Epoxy- Amine Cure Reactions, *Macromolecules* (2007) 4370–4377.
- [8] T. Sabu, C. Sinturel, T. Raju, *Micro- and nanostructured epoxy/rubber blends*, Wiley-VCH, Weinheim, Germany, 2014.
- [9] D. Ratna, *Handbook of thermoset resins*, first ed., iSmithers, Shawbury, Shrewsbury, 2009.
- [10] Information on <https://polymerinnovationblog.com/epoxy-cure-chemistry-part-4-nucleophiles-action/>
- [11] I. Hamerton, *Recent developments in epoxy resins*, Rapra Technology Ltd, Shawbury, Shrewsbury, 1996.
- [12] A. Chaloupka, *Development of a dielectric sensor for the real-time in-mold characterization of carbon fiber reinforced thermosets*. PhD, Augsburg, 2018.
- [13] W.J. Blank, Z.A. He, M. Picci (Eds.), *Catalysis of the epoxy-carboxyl reaction*, 2002.
- [14] D. Montarnal, M. Capelot, F. Tournilhac, L. Leibler, Silica-Like Malleable Materials from Permanent Organic Networks, *Science* (2011) 965–968.
- [15] W. Denissen, J.W. Winne, F.E. Du Prez, Vitrimers: permanent organic networks with glass-like fluidity. Minireview, *Chemical Science* (2016) 30–38.
- [16] F. García, M.M.J. Smulders, Dynamic covalent polymers, *Journal of Polymer Science* (2016) 3551–3577.
- [17] M. Capelot, *Step-growth Polymerization, Supramolecular Polymers and Vitrimers*, 2013.
- [18] F. Sordo, V. Michaud, Processing and damage recovery of intrinsic self-healing glass fiber reinforced composites, *Smart Mater. Struct.* 25 (2016) 84012.
- [19] Information on <https://www.arkema.com/en/media/news/news-details/Self-healing-elastomer-enters-industrial-production/>
- [20] W. Zou, J. Dong, Y. Luo, Q. Zhao, T. Xie, Dynamic Covalent Polymer Networks: from Old Chemistry to Modern Day Innovations, *Advanced materials* (Deerfield Beach, Fla.) 29 (2017).
- [21] J.P. Brutman, P.A. Delgado, M.A. Hillmyer, Polylactide Vitrimers, *ACS Macro Lett.* 3 (2014) 607–610.
- [22] J. Han, T. Liu, C. Hao, S. Zhang, B. Guo, J. Zhang, A Catalyst-Free Epoxy Vitrimer System Based on Multifunctional Hyperbranched Polymer, *Macromolecules* 51 (2018) 6789–6799.
- [23] X. Kuang, Y. Zhou, Q. Shi, T. Wang, H.J. Qi, Recycling of Epoxy Thermoset and Composites via Good Solvent Assisted and Small Molecules Participated Exchange Reactions, *ACS Sustainable Chem. Eng.* 6 (2018) 9189–9197.
- [24] Y. Zhou, J.G.P. Goossens, R.P. Sijbesma, J.P.A. Heuts, Poly(butylene terephthalate)/Glycerol-based Vitrimers via Solid-State Polymerization, *Macromolecules* 50 (2017) 6742–6751.

References

- [25] Z. Pei, Y. Yang, Q. Chen, E.M. Terentjev, Y. Wei, Y. Ji, Mouldable liquid-crystalline elastomer actuators with exchangeable covalent bonds, *Nature materials* 13 (2014) 36–41.
- [26] Y. Yang, Z. Pei, Z. Li, Y. Wei, Y. Ji, Making and Remaking Dynamic 3D Structures by Shining Light on Flat Liquid Crystalline Vitrimer Films without a Mold, *Journal of the American Chemical Society* 138 (2016) 2118–2121.
- [27] E. Chabert, J. Vial, J.-P. Cauchois, M. Mihaluta, F. Tournilhac, Multiple welding of long fiber epoxy vitrimer composites, *Soft Matter* 12 (2016) 4838–4845.
- [28] E. Amendola, S.D. Iacono, A. Pastore, M. Curcio, A. Iadonisi, Epoxy Thermosets with Self-Healing Ability, *MSCE* 03 (2015) 162–167.
- [29] Q. Tian, Y.C. Yuan, M.Z. Rong, M.Q. Zhang, A thermally remendable epoxy resin, *J. Mater. Chem.* 19 (2009) 1289.
- [30] D.H. Turkenburg, H.R. Fischer, Diels-Alder based, thermo-reversible cross-linked epoxies for use in self-healing composites, *Polymer* 79 (2015) 187–194.
- [31] Y. Min, S. Huang, Y. Wang, Z. Zhang, B. Du, X. Zhang, Z. Fan, Sonochemical Transformation of Epoxy–Amine Thermoset into Soluble and Reusable Polymers, *Macromolecules* 48 (2015) 316–322.
- [32] Inhestern, Thermisch reversibel vernetzte Polymermatrices für neuartige Faserverbund-Werkstoffe. PhD, 2016.
- [33] P. Taynton, K. Yu, R.K. Shoemaker, Y. Jin, H.J. Qi, W. Zhang, Heat- or water-driven malleability in a highly recyclable covalent network polymer, *Advanced materials (Deerfield Beach, Fla.)* 26 (2014) 3938–3942.
- [34] P. Taynton, H. Ni, C. Zhu, K. Yu, S. Loob, Y. Jin, H.J. Qi, W. Zhang, Repairable Woven Carbon Fiber Composites with Full Recyclability Enabled by Malleable Polyimine Networks, *Advanced materials (Deerfield Beach, Fla.)* 28 (2016) 2904–2909.
- [35] Information on <https://www.mallinda.com/>
- [36] W. Denissen, M. Driesbeke, R. Nicolaÿ, L. Leibler, J.M. Winne, F.E. Du Prez, Chemical control of the viscoelastic properties of vinylogous urethane vitrimers, *Nature communications* 8 (2017) 14857.
- [37] W. Denissen, G. Rivero, R. Nicolaÿ, L. Leibler, J.M. Winne, F.E. Du Prez, Vinylogous Urethane Vitrimers, *Adv. Funct. Mater.* 25 (2015) 2451–2457.
- [38] S. Zechel, R. Geitner, M. Abend, M. Siegmann, M. Enke, N. Kuhl, M. Klein, J. Vitz, S. Gräfe, B. Dietzek, M. Schmitt, J. Popp, U.S. Schubert, M.D. Hager, Intrinsic self-healing polymers with a high E-modulus based on dynamic reversible urea bonds, *NPG Asia Mater* 9 (2017) e420–e420.
- [39] J. Liu, Y. Liu, Y. Wang, J. Zhu, J. Yu, Z. Hu, Disulfide bonds and metal-ligand co-crosslinked network with improved mechanical and self-healing properties, *Materials Today Communications* 13 (2017) 282–289.
- [40] W. Post, A. Cohades, V. Michaud, S. van der Zwaag, S.J. Garcia, Healing of a glass fibre reinforced composite with a disulphide containing organic-inorganic epoxy matrix, *Composites Science and Technology* 152 (2017) 85–93.
- [41] Y. Li, Y. Zhang, O. Rios, J.K. Keum, M.R. Kessler, Photo-responsive liquid crystalline epoxy networks with exchangeable disulfide bonds, *RSC Adv.* 7 (2017) 37248–37254.
- [42] L. Zhang, L. Chen, S.J. Rowan, Trapping Dynamic Disulfide Bonds in the Hard Segments of Thermoplastic Polyurethane Elastomers, *Macromol. Chem. Phys.* 218 (2017) 1600320.
- [43] A. Rekondo, R. Martin, A. Ruiz de Luzuriaga, G. Cabañero, H.J. Grande, I. Odriozola, Catalyst-free room-temperature self-healing elastomers based on aromatic disulfide metathesis, *Mater. Horiz.* 1 (2014) 237–240.
- [44] X. Jian, Y. Hu, W. Zhou, L. Xiao, Self-healing polyurethane based on disulfide bond and hydrogen bond, *Polym Adv Technol* 29 (2018) 463–469.

- [45] T. Liu, C. Hao, S. Zhang, X. Yang, L. Wang, J. Han, Y. Li, J. Xin, J. Zhang, A Self-Healable High Glass Transition Temperature Bioepoxy Material Based on Vitriimer Chemistry, *Macromolecules* 51 (2018) 5577–5585.
- [46] S. Ji, J. Xia, H. Xu, Dynamic Chemistry of Selenium: Se–N and Se–Se Dynamic Covalent Bonds in Polymeric Systems, *ACS Macro Lett.* 5 (2016) 78–82.
- [47] Y. Zhou, High-performance poly(butylene terephthalate) vitrimers, 2017.
- [48] R. Martin, A. Rekondo, A.R. de Luzuriaga, P. Casuso, D. Dupin, G. Cabañero, H.J. Grande, I. Odriozola, Dynamic sulfur chemistry as a key tool in the design of self-healing polymers, *Smart Mater. Struct.* 25 (2016) 84017.
- [49] J.M. Matxain, J.M. Asua, F. Ruipérez, Design of new disulfide-based organic compounds for the improvement of self-healing materials, *Physical chemistry chemical physics PCCP* 18 (2016) 1758–1770.
- [50] R. Caraballo, M. Rahm, P. Vongvilai, T. Brinck, O. Ramström, Phosphine-catalyzed disulfide metathesis, *Chemical communications (Cambridge, England)* (2008) 6603–6605.
- [51] A. Rekondo, R. Martin, A. Ruiz de Luzuriaga, G. Cabañero, H.J. Grande, I. Odriozola, Catalyst-free room-temperature self-healing elastomers based on aromatic disulfide metathesis, *Mater. Horiz.* 1 (2014) 237–240.
- [52] R.J. Sarma, S. Otto, J.R. Nitschke, Disulfides, imines, and metal coordination within a single system: interplay between three dynamic equilibria, *Chemistry (Weinheim an der Bergstrasse, Germany)* 13 (2007) 9542–9546.
- [53] A.M. Belenguer, T. Friščić, G.M. Day, J.K.M. Sanders, Solid-state dynamic combinatorial chemistry: reversibility and thermodynamic product selection in covalent mechanosynthesis, *Chem. Sci.* 2 (2011) 696.
- [54] R.J. Sarma, S. Otto, J.R. Nitschke, Disulfides, imines, and metal coordination within a single system: interplay between three dynamic equilibria, *Chemistry (Weinheim an der Bergstrasse, Germany)* 13 (2007) 9542–9546.
- [55] I. Azcune, I. Odriozola, Aromatic disulfide crosslinks in polymer systems: Self-healing, reprocessability, recyclability and more, *European Polymer Journal* 84 (2016) 147–160.
- [56] T. Ohishi, Y. Iki, K. Imato, Y. Higaki, A. Takahara, H. Otsuka, Insertion Metathesis Depolymerization of Aromatic Disulfide-containing Dynamic Covalent Polymers under Weak Intensity Photoirradiation, *Chem. Lett.* 42 (2013) 1346–1348.
- [57] Z.Q. Lei, H.P. Xiang, Y.J. Yuan, M.Z. Rong, M.Q. Zhang, Room-Temperature Self-Healable and Remoldable Cross-linked Polymer Based on the Dynamic Exchange of Disulfide Bonds, *Chem. Mater.* 26 (2014) 2038–2046.
- [58] U. Lafont, H. van Zeijl, S. van der Zwaag, Influence of cross-linkers on the cohesive and adhesive self-healing ability of polysulfide-based thermosets, *ACS applied materials & interfaces* 4 (2012) 6280–6288.
- [59] J. Canadell, H. Goossens, B. Klumperman, Self-Healing Materials Based on Disulfide Links, *Macromolecules* 44 (2011) 2536–2541.
- [60] A. Takahashi, T. Ohishi, R. Goseki, H. Otsuka, Degradable epoxy resins prepared from diepoxide monomer with dynamic covalent disulfide linkage, *Polymer* (2016) 319–326.
- [61] G.C. Tesoro, V. Sastri, Reversible Crosslinking in Epoxy Resins. I. Feasibility Studies, *Journal of Applied Polymer Science* (1990) 1425–1437.
- [62] B. Gyarmati, Á. Némethy, A. Szilágyi, Reversible disulphide formation in polymer networks: A versatile functional group from synthesis to applications, *European Polymer Journal* 49 (2013) 1268–1286.
- [63] P.A. Fernandes, M.J. Ramos, Theoretical insights into the mechanism for thiol/disulfide exchange, *Chemistry (Weinheim an der Bergstrasse, Germany)* 10 (2004) 257–266.
- [64] R. Singh, G.M. Whitesid, Thiol-disulfide interchange, *The Chemistry of Sulfur-Containing Functional Groups* (1993) 633–658.

References

- [65] R. Singh, G.V. Lamoureux, W.J. Lees, G.M. Whitesides, Reagents for rapid reduction of disulfide bonds 251 (1995) 167–173.
- [66] V. Sastri, G.C. Tesoro, Reversible Crosslinking in Epoxy Resins. II. New Approaches (1990).
- [67] H. Lengsfeld, H. Mainka, V. Altstädt, Carbonfasern: Herstellung, Anwendung, Verarbeitung, Carl Hanser Verlag GmbH & Co. KG, 2019.
- [68] G.W. Ehrenstein, Faserverbund-Kunststoffe: Werkstoffe - Verarbeitung - Eigenschaften, secondnd completely revised edition, Carl Hanser Verlag GmbH & Co. KG, München, 2006.
- [69] J. Xue, Tensile strength and thermal residual stress of CARALL and UACS/AL laminates. PhD, Ottawa, Canada, 2012.
- [70] M. Sadighi, R.C. Alderliesten, R. Benedictus, Impact resistance of fiber-metal laminates: A review, International Journal of Impact Engineering 49 (2012) 77–90.
- [71] D. Stefaniak, E. Kappel, B. Kolesnikov, C. Hühne (Eds.), Improving the mechanical performance of unidirectional cfrp by metal-hybridization, 2012.
- [72] A. Vlot, J.W. Gunnink, Fibre Metal Laminates: An Introduction, Springer Netherlands, Dordrecht, 2001.
- [73] M. Stoll, Behavior of Fiber-Metal-Elastomer-Hybrid-Laminates.
- [74] T. Sinmazçelik, E. Avcu, M.Ö. Bora, O. Çoban, A review: Fibre metal laminates, background, bonding types and applied test methods, Materials & Design 32 (2011) 3671–3685.
- [75] R. Alderliesten, Fatigue and Fracture of Fibre Metal Laminates, firstst edition, Springer International Publishing, Cham, 2017.
- [76] S.E. Moussavi-Torshizi, S. Dariushi, M. Sadighi, P. Safarpour, A study on tensile properties of a novel fiber/metal laminates, Materials Science and Engineering: A 527 (2010) 4920–4925.
- [77] A. Chlupova, V. Kozak, Fatigue crack growth and delamination in fiber metal laminate (Glare) during loading with positive mean stress, 18th International Conference Engineering Mechanics (2012) 531–536.
- [78] R. Marissen, Fatigue crack growth in ARALL: A hybrid aluminium-aramid composite material: Crack growth mechanisms and quantitative predictions of the crack growth rates. PhD, 1988.
- [79] G. Roebroeks, Towards GLARE: The development of a fatigue insensitive and damage tolerant aircraft material (1991).
- [80] C.A. R Vermeeren, Ultra high modulus carbon fibres in ARALL laminates, Report, 1990.
- [81] W.-X. Wang, Y. Takao, T. Matsubara, Galvanic corrosion-resistant carbon fiber metal laminates (2007).
- [82] J. Lopes, M. Freitas, D. Stefaniak, P.P. Camanho, Inter-laminar shear stress in hybrid CFRP/austenitic steel, Frattura ed Integrità Strutturale 9 (2015) 67–79.
- [83] X. Li, X. Zhang, H. Zhang, J. Yang, A.B. Nia, G.B. Chai, Mechanical behaviors of Ti/CFRP/Ti laminates with different surface treatments of titanium sheets, Composite Structures 163 (2017) 21–31.
- [84] P. Cortés, W.J. Cantwell, The fracture properties of a fibre–metal laminate based on magnesium alloy, Composites Part B: Engineering 37 (2005) 163–170.
- [85] D. Nestler, H. Jung, S. Arnold, B. Wielage, S. Nendel, L. Kroll, Thermoplastische Hybridlaminat mit variabler Metallkomponente, Mat.-wiss. u. Werkstofftech 45 (2014) 531–536.
- [86] P. Cortés, W.J. Cantwell, The Impact Properties of High-temperature Fiber-Metal Laminates, Journal of Composite Materials 41 (2007) 613–632.
- [87] M. Biron, Thermoplastics and thermoplastic composites, thirdrd edition, William Andrew, Applied Science Publishers, Oxford, United Kingdom, Cambridge, MA, United States, 2018.

- [88] D.A. Kissounko, P. Taynton, C. Kaffer, New material: vitrimers promise to impact composites, *Reinforced Plastics* 62 (2018) 162–166.
- [89] C. Dreyer, M. Bauer, D. Söthje, C. Braune, *Chemical recycling and repair of (fiber-reinforced) thermosetting resins with cyanurate structures*, Nevada, 2014.
- [90] Y. Yuan, Y. Sun, S. Yan, J. Zhao, S. Liu, M. Zhang, X. Zheng, L. Jia, Multiply fully recyclable carbon fibre reinforced heat-resistant covalent thermosetting advanced composites, *Nature communications* 8 (2017) 14657.
- [91] G. Höhne, W.F. Hemminger, H.-J. Falmmersheim, *Differential Scanning Calorimetry*, secondnd edition, Springer, 2003.
- [92] G.W. Ehrenstein, G. Riedel, P. Trawiel, *Praxis der Thermischen Analyse von Kunststoffen*, second ed., Hanser, 2003.
- [93] P.J. Halley, M.E. Mackay, G.A. George, Determining the gel point of an epoxy resin by various theological methods, *High Performance Polymers* 6 (1994) 405–414.
- [94] H.H. Winter, Can the gel point of a cross-linking polymer be detected by the $G' - G''$ crossover?, *Polymer Engineering and Science* 27 (1987) 1698–1792.
- [95] ASTM International, Standard Test Method for Assignment of the Glass Transition Temperature By Dynamic Mechanical Analysis, E1640-07, Information on www.astm.org
- [96] Information on <https://www.skz.de/en/research/technicalfacilities/pruefverfahren1/rheolog-eigenschaften1/4863.Rotational-rheometer.html>
- [97] Information on <https://analytik.news/fachartikel/2013/17.html>
- [98] W. Grellmann, S. Seidler, P. Anderson, *Polymer Testing*, second., Hanser, 2014.
- [99] W. Brostow, V. Castano, M. Deng, A.M. Donald, N.A. D'Souza, B. Erman, *Performance of Plastics*, Hanser, Munich, 2001.
- [100] ISO 14126:1999, Bestimmung der Druckeigenschaften in der Laminebene.
- [101] Information on http://www.substech.com/dokuwiki/doku.php?id=flexural_strength_tests_of_ceramics
- [102] G.W. Ehrenstein, *Faserverbund-Kunststoffe: Werkstoffe - Verarbeitung - Eigenschaften*, second ed., 2006.
- [103] A. Monden, Adhäsion zwischen epoxidharzbasiertem CFK und oberflächenmodifiziertem Stahl: Grenzschnittversagen von Hybridlaminaten unter Mode I, Mode II und Mixed-Mode Belastung. PhD, Augsburg, 2016.
- [104] ASTM International, Standard Test Method for Shear Properties of Composite Materials by V-Notched Rail Shear Method, D7078/D7078M, West Conshohocken, PA, Information on www.astm.org
- [105] M. Salviato, K. Kirane, Z.P. Bažant, G. Cusatis, Mode I and II Interlaminar Fracture in Laminated Composites: A Size Effect Study, *Journal of applied mechanics* 86 (2019) 100.
- [106] S. Hashemi, A.J. Kinloch, J.G. Williams, Corrections needed in double-cantilever beam tests for assessing the interlaminar failure of fibre-composites, *J Mater Sci Lett* 8 (1989) 125–129.
- [107] W.S. Johnson, J.E. Masters, T.K. O'Brien, R.H. Martin, Round Robin Testing for Mode I Interlaminar Fracture Toughness of Composite Materials, *Journal of Composites Technology and Research* 15 (1993) 269.
- [108] J.C. Both, *Tragfähigkeit von CFK-Metall-Laminaten unter mechanischer und thermischer Belastung*, 2014.
- [109] Information on <https://adhesives.specialchem.com/product/p-huntsman-araldite-epn-1180>
- [110] Huntsman, Data Sheet: Tactix® 742. Solid trifunctional epoxy resin, Basel, Switzerland, 2012.
- [111] C. Probst, *Polysulfides - Resistive and Versatile*. Thioplast G, Greiz.
- [112] Information on <https://polymer-additives.specialchem.com/product/a-huntsman-aradur-9664-1>
- [113] Information on <https://coatings.specialchem.com/product/r-huntsman-araldite-ly-1564>

References

- [114] Sigma-Aldrich, Safety Data Sheet: 4-Aminophenyl disulfide, sixth.sixth, 2020.
- [115] Sigma-Aldrich, Safety Data Sheet: 3,3'-Dithiodipropionic acid, sixth.sixth, 2019.
- [116] Nouryon, Safety Data Sheet: Thioplast EPS 70, fourth ed., 2019.
- [117] Nouryon, Safety Data Sheet: Thioplast G4, second ed., 2019.
- [118] Nouryon, Safety Data Sheet: Thioplast EPS 25, second ed., 2017.
- [119] H.Q. Pham, M.J. Marks (Eds.), Epoxy Resins, Wiley-VCH Verlag GmbH & Co. KGaA, 2005.
- [120] SGL Carbon GmbH, The Enablers: Our continous carbon fiber tows. Sigrafil®.
- [121] W. Krenkel (Ed.), Ceramic matrix composites: Fiber reinforced ceramics and their applications, Wiley-VCH, Weinheim, 2008.
- [122] P.J. Flory, Molecular Size Distribution in Three Dimensional Polymers. I. Gelation 1, J. Am. Chem. Soc. 63 (1941) 3083–3090.
- [123] S. CAO, Z. WU, Tensile properties of FRP composites at elevated and high temperatures, Journal of applied mechanics 11 (2008) 963–970.
- [124] Sigma-Aldrich, Safety Data Sheet: Ethylene glycol bis-mercaptoacetate for synthesis, sixth.second, 2021.

List of Figures

Figure 1.1: Target criteria for resin development	2
Figure 2.1: Schematic structure of polymers (following [2])	3
Figure 2.2: Microstructure of amorphous and semi-crystalline thermoplastic polymers (following [2])	4
Figure 2.3: Schematic TTT-diagram for thermosetting resins [3]	5
Figure 2.4: Structural chemical formula of the oxirane ring (epoxy group) (following [6])	7
Figure 2.5: Schematic epoxy-amine network structure [10]	8
Figure 2.6: Schematic representation of associative and dissociative CANs [15]	11
Figure 2.7: Representation of viscosity change of a) elastomer and b) thermoset vitrimers [15]	13
Figure 2.8: Overview of elastic modulus versus healing temperature of a wide range of intrinsic self-healing polymer matrices developed in the past decade [40].....	16
Figure 2.9: [2+1] Radical mediated disulfide exchange mechanism [55]	17
Figure 2.10: A) Disulfide-containing diepoxide BGPDS [60], B) Diphenyl disulfide (DPDS) [60], C) Methylene dianiline (MDA) [61], D) 4-Aminophenyl disulfide (APhD) [61].....	22
Figure 2.11: Layer structure of FML [69]	30
Figure 2.12: Crack growth curve of aluminum 2024-T3 and Glare FMLs for constant amplitude fatigue loading [72].....	31
Figure 2.13: Delamination and fiber bridging in FMLs [72]	32
Figure 2.14: Schematic illustration of stress-strain curves of aluminum, FRP and FML [76]	32
Figure 2.15: Types and levels of damage in FML [77]	33
Figure 3.1: Oscillating plate-plate rheometer [96]	39
Figure 3.2: Compression test with shear loading [100]	42
Figure 3.3: Schematic 3-point and 4-point setup for bending test [101]	44
Figure 3.4: Schematic ILS stress distribution [103].....	46
Figure 3.5: V-notched rail shear test setup [104]	48
Figure 3.6: Scheme of DCB specimen with hinges [105].....	50
Figure 3.7: $C_{1/3}$ over crack propagation a to determine $ \Delta $	51
Figure 3.8: Schematic charpy impact test setup	52
Figure 4.1: Molecular structure of single resin components used [109–115]	54
Figure 4.2: Molecular structure of the disulfide containing component of the commercially available resin mixture Thioplast EPS70 [111]	55
Figure 4.3: A Components of second resin series	59

List of Figures

Figure 4.4: Neat resin specimens for flow tests	65
Figure 4.5: Hand laminating of plates with woven carbon fiber fabric	66
Figure 4.6: Preparation of CFRP plates for butt-joint test with separating foil	67
Figure 4.7: FML plate with outer aluminum layers	67
Figure 5.1: Example of modulus crossover at DMA during isothermal curing	70
Figure 5.2: Gel times of first resin series	71
Figure 5.3: Gel time of second resin series	72
Figure 5.4: Overlay of TGA curves of first resin series	81
Figure 5.5: Mass loss during cure at 180 °C.....	84
Figure 5.6: Stress-strain diagram of tensile test of second resin series polymers.....	86
Figure 5.7: Stress-strain diagram of bending test of first resin series polymers	86
Figure 5.8: Influence of mass percent of EPS70 in component A of the resin on tensile stiffness E_t	87
Figure 5.9: Influence of mass percent of EPS70 in component A of the resin on bending stiffness E_f	87
Figure 5.10: G_{Ic} values for different resin systems used in CFRP	91
Figure 5.11: Influence of resin system on impact resistance of CFRP	92
Figure 5.12: Comparison of bending strength of woven fabric CFRP with M1.6, M1.7, M2.4 and E420 reference as matrix	93
Figure 5.13: Bending modulus values of woven fabric CFRP with M1.6, M1.7, M2.4 and E420 reference as matrix	94
Figure 5.14: Comparison of the ILSS strength of CFRP and FML with resin 1c, 1e, 1f, 1g.....	96
Figure 5.15: G_{Ic} values for FML with different resin systems.....	97
Figure 5.16: ILSS strength τ_{ILSS} of FML with different resins	98
Figure 5.17: Influence of resin system on Charpy impact resistance of FML	98
Figure 5.18: Bending strength σ_f values of woven fabric FML with M1.6, M1.7, M2.4	99
Figure 5.19: Bending modulus E_f values of woven fabric FML with M1.6, M1.7, M2.4.....	100
Figure 5.20: Exemplary DMA curve for 1e CFRP	106
Figure 5.21: Glass transition of vitrimer CFRP of second resin series measured by DMA.....	107
Figure 5.22: Mass gain of vitrimer CFRP due to accelerated conditioning (H_2O)	110
Figure 5.23: Effect of accelerated conditioning on bending strength of vitrimer CFRP.....	111
Figure 5.24: Decrease of T_g of epoxy resin 1c due to moisture uptake measured by DMA.....	112
Figure 5.25: Effect of accelerated conditioning on bending strength σ_f of vitrimer CFRP	113
Figure 5.26: Effect of accelerated conditioning on bending stiffness of vitrimer CFRP	114

Figure 5.27: Effect of accelerated conditioning on bending stiffness E_f of vitrimer CFRP	115
Figure 5.28: Effect of salt spray test on bending strength σ_f of vitrimer CFRP after 10, 20 and 30 days of conditioning	116
Figure 5.29: Effect of salt spray test on bending stiffness E_f of vitrimer CFRP after 10, 20 and 30 days of conditioning	117
Figure 5.30: Effect of salt spray test on bending strength σ_f of vitrimer FML	118
Figure 5.31: Effect of salt spray test on bending stiffness E_f of vitrimer FML	119
Figure 5.32: Effect of salt spray test on bending strength σ_f of vitrimer FML	120
Figure 5.33: Effect of salt spray test on bending stiffness E_f of vitrimer FML	121
Figure 5.34: Change of flexural strength σ_f of CFRP samples due to chemical exposure	122
Figure 5.35: Change of bending modulus E_f of CFRP samples due to chemical exposure.....	123
Figure 5.36: Relaxation times of UD CFRP of first and second resin series	128
Figure 5.37: Relaxation after 10 minutes over ΔT for mixtures with 20% proportion of dynamic bonds.....	131
Figure 5.38: Influence of static base resins on flow behavior tested with mixture 13, 51 and M2.1	132
Figure 5.39: Influence of dynamic hardeners on flow behavior tested with mixtures VME02, M1.6 and M2.4.....	133
Figure 5.40: Molecular structure of recycling chemical glycol dimercaptoacetate [124]	136
Figure 5.41: Dimensional changes of resin specimen 1g (upper, yellow) and 2i (lower, brown) during recycling.....	137
Figure 5.42: Mass change of resin specimen 1g and 2i during recycling.....	138
Figure 5.43: GPC measurement of dissolved resin 1g with RI detector (red) and UV detector (blue)	139
Figure 5.44: GPC measurement of dissolved resin 2i with RI detector (red line) and UV detector (blue line).....	140
Figure 5.45: Dissolution of vitrimer resin on heating plate	141
Figure 5.46: Comparison of fracture toughness of original and repaired CFRP with resins 1c, 1e, 1f and 1g.....	145
Figure 5.47: Reparability of 1e FML	146
Figure 5.48: Butt-joint test results of pressed (original) and repaired CFRP specimen with M1.7 resin.....	147
Figure 5.49: Thermal delamination of vitrimer FML to metal and CFRP	147

List of Figures

Figure 5.50: Steps of chemical delamination: separating fiber and metal layers as well as fiber and resin matrix of a vitrimer FML sample.....	148
Figure 5.51: Target properties for resin development.....	152
Figure 5.52: Bandwidth of key properties of resin mixtures tested.....	160
Figure 6.1: Influence of EPS70 on T_g of first resin series.....	180
Figure 6.2: Influence of EPS70 on T_g of second resin series.....	180
Figure 6.3: T_g values of first resin series (DMA, criterion G'' max).....	181
Figure 6.4: T_g values of second resin series (DMA, criterion G'' max).....	181
Figure 6.5: Degradation temperature T_d of first resin series.....	184
Figure 6.6: Degradation temperature T_d of second resin series.....	184
Figure 6.7: DMA results for FML samples with resin 1g.....	187
Figure 6.8: DMA results for FML samples with resin 2i.....	188
Figure 6.9: DMA results for FML samples with resin 1c.....	189
Figure 6.10: Progression of mass of vitrimer CFRP during exposure to HCl	190
Figure 6.11: Progression of mass of vitrimer CFRP during exposure to $NaOH$	191
Figure 6.12: Progression of mass of vitrimer CFRP during exposure to $Ca(OH)_2$	192
Figure 6.13: Progression of mass of vitrimer CFRP during exposure to $CaCl_2$	193
Figure 6.14: GPC measurement results of M1.5 and M1.6 with smaller meshes using RI detector.....	196
Figure 6.15: GPC measurement results of M1.5 and M1.6 with smaller meshes using UV detector.....	196
Figure 6.16: Comparison of GPC measurement results of mixtures with smaller and wider meshes using RI detector.....	197
Figure 6.17: Comparison of GPC measurement results of mixtures with smaller and wider meshes using UV detector.....	197
Figure 6.18: CFRP plate with 1c repaired (left) and original (right).....	198
Figure 6.19: CFRP plate with 1e repaired (left) and original (right).....	199
Figure 6.20: CFRP plate with 1f repaired (left) and original (right).....	199
Figure 6.21: CFRP plate with 1g repaired (left) and original (right).....	200

List of Tables

Table 2.1: Calculated values of various disulfide bonds [49]	19
Table 2.2: Comparison of similar diepoxides and diamines with and without a disulfide bond [60]	23
Table 4.1: Composition of resin mixture EPS70 [116]	55
Table 4.2: Parameters of resins and hardeners from the respective product data sheets for calculation of resin formulations [109–118]	56
Table 4.3: Base resin components in comparison [111, 116, 118]	57
Table 4.4: Hardener components in comparison [111, 114, 115, 117].....	57
Table 4.5: Material properties of the employed carbon fiber type [120]	58
Table 4.6: Resin formulations of first and second resin series.....	60
Table 4.7: Resin formulations of mixtures to test component influences, of mixtures with 20% proportion of dynamic bonds and of mixtures to optimize resin properties.....	62
Table 4.8: Resin formulation of EPS70-REF	63
Table 4.9: Main properties of vitrimer prepreg materials of first and second resin series.....	64
Table 5.1: Influence of resin components on gel time and cure time	75
Table 5.2: Influence of hardener components on gel time and cure time.....	76
Table 5.3: Influence of base resin components on T_g	79
Table 5.4: Influence of hardener components on T_g	79
Table 5.5: Residual mass of EPS70 at isothermal temperatures measured by TGA	82
Table 5.6: Comparison of degradation temperature $T_d, 95\%$ under N_2 and under air	83
Table 5.7: Mechanical testing results of first and second resin series CFRP materials.....	89
Table 5.8: Mechanical testing results of first and second resin series FML materials (layer structure 3/2).....	95
Table 5.9: Benchmarking of polymer materials (source for values of thermoplastics: [87]).....	101
Table 5.10: Benchmarking of CFRP with PP, PA6, E420 and VME02 as matrix material.....	102
Table 5.11: Benchmarking of CFRP with vitrimer epoxy matrix 1c and 1f in comparison to SGL epoxy resin E420 and SGL PA6 as matrix material.....	103
Table 5.12 Influence of fiber geometries on relaxation (with resin 2f).....	127
Table 5.13: Flowability of optimized resin mixtures	134
Table 5.14: Dissolution times (recycling) of resins of first and second series and E420	136
Table 5.15: Evaluation matrix for selection of three vitrimer resin mixtures	143
Table 5.16: Temperatures set for repair tests of resin 1c, 1e, 1f and 1g.....	144

List of Tables

Table 5.17: Influence of base resin components on relaxation	149
Table 5.18: Influence of hardener components on relaxation	149
Table 5.19: Key values of mixture M1.7	150
Table 5.20: Key values of mixture M2.4	151
Table 5.21: Key values of mixture M1.6	151
Table 5.22: Influence of base resin components on resin properties	153
Table 5.23: Influence of base hardener components on resin properties	153
Table 5.24: Key values of the three mixtures selected	158
Table 5.25: Gel time, cure time, T_g from DMA, decomposition temperature and normalized modulus after 10 minutes of all resins tested	159
Table 6.1: Gel times of first resin series	178
Table 6.2: Gel times of second resin series.....	178
Table 6.3: Gel times of all other resins	178
Table 6.4: Cure times of all mixtures	179
Table 6.5: T_g of all other resins (5 K/min, criterion max. G'')	182
Table 6.6: Glass transition values of resins (rheometry with 5 K/min).....	183
Table 6.7: Degradation temperature of selected resin mixtures.....	185
Table 6.8: Fiber volume fractions of CFRP-plates for the mechanical tests.....	185
Table 6.9: Poisson ratios and V-notched rail shear test results of CFRP of first resin series ...	186
Table 6.10: Characteristic values of glass transition of vitrimer CFRP measured by DMA	186
Table 6.11: Normalization and average of resin mass fraction of CFRP samples from accelerated conditioning.....	189
Table 6.12: Residual modules of the other resins.....	194
Table 6.13:Relaxation measurement results	195

Acknowledgements

First of all, I would like to express my special thanks to Prof. Dr. Markus Sause for supervising and guiding my work over the years.

I would like to thank Prof. Dr.-Ing. Dietmar Koch for taking over the secondary appraisal of my work without any hesitation.

My special thanks go to the SGL Carbon GmbH for the opportunity to conduct my doctoral thesis, the pleasant and collegial working atmosphere and the three instructive years I was allowed to research and spend there. In particular, I would like to thank Dr. Max von Bistram and Dr. Norma Minar for their supervision of my work within the company and for their advice at any time.

Furthermore, I would like to thank my three students Pascal Boxler, Jacopo Zepponi and Christian Dilly for the good cooperation and their contribution to this thesis.

Not mentioned by name, but nevertheless indispensable for this thesis, I would like to express my sincere thanks to all the employees of SGL who supported me in word and deed. I would like to thank the mechanical testing laboratory, the chemical laboratory and the staff of the technical center.

Appendix

Gel Times

Table 6.1: Gel times of first resin series

Resin	1=E420	1a	1b	1c	1d	1e	1f	1g
Gel time [s]	12	15	29	31	35	38	45	68

Table 6.2: Gel times of second resin series

Resin	2=VME02	2a	2b	2c	2d	2e	2f	2g	2h	2i
Gel time [s]	548	673	784	844	821	849	878	928	1674	1857

Table 6.3: Gel times of all other resins

Influence of EPS25 compared to EPS70									
Resin	11	12	13		13	EPS70-Ref			
Gel time [min]	27	30	35		35	32			
Influence of DTPA									
Resin	21=11	22	23						
Gel time [min]	27	9	6						
Influence of static base resins (literature)									
Resin	21=11	50	70						
Gel time [min]	-	-	-						
Influence of static base resins									
Resin	13	51	M2.1						
Gel time [min]	35	8	16						
Influence of dynamic hardeners					Influence of APhD				
Resin	22	23	M2.2	M2.3		11	2=VME02		
Gel time [min]	9	6	16	51		27	6*		
Mixtures with 20% proportion of dynamic bonds set									
Resin	VME02	M1.6	M1.7	M2.4	M2.5	M2.6	M2.7		
Gel time [min]	6*	6	30	43	14	45	47		
Optimized/Multi-component mixtures									
Resin	52	53	56	71	M1.1	M1.2	M1.3	M1.4	M1.5
Gel time [min]	19	20	24	15	6	11	11	4	5

*@ 150 °C

Cure Times

Table 6.4: Cure times of all mixtures

Resin	Cure Time @ 150 °C [min]	Cure Time @ 180 °C [min]
1c	10	
1e	10	
1f	10	
1g	10	
2b	45	
2f	60	
2g	65	
2i	85	
11		108
12		85
13		70
21		108
22		60
23		50
51		50
52		50
53		70
56		70
71		45
M1.1		55
M1.2		70
M1.3		55
M1.4		40
M1.5		65
M1.6		60
M1.7		95
M2.1		75
M2.2		70
M2.3		120
M2.4		110
M2.5		60
M2.6		120
M2.7		110
EPS70-Ref		85

Glass Transition Temperature - DSC

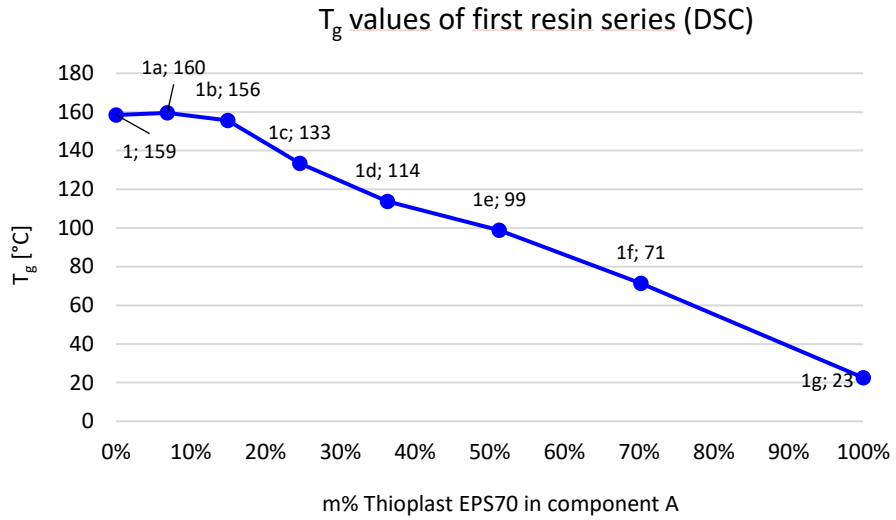


Figure 6.1: Influence of EPS70 on T_g of first resin series

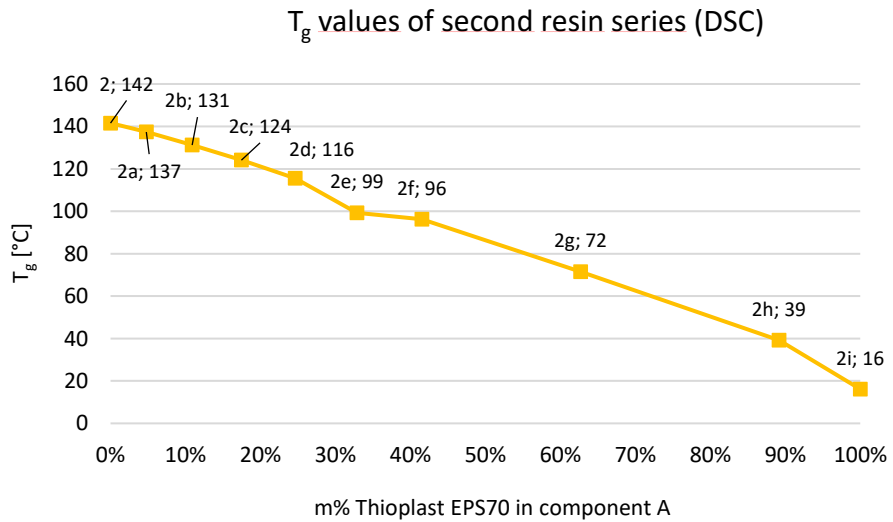


Figure 6.2: Influence of EPS70 on T_g of second resin series

Glass Transition Temperature – Rheological Measurements

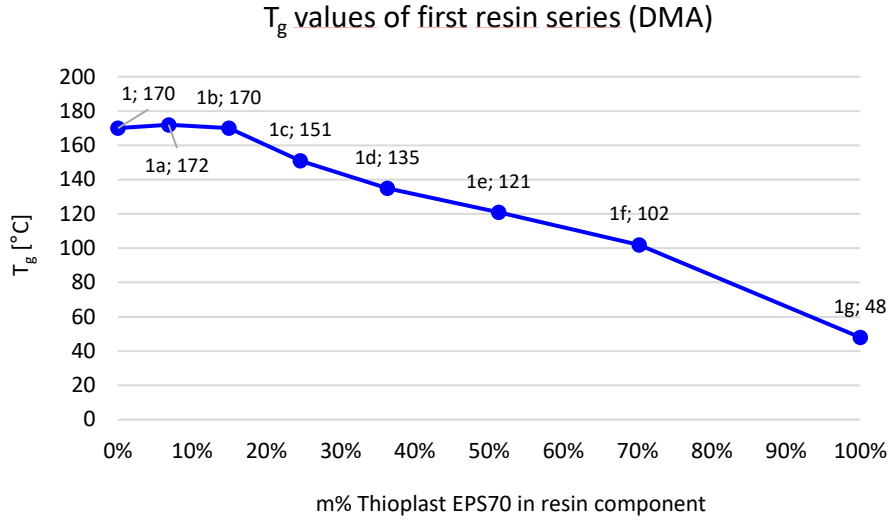


Figure 6.3: T_g values of first resin series (DMA, criterion G'' max)

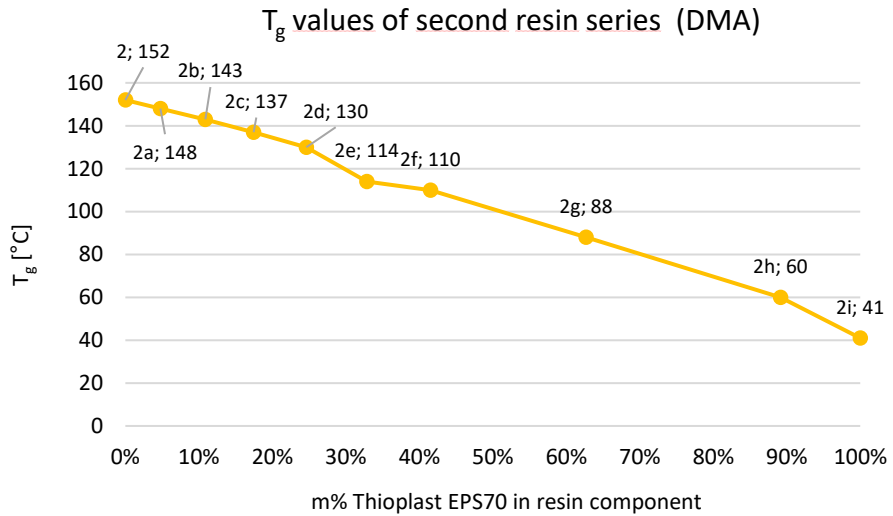


Figure 6.4: T_g values of second resin series (DMA, criterion G'' max)

Appendix

Table 6.5: T_g of all other resins (5 K/min, criterion max. G'')

Influence of EPS25				compared to EPS70						
Resin	11	12	13		13	EPS70-Ref				
T_g [°C]	189	127	84		84	104				
Influence of DTPA										
Resin	21=11	22	23							
T_g [°C]	189	143	115							
Influence of static base resins (literature)										
Resin	21=11	50	70							
T_g [°C]	189	265*	340*							
Influence of static base resins										
Resin	13	51	M2.1							
T_g [°C]	110	127	139							
Influence of dynamic hardeners					Influence of APhD					
Resin	22	23	M2.2	M2.3		11	VME02			
T_g [°C]	148	121	126	68		189	136			
Mixtures with 20% proportion of dynamic bonds set										
Resin	VME02	M1.6	M1.7	M2.4	M2.5	M2.6	M2.7			
T_g [°C]	130**	111	122	134	107	117	126			
Optimized/Multi-component mixtures										
Resin	52	53	56	71	M1.1	M1.2	M1.3	M1.4	M1.5	
T_g [°C]	89	60	36	100	104	106	79	≈20	138	

*criterion G' Onset for DMA

**cured @ 150 °C

Table 6.6: Glass transition values of resins (rheometry with 5 K/min)

Resin	$T_{g,Onset}$ [°C]	$T_{g,maxG''}$ [°C]	$T_{g,Endset}$ [°C]	$\Delta T_{(Endset- Onset)}$ [°C]
1c	110	121	154	44
1e	90	100	130	40
1f	80	91	123	43
1g	50	54	81	31
2b	117	126	140	23
2f	90	99	120	30
2g	66	72	88	22
2i	42	43	66	
V11	189	193	207	18
V12	127	132	147	20
V13	84	110	125	41
V21	189	193	207	18
V22	143	148	157	14
V23	115	121	133	18
V51	113	126	153	40
V52	84	89	112	28
V53	55	60	76	21
V56	33	36	57	24
V71	89	100	133	44
M1.1	99	104	116	17
M1.2	90	105	131	41
M1.3	71	76	91	20
M1.4	-	≈20	-	-
M1.5	132	138	153	21
M1.6	108	111	121	13
M1.7	118	122	136	18
M2.1	121	139	170	49
M2.2	117	126	145	28
M2.3	66	68	99	33
M2.4	129	134	146	17
M2.5	100/100	107	122	22
M2.6	114	117	127	13
M2.7	122	126	139	17
EPS70-Ref	95	104	124	29

Degradation Temperatures

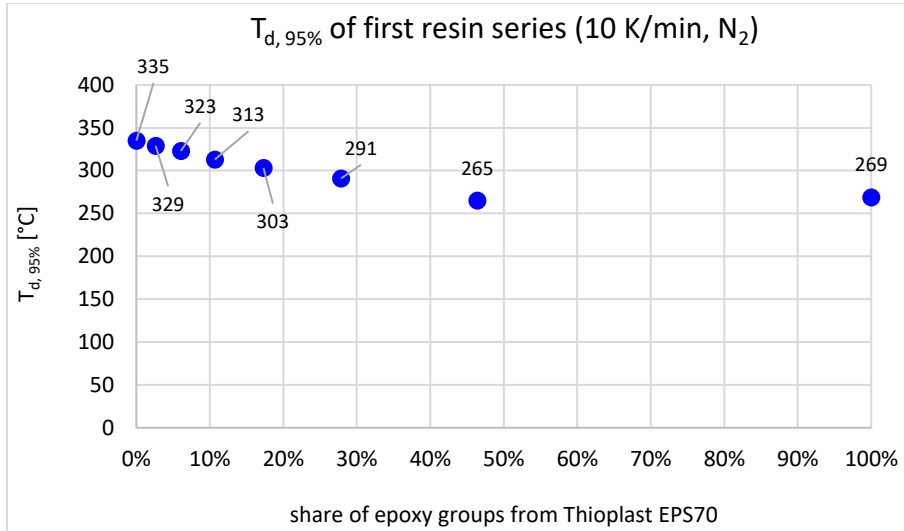


Figure 6.5: Degradation temperature $T_{d,95\%}$ of first resin series

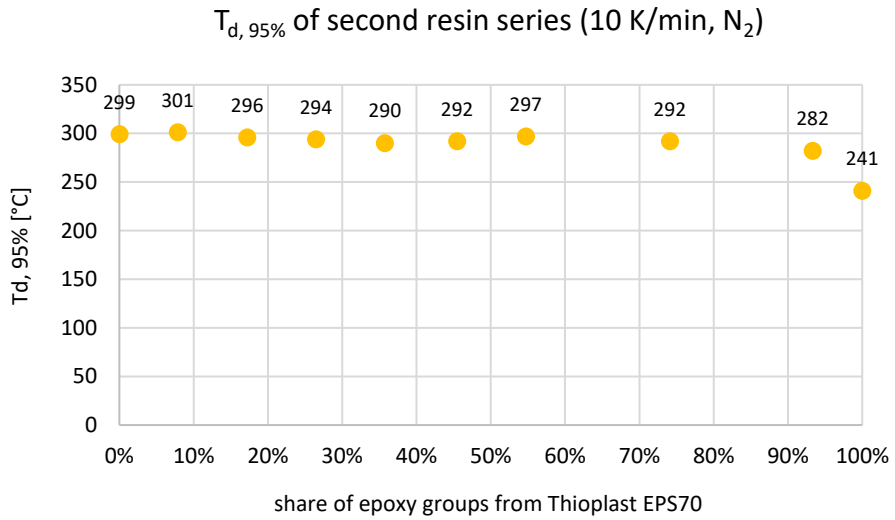


Figure 6.6: Degradation temperature $T_{d,95\%}$ of second resin series

Table 6.7: Degradation temperature of selected resin mixtures

Resin	T_d [°C]	
	5% mass loss in total	2% mass loss in 2 nd step
M1.1	257	
M1.3		(253)
M1.5		(281)
M1.6	306	
M1.7		(281)
M2.1	270	
M2.4	250	
M2.5	285	
M2.6	281	
M2.7		(279)
13		(266)
23	316	
EPS70Ref	291	

Mechanical Performance of CFRP at Room Temperature

Table 6.8: Fiber volume fractions of CFRP-plates for the mechanical tests

Resin		0° Tensile test		Bending 0° & 90°, Compression 0° & 90°		±45° Tensile test (pseudo-shear)		ILSS test	
		FVF	s	FVF	s	FVF	s	FVF	s
1c		52.0%	2.2%	56.0%	0.4%	54.8%	0.4%	59.5%	1.4%
1e		53.0%	1.4%	56.2%	0.2%	54.5%	1.1%	62.3%	3.3%
1f		52.8%	2.9%	56.9%	1.0%	55.7%	3.8%	64.3%	0.3%
1g		58.2%	3.0%	63.8%	1.1%	65.2%	2.9%	67.7%	1.1%
2b		57.2%	2.8%	69.2%	1.6%	64.4%	1.5%	71.6%	0.0%
2f		61.8%	2.5%	67.2%	0.0%	67.0%	1.3%	69.4%	0.1%
2g		59.8%	0.2%	59.0%	1.3%	61.8%	1.6%	52.8%	2.1%
2i		60.8%	3.3%	56.0%	1.9%	52.3%	1.7%	50.8%	1.8%

Appendix

Table 6.9: Poisson ratios and V-notched rail shear test results of CFRP of first resin series

Parameter	Standard	1c	1e	1f	1g	Unit
Poisson ratio $\parallel\perp$ of neat resin	ISO 527-5	2.59	2.41	2.29	*	[1]
Poisson ratio $\parallel\perp$ of CFRP	ISO 527-5		3.19	3.13		[1]
Poisson ratio $\perp\parallel$ of CFRP	ISO 527-2		0.56	0.64		[1]
Shear strength	ASTM D 7078		40	34		MPa
Shear modulus			3.2	2.4		GPa

*Could not be determined because of the low T_g and the resulting high elasticity of the material

Mechanical Stability of the CFRP at Elevated Temperatures (DMA Measurements)

Table 6.10: Characteristic values of glass transition of vitrimer CFRP measured by DMA

Resin	Onset G' [°C]	Maximum G'' [°C]	T_g Endset [°C]	Broadness of glass transition [°C]
1c	110	121	154	43
1e	90	100	130	41
1f	80	91	123	43
1g	50	54	81	31
VME02	128	136	145	17
2b	117	126	140	23
2f	90	99	120	30
2g	66	72	88	22
2i	42	43	66	25

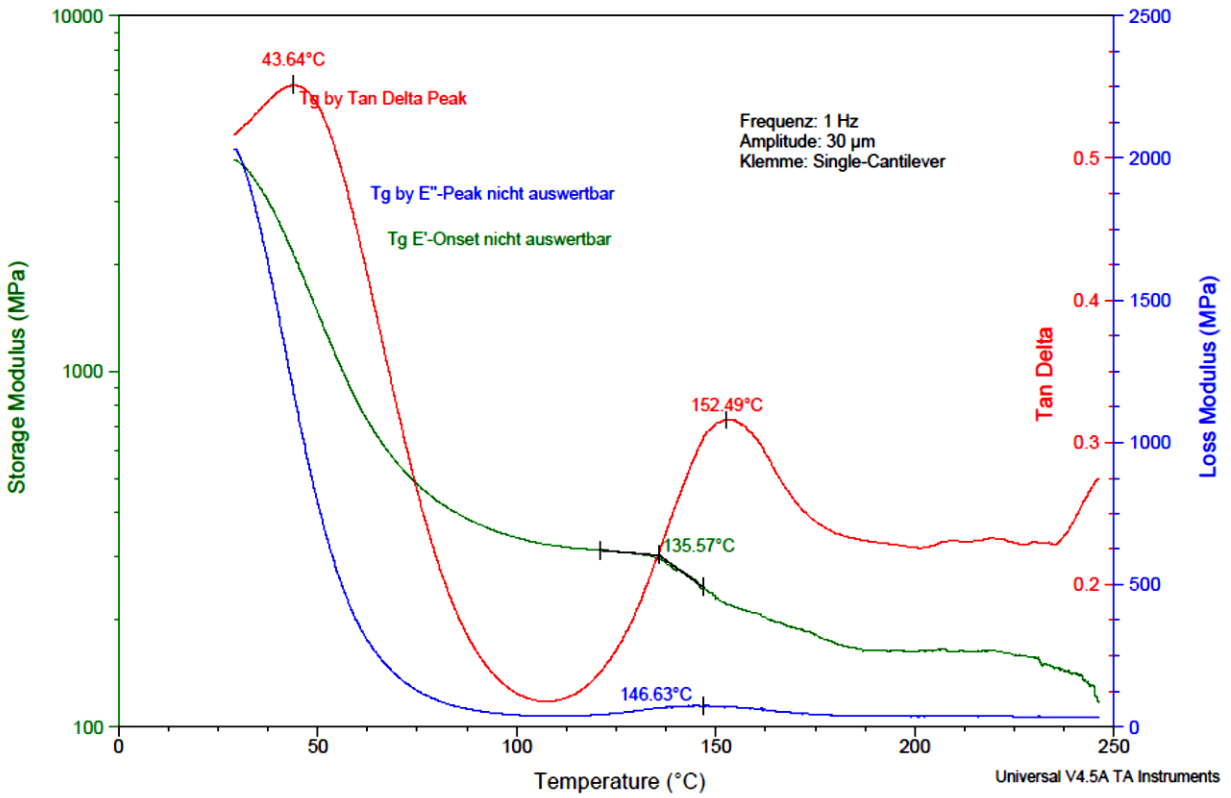
Mechanical Stability of the FML at Elevated Temperatures (DMA Measurements)

Figure 6.7: DMA results for FML samples with resin 1g

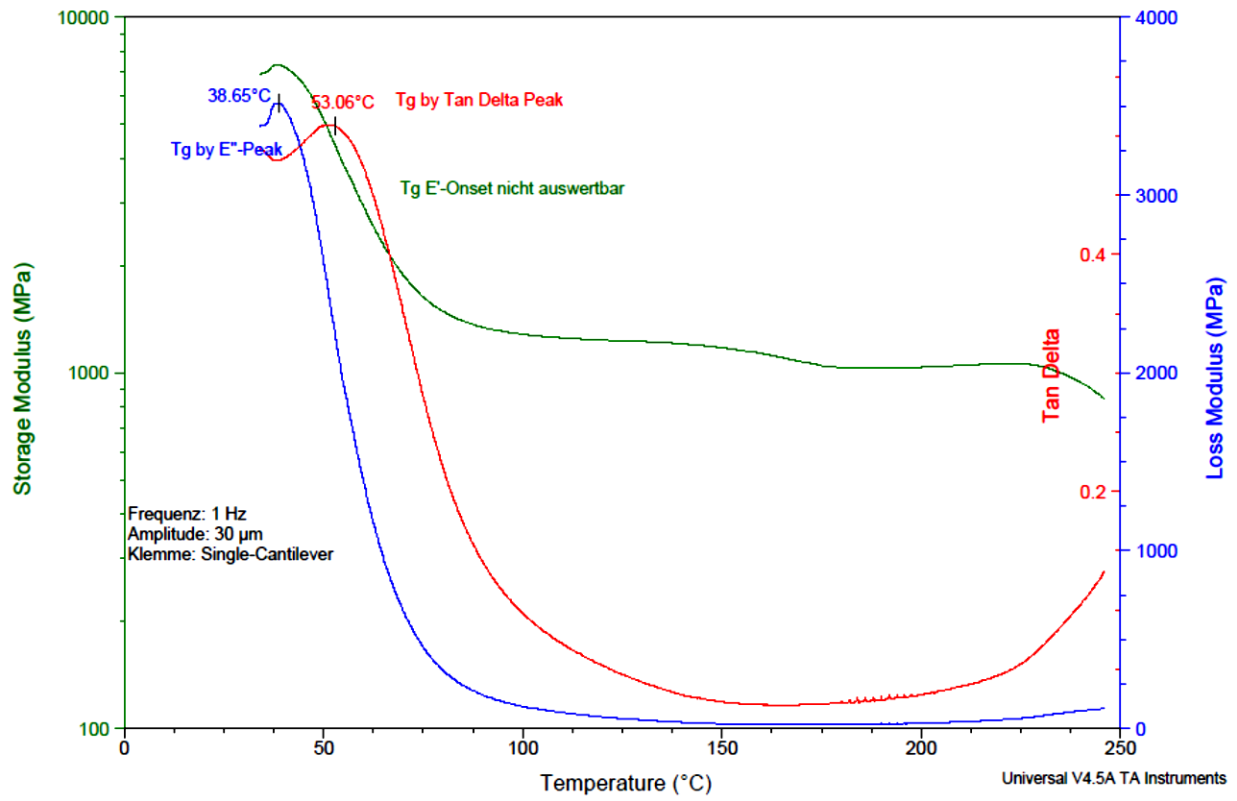


Figure 6.8: DMA results for FML samples with resin 2i

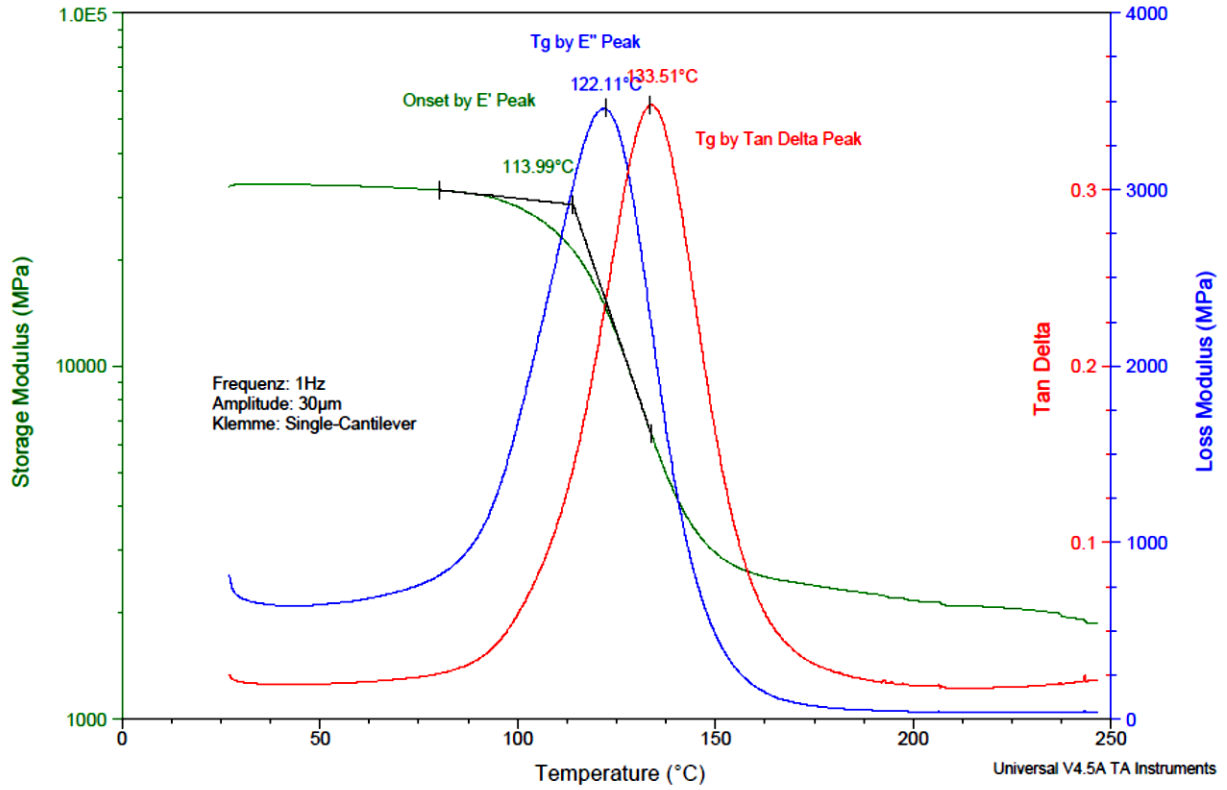


Figure 6.9: DMA results for FML samples with resin 1c

Water Absorption and Media Resistivity – Resin Mass Fractions

Table 6.11: Normalization and average of resin mass fraction of CFRP samples from accelerated conditioning

Resin	E420	1c	1e	1f	1g	2f	PA6	
Fiber Volume Fraction [%]	48.80	59.80	52.50	60.90	53.70	66.50	64.45	
Resin Mass Fraction [%]	26.98	30.90	37.60	30.00	36,50	25.10	41.16	Ø 41.16

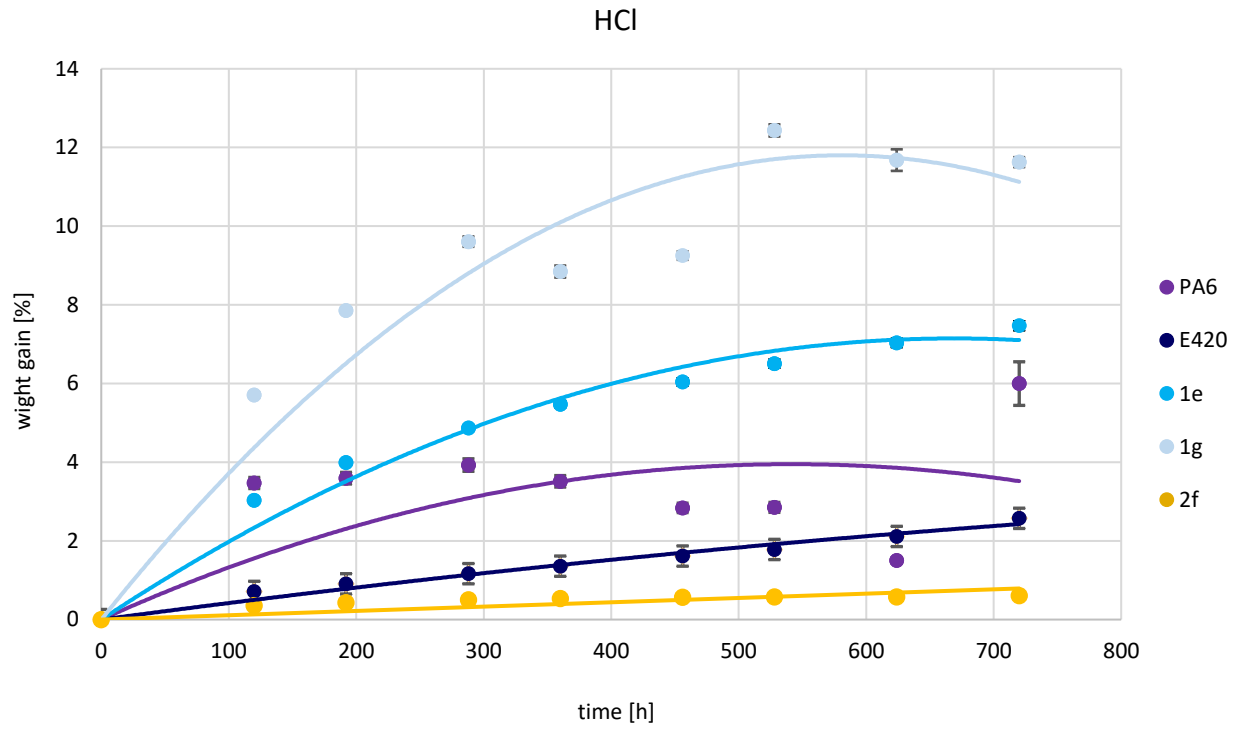


Figure 6.10: Progression of mass of vitrimer CFRP during exposure to *HCl*

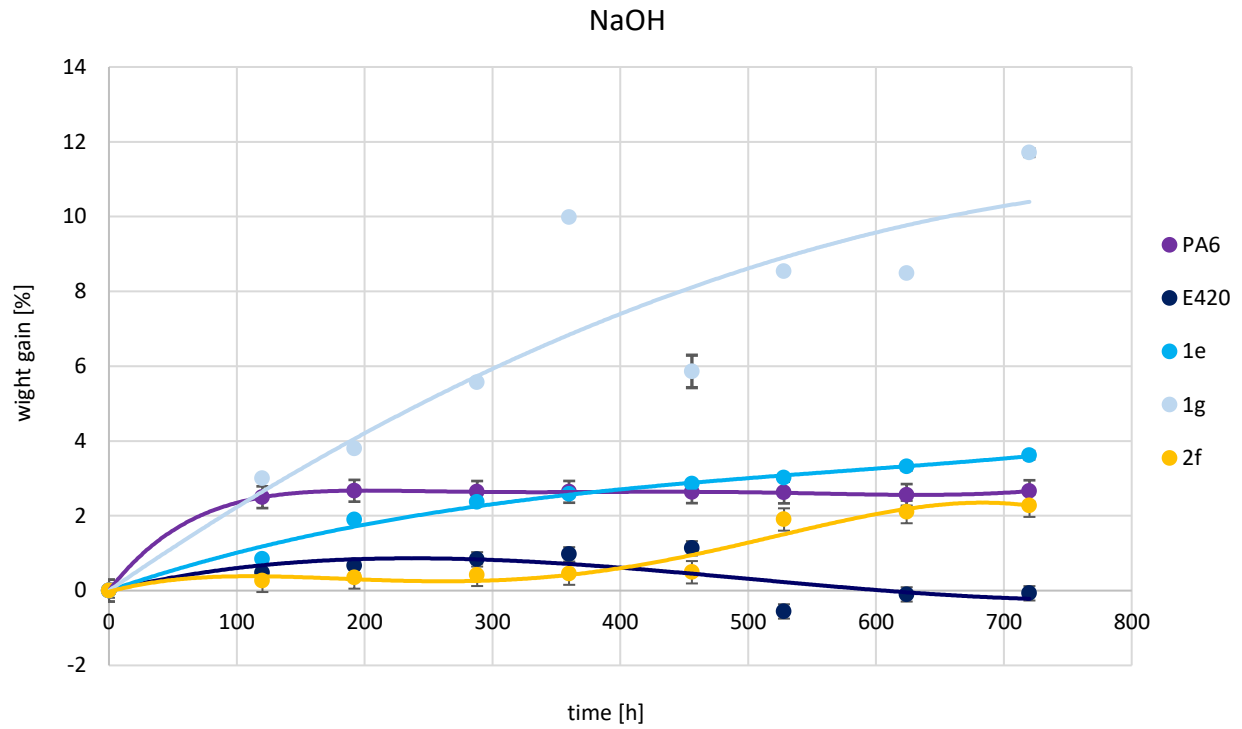


Figure 6.11: Progression of mass of vitrimer CFRP during exposure to $NaOH$

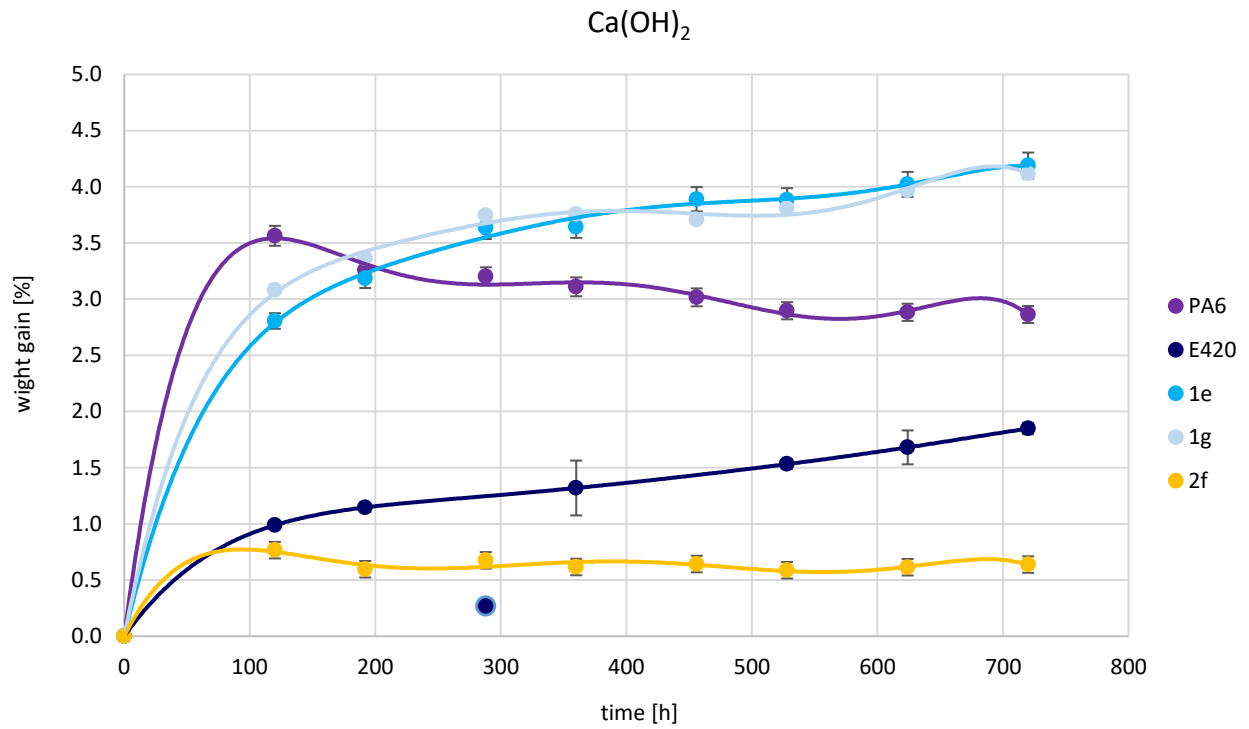


Figure 6.12: Progression of mass of vitrimer CFRP during exposure to Ca(OH)_2

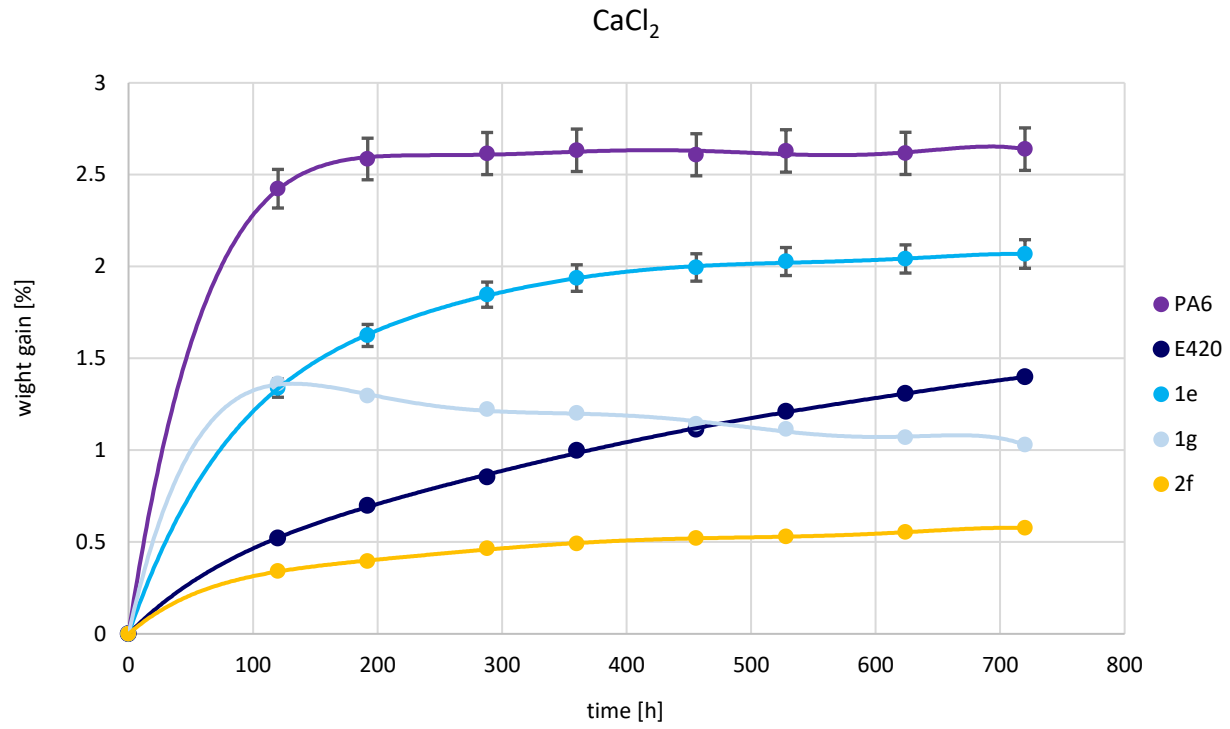


Figure 6.13: Progression of mass of vitrimer CFRP during exposure to CaCl_2

Dynamic Properties – Relaxation Behavior

Table 6.12: Residual modulus of the other resins

Influence of EPS25 compared to EPS70									
Resin	11	12	13		13	EPS70-Ref			
Proportion of dynamic bonds	0%	13%	25%						
Residual Modulus 10 min @ 180 °C	/ (>82%)	82%	70%						
Residual Modulus 1 h @ 180 °C	/ (>71%)	71%	55%						
Influence of DTPA									
Resin	21=11	22	23						
Proportion of dynamic bonds	0%	7%	13%						
Residual Modulus 10 min @ 180 °C	/ (>82%)	87%	53%						
Residual Modulus 1 h @ 180 °C	/ (>71%)	77%	45%						
Influence of static base resins									
Resin	13	51	M2.1						
Proportion of dynamic bonds	0%	0%	0%						
Residual Modulus 10 min @ 180 °C	70%	81%	85%						
Residual Modulus 1 h @ 180 °C	55%	67%	76%						
Influence of dynamic hardeners					Influence of APHD				
Resin	22	23	M2.2	M2.3		11	VME02		
Proportion of dynamic bonds	7%	13%	7%	33%		0%	20%		
Residual Modulus 10 min @ 180 °C	87%	53%	81%	35%		/ (>82%)	35%		
Residual Modulus 1 h @ 180 °C	77%	45%	70%	25%		/ (>71%)	29%		
Mixtures with 20% proportion of dynamic bonds set									
Resin	VME02	M1.6	M1.7	M2.4	M2.5	M2.6	M2.7		
Proportion of dynamic bonds	20%	20%	20%	20%	20%	20%	20%		
Residual Modulus 10 min @ 180 °C	35%	48%	25%	36%	35%	77%	70%		
Residual Modulus 1 h @ 180 °C	29%	34%	17%	29%	55%	36%	55%		
Optimized/Multi-component mixtures									
Resin	52	53	56	71	M1.1	M1.2	M1.3	M1.4	M1.5
Proportion of dynamic bonds	28%	45%	55%	34%	34%	38%	57%	11%	28%
Residual Modulus 10 min @ 180 °C	67%	25%	/	68%	76%	66%	/	53%	67%
Residual Modulus 1 h @ 180 °C	49%	14%	/	54%	61%	49%	/	41%	49%

Relaxation Measurement Results

Table 6.13: Relaxation measurement results

Resin	T _{g,endset} [°C]	T [°C]	ΔT [°C]	Modulus G' Max (G ₀) [MPa]	Modulus G' Min (G after 60min) [MPa]	G/G ₀ after 10 min	G/G ₀ after 60 min
M1.1	113	163	50	6015	4130	82%	69%
	113	180	67	5986	3658	76%	61%
	113	200	87	6425	3075	66%	48%
M1.2	131	180	49	4769	2817	71%	59%
	131	200	69	7016	3396	68%	48%
M1.3	90	140	50	4462	3118	82%	70%
	90	180	90	5475	2689	66%	49%
	90	200	110	4211	2119	62%	50%
M1.5	152	180	28	11015	4489	53%	41%
M1.6	94	180	86	1820	623	48%	34%
M1.7	87	180	93	544	94	25%	17%
M2.1	170	180	10	10700	8116	85%	76%
M2.2	145	180	35	12245	8578	81%	70%
M2.3	85	180	95	2459	625	35%	25%
M2.4	146	158	12	3355	1325	47%	39%
M2.4	146	180	34	5273	1539	36%	29%
	146	200	54	5274	1491	35%	28%
	122	173	51	7176	4021	66%	56%
M2.5	122	180	58	8473	4661	65%	55%
	122	200	78	8154	3295	55%	40%
	127	154	27	3248	2020	76%	62%
M2.6	127	180	53	4245	1533	57%	36%
	127	200	73	3805	1002	46%	26%
	139	150	11	1854	987	70%	53%
M2.7	139	200	61	2343	945	61%	40%
	139	180	41	2474	1368	73%	55%
	VME02	149	180	31	10127	2924	35%
149		200	51	3646	905	38%	25%

Recycling of Vitrimers Neat Resin – GPC Measurements

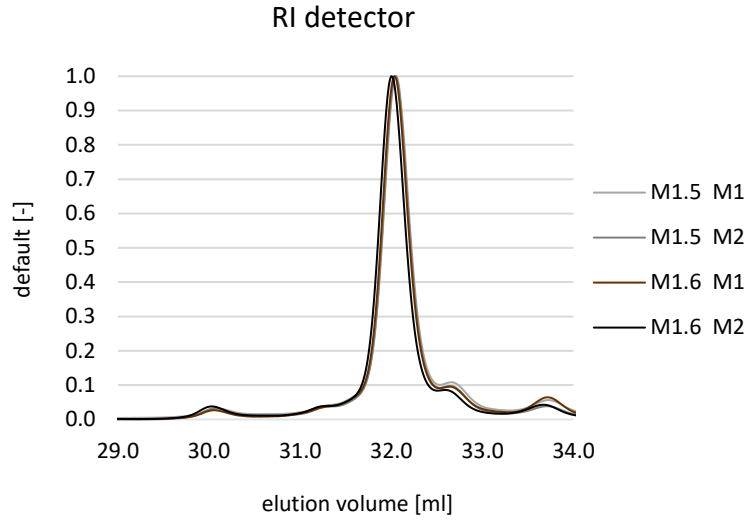


Figure 6.14: GPC measurement results of M1.5 and M1.6 with smaller meshes using RI detector

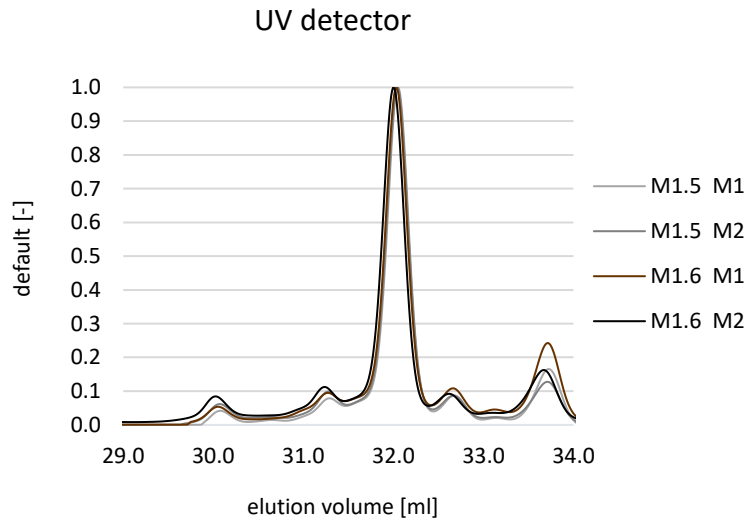


Figure 6.15: GPC measurement results of M1.5 and M1.6 with smaller meshes using UV detector

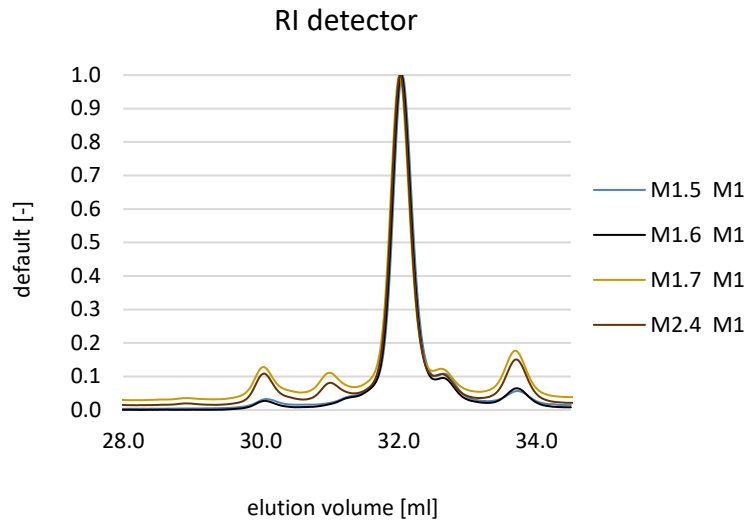


Figure 6.16: Comparison of GPC measurement results of mixtures with smaller and wider meshes using RI detector

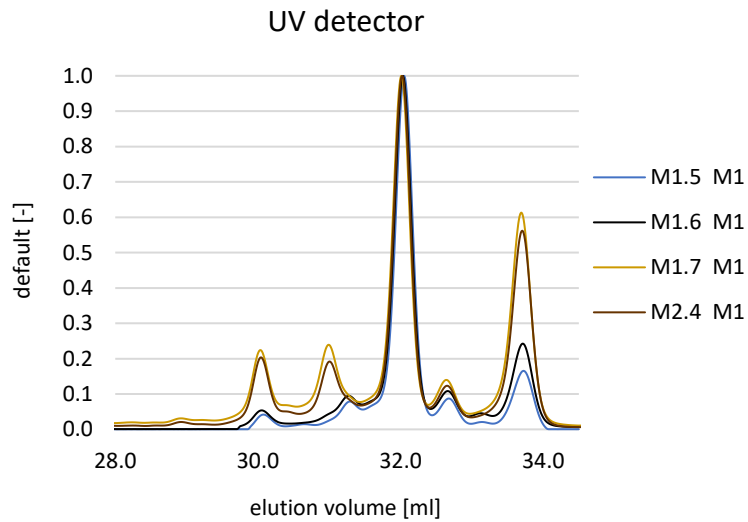


Figure 6.17: Comparison of GPC measurement results of mixtures with smaller and wider meshes using UV detector

Dynamic Properties – Repair Potential (C-Scan Images)

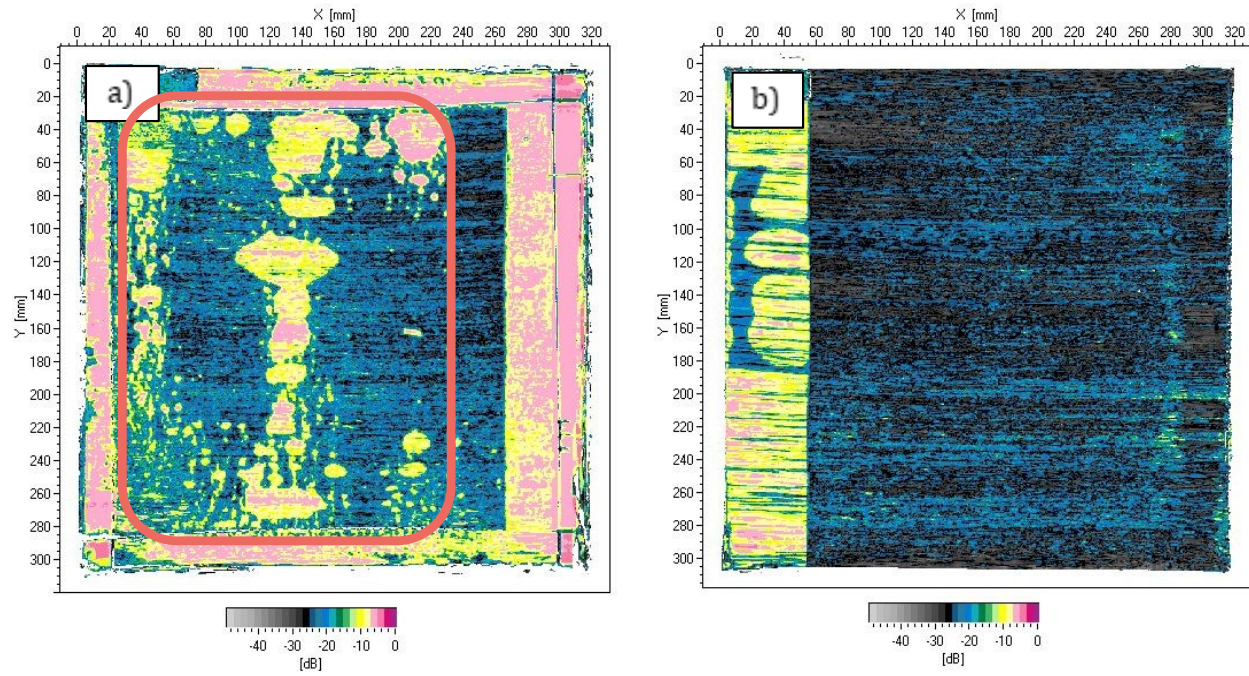


Figure 6.18: CFRP plate with 1c repaired (left) and original (right)

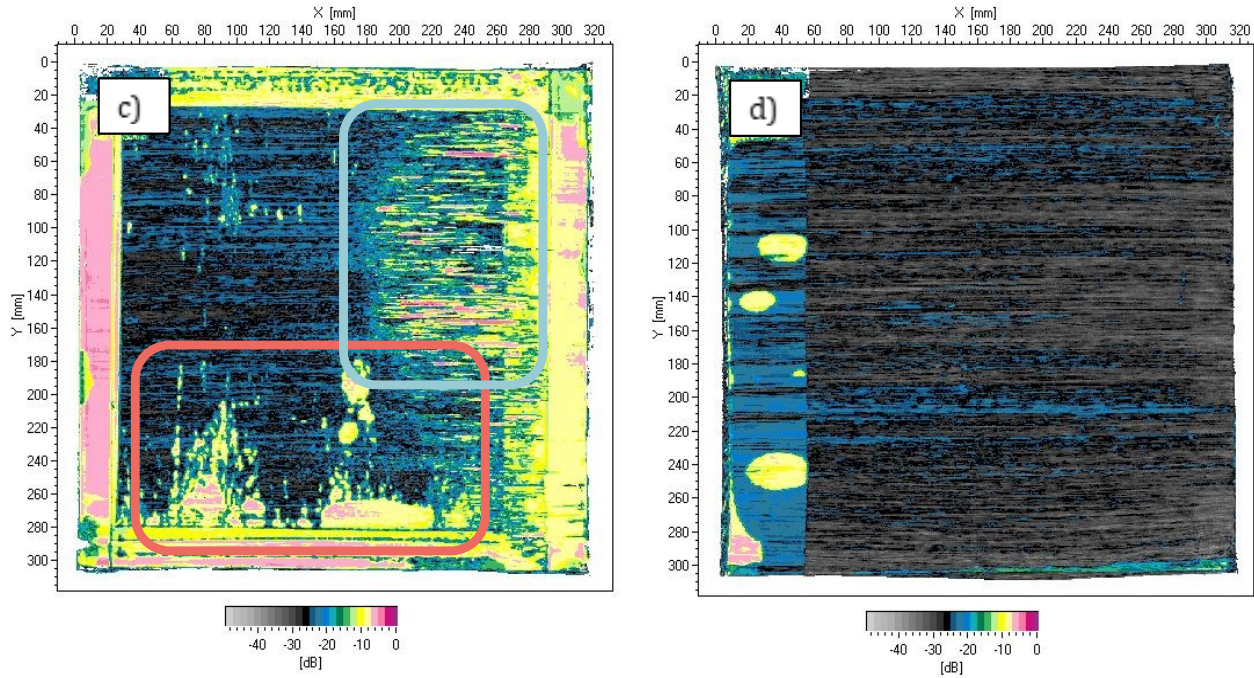


Figure 6.19: CFRP plate with 1e repaired (left) and original (right)

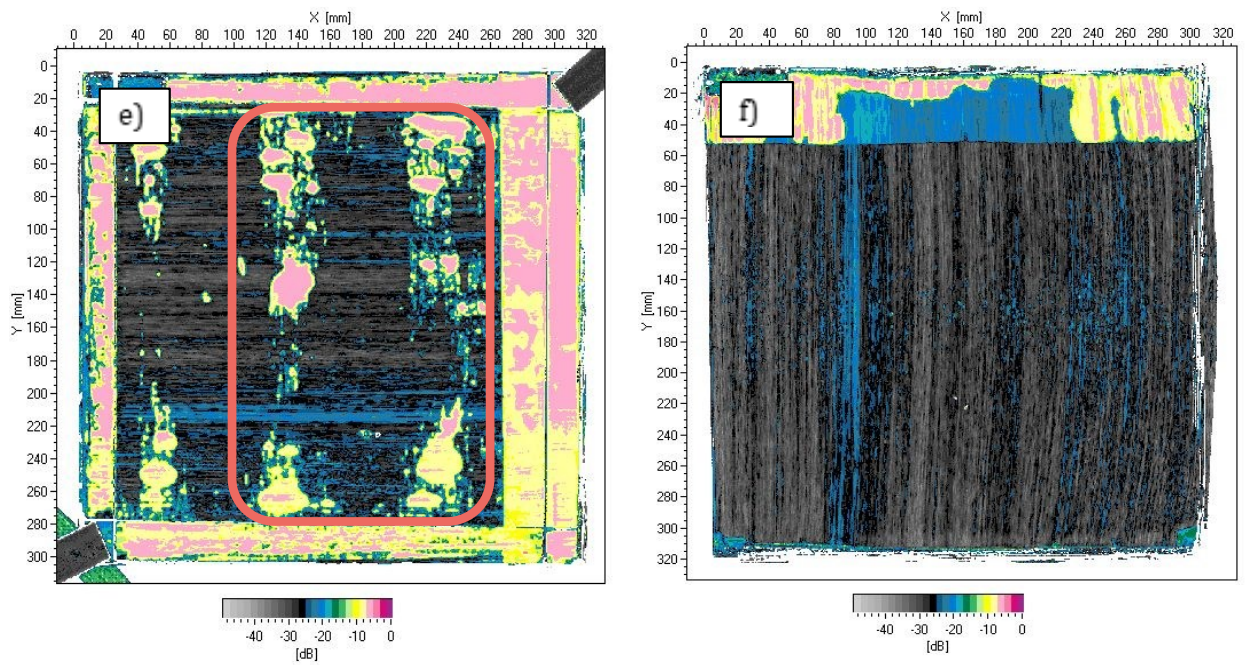


Figure 6.20: CFRP plate with 1f repaired (left) and original (right)

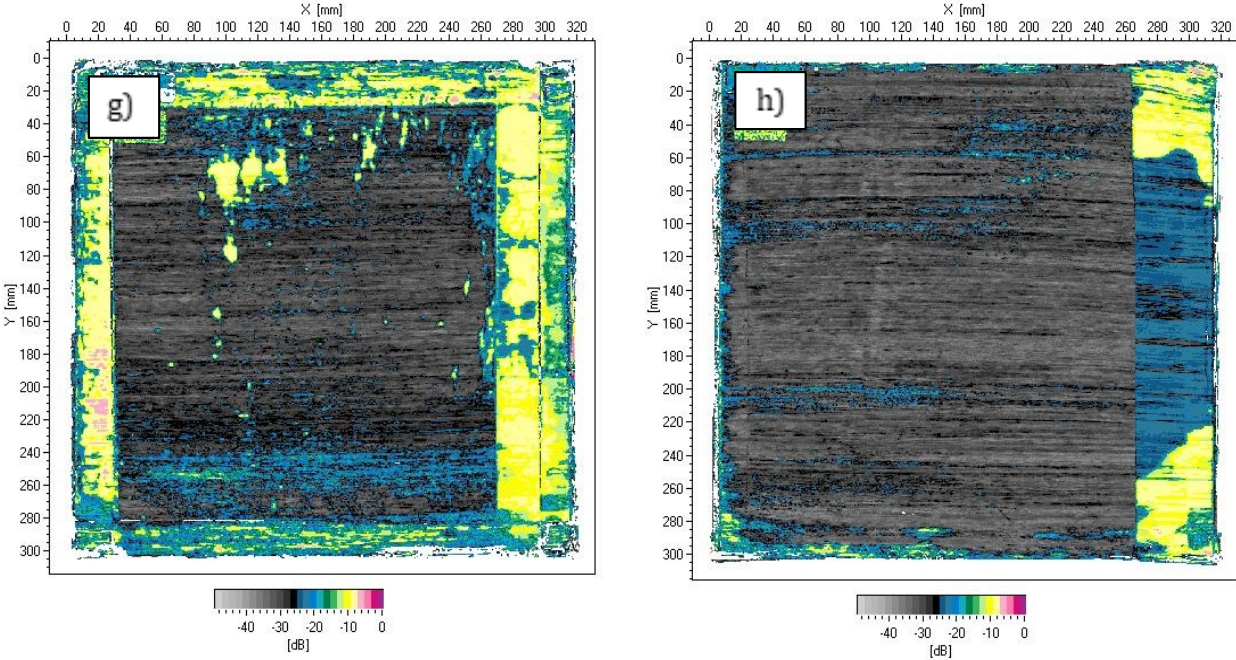


Figure 6.21: CFRP plate with 1g repaired (left) and original (right)